Robust Multivariable Control Design

An Application to a Bank-to-Turn Missile

Author: Yashren Reddi

Supervisor: Prof. Edward Boje

2011

UNIVERSITY OF KWAZULU-NATAL

As the candidate's Supervisor I agree/do not agree to the submission of this thesis

....

Declaration

I .... declare that

(i) The research reported in this dissertation, except where otherwise indicated, is my original work.
(ii) This dissertation has not been submitted for any degree or examination at any other university.
(iii) This dissertation does not contain other persons' data, pictures, graphs or other information, unless specifically acknowledged as being sourced from other persons.
(iv) This dissertation does not contain other persons' writing, unless specifically acknowledged as being sourced from other researchers. Where other written sources have been quoted, then:
   a) their words have been re-written but the general information attributed to them has been referenced;
   b) where their exact words have been used, their writing has been placed inside quotation marks, and referenced.
(v) Where I have reproduced a publication of which I am an author, co-author or editor, I have indicated in detail which part of the publication was actually written by myself alone and have fully referenced such publications.
(vi) This dissertation does not contain text, graphics or tables copied and pasted from the Internet, unless specifically acknowledged, and the source being detailed in the dissertation and in the References sections.

Signed: ....

Abstract

Multi-input multi-output (MIMO) control system design is much more difficult than single-input single output (SISO) design due to the combination of cross-coupling and uncertainty. An investigation is undertaken into both the classical Quantitative Feedback Theory (QFT) and modern H-infinity frequency domain design methods. These design tools are applied to a bank-to-turn (BTT) missile plant at multiple operating points for a gain scheduled implementation. A new method is presented that exploits both QFT and H-infinity design methods. It is shown that this method gives insight into the H-infinity design and provides a classical approach to tuning the final H-infinity controller. The use of "true" inversion-free design equations, unlike the theory that appears in current literature, is shown to provide less conservative bounds at frequencies near and beyond the gain cross-over frequency. All of the techniques investigated and presented are applied to the BTT missile to show their application to a practical problem. It was found that the H-infinity design method was able to produce satisfactory controllers at high angles of attack where there were no QFT solutions found. Although an H-infinity controller was produced for all operating points except the last, the controllers were found to be of very high-order, contain very poorly damped second order terms and generally more conservative, as opposed to the QFT designs. An investigation into simultaneous stabilization of multiple plants using H-infinity is also presented. Although a solution to this was not found, a strongly justified case to entice further investigation is presented.

Acknowledgements

I would like to thank my supervisor, Professor Edward Boje, for the peculiar but effective guidance and thought-provoking questions I received throughout my time doing research at the university. The financial assistance of the National Research Foundation (NRF) towards this research is also acknowledged.

Table of Contents

1. Introduction

In order to make a machine do what it is intended to do in the real world, a control system is required. With the presence of uncertainty, feedback control in particular is required. Linear single-input single-output (SISO) designs are fairly well understood and there are robust design techniques such as SISO Quantitative Feedback Theory (QFT) that allows the designer to find an optimal controller design without iteration. In multi-input multi-output (MIMO) systems there is generally cross-coupling in the system. The cross-coupling in conjunction with the uncertainty in most cases lead to non-trivial problems.

Some of the available design techniques for MIMO systems are investigated. After a deep study of these techniques, they are applied to a MIMO problem. The problem is to design a controller to meet reference tracking specifications and stability specifications for a bank-to-turn missile multivariable plant.

Chapter two presents the theory that is applied in later sections to the missile problem. There are three main theory subsections. The first two describes QFT and H-infinity theory and the last subsection describes a new methodology that combines both QFT and H-infinity. The fundamental principles behind QFT are first introduced in Section 2.1.1; this is done for the SISO case. Sections 2.1.2 - 2.1.6 describe the original and more recent contributions to MIMO QFT. An alternative to the original MIMO QFT design equations which may provide better results are given in Section 2.1.7. Section 2.1.8 details the stability of MIMO systems in the QFT framework. To complete the exposition of MIMO QFT, Section 2.1.9 discusses the generation and use of uncertainty templates in QFT.

With the intensive research on optimization in control design done over the past four decades, it would be ignorant not to study the rich material on modern control design. Section 2.2 presents the modern feedback approach to design. State-feedback concept of control is presented first as a primer to H-infinity optimization. The solution to the H-infinity problem is investigated in Section 2.2.2 with the intention to modify the solution so that the simultaneous stabilization problem may be solved. The description of the simultaneous stabilization problem and the research done towards a solution are shown in Section 2.2.3. Section 2.2.4 concludes the section on modern control with the presentation of how H-infinity design methodology is applied for practical problems.

Section 2.3 documents an attractive new design methodology that combines the advantages of both H-infinity design and QFT.

Chapter three contains a description of the plant model, specifications for the design and an analysis of the plant.

The application of the theory in Chapter 2 (in the order of presentation) is detailed for the missile problem in Chapters 4-6. To conclude the dissertation Section 7 gives a deep discussion and conclusion from the results obtained in the application section.

2. Theory

This section contains the relevant theory for design of linear time-invariant controllers. The philosophy of Quantitative Feedback Theory (QFT) is expounded in Section 2.1. Section 2.2 describes modern control design methods such as H-infinity control and other state-feedback approaches. In the last theory section (2.3), QFT and H-infinity are united to exploit each design method.

2.1. Quantitative Feedback Theory

2.1.1. Introduction to SISO QFT Design

The task of a control engineer is to design a system such that the client specifications around the plant are met. The plant represents the dynamics of the system to be controlled. For all practical cases, the plant is uncertain but can be quantified. Neglecting the implementation of the controller elements, the control system usually contains sensors, actuators and the plant itself. The symbols used to represent the physical units and the signals in the control system are given in Table 2.1.1. The classical block diagram that shows the interconnection of the physical units and signals stated in Table 2.1.1 is shown in Fig. 2.1.1.1.

Table 2.1.1 Symbols that represent physical units and signals

Physical Units	**Symbol in complex domain**
Plant	$P(s)$
Sensor	$H(s)$
Pre-filter	$F(s)$
Feedback controller	$G(s)$
Signals	
Reference	$r(s)$
Output	$y(s)$
Noise	$n(s)$
Output disturbance	$d_o(s)$
Input disturbance	$d_i(s)$
Input	$u(s)$

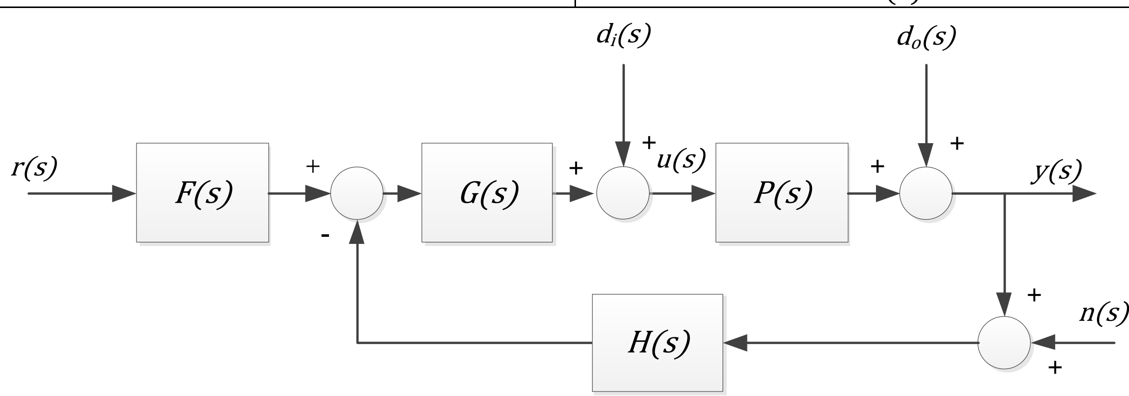

Figure 2.1.1.1 Classical control system block diagram

The three common reasons for using feedback is to,

- Reduce uncertainty,
- Stabilize an open-loop unstable system,
- Reject disturbances, even when there is no plant uncertainty.

The progenitor of QFT, Prof. Isaac Horowitz made an important observation. He realized that fixed, stable systems (no uncertainty) do not require feedback to satisfy specifications. The specifications can be achieved by shaping the pre-filter appropriately. His subsequent thought was what formed the fundamental philosophy of QFT. Horowitz' idea was that the amount of feedback should be directly related to the amount of uncertainty in the system (Horowitz, 2001, pg 887); this idea explains the etymology of the title of the design philosophy.

The following describe the specifications that may be desired by the client:

- Reference tracking – The requirement for the output of the plant to follow (track) the reference signal
- Output/input disturbance rejection – The requirement for the attenuation of disturbances seen at the plant output due to disturbances at the plant output/input
- Robust stability margins – The stability requirement that takes unstructured uncertainties into account (uncertainties that are not a result of parameter uncertainty - structured uncertainty)
- Sensor noise rejection – The requirement for the transfer of sensor noise to the plant input to be below some specified level

One of the attractions of QFT is that all the above stated requirements can be mapped to constraints on the controller during design time, whereas other methods may allow only certain requirements to be mapped and force an iterative approach to solving the whole problem.

To expound the idea of SISO QFT, the reference tracking design problem is developed further. The reference tracking problem is to design a feedback controller $G(s)$, and a pre-filter $F(s)$ such that the closed-loop reference to output magnitude response for all plants within the uncertain set lie between the upper bound, $|A(j\omega)|$ and lower bound, $|B(j\omega)|$. A typical set of upper and lower magnitude bounds are illustrated in Fig. 2.1.1.2. The frequency domain bounds are usually generated from reasonably desired time-domain responses.

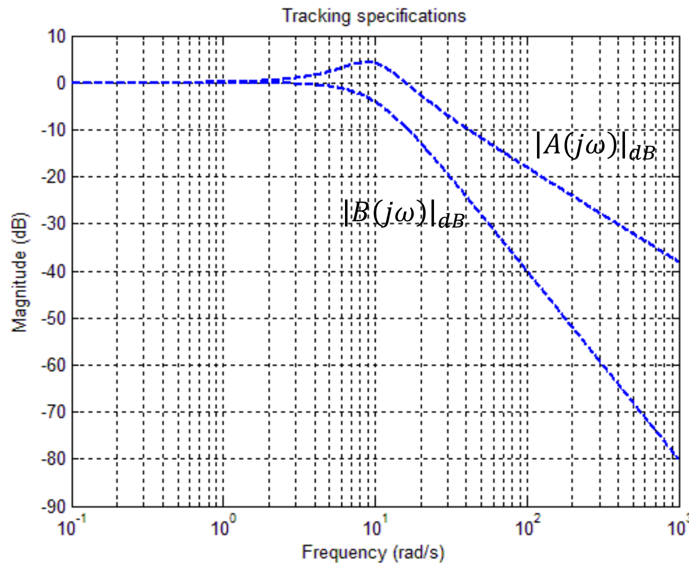

Figure 2.1.1.2 Magnitude response of the tracking specifications

The Numerical Approach

Taking the sensor to be ideal (for simplicity), defining the loop gain $L = PG$ and neglecting the dependence on the complex variable s for simplicity, the reference to output transfer function for the system shown in Fig. 2.1.1.1 is given by

$$T_{y/r} = \frac{L}{1+L}F. \tag{2.1.1.1}$$

The tracking specifications will be met if the maximum change of the logarithm of Eq. (2.1.1.1) is less than the change of the logarithm of the tracking specifications (Yaniv, 1999, pg 75). Assuming loop i results in the maximum and loop j results in the minimum, the following must be satisfied

$$max\Delta log|T_{y/r}| = log\left|\frac{L_i}{1+L_i}F\right| - log\left|\frac{L_j}{1+L_j}F\right| \leq log|A(j\omega)| - log|B(j\omega)| \tag{2.1.1.2}$$

The pre-filter is fixed hence it gets cancelled in Eq. (2.1.1.2) when extracted from the logarithm. By simplifying Eq. (2.1.1.2) one obtains

$$\left|\frac{P_i}{P_j}\frac{1+GP_j}{1+GP_i}\right| \leq \frac{|A(j\omega)|}{|B(j\omega)|}. \tag{2.1.1.3}$$

Equation (2.1.1.3) is a linear fractional mapping on the controller G and after further manipulation one finally obtains a quadratic function which must be solved to obtain $|G|$ for some controller phase angle. This is the approach one would take to design a controller using a computing machine. The quadratic function must be solved for each ordered pair of plants in the plant set and the intersection of the constraints are the final gain to be satisfied. This must be done for a set of design frequencies and phase angles. The result of this computation is controller gain requirements for the set of phase angles chosen. The design task is to shape the controller such that it satisfies the constraints. Generally, a nominal loop $(L_0 = P_0G)$ is chosen which is shaped by the designer; this is more relevant to the graphical approach to the QFT design. A tacit constraint is that $(1+PG)$ does not have any right-hand plane (RHP) zero for all plants.

The Graphical Approach

QFT is well known for the use of templates in the graphical design procedure. A QFT template encapsulates the phase and gain of an uncertain plant at a particular frequency i.e. it is a physical representation of the uncertainty. Assuming the uncertain plant is given by a set of discrete functions, the template can be generated by determining the plant value for each plant in the set. Generally the discrete set of plant values is plotted on a graph that displays phase versus magnitude. Templates are generated for a finite set of frequencies ("working frequencies"). These frequencies are chosen such that the resulting templates appear significantly different from each other.

The graphical approach is an elegant way of designing because once the uncertainty is captured in the templates, the designer requires only a single loop to work with: the nominal loop. The nominal loop is the loop obtained when the controller is multiplied by one of the plants from the uncertain set; the plant chosen is referred to as the nominal plant. The point on the template that is an evaluation of the nominal plant is called the handle. The handle is an important concept that unites the nominal loop and the template.

In order to solve the reference tracking problem a graphical interpretation of Eq. (2.1.1.2) is required. The Nichols chart must be used to design for reference tracking since it contains the loci of the complementary sensitivity. The nominal loop gain that satisfies the reference tracking constraint is gain that occurs at the handle of the template when the maximum change of the complementary sensitivity loci intersecting the template is less than or equal to the specifications for some nominal loop phase angle. One can imagine the tedious physical requirement in order to obtain a smooth boundary.

An additional constraint may be a $3dB$ robust stability margin for unstructured uncertainties. This means that the system must have a worst-case gain margin of $10.69dB$ and phase margin of $41.46°$ (Sidi, 2001, pg 52). The design uses the Inverse Nichols chart as the domain which is a graph similar to the Nichols chart except that the loci are of the sensitivity function. The gain cross-over frequency ω_{gc} is the frequency where the nominal loop has a gain of $0dB$. It is an important frequency because it gives the designer knowledge about the bandwidth of the loop. The robust stability bounds are calculated at frequencies "near" the gain cross-over frequency. In order to obtain the nominal loop robust stability bound the designer must shift the template around the $3dB$ locus in the Inverse Nichols chart such that the template makes contact with the $3dB$ locus (Eitelberg, 2006, pg 94). While performing this operation, the nominal bound is obtained by delineating the points over which the handle falls.

When the bound generation is complete, an intersection of the bounds must be done. The nominal loop must then be shaped to satisfy the graphical constraints. The resulting controller provides the required feedback to reduce the closed-loop uncertainty to levels that allow the final pre-filter shaping to meet the absolute tracking specifications.

The final step is to design the pre-filter. As stated earlier, the feedback controller is responsible for reducing the closed-loop uncertainty and the pre-filter shapes the final reference to output response. As bounds were found for the loop gain that allowed $G(s)$ to be derived, bounds on the pre-filter $F(s)$ can also be found. Manually, this can be achieved by placing the template on the nominal open-loop gain L_0, with the handle of the template coinciding with the nominal loop transfer functions at the respective template frequency. The pre-filter upper bound at some frequency ω_i is given by $|A(j\omega_i)|_{dB} - \left|T_{max}^{template}(j\omega_i)\right|_{dB}$, where $\left|T_{max}^{template}(j\omega_i)\right|$ is the maximum value of the intersection of the complementary sensitivity loci with the plant template at ω_i. Similarly, the lower bound is given by $|B(j\omega_i)|_{dB} - \left|T_{min}^{template}(j\omega_i)\right|_{dB}$. The pre-filter $F(s)$ is designed to be minimum phase and to lie within these bounds.

Controller Preferences

An attractive feature unique to QFT is the transparency in design. At every stage of the design the designer can clearly "see" the effect of making changes to the system. The controller is actively constructed by the designer using the QFT philosophy as a guide. This allows the designer to make trade-offs while designing between meeting boundary constraints and enforcing preferences on the controller. The three important preferences in controller design are

- Minimum controller gain,
- Minimum controller order and,
- Limiting minimum damping factor in controller elements.

Assuming ideal sensor, the sensor noise to plant input transfer function is given by

$$T_{u/n} = \frac{-G}{1+L}. \tag{2.1.1.4}$$

For a strictly proper loops (all real systems), the signal transfer from sensor to plant input goes with the controller gain at high frequency ($\lim_{\omega\to\infty}|L(j\omega)| \to 0$). This means that the noise at the sensor will be amplified via the controller if the gain of the controller is high at high frequency. All signals going to the plant input must pass the controller. Since the power transfer to the plant input is related to the integral of the magnitude of the controller frequency response and the error signal, the controller magnitude must be minimized in order to prevent actuator saturation. Unnecessarily high controller gain can be thought of as excessive actuation which will lead to quicker deterioration of the actuators.

Whether the controller is implemented digitally or using analog components an element of uncertainty is contributed by each element (pole/zero) of the controller. Hence, to reduce the unaccounted uncertainty in the controller implementation the designer must aim for minimum order controllers.

It is also not desired to have very small damping factors in the controller elements. This is because the dynamics is very sensitive to the accuracy of the implementation. Small changes in the damping factor or corner frequency may result in large changes to the loop which in most cases no provision is made during the design.

2.1.2. Introduction to MIMO QFT: Design for Output Disturbance Rejection

The fundamental idea of QFT design: the amount of feedback in the system must be directly related to the amount of uncertainty in the system - this is very clear in SISO systems. If there is no uncertainty in the system and the system is stable, there is no need for feedback to meet reference tracking requirement. For the MIMO plant case, feedback is not only required to stabilize and reduce uncertainty in the closed-loop response, but may also be required to reduce the cross-coupling in the system. MIMO QFT is a diagonal type of control system design approach. For this reason the controller $\boldsymbol{G}$ is assumed to be diagonal except where specified. The subsequent three sections show the design equations required for applying the QFT methodology for cases of output-disturbance rejection, reference tracking and input-disturbance rejection problems. For further reference, the following is a list of some of the fundamental papers that present the MIMO QFT technique: Horowitz, I. (1979), Horowitz, I. and Sidi, M. (1980), Horowitz, I. and Loecher, C. (1981), Horowitz, I. (1982) and Yaniv, O and Horowitz, I. (1986).

Design for Output-Disturbance Rejection

The output-disturbance rejection problem requires the design of the controller $\boldsymbol{G}$ that results in the magnitude of the disturbance to output frequency response for all plant cases to be below the sensitivity specification. Figure 2.1.2.1 shows the general structure of a MIMO feedback control system. Bold symbols are used to indicate transfer function matrices. The symbols and signals in Fig. 2.1.2.1 are synonymous with those that appear in Table 2.1.1 except the former refer to matrices. All of the control blocks are $n \times n$ matrices and the signals are column vectors of dimension n. For all following sections the sensor matrix $\boldsymbol{H}$ is set equal to the identity matrix $\boldsymbol{I}$ to be concise in the derivation, without loss of generality. It is also assumed that the sensors and the filters are constructed with negligible uncertainty and the plant is the only element that introduces significant uncertainty into the system.

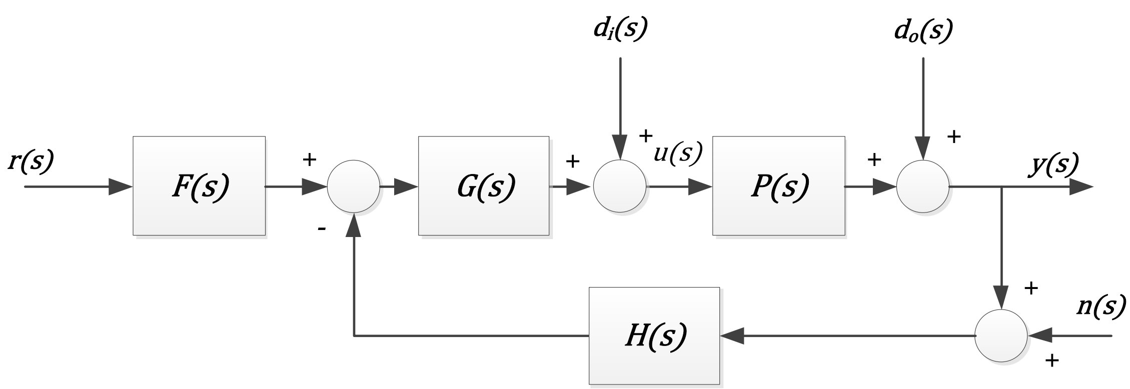

Figure 2.1.2.1 Classical MIMO control system feedback structure

The general specification for output disturbance rejection is of the form shown in Fig.2.1.2.2; the upper bound for the diagonal channels are $|A_{ii}(j\omega)|$ and $|A_{ij}(j\omega)|$ for the off-diagonal channels. Both channels of the system have a wash-out characteristic at low frequency. At high frequency the diagonal channel response goes to $0dB$ and the off-diagonal channel rolls down. These high frequency qualitative descriptions can be succinctly expressed as $\lim_{\omega\to\infty} \boldsymbol{S} = \lim_{\omega\to\infty}(\boldsymbol{I}+\boldsymbol{L})^{-\mathbf{1}} = \boldsymbol{I}$.

Conventionally, $\boldsymbol{T}(s)$ is used to denote the complementary sensitivity, but in the following sections $\boldsymbol{T}(s)$ is used to denote a transfer function matrix specific for different sections. In the exposition below it is used to describe the output-disturbance to output response in the frequency domain.

Rule for determining transfer functions from block diagrams (Skogestad and Postlethwaite, 2005, pp 68-69): To obtain the transfer function that describes the signal transfer from some input signal to output signal, start at the output signal moving against the signal flow. Write each block as they are encountered. When you exit a loop, write $(\boldsymbol{I}+\boldsymbol{L})^{-1}$: for negative feedback. The loop gain $\boldsymbol{L}$ is the product of the matrices in the loop, in the order in which they are encountered when travelling against signal flow from the loop break point.

Applying the above rule, one gets the following for the output disturbance transfer function

$$\boldsymbol{T}(s) = [\boldsymbol{I}+\boldsymbol{P}(s)\boldsymbol{G}(s)]^{-\mathbf{1}}. \qquad (2.1.2.1)$$

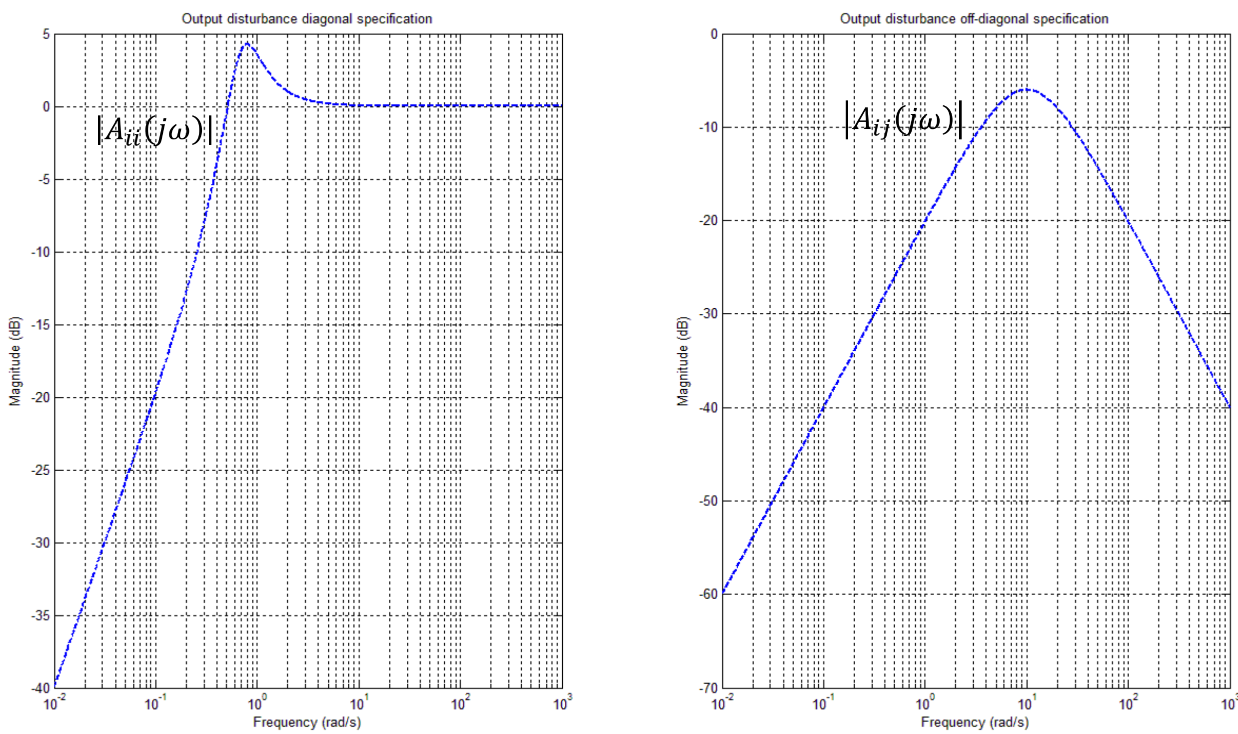

Figure 2.1.2.2 Output disturbance rejection specifications for diagonal channels (left) and off-diagonal channels (right)

Equation (2.1.2.1) can be manipulated so that design equations can be formed i.e. writing each row so that the diagonal elements of $\boldsymbol{G}$ can be designed independently. Since the sensor is diagonal, it can be absorbed into the plant or controller. Hence it does not pose a difficulty in the derivation of the QFT design equations. The dependence on the complex variable s is excluded for notation simplicity. The symbol $\boldsymbol{T}$ is used to denote the signal transmission from output disturbance to plant output (in the complex domain) for this section.

$$\boldsymbol{T} = [\boldsymbol{I} + \boldsymbol{PG}]^{-1}, \tag{2.1.2.2}$$

$$[\boldsymbol{I} + \boldsymbol{PG}]\boldsymbol{T} = \boldsymbol{I}. \tag{2.1.2.3}$$

Both sides of the Eq. (2.1.2.3) are multiplied on the left by the inverse of the plant (represented by $\widehat{\boldsymbol{P}}$) to obtain

$$\left[\widehat{\boldsymbol{P}} + \boldsymbol{G}\right]\boldsymbol{T} = \widehat{\boldsymbol{P}}. \tag{2.1.2.4}$$

A common manipulation in QFT literature known as a diagonal splitting is done next, which splits the matrix $\widehat{\boldsymbol{P}}$ into the sum of two matrices: $\widehat{\boldsymbol{P}}_{\boldsymbol{D}}$ containing the diagonal entries and $\widehat{\boldsymbol{P}}_{\boldsymbol{O}}$ containing the off-diagonal entries (Boje, 2002b). Different types of splitting of the plant may lead to different interpretations.

$$\left[\widehat{\boldsymbol{P}}_{\boldsymbol{D}} + \widehat{\boldsymbol{P}}_{\boldsymbol{O}} + \boldsymbol{G}\right]\boldsymbol{T} = \widehat{\boldsymbol{P}} \tag{2.1.2.5}$$

Extracting the diagonal matrices as a common factor

$$\left(\widehat{\boldsymbol{P}}_{\boldsymbol{D}} + \boldsymbol{G}\right)\left[\boldsymbol{I} + \left(\widehat{\boldsymbol{P}}_{\boldsymbol{D}} + \boldsymbol{G}\right)^{-\boldsymbol{1}}\widehat{\boldsymbol{P}}_{\boldsymbol{O}}\right]\boldsymbol{T} = \widehat{\boldsymbol{P}}. \tag{2.1.2.6}$$

Manipulation proceeds to obtain the design equation which turn out to be implicit in the output disturbance rejection matrix transfer function

$$\left[\boldsymbol{I} + \left(\widehat{\boldsymbol{P}}_{\boldsymbol{D}} + \boldsymbol{G}\right)^{-\boldsymbol{1}}\widehat{\boldsymbol{P}}_{\boldsymbol{O}}\right]\boldsymbol{T} = \left(\widehat{\boldsymbol{P}}_{\boldsymbol{D}} + \boldsymbol{G}\right)^{-\boldsymbol{1}}\widehat{\boldsymbol{P}}, \tag{2.1.2.7}$$

$$\boldsymbol{T} = \left(\widehat{\boldsymbol{P}}_{\boldsymbol{D}} + \boldsymbol{G}\right)^{-\boldsymbol{1}}\widehat{\boldsymbol{P}} - \left(\widehat{\boldsymbol{P}}_{\boldsymbol{D}} + \boldsymbol{G}\right)^{-\boldsymbol{1}}\widehat{\boldsymbol{P}}_{\boldsymbol{O}}\boldsymbol{T}. \tag{2.1.2.8}$$

A conservative design is one in which the system specifications are met with unnecessarily large control effort. Equation (2.1.2.8) gives the first indication of a conservative design because the design equation is implicit in the disturbance to output response which is not known a priori (during design). This will be elucidated in the scalar equivalent equations to follow. The (i, j) element of $\widehat{\boldsymbol{P}} = \boldsymbol{P}^{-\boldsymbol{1}}$ are defined as $1/q_{ij}$ which is common in QFT literature. To obtain the design equations, the matrix transfer function in Eq. (2.1.2.8) is written in its scalar form. The design equations for a $n \times n$ system are

$$t_{ij} = \frac{q_{ii}}{1 + g_i q_{ii}}\left(\frac{1}{q_{ij}} - \sum_{k=1, k\neq i}^{n} \frac{1}{q_{ik}} t_{kj}\right), \qquad i, j = 1, \dots, n. \tag{2.1.2.9}$$

Since the plant for which the application of MIMO QFT is applied to in this thesis is a 2×2 system, the explicit equations for a 2×2 system are stated. Expanding Eq. (2.1.2.9) for $n = 2$, gives the design equations for a 2×2 system as

$$t_{11} = \frac{1}{1 + q_{11}g_1}\left(1 - \frac{q_{11}}{q_{12}} t_{21}\right), \tag{2.1.2.10}$$

$$t_{12} = \frac{q_{11}/q_{12}}{1 + q_{11}g_1}(1 - t_{22}), \tag{2.1.2.11}$$

$$t_{21} = \frac{q_{22}/q_{21}}{1 + q_{22}g_2}(1 - t_{11}), \tag{2.1.2.12}$$

$$t_{22} = \frac{1}{1 + q_{22}g_2}\left(1 - \frac{q_{22}}{q_{21}}t_{12}\right). \tag{2.1.2.13}$$

Equations (2.1.2.10) and (2.1.2.11) are used for loop one design. The remaining two equations are used for loop two design. The above scalar equations show clearly that the design of each loop depends on the unknown disturbance to output transfer functions. For example, if loop one is designed first, it requires the disturbance to output response of t_{21} which is not known at that stage of the design. To overcome this obstacle in the design, it is presumed that the specifications will be met and the term t_{21} is over-bounded by imposing the Schwarz inequality. This is one of the entry points for conservatism in the MIMO QFT design.

Applying the Schwarz inequality and using the specification bounds, the following design equations are obtained with $l_i = q_{ii}g_i$ for $i = 1,2$

$$t_{11} \le \left|\frac{1}{1 + l_1}\right|\left(1 + \left|\frac{q_{11}}{q_{12}}\right||A_{21}|\right) \le |A_{11}|, \tag{2.1.2.14}$$

$$t_{12} \le \left|\frac{q_{11}/q_{12}}{1 + l_1}\right|(1 + |A_{22}|) \le |A_{12}|, \tag{2.1.2.15}$$

$$t_{21} \le \left|\frac{q_{22}/q_{21}}{1 + l_2}\right|(1 + |A_{11}|) \le |A_{21}|, \tag{2.1.2.16}$$

$$t_{22} \le \left|\frac{1}{1 + l_2}\right|\left(1 + \left|\frac{q_{22}}{q_{21}}\right||A_{12}|\right) \le |A_{22}|. \tag{2.1.2.17}$$

Boundaries are found by determining the nominal loop gain that ensures the respective constraint is satisfied for all plants in the set.

An improvement of the MIMO QFT design technique (Horowitz, 1982) can be obtained by substituting the known information after completion of a loop design. If loop one is designed first in the 2×2 system, t_{11} and t_{12} can be substituted into t_{21} and t_{22} so that the design of the last loop is exact (no overdesign for the last design step).

Defining $\gamma^2 = \frac{q_{11}q_{22}}{q_{12}q_{21}}$, and assuming loop one is designed first, the exact design equations (2×2 system) for loop two are

$$t_{21} = \frac{(q_{22}/q_{21})l_1}{(1 + l_1)(1 + l_2) - \gamma^2}, \tag{2.1.2.18}$$

$$t_{22} = \frac{1 + l_1 - \gamma^2}{(1 + l_1)(1 + l_2) - \gamma^2}. \tag{2.1.2.19}$$

If loop two is designed first, the exact design equations for loop one are

$$t_{11} = \frac{1 + l_2 - \gamma^2}{(1 + l_1)(1 + l_2) - \gamma^2}, \tag{2.1.2.20}$$

$$t_{12} = \frac{(q_{11}/q_{12}) l_2}{(1 + l_1)(1 + l_2) - \gamma^2}. \tag{2.1.2.21}$$

So far the theory describes the required loop gains for each loop in order to achieve the magnitude specification. In Section 2.1.8, the stability of the MIMO system is investigated and further requirements on l_i are imposed to ensure stability of the closed-loop system.

2.1.3. Design for Reference Tracking

The reference tracking problem is a very prevalent one in industry. The reference tracking problem is: given a reference signal $\boldsymbol{r}$, the output of the plant $\boldsymbol{y}$ must track the reference within some bounds in the presence of plant uncertainty. The controller is designed to reduce the closed-loop uncertainty and ensure stability, and a pre-filter is designed to shape the absolute reference to output response. When the diagonal channels are required to have conventional (SISO) tracking specifications and the off-diagonal channel responses are required to be minimized, the system specification is said to be basically non-interacting (BNIA) in the QFT literature. The typical reference to output specification for a diagonal channel is the same as the SISO system specifications. The off-diagonal channels of a BNIA system typically have band-passing characteristics like those that appear in Fig. 2.1.2.2.

In this section, $\boldsymbol{T}$ is used to denote the reference to output response in the complex domain. The rule to obtain the transfer function matrix is applied for reference tracking to the block diagram in Fig. 2.1.2.1 to obtain

$$\boldsymbol{T} = \boldsymbol{PG}[\boldsymbol{I} + \boldsymbol{HPG}]^{-1}\boldsymbol{F}. \tag{2.1.3.1}$$

Assuming the sensor is ideal ($\boldsymbol{H} \to \boldsymbol{I}$ in the frequency range of interest), and applying the push-through rule (Skogestad and Postlethwaite, 2005, pg 68) twice, Eq. (2.1.3.1) can be simplified to

$$\boldsymbol{T} = [\boldsymbol{I} + \boldsymbol{PG}]^{-1}\boldsymbol{PGF}. \tag{2.1.3.2}$$

The tracking specification can be written mathematically as

$$|\boldsymbol{B}(j\omega)|_{ij} \leq |\boldsymbol{T}(j\omega)|_{ij} \leq |\boldsymbol{A}(j\omega)|_{ij}. \tag{2.1.3.3}$$

The matrices $\boldsymbol{A}$ and $\boldsymbol{B}$ contain the upper and lower bounds for each channel. Obviously for non-interacting channels the lower bound will be zero. An upper bound must be specified because only partial decoupling can occur for uncertain systems.

Performing a similar matrix manipulation as done in Section 2.1.2, the following equation for the reference tracking response is obtained

$$\boldsymbol{T} = \left(\widehat{\boldsymbol{P}}_{\boldsymbol{D}} + \boldsymbol{G}\right)^{-1}\boldsymbol{GF} - \left(\widehat{\boldsymbol{P}}_{\boldsymbol{D}} + \boldsymbol{G}\right)^{-1}\widehat{\boldsymbol{P}}_{\boldsymbol{O}}\boldsymbol{T}. \tag{2.1.3.4}$$

As a reminder, the elements of $\widehat{\boldsymbol{P}} = \boldsymbol{P}^{-1}$ are $1/q_{ij}$. To obtain the design equations, the matrix transfer function in Eq. (2.1.3.4) is written in its scalar form. For an $n \times n$ system, the design equations are,

$$t_{ij} = \frac{1}{1 + g_i q_{ii}}\left(g_i q_{ii} f_{ij} - q_{ii} \sum_{k=1, k\neq i}^{n} \frac{1}{q_{ik}} t_{kj}\right), \qquad i, j = 1, \dots, n. \tag{2.1.3.5}$$

Evaluating Eq. (2.1.3.5) for $n = 2$, gives the design equations for a 2×2 system as

$$t_{11} = \frac{1}{1 + l_1}\left(l_1 f_{11} - \frac{q_{11}}{q_{12}} t_{21}\right), \tag{2.1.3.6}$$

$$t_{12} = \frac{1}{1 + l_1}\left(l_1 f_{12} - \frac{q_{11}}{q_{12}} t_{22}\right), \tag{2.1.3.7}$$

$$t_{21} = \frac{1}{1+l_2}\left(l_2 f_{21} - \frac{q_{22}}{q_{21}} t_{11}\right), \tag{2.1.3.8}$$

$$t_{22} = \frac{1}{1+l_2}\left(l_2 f_{22} - \frac{q_{22}}{q_{21}} t_{12}\right). \tag{2.1.3.9}$$

Equations (2.1.3.6)–(2.1.3.9) can be thought of as equivalent SISO systems decomposed from the original MIMO system. The first term in the equations is similar to the reference tracking design equation for SISO system [Eq. (2.1.1.1)]. The second term can be thought of as an equivalent "disturbance" to the system. The cross-coupling in the system manifests itself as an equivalent disturbance in the equivalent SISO systems.

After applying the Schwarz inequality to equations above, it should be observed that by making the upper bound of the off-diagonal channel $|A_{ij}|$ smaller results in a lower loop gain requirement in the jth loop but this has an effect of increasing the required loop gain in the ith loop.

For further manipulations to come, the equivalent disturbance is defined as

$$\alpha_{ij} = \left| q_{ii} \sum_{k=1,k\neq i}^{n} \frac{1}{q_{ik}} \right| |t_{kj}| = \left| q_{ii} \sum_{k=1,k\neq i}^{n} \frac{1}{q_{ik}} \right| |A_{kj}|. \tag{2.1.3.10}$$

The traditional MIMO QFT design of l_i requires allocating a reserve for the variation of the cross-coupling term for the independent design of l_i and f_{ij}. This involves splitting the specifications as illustrated below.

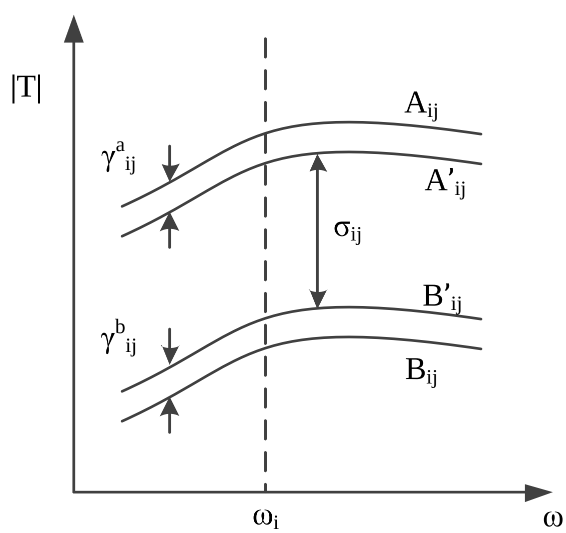

Figure 2.1.3.1 Illustration of splitting of the tracking specifications for design purpose

The above and below cross-coupling allocations are denoted by γ_{ij}^a and γ_{ij}^b, respectively. In the original QFT synthesis process each of the stated allocations where made equal to each other i.e. $\gamma_{ij}^a = \gamma_{ij}^b = \gamma_{ij}$ and γ_{ij} was chosen arbitrarily, this gives rise to a conservative design. The conservativeness can be reduced by numerical iteration until the "actual" magnitude variation of the cross-coupling term is equal to half the variation of the diagonal term (Houpis, 2006, pg 181). This will result in the optimal choice for the allocation reserve when $\gamma_{ij}^{a} = \gamma_{ij}^{b} = \gamma_{ij}$.

An automatic procedure for the generation of tracking bounds is provided in (Boje, 2004). Using this method there is no explicit allocation in the upper and lower cross-coupling reserves and they are in general not equal. The result of the paper is that after some manipulation of the fundamental tracking bound equation, a quartic inequality in terms of the controller gain and phase, and ordered-pair of plants is found. The solution of the quartic inequality gives rise to feasible regions for the controller. Unlike the traditional QFT design, the direction towards reducing the number of significant parameter-space points is unclear. Hence the one problem with this method is that a copious number of calculations are required in order to obtain the bounds.

The tracking specification can be writing as

$$\left|\left|\frac{f_{ij} l_i^{[y]}}{1 + l_i^{[y]}}\right| - \left|\frac{1}{1 + l_i^{[y]}}\right| \alpha_{ij}^{[y]}\right| \leq |t_{ij}| \leq \left|\frac{f_{ij} l_i^{[x]}}{1 + l_i^{[x]}}\right| + \left|\frac{1}{1 + l_i^{[x]}}\right| \alpha_{ij}^{[x]}. \qquad (2.1.3.11)$$

The superscript x refers to elements derived from a plant that maximizes the right side of Eq. (2.1.3.11) and the superscript y refers to the elements derived from a plant that minimized the left side of Eq. (2.1.3.11). The mathematical manipulation performed attempts to eliminate f_{ij} to allow independent design of l_i. Equation (2.1.3.12) is quartic in the controller gain g_i and is the design equation used for loop i.

$$\frac{\left|l_i^{[x]}\right|}{\left|l_i^{[y]}\right|} \leq \frac{A_{ij}\left|1 + l_i^{[x]}\right| - \alpha_{ij}^{[x]}}{B_{ij}\left|1 + l_i^{[y]}\right| - \alpha_{ij}^{[y]}} \qquad (2.1.3.12)$$

The solution for controller gain from Eq. (2.1.3.12) needs to be calculated for each frequency and phase angle, and for all ordered-pairs of plants in the set. The intersection of the individual solutions gives the global QFT bounds for the controller gain. By multiplying the solution with the nominal equivalent plant q_{ii0}, one gets the nominal loop boundary.

The automatic procedure above is less conservative than the original MIMO QFT procedure.

Design Equations for Final Loop

Multiplying both sides of Eq. (2.1.3.2) by $\boldsymbol{P}^{-1}[\boldsymbol{I} + \boldsymbol{PG}]^{-1}$ from the left result in

$$[\boldsymbol{P}^{-1} + \boldsymbol{G}]\boldsymbol{T} = \boldsymbol{GF}. \qquad (2.1.3.13)$$

Although not the optimal choice, $\boldsymbol{F}$ is chosen to be diagonal to simplify the design. Writing Eq. (2.1.3.13) in terms of its scalar elements for a 2×2 system

$$\begin{bmatrix} 1/q_{11} + g_1 & 1/q_{12} \\ 1/q_{21} & 1/q_{22} + g_2 \end{bmatrix}\begin{bmatrix} t_{11} & t_{12} \\ t_{21} & t_{22} \end{bmatrix} = \begin{bmatrix} g_1 & 0 \\ 0 & g_2 \end{bmatrix}\begin{bmatrix} f_{11} & 0 \\ 0 & f_{22} \end{bmatrix}. \qquad (2.1.3.14)$$

If row one is designed first, row two can be designed exactly. To get the exact design equations for loop two, both sides of Eq. (2.1.3.14) must be multiplied by $\begin{bmatrix} 1 & 0 \\ -\frac{1/q_{21}}{1/q_{11}+g_1} & 1 \end{bmatrix}$ from the left to make the element $\left[\boldsymbol{P^{-1}} + \boldsymbol{G}\right]_{21} = 0$. This matrix multiplication is equivalent to the row operation

$$R_2 \leftarrow R_2 - \frac{1/q_{21}}{1/q_{11} + g_1} R_1.$$

By performing the above step the following is obtained

$$\begin{aligned} &\begin{bmatrix} 1/q_{11} + g_1 & 1/q_{12} \\ 0 & \dfrac{1}{q_{22}} - \dfrac{1}{1/q_{11} + g_1} \cdot \dfrac{1}{q_{21}} \dfrac{1}{q_{12}} + g_2 \end{bmatrix} \begin{bmatrix} t_{11} & t_{12} \\ t_{21} & t_{22} \end{bmatrix} \\ &= \begin{bmatrix} g_1 & 0 \\ -\dfrac{1}{1/q_{11} + g_1} \cdot \dfrac{1}{q_{21}} g_1 & g_2 \end{bmatrix} \begin{bmatrix} f_{11} & 0 \\ 0 & f_{22} \end{bmatrix}. \end{aligned} \tag{2.1.3.15}$$

By defining

$$q'_{21} = (1/q_{11} + g_1) q_{21}, \tag{2.1.3.16}$$

$$q'_{22} = 1 \Big/ \left(\frac{1}{q_{22}} - \frac{1}{1/q_{11} + g_1} \cdot \frac{1}{q_{21}} \frac{1}{q_{12}} \right), \tag{2.1.3.17}$$

the second row exact design equations can be written as

$$\begin{aligned} t_{21} &= \frac{-\dfrac{1}{1/q_{11} + g_1} \cdot \dfrac{1}{q_{21}} g_1 f_{11}}{\left(\dfrac{1}{q_{22}} - \dfrac{1}{1/q_{11} + g_1} \cdot \dfrac{1}{q_{21}} \dfrac{1}{q_{12}} \right) + g_2} = \frac{-\dfrac{1}{1/q_{11} + g_1} \cdot \dfrac{1}{q_{21}} q'_{22} g_1 f_{11}}{1 + q'_{22} g_2} = \\ &= \frac{-(q'_{22}/q'_{21}) g_1 f_{11}}{1 + q'_{22} g_2}. \end{aligned} \tag{2.1.3.18}$$

$$t_{22} = \frac{g_2 f_{22}}{\left(\dfrac{1}{q_{22}} - \dfrac{1}{1/q_{11} + g_1} \cdot \dfrac{1}{q_{21}} \dfrac{1}{q_{12}} \right) + g_2} = \frac{g_2 f_{22}}{\dfrac{1}{q'_{22}} + g_2} = \frac{q'_{22} g_2 f_{22}}{1 + q'_{22} g_2} \tag{2.1.3.19}$$

Eq. (2.1.3.17) is the transfer function of the equivalent plant from input 2 to output 2 with loop one closed.

If the second row is design first, a similar procedure is performed except the element $\left[\boldsymbol{P^{-1}} + \boldsymbol{G}\right]_{21}$ is made zero by multiplying both sides of Eq. (2.1.3.14) by $\begin{bmatrix} 1 & -\frac{1/q_{12}}{1/q_{22}+g_2} \\ 0 & 1 \end{bmatrix}$ from the left. This is equivalent to row operation

$$R_1 \leftarrow R_1 - \frac{1/q_{12}}{1/q_{22} + g_2} R_2.$$

By defining

$$q'_{12} = (1/q_{22} + g_2)q_{12}, \tag{2.1.3.20}$$

$$q'_{11} = 1/\left(\frac{1}{q_{11}} - \frac{1}{1/q_{22} + g_2} \cdot \frac{1}{q_{21}}\frac{1}{q_{12}}\right), \tag{2.1.3.21}$$

the first row exact design equations can be written as

$$t_{11} = \frac{g_1 f_{11}}{\left(\frac{1}{q_{11}} - \frac{1}{1/q_{22} + g_2}\frac{1}{q_{12}}\frac{1}{q_{21}}\right) + g_1} = \frac{q'_{11} g_1 f_{11}}{1 + q'_{11} g_1} \tag{2.1.3.22}$$

$$t_{12} = -\frac{\frac{1}{1/q_{22} + g_2}\frac{1}{q_{12}} g_2 f_{22}}{\left(\frac{1}{q_{11}} - \frac{1}{1/q_{22} + g_2}\frac{1}{q_{12}}\frac{1}{q_{21}}\right) + g_1} = -\frac{\frac{1}{1/q_{22} + g_2}\frac{1}{q_{12}} q'_{11} g_2 f_{22}}{1 + q'_{11} g_1} \tag{2.1.3.23}$$

$$= -\frac{(q'_{11}/q'_{12}) g_2 f_{22}}{1 + q'_{11} g_1}$$

The explicit equations for the output response are given by Eqs (2.1.3.24)-(2.1.3.27). These equations are very useful for checking the final system performance when the equivalent plants are available. They are obtained by simply solving Eqs (2.1.3.6)-(2.1.3.9) explicitly. As defined earlier, $\gamma^2 = \frac{q_{11}q_{22}}{q_{12}q_{21}}$.

$$t_{11} = \frac{f_{11} l_1 (1 + l_2) - \frac{q_{11}}{q_{12}} f_{21} l_2}{(1 + l_1)(1 + l_2) - \gamma^2}, \tag{2.1.3.24}$$

$$t_{12} = \frac{f_{12} l_1 (1 + l_2) - \frac{q_{11}}{q_{12}} f_{22} l_2}{(1 + l_1)(1 + l_2) - \gamma^2}, \tag{2.1.3.25}$$

$$t_{21} = \frac{f_{21} l_2 (1 + l_1) - \frac{q_{22}}{q_{21}} f_{11} l_1}{(1 + l_1)(1 + l_2) - \gamma^2}, \tag{2.1.3.26}$$

$$t_{22} = \frac{f_{22} l_2 (1 + l_1) - \frac{q_{22}}{q_{21}} f_{12} l_1}{(1 + l_1)(1 + l_2) - \gamma^2}. \tag{2.1.3.27}$$

2.1.4. Design for Input Disturbance Rejection

Applying the rule to obtain the transfer function matrix for input disturbance to plant output, one gets

$$\boldsymbol{T} = \boldsymbol{P}[\boldsymbol{I} + \boldsymbol{GHP}]^{-1}. \tag{2.1.4.1}$$

Assuming an ideal sensor and applying the push-through rule once Eq. (2.1.4.1) becomes

$$\boldsymbol{T} = [\boldsymbol{I} + \boldsymbol{PG}]^{-1}\boldsymbol{P}. \tag{2.1.4.2}$$

After performing the usual QFT manipulations such as diagonal splitting the transfer function design matrix that is obtained is

$$\boldsymbol{T} = \left(\widehat{\boldsymbol{P}}_{\boldsymbol{D}} + \boldsymbol{G}\right)^{-1} - \left(\widehat{\boldsymbol{P}}_{\boldsymbol{D}} + \boldsymbol{G}\right)^{-1}\widehat{\boldsymbol{P}}_{\boldsymbol{O}}\boldsymbol{T}. \tag{2.1.4.3}$$

To obtain design equations, the matrix transfer function in Eq. (2.1.4.3) is written in its scalar form. For an $n \times n$ system, the design equations are given by

$$t_{ij} = \frac{q_{ii}}{1 + g_i q_{ii}}\left(1 - \sum_{k=1,k\neq i}^{n} \frac{1}{q_{ik}} t_{kj}\right), \qquad i,j = 1, \dots, n. \tag{2.1.4.4}$$

Expanding Eq. (2.1.4.4) for $n = 2$, gives the design equations for a 2×2 system as

$$t_{11} = \frac{q_{11}}{1 + q_{11}g_1}\left(1 - \frac{t_{21}}{q_{12}}\right), \tag{2.1.4.5}$$

$$t_{12} = \frac{q_{11}}{1 + q_{11}g_1}\left(1 - \frac{t_{22}}{q_{12}}\right), \tag{2.1.4.6}$$

$$t_{21} = \frac{q_{22}}{1 + q_{22}g_2}\left(1 - \frac{t_{11}}{q_{21}}\right), \tag{2.1.4.7}$$

$$t_{22} = \frac{q_{22}}{1 + q_{22}g_2}\left(1 - \frac{t_{12}}{q_{21}}\right). \tag{2.1.4.8}$$

The Schwarz inequality is then applied to Eqs (2.1.4.5)-(2.1.4.8) as was performed in the other design problems.

2.1.5. Non-diagonal Controller Design

A non-diagonal controller is a controller that does not contain diagonal entries only. As stated in earlier sections the traditional MIMO QFT design assumes diagonal controllers. It is intuitive that non-diagonal controllers may result in less conservative designs as there are more degrees of freedom. The increase in number of degrees of freedom in the controller generally complicates the design. An uncomplicated way to form a non-diagonal controller is to multiply a plant pre-compensator with a QFT diagonal controller, this is the approach suggested by Horowitz (Horowitz, 2001, pg 905).

There are two classes of pre-compensators. The first is the static pre-compensator. A static pre-compensator is one that does not depend on frequency. It is usually chosen to be the inverse of the plant at the cross-over frequency to provide decoupling at that frequency (generally $|\boldsymbol{L}|$ is large at low frequency and low at high frequency). Since the matrix will be complex, a real approximation must be obtained. This may be done using the ALIGN algorithm developed by Kouvaritakis (Maciejowski, 1988, pg 145). An example of an implementation of this idea for controller design for a turbo fan engine can be found in (Boje and Nwokah, 2001).

The second class of pre-compensators are the dynamic pre-compensators. The dynamic pre-compensators depend on frequency. For a fixed, stable and minimum phase plant, it is understood that pre-compensating the plant with the inverse results in complete decoupling (neglecting implementation consequences). This is true because after pre-compensation the equivalent plant is the identity matrix. For plants that are uncertain, and may be unstable and non-minimum phase, this approach to decoupling loses meaning. The method provided by Boje (2002b) is a quantitative approach for designing a pre-compensator for the uncertain plant to reduce the cross-coupling in the system. It will be shown that reduction in cross-coupling results in a less conservative QFT design. Figure (2.1.5.1) shows a control system for disturbance rejection with a diagonal controller $\boldsymbol{G}$ and a pre-compensator $\boldsymbol{K}$. This section is based on quantitative design of non-diagonal controllers by Boje (2002b).

An alternative non-diagonal controller design approach is given in Garcia-Sanz, M., Eguinoa, I. and Bennani, S. (2009). This approach also attempts to diagonalize the plant via pre-compensation. The design of the pre-compensator is not quantitative as in the method used in Boje (2002b).

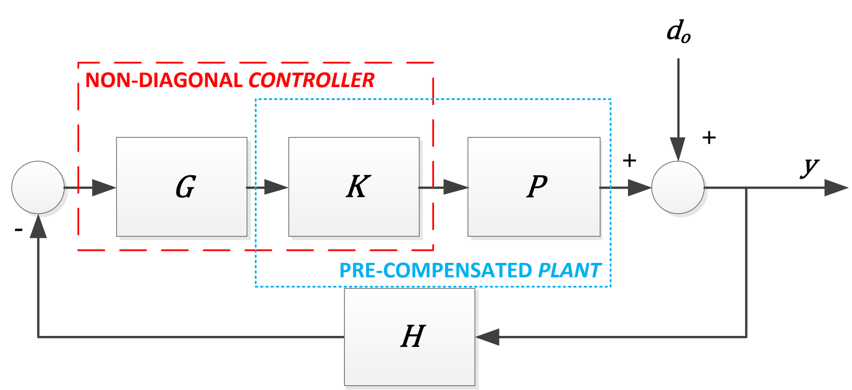

Figure 2.1.5.1 Control system structure for output disturbance rejection showing non-diagonal controller

The process of designing a non-diagonal controller has two main steps. The first step is to design the pre-compensator which attempts to reduce the worst case interaction in the system, and the second step is to perform the usual MIMO QFT design of $\boldsymbol{G}$. Another motivation for reducing the cross-coupling in the system is that the MIMO closed-loop system stability can be inferred directly from the individual loop stability if the worst case cross-coupling is reduced sufficiently.

A measure for the cross-coupling in the system is given by the Perron root of the interaction matrix. The interaction matrix is defined as

$$\boldsymbol{X} = \left(\widehat{\boldsymbol{P}}_{\boldsymbol{D}} + \boldsymbol{G}\right)^{-\mathbf{1}} \widehat{\boldsymbol{P}}_{\boldsymbol{O}}. \tag{2.1.5.1}$$

The interaction matrix appears in the QFT transfer function matrix design Eqs (2.1.2.8), (2.1.3.4), (2.1.4.3).

The Perron root of a matrix is the maximum eigenvalue of the element-wise absolute value of the matrix. The interaction index is given by the Perron root of the interaction matrix in Eq. (2.1.5.1). The closed-loop interaction index is denoted by γ_c and the open-loop interaction index is denoted by γ_o. After simplification, the interaction for a 2×2 system becomes

$$\gamma_c(\boldsymbol{X}) = \max_{P \in \{P\}} \left\{ \sqrt{abs\left[\frac{q'_{11}q'_{22}}{q'_{12}q'_{21}} \frac{1}{(1+l'_1)(1+l'_2)}\right]} \right\}. \tag{2.1.5.2}$$

The primed elements in Eq. (2.1.5.2) indicate that they have been derived from the modified plant $\boldsymbol{P}' = \boldsymbol{PK}$. The equation for the interaction index shows that the cross-coupling in the system can be reduced by either reducing the ratios q'_{11}/q'_{12} and/or q'_{22}/q'_{21} (by appropriate design of $\boldsymbol{K}$**)** or by having low individual loop sensitivity. During the pre-compensator design stage it is useful to know the open-loop interaction index; this is obtained by simply substituting $l_1 = l_2 = 0$ into Eq. (2.1.5.2) to get

$$\gamma_o(\boldsymbol{X}) = \max_{P \in \{P\}} \left\{ \sqrt{abs\left(\frac{q'_{11}q'_{22}}{q'_{12}q'_{21}}\right)} \right\} \tag{2.1.5.3}$$

It is shown in (Limebeer, 1982) that if the interaction index is made less than unity for all frequencies, stability of the MIMO system will be guaranteed by the stability of the individual loops (sufficient but not necessary condition). If this stability criterion is to be used, it would of course be of huge benefit to reduce the interaction index by some other means rather than by high individual loop gains. Having high loop gain may not even be possible to achieve in certain design cases (due to delay or non-minimum phase). The design of $\boldsymbol{K}$ is performed to target the reduction of the ratios q'_{11}/q'_{12} and q'_{22}/q'_{21} at frequencies near and above the gain cross-over frequencies to ease the demand of individual loop gains. It can be deduced from the assessment of QFT design equations, for all type of problems (output disturbance rejection, reference tracking,…), that the reduction in the above stated ratios also reduces the conservativeness of the design (because the magnitude of the equivalent disturbance term is reduced).

The first step of the design of a pre-compensator is to create a pre-compensator structure. The structure chosen by Boje (2002b) for a 2×2 system consists of the product of two unimodular matrices $\boldsymbol{K_1}$ and $\boldsymbol{K_2}$ such that the pre-compensated plant inverse is given by

$$\widehat{\boldsymbol{P}}' = (\boldsymbol{PK})^{-1} = (\boldsymbol{PK}_1\boldsymbol{K}_2)^{-1} = \widehat{\boldsymbol{K}}_2\widehat{\boldsymbol{K}}_1\widehat{\boldsymbol{P}}. \tag{2.1.5.4}$$

As will be seen in the next equation, the purpose of each matrix $\boldsymbol{K_i}$ is to modify the ith row of the equivalent plant. The expansion of Eq. (2.1.5.4) gives the following in terms of the scalar elements

$$\widehat{\boldsymbol{P}}' = \widehat{\boldsymbol{K}}_2\widehat{\boldsymbol{K}}_1\widehat{\boldsymbol{P}} = \begin{bmatrix} 1 & 0 \\ \hat{k}_{21} & 1 \end{bmatrix}\begin{bmatrix} 1 & \hat{k}_{12} \\ 0 & 1 \end{bmatrix}\begin{bmatrix} 1/q_{11} & 1/q_{12} \\ 1/q_{21} & 1/q_{22} \end{bmatrix} \tag{2.1.5.5}$$

$$= \begin{bmatrix} 1/\dfrac{q_{11}}{1+\hat{k}_{12}\dfrac{q_{11}}{q_{21}}} & 1/\dfrac{q_{12}}{1+\hat{k}_{12}\dfrac{q_{12}}{q_{22}}} \\ 1/1+\hat{k}_{21}\dfrac{q_{21}}{q'_{11}} & 1/\dfrac{q_{21}}{1+\hat{k}_{21}\dfrac{q_{21}}{q'_{11}}} \end{bmatrix} \triangleq \begin{bmatrix} 1/\mathrm{q}'_{11} & 1/\mathrm{q}'_{12} \\ 1/\mathrm{q}'_{21} & 1/\mathrm{q}'_{22} \end{bmatrix}.$$

Using Eq. (2.1.5.5) the ratios q'_{11}/q'_{12} and q'_{22}/q'_{21} are calculated as

$$\frac{q'_{11}}{q'_{12}} = \frac{q_{11}}{q_{12}}\frac{1+\hat{k}_{12}\,q_{12}/q_{22}}{1+\hat{k}_{12}\,q_{11}/q_{21}} = \frac{q_{11}}{q_{12}}\beta_1, \tag{2.1.5.6}$$

$$\frac{q'_{22}}{q'_{21}} = \frac{q_{22}}{q_{21}}\frac{1+\hat{k}_{21}\,q_{21}/q'_{11}}{1+\hat{k}_{21}\,q_{22}/q'_{12}} = \frac{q_{22}}{q_{21}}\beta_2. \tag{2.1.5.7}$$

Equations (2.1.5.6) and (2.1.5.7) show that the interaction index for a fixed plant can be made equal to zero by choosing $\hat{k}_{\mathrm{ij}} = -\,q_{\mathrm{jj}}/q_{\mathrm{ij}}$. This is equivalent to pre-compensating the plant with its inverse. The problem is more difficult when the $q's$ are uncertain. The factor $\hat{k}_{\mathrm{ij}}$ needs to be chosen so that β_{i} is less than unity or some chosen upper limit for all plant cases (NB. that when $\hat{k}_{\mathrm{ij}} = 0 \;\; \forall\, i,j;\; i \neq j$ there is no change in the interaction index). The design of $\hat{k}_{\mathrm{ij}}$ is done based on the open-loop interaction index. At low frequency, the closed-loop sensitivity usually requires high loop gain. Hence it dominates the interaction index at low frequency. This results in a low interaction index at low frequencies. To minimize the gain cross-over frequencies of each loop, $\boldsymbol{K}$ needs to be designed to reduce the interaction index at frequencies near and greater than each loop gain cross-over frequency. The frequency points chosen are within the set that gives an interaction index greater than unity. For each of the frequency points chosen in the set, the linear fractional mapping given by Eq. (2.1.5.8) is plotted.

$$\left|\frac{1+\hat{k}_{\mathrm{ij}}\,q_{\mathrm{ij}}/q_{\mathrm{jj}}}{1+\hat{k}_{\mathrm{ij}}\,q_{\mathrm{ii}}/q_{\mathrm{ji}}}\right| \leq \alpha_i(\omega) \tag{2.1.5.8}$$

The factor $\alpha_i(\omega)$ is chosen by the designer and represents the reduction required. A plot of the linear fractional mapping above gives rise to level curves for different α_i values. The designer's task is to shape $\hat{k}_{\mathrm{ij}}(\omega)$ so that it lies within the level curves that give the required reduction, at the specified frequencies. It is important to keep $|\hat{k}_{\mathrm{ij}}|$ small during the design because it represents the amplification of signals across off-diagonal channels (cross-feed). If $|\hat{k}_{\mathrm{ij}}|$ is kept small, the diagonal gain cross-over frequency does not lose significant meaning from the SISO case. If the pre-compensation of the plant results in the peak interaction index being less than unity for frequencies above the gain cross-over frequencies, it eases the requirement on $\boldsymbol{G}$. The second stage of the non-diagonal controller design is to design the diagonal controller $\boldsymbol{G}$ with the MIMO QFT design process. The diagonal controller is designed to meet closed-loop system requirements such as, ensuring stability of the closed-loop system, reducing sensitivity to output/input disturbance or reference tracking specifications. The use of the pre-compensator eases the design of $\boldsymbol{G}$ for all the cases above.

2.1.6. Design using Tracking Error Specifications

In Section 2.1.3, it was stated that conservatism was introduced in the reference tracking design due to allocating bounds for the cross-coupling terms in the design equations. The design method in (Boje, 2002a) uses tracking error specifications to design for reference tracking. Because the tracking error specification takes into account phase information it may lead to less conservative designs. Additionally, this method circumvents the usually conservative contribution through reserve allocation (for equivalent disturbance terms).

The design begins with a client specified model $\boldsymbol{M}(s)$; this is the desired reference to output behaviour. The model must be a realistic expectation of the system i.e. must correctly represent delays, non-minimum phase etc. The specifications are of disk form around the model $\boldsymbol{M}(s)$. The relative tracking error, $\boldsymbol{E}_{\boldsymbol{k}}^{\boldsymbol{r}}$ represents the error between the model and the output of kth plant. The magnitude of the relative tracking error is required to be less than the disk specification, represented by $\boldsymbol{A}_{ij}(j\omega)$ in Eq. (2.1.6.1) for the jth input to the ith output.

$$\left|(\boldsymbol{I}+\boldsymbol{L}_{\boldsymbol{k}})^{-\boldsymbol{1}}\boldsymbol{L}_{\boldsymbol{k}}\boldsymbol{F}-\boldsymbol{M}\right| \triangleq |\boldsymbol{E}_{\boldsymbol{k}}^{\boldsymbol{r}}(j\omega)|_{ij} \leq \boldsymbol{A}_{ij}(j\omega) \tag{2.1.6.1}$$

The crucial step to obtaining design equations shown in (Boje, 2002a), which was initially identified in a SISO implementation of the same idea in (Eitelberg, 2000), is to take the error between two plants i and k. The relative tracking error between plant i and k are

$$\boldsymbol{E}_{\boldsymbol{i}}^{\boldsymbol{r}}-\boldsymbol{E}_{\boldsymbol{k}}^{\boldsymbol{r}}=(\boldsymbol{I}+\boldsymbol{L}_{\boldsymbol{k}})^{-1}\left(\boldsymbol{L}_{\boldsymbol{k}}\hat{\boldsymbol{L}}_{\boldsymbol{i}}-\boldsymbol{I}\right)(\boldsymbol{M}-\boldsymbol{E}_{\boldsymbol{i}}^{\boldsymbol{r}}) \tag{2.1.6.2}$$

To obtain design equations from Eq. (2.1.6.2), the ith plant is chosen as the nominal plant which is required to have a relative error $|\boldsymbol{E}_{\boldsymbol{i}}^{\boldsymbol{r}}|=|\boldsymbol{E}_{\boldsymbol{0}}^{\boldsymbol{r}}|\approx\boldsymbol{0}$. Simplifying Eq. (2.1.6.2) by substituting the nominal plant and multiplying both sides on the left by $\widehat{\boldsymbol{P}}_{\boldsymbol{k}}(\boldsymbol{I}+\boldsymbol{L}_{\boldsymbol{k}})$ gives

$$\left(\widehat{\boldsymbol{P}}_{\boldsymbol{k}}+\boldsymbol{G}\right)\boldsymbol{E}_{\boldsymbol{k}}^{\boldsymbol{r}}=\left(\widehat{\boldsymbol{P}}_{\boldsymbol{k}}-\widehat{\boldsymbol{P}}_{\boldsymbol{0}}\right)\boldsymbol{M}. \tag{2.1.6.3}$$

Define $\left[\widehat{\boldsymbol{P}}_{\boldsymbol{k}}\boldsymbol{M}\right]_{ij}=1/q_{ij}^{m}$ and let the superscript 0 represent the nominal case. For simplicity, also let the elements $\left(1/q_{ij}^{m}-1/q_{ij}^{0m}\right)=1/q_{ij}^{*}$. For a 2×2 system, Eq. (2.1.6.3) in terms of the elements defined is

$$\begin{bmatrix}\dfrac{1}{q_{11}}+g_1 & \dfrac{1}{q_{12}}\\ \dfrac{1}{q_{21}} & \dfrac{1}{q_{22}}+g_2\end{bmatrix}\begin{bmatrix}e_{11} & e_{12}\\ e_{21} & e_{22}\end{bmatrix}=\begin{bmatrix}1/q_{11}^{*} & 1/q_{12}^{*}\\ 1/q_{21}^{*} & 1/q_{22}^{*}\end{bmatrix} \tag{2.1.6.4}$$

Assuming loop one is designed first, the implicit design equations for loop one are

$$e_{11}=\frac{1}{1+l_1}\left(q_{11}/q_{11}^{m}-q_{11}/q_{11}^{m0}-q_{11}/q_{12}e_{21}\right), \tag{2.1.6.5}$$

$$e_{12}=\frac{1}{1+l_1}\left(q_{11}/q_{12}^{m}-q_{11}/q_{12}^{m0}-q_{11}/q_{12}e_{22}\right). \tag{2.1.6.6}$$

In order to get loop two equations, both sides of Eq. (2.1.6.4) are multiplied by $\begin{bmatrix} 1 & 0 \\ -\frac{1}{\frac{1}{q_{11}}+g_1}\frac{1}{q_{21}} & 1 \end{bmatrix}$ from the left to get

$$\begin{bmatrix} \dfrac{1}{q_{11}}+g_1 & \dfrac{1}{q_{12}} \\ 0 & \dfrac{1}{q_{22}}-\dfrac{1}{\dfrac{1}{q_{11}}+g_1}\dfrac{1}{q_{12}}\dfrac{1}{q_{21}}+g_2 \end{bmatrix}\begin{bmatrix} e_{11} & e_{12} \\ e_{21} & e_{22} \end{bmatrix} = \begin{bmatrix} 1/q_{11}^{*} & 1/q_{12}^{*} \\ \dfrac{1}{q_{21}^{*}}-\dfrac{1}{\dfrac{1}{q_{11}}+g_1}\dfrac{1}{q_{21}}\dfrac{1}{q_{11}^{*}} & \dfrac{1}{q_{22}^{*}}-\dfrac{1}{\dfrac{1}{q_{11}}+g_1}\dfrac{1}{q_{21}}\dfrac{1}{q_{12}^{*}} \end{bmatrix}. \tag{2.1.6.7}$$

Define the new equivalent plant of loop two that takes into account g_{11} by

$$\frac{1}{q_{22}'}=\frac{1}{q_{22}}-\frac{1}{1/q_{11}+g_1}\frac{1}{q_{12}}\frac{1}{q_{21}}. \tag{2.1.6.8}$$

Defining $l_2'=g_2q_{22}'$ and solving for the error terms of row two in Eq. (2.1.6.7), one gets the following loop two design equations

$$e_{21}=\frac{q_{22}'}{1+l_2'}\left(\frac{1}{q_{21}^{*}}-\frac{q_{11}}{1+l_1}\frac{1}{q_{21}}\frac{1}{q_{11}^{*}}\right), \tag{2.1.6.9}$$

$$e_{22}=\frac{q_{22}'}{1+l_2'}\left(\frac{1}{q_{22}^{*}}-\frac{q_{11}}{1+l_1}\frac{1}{q_{21}}\frac{1}{q_{12}^{*}}\right), \tag{2.1.6.10}$$

The second phase of the design is to design the pre-filter $\boldsymbol{F}$. Making use of the fact that the nominal tracking error was designed to be zero or small, the tracking error is

$$|\boldsymbol{E}_{\mathbf{0}}^{r}|=\left|\boldsymbol{M}-\boldsymbol{T}_{\mathbf{0}\boldsymbol{Y}/\boldsymbol{R}}\right|=|\boldsymbol{M}-\boldsymbol{T}_{\mathbf{0}}\boldsymbol{F}|=\mathbf{0}. \tag{2.1.6.11}$$

In this case, $\boldsymbol{T}_{\mathbf{0}}$ represents the complementary sensitivity. Solving for $\boldsymbol{F}$ in Eq. (2.1.6.11) gives

$$\boldsymbol{F}=\boldsymbol{F}_{\mathbf{0}}=\widehat{\boldsymbol{T}}_{\mathbf{0}}\boldsymbol{M}. \tag{2.1.6.12}$$

As stated in (Boje, 2002a), by the realistic choice of $\boldsymbol{M}$, the designer can ensure $\boldsymbol{F}$ is strictly proper and stable. The operation in Eq. (2.1.6.12) may result in a high order pre-filter. To allow for the tuning of $\boldsymbol{F}$, bounds are placed on the pre-filter elements based on the tracking error specifications. This is equivalent to stating that the pre-filter elements are allowed to vary around the nominal i.e. $\boldsymbol{F}=\boldsymbol{F}_{\mathbf{0}}+\boldsymbol{\delta F}$. This of course is only possible if the controller is made conservative. The relative error is given by

$$|\boldsymbol{E}^{r}|_{ij}=|\boldsymbol{M}-\boldsymbol{T}\boldsymbol{F}-\boldsymbol{T}\delta\boldsymbol{F}|_{ij}. \tag{2.1.6.13}$$

Applying the Schwarz inequality to the above equation, one gets

$$|\boldsymbol{E}^{r}|_{ij}\leq|\boldsymbol{M}-\boldsymbol{T}\boldsymbol{F}|_{ij}+|\boldsymbol{T}\delta\boldsymbol{F}|_{ij}. \tag{2.1.6.14}$$

Following the manipulation in (Boje, 2002a), the bound on the radius of the elements of $\boldsymbol{F}$ for the jth column are determined to be

$$\left|\delta f_j\right| \leq \min_i \left\{\left(A_{ij} - |\boldsymbol{M} - \boldsymbol{T}\boldsymbol{F}_0|_{ij}\right) \min_{\boldsymbol{P}\in\{P\}} \left(1/\sum_{k=1}^{n} |t_{ik}|\right)\right\}. \tag{2.1.6.15}$$

2.1.7. Bounds using Inversion-free QFT

In the original MIMO QFT design methodology, the design equations are a function of the elements of the plant inverse. It turns out that when the plant elements are used in the design equation instead of the inverse elements, different bounds may be obtained. It is important that plant inversion is not implicit in the design equations because that will result in the same bounds as those generated using the original formulation. Both bounds may be conservative but one may be more restrictive than the other, hence the union of the bounds are taken, which may yield an overall less conservative design. This section is based on unpublished material by Boje and Chait on the use of inversion-free techniques to obtain less conservative bounds on loop gains.

The following derivation, results in design equations that appear in the QFT literature that are called "inversion-free" or "direct" design equations (Park, Yossi and Steinbuch, 1997). These are not truly inversion-free because plant inversion is implicit in the design equations. The determinant of the plant appearing in the design equations indicates that inversion is implicit. The derivation in this section is done for disturbance rejection. It is found that the plant inversion is indeed implicit and is confirmed by the fact that the original QFT formulation and the "inversion-free" method produce the same bounds. From Eq. (2.1.2.3), $\boldsymbol{G}$ is extracted as a common factor to the right, giving

$$\left(\widehat{\boldsymbol{G}}+\boldsymbol{P}\right)\boldsymbol{G}\,\boldsymbol{T}=\boldsymbol{I}. \tag{2.1.7.1}$$

Performing diagonal splitting of the plant

$$\left(\widehat{\boldsymbol{G}}+\boldsymbol{P_D}+\boldsymbol{P_O}\right)\boldsymbol{G}\,\boldsymbol{T}=\boldsymbol{I}. \tag{2.1.7.2}$$

Taking the diagonal matrices as a common factor

$$\left(\widehat{\boldsymbol{G}}+\boldsymbol{P_D}\right)\left(\boldsymbol{I}+\left(\widehat{\boldsymbol{G}}+\boldsymbol{P_D}\right)^{-1}\boldsymbol{P_O}\right)\boldsymbol{G}\,\boldsymbol{T}=\boldsymbol{I}. \tag{2.1.7.3}$$

After some further manipulation and solving for $\boldsymbol{T}$

$$\boldsymbol{T}=\widehat{\boldsymbol{G}}\left(\widehat{\boldsymbol{G}}+\boldsymbol{P_D}\right)^{-1}[\boldsymbol{I}-\boldsymbol{P_o}\boldsymbol{G}\,\boldsymbol{T}]. \tag{2.1.7.4}$$

For a 2×2 system, the scalar design equations are

$$t_{11}=\frac{1}{1+p_{11}g_1}(1-p_{12}g_2t_{21}), \tag{2.1.7.5}$$

$$t_{12}=\frac{-p_{12}g_2t_{22}}{1+p_{11}g_1}, \tag{2.1.7.6}$$

$$t_{21}=\frac{-p_{21}g_1t_{11},}{1+p_{22}g_2} \tag{2.1.7.7}$$

$$t_{22}=\frac{1}{1+p_{22}g_2}(1-p_{21}g_1t_{12}). \tag{2.1.7.8}$$

From assessing the equations above it can be observed that g_2 in Eq. (2.1.7.5) can be eliminated by using Eq. (2.1.7.7). Defining $\bar{\gamma}^2=\frac{p_{11}p_{22}}{p_{12}p_{21}}$, the simplified version for the design of t_{11} is given by

$$t_{11} = \frac{1 + \frac{p_{12}}{p_{22}} t_{21}}{1 + (1 - 1/\bar{\gamma}^2) l_1}. \tag{2.1.7.9}$$

Similarly, the other design equations are

$$t_{12} = \frac{\frac{-p_{12}}{p_{22}} + \frac{p_{12} t_{22}}{p_{22}}}{1 + (1 - 1/\bar{\gamma}^2) l_1}, \tag{2.1.7.10}$$

$$t_{21} = \frac{\frac{-p_{21}}{p_{11}} + \frac{p_{21} t_{11}}{p_{11}}}{1 + (1 - 1/\bar{\gamma}^2) l_2}, \tag{2.1.7.11}$$

$$t_{22} = \frac{1 + \frac{p_{21}}{p_{11}} t_{12}}{1 + (1 - 1/\bar{\gamma}^2) l_2}. \tag{2.1.7.12}$$

For the purpose of this thesis, the equations above will be referred to as the inversion-free equations as it is used in the current literature. The following design equations will be referred to as the true inversion-free design equations. A truly inversion-free design can be obtained by multiplying Eq. (2.1.2.3) on both sides from the right by $(\boldsymbol{I} + \boldsymbol{PG})\widehat{\boldsymbol{G}}$, to obtain

$$\boldsymbol{T}\left(\widehat{\boldsymbol{G}} + \boldsymbol{P}\right) = \widehat{\boldsymbol{G}}. \tag{2.1.7.13}$$

Writing Eq. (2.1.7.13) in terms of its scalar elements

$$\begin{bmatrix} t_{11} & t_{12} \\ t_{21} & t_{22} \end{bmatrix} \begin{bmatrix} \frac{1 + l_1}{g_1} & p_{12} \\ p_{21} & \frac{1 + l_2}{g_2} \end{bmatrix} = \begin{bmatrix} \frac{1}{g_1} & 0 \\ 0 & \frac{1}{g_2} \end{bmatrix}. \tag{2.1.7.14}$$

Simplify the above equation by multiplying both sides from the right by $\begin{bmatrix} \frac{g_1}{1+l_1} & 0 \\ 0 & \frac{g_2}{1+l_2} \end{bmatrix}$, one gets

$$\begin{bmatrix} t_{11} & t_{12} \\ t_{21} & t_{22} \end{bmatrix} \begin{bmatrix} 1 & \frac{p_{12} g_2}{1 + l_2} \\ \frac{p_{21} g_1}{1 + l_1} & 1 \end{bmatrix} = \begin{bmatrix} \frac{1}{1 + l_1} & 0 \\ 0 & \frac{1}{1 + l_2} \end{bmatrix}. \tag{2.1.7.15}$$

Decomposing Eq. (2.1.7.15) results in the following design equations

$$t_{11} = \frac{1 - p_{21} g_1 t_{12}}{1 + l_1}, \tag{2.1.7.16}$$

$$t_{21} = -\frac{p_{21} g_1}{1 + l_1} t_{22}, \tag{2.1.7.17}$$

$$t_{12} = -\frac{p_{12} g_2 t_{11}}{1 + l_2}, \tag{2.1.7.18}$$

$$t_{22} = \frac{1 - p_{12} g_2 t_{21}}{1 + l_2}. \tag{2.1.7.19}$$

Equations (2.1.7.16) and (2.1.7.17) are used for loop one design and Eqs (2.1.7.18) and (2.1.7.19) are used for loop two design. When designing the first loop, the equations above become useful because they can provide alternative bounds, which if satisfied, will ensure specifications are met. The advantage of incorporating the inversion-free method in the design procedure is to possibly create less conservative bounds. Since both methods produce bounds that are conservative and generally not the same, the union of the bounds will result in bounds that may be less conservative than the individual methods. The second loop design will proceed as usual using the exact bounds

2.1.8. Stability of MIMO Systems

Ensuring stability of closed-loop systems under all system circumstances is indispensible in real world applications. For MIMO systems the extension of the SISO Nyquist criterion is used to assess stability. The return difference for the multivariable plant is given by

$$\boldsymbol{D} = \boldsymbol{I} + \boldsymbol{L}(s). \tag{2.1.8.1}$$

The inverse of the return difference appears in all closed-loop transfers. Hence for the system to be stable, $\boldsymbol{D}^{-1}$ cannot have any right-hand plane (RHP) poles. The inverse of $\boldsymbol{D}$ is given by

$$\boldsymbol{D}^{-1} = \frac{adj\big(\boldsymbol{I} + \boldsymbol{L}(s)\big)}{det\big(\boldsymbol{I} + \boldsymbol{L}(s)\big)}. \tag{2.1.8.2}$$

This is equivalent to stating that the system is closed-loop stable if and only if $det\big(\boldsymbol{I} + \boldsymbol{L}(s)\big)$ has no RHP zeros. By the application of the Nyquist criterion, it can be said that the closed-loop system is stable provided that the image of $det\big(\boldsymbol{I} + \boldsymbol{L}(s)\big)$ as s goes around the usual Nyquist contour encircles the origin p times in the anticlockwise direction, where p is the number of unstable Smith-McMillan poles (Maciejowski, 1989, pg 59). Alternatively, one can plot the eigenvalues of $\boldsymbol{L}(s)$ (characteristic loci as s is varied) and count the encirclements of the -1 point. If there are p unstable Smith-McMillan poles, the system is stable if and only if the net encirclement of the -1 point is anticlockwise and equal to p (Maciejowski, 1989, Theorem 2.9). This stability criterion allows one to test for stability but does not clearly indicate how it can be applied during the shaping of individual loops.

Interpreting Stability from a QFT Design Perspective

The closed-loop system will be stable if there are no RHP zeros in the factor $[(1 + \mathrm{l}_1)(1 + \mathrm{l}_2) - \gamma^2]$ in a 2×2 system. It is found that this factor appears in the denominator of all the explicit closed-loop scalar equations for a 2×2 system, as found in Eqs. (2.1.2.18) - (2.1.2.21). It is shown below that this common denominator is equal to the determinant of the return difference $\big(\boldsymbol{I} + \boldsymbol{L}(s)\big)$ for a 2×2 system. The characteristic equation of the system is given by

$$\det(\boldsymbol{I} + \boldsymbol{P}\boldsymbol{G}) = 0. \tag{2.1.8.3}$$

The plant inverse is given by

$$\widehat{\boldsymbol{P}} = \begin{bmatrix} 1/q_{11} & 1/q_{12} \\ 1/q_{21} & 1/q_{22} \end{bmatrix}. \tag{2.1.8.4}$$

The plant in terms of q's

$$\boldsymbol{P}(q) = \big(\widehat{\boldsymbol{P}}\big)^{-1} = \frac{1}{\det\big(\widehat{\boldsymbol{P}}\big)} adj\big(\widehat{\boldsymbol{P}}\big) = \frac{1}{\dfrac{1}{q_{11}q_{22}} - \dfrac{1}{q_{12}q_{21}}} \begin{bmatrix} 1/q_{22} & -1/q_{12} \\ -1/q_{21} & 1/q_{11} \end{bmatrix}, \tag{2.1.8.5}$$

$$= \frac{q_{11}q_{22}q_{12}q_{21}}{q_{12}q_{21} - q_{11}q_{22}} \begin{bmatrix} 1/q_{22} & -1/q_{12} \\ -1/q_{21} & 1/q_{11} \end{bmatrix},$$

$$= \frac{1}{1-\gamma^2} \begin{bmatrix} q_{11} & -q_{11}q_{22}/q_{12} \\ -q_{11}q_{22}/q_{21} & q_{22} \end{bmatrix}.$$

Calculating the return difference in terms of $q's$

$$\boldsymbol{I}+\boldsymbol{PG}=\begin{bmatrix} 1+\dfrac{q_{11}g_1}{1-\gamma^2} & \dfrac{-q_{11}q_{22}g_2/q_{12}}{1-\gamma^2} \\ \dfrac{-q_{11}g_1q_{22}/q_{21}}{1-\gamma^2} & 1+\dfrac{q_{22}g_2}{1-\gamma^2} \end{bmatrix}. \tag{2.1.8.6}$$

Expressing the determinant of return difference in terms of $q's$

$$\det(\boldsymbol{I}+\boldsymbol{PG})=0=\left(1+\frac{q_{11}g_1}{1-\gamma^2}\right)\left(1+\frac{q_{22}g_2}{1-\gamma^2}\right)+\frac{-q_{11}^2q_{22}^2g_1g_2/(q_{12}q_{21})}{(1-\gamma^2)^2}, \tag{2.1.8.7}$$

$$=[(1-\gamma^2)+q_{11}g_1][(1-\gamma^2)+q_{22}g_2]-q_{11}^2q_{22}^2g_1g_2/(q_{12}q_{21}),$$

$$=(1-\gamma^2)^2+q_{11}g_1(1-\gamma^2)+q_{22}g_2(1-\gamma^2)+q_{11}g_1q_{22}g_2-\gamma^2q_{11}q_{22}g_1g_2,$$

$$=(1-\gamma^2)^2+q_{11}g_1(1-\gamma^2)+q_{22}g_2(1-\gamma^2)+(1-\gamma^2)q_{11}q_{22}g_1g_2,$$

$$=(1-\gamma^2)+q_{11}g_1+q_{22}g_2+q_{11}q_{22}g_1g_2=0,$$

$$=1-\gamma^2+l_1+l_2+l_1l_2,$$

$$=(1+l_1)(1+l_2)-\gamma^2.$$

By the application of the Nyquist criterion, it can be concluded that the closed-loop system is stable if and only if the loci $[(1+l_1)(1+l_2)-\gamma^2]$ do not encircle the origin (Houpis, 2006, pg 203). At high frequency the magnitude of both loop gains goes to zero for strictly proper plants and at least proper controllers. This implies that the characteristic equation at high frequency is $1-\gamma^2=0$. Therefore, at high frequency, the magnitude of γ^2 must be less than unity to prevent encirclement (sufficient condition). This criterion is less severe than Rosenbrock's diagonal dominance criterion which requires dominance at all frequencies. Equation (2.1.8.7) also implies that if the last loop is stable, the closed-loop system will be stable.

Implication for Loop Shaping Concerning Stability

Based on the Eq. (2.1.8.7) , stability can be ensured if each loop is design to be stable (i.e. there are no RHP zeros of the individual loop characteristic equation), the controller $\boldsymbol{G}$ is stable and there are no pole-zero cancellations in the individual loop gain. This is not a necessary condition. If there are unstable loops in the system, making the last loop stable (using the exact equations) will result in a stable MIMO closed-loop system. It is shown in (Yaniv, 1999, pg 103) that for a 2×2 system, the first loop can be designed to be unstable provided the RHP zero of $1+l$ (for the first loop) is far from the origin. The RHP zero (of the characteristic equation) of the first loop appears as a RHP zero of the second loop equivalent plant, q_2^{eq}. If the RHP zero (of the characteristic equation) of the unstable loop is close to the origin, it will provide too much phase lag in the second loop to meet specifications.

Assessing Stability using the Nichols Plot

Traditionally, the Nyquist plot is used to check if the closed-loop system is stable based on the open-loop transfer function. Although it allows for the designer to easily assess stability, it is not a convenient design tool for shaping the individual loops i.e. it is difficult to see the sensitivity and complementary sensitivity of the resulting system. The Nichols plot allows one to view the sensitivity and complementary sensitivity of the system, hence the stability margins. To interpret stability in the Nichols chart it is essential to track the mapping from the complex plane (Nyquist Chart) to the Nichols chart. A more comprehensive stability analysis using the Nichols chart is given in (Cohen, N., Chait, Y., Yaniv, O. and Borghesani, C., 1992).

An alternative interpretation of the Nyquist criterion is given by (Vidyasagar, Bertschmann and Sallaberger, 1988). A ray should be imagined to exist connecting the Nyquist point $(-1, j0)$ to any other point with infinite radius. If the image of $L(s)$ crosses the ray in a clockwise direction, it is counted as positive; and negative if the crossing is in an anticlockwise direction. The net crossing/s of the ray is equal to the number of encirclements of the Nyquist point. To understand the mapping from the Nyquist Chart to the Nichols chart, an example is used. An unstable open-loop transfer function is used, given by

$$\mathrm{L(s)} = \frac{0.5}{\left(\left(\frac{\mathrm{s}}{5}\right)^2 + 2 \cdot 0.4 \cdot \frac{\mathrm{s}}{5} + 1\right)(\mathrm{s} - 1)} \cdot \mathrm{k}, \tag{2.1.8.8}$$

where k is the proportional gain feedback term. The corresponding Nyquist and Nichols plot are shown in Fig. 2.1.8.1, when $k = 1$.

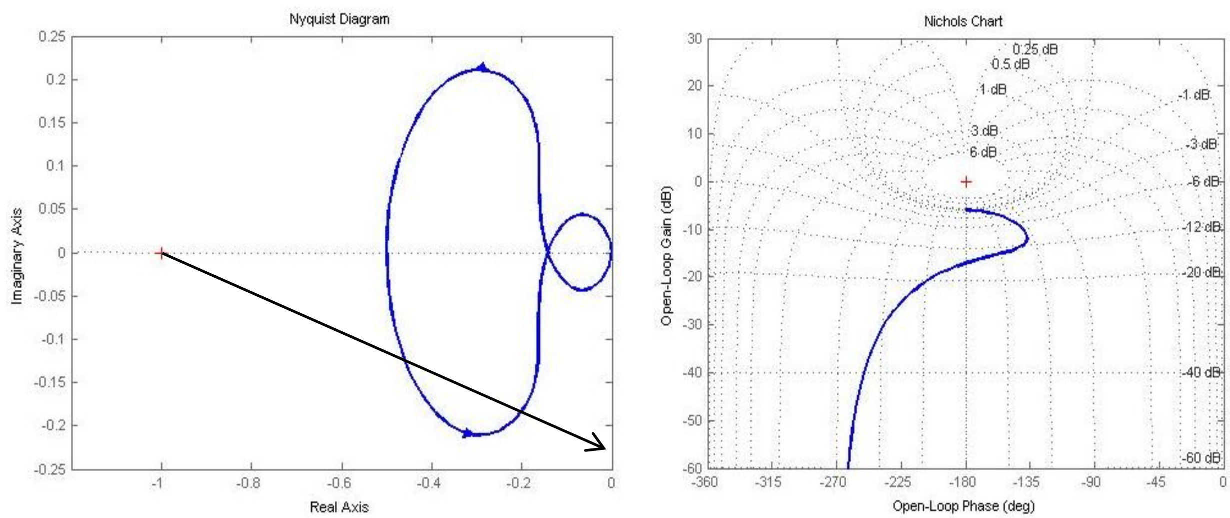

Figure 2.1.8.1 Nyquist plot and corresponding mapping to Nichols Chart of $L(s)$ for $k = 1$

In the Nyquist plot in Fig. 2.1.8.1, a ray extends from the Nyquist point in the Nyquist diagram with an infinite length. If the crossings' on the ray are counted with the rules above, relative to the respective centre's based on the curvature of the image of $L(s)$, it is noticed that the net crossing is zero irrespective of the angle of the projected ray from the Nyquist point. It is important to note that there are zero crossings of the line above the Nyquist point in the Nichols chart. The system is clearly closed-loop unstable based on the Nyquist criterion.

In Fig. 2.1.8.2 the feedback gain is $k = 3.8$, there is one crossing of the ray in the Nyquist plot. It is seen that this gets reflected as the loop gain $L(s)$ starting at a point above the Nyquist point (but no crossing the $-\pi\ rad$ phase line). Let the line above the Nyquist point in the Nichols chart be called the Nyquist line. If $L(j\omega)$ crosses from the left of the Nyquist line to the right, it represents two anticlockwise encirclements, and if it crosses from the right of the Nyquist line to the left, it represents two clockwise encirclements of the Nyquist point. For the system with $k = 3.8$, stability of the system can be assessed as follows. Since the loop gain begins at the Nyquist line and goes to the right, there must be one anticlockwise encirclement of the Nyquist point. Also there are no other crossings across the Nqyuist line, hence the total number of encirclements of the Nyquist point is -1. Since there is one RHP pole in $L(s)$, $N = -P$ hence the closed-loop system is stable.

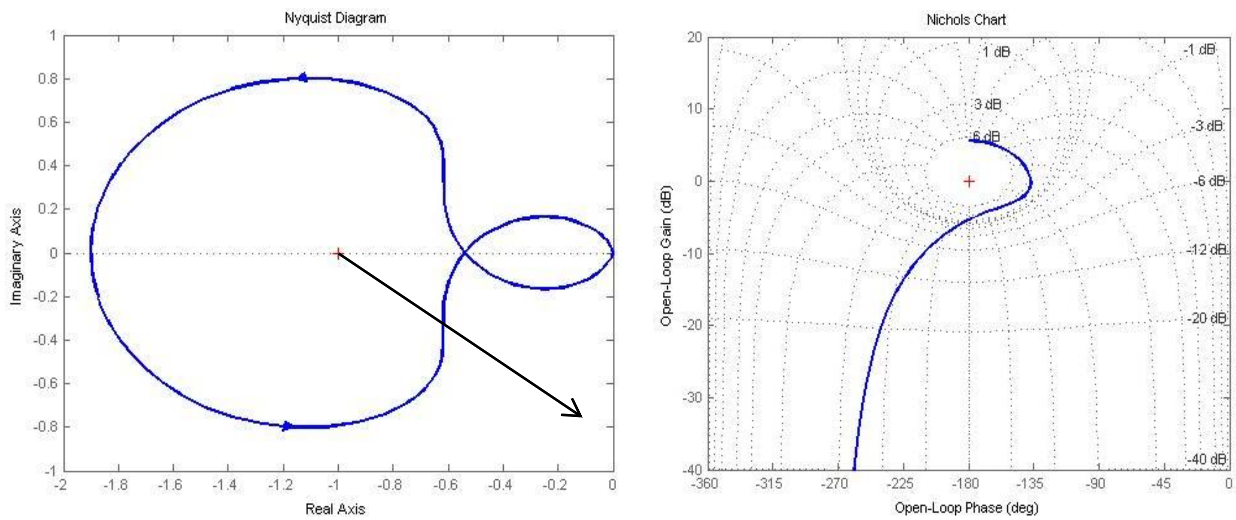

Figure 2.1.8.2 Nyquist plot and corresponding mapping to Nichols chart of $\boldsymbol{L(s)}$ for $\boldsymbol{k = 3.8}$

An interesting note on the mapping is that a ray in the Nyquist plot maps to a line of constant phase of $\left(\frac{1}{1+L}\right)$ in the inverse Nichols chart.

2.1.9. Boundary of Templates

As stated in Section 2.1.1, the generation of templates is an essential part of the QFT design procedure as it gives insight on the design and is required for the graphical design approach. The design of a robust controller requires a bound on the uncertainty. Using the Maximum Principle (Munkres, 2000), only the boundary of the uncertainty template is required to obtain a robust controller provided there is no finite escape in the boundary. Modern control design methods like H_∞ design use disk specifications to bound the uncertainty which is generally conservative. QFT uses the actual plant uncertainty. This poses a problem when dealing with plants that have high plant uncertainty dimensions. For n uncertain parameters in a particular plant, and m points chosen within the sets, the number of plant evaluations for a single frequency, for all possible parameter combinations are equal to m^n. Since only the outer edge of the template is used in design, a drastic improvement in efficiency can be obtained by determining the parameters (in the parameter space) that will result in a mapping that resides on the boundary of the template.

Although, there may be interior points of the parameter space that results in a mapping to the boundary of the template, it is found (through experimentation) that the majority of the points that make up the boundary of the template are a result of the mapping of the boundary of the parameter space (may be a hypercube). To determine these interior points, a method is provided in (Garcia-Sanz and Vital, 1999). The idea is that a mapping of a multi-dimensional ball (some small radius ϵ , hence is an interior point) from the parameter space to $\mathbb{R}^2$, results in a disk (centred on an interior point) in $\mathbb{R}^2$ if the rank of the Jacobian matrix of the mapping is equal to 2. In other words, if the rank of the Jacobian matrix for an interior point (in the parameter space) is less than 2, it implies that the resulting disk in $\mathbb{R}^2$ has zero radius and must be a boundary point of the template.

An example is taken from (Garcia-Sanz and Vital, 1999) to illustrate the idea. An uncertain plant is given by

$$P(s) = \frac{1}{s^2 + 2 \cdot 0.02 \cdot s \cdot \omega_n + \omega_n^2}\ e^{-s\tau} \qquad \omega_n \in [0.7,1.2], \tau \in [0,2] \tag{2.1.9.1}$$

The Jacobian matrix of the mapping from the parameter space to the complex plane for the plant in Eq. (2.1.9.1) is given by

$$J(P) = \begin{bmatrix} \dfrac{\partial Re\ P(j\omega)}{\partial \omega_n} & \dfrac{\partial Re\ P(j\omega)}{\partial \tau} \\ \dfrac{\partial Im\ P(j\omega)}{\partial \omega_n} & \dfrac{\partial Im\ P(j\omega)}{\partial \tau} \end{bmatrix}. \tag{2.1.9.2}$$

By analysis, it may be possible to find a solution to when the Jacobian of the mapping loses rank. If this is not possible, one can use brute force together with the Jacobian theory to find parameter points close to the boundary. A large number of points can be chosen, and instead of checking the rank of the Jacobian matrix, one could check the condition number since it is unlikely that one may find the exact interior point that result in a boundary point through brute force. If a relatively high condition number occurs, it means that the matrix is "close" to losing rank and will be close to a boundary point.

To find the boundary of the template, a mapping of the all sides of the hypercube (parameter space) must be plotted. This is equivalent to fixing all parameters at their end points and varying one parameter (must be done for all combinations of end points). The blue asterisks in Fig. 2.1.9.1 are a result of plotting the edges of the hypercube and the black dots are a result of choosing points that give a condition number of the Jacobian matrix greater than 250. The magenta circles are a plot of 2500 plant parameter interior points.

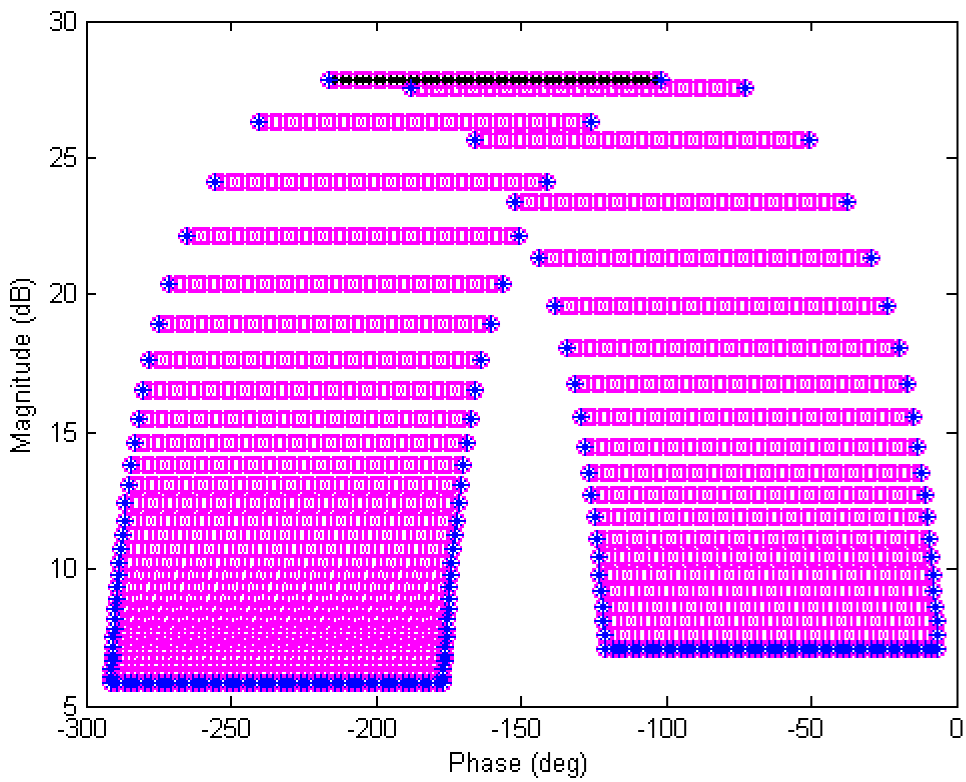

Figure 2.1.9.1 Plant template for $\omega = 1rad/s$; blue '*' - boundary of parameter space mapping; magneta 'o' – 2500 points evenly selected within parameter space; black '.' - cond(Jacobian) > 250

The combination of the parameter space boundary mapping and the use of the Jacobian theory result in a set of *essential* points that encapsulate the uncertainty. In order to get the boundary of the reduced set, one could use methods such as finding the non-convex hull in (Boje, 2000).

2.2. Modern Control Theory

The section contains the theory relating to state-feedback control system design techniques.

2.2.1. State-Feedback Control

The state-feedback control problem is to obtain a controller $\boldsymbol{K}$ that drives the plant input by implementing a linear combination of the plant's state variable such that the closed-loop system is stable and the performance requirements are met. Since the control input is a linear combination of the state of the plant, the controller will be a simple gain matrix. A state-feedback control system structure is shown in Fig. 2.2.1.1 (Franklin, Powell and Emami-Naeini, 2006, pg 482).

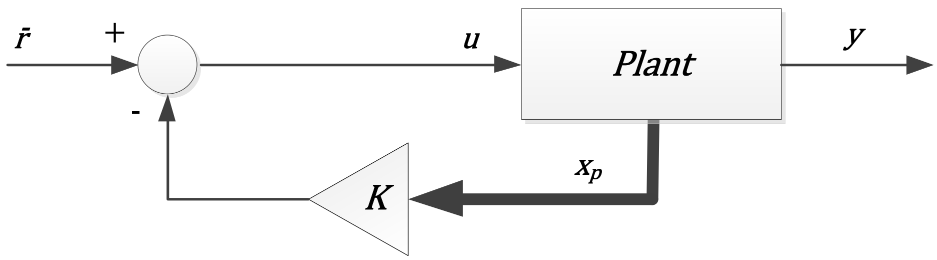

Figure 2.2.1.1 State-feedback control structure

The state of the plant $\boldsymbol{x}_p$ is a column vector extracted from the plant and fed into the state-feedback gain $\boldsymbol{K}$ in Fig. 2.2.1.1. The signal $\bar{\boldsymbol{r}}$ is derived from the reference to the system and a loop transfer recovery block. When $\bar{\boldsymbol{r}}$ is zero, the state-feedback problem is referred to as a regulating state-feedback problem. This approach to solving the feedback problem may have become common due to the easy stability analysis that this method presents (at least for a fixed plant case). The ease of the stability analysis can be seen from Eq. (2.2.1.1), by letting the reference equal to zero (NB. the dependence of time is excluded in the analysis as this thesis focuses on linear time-invariant systems)

$$\dot{\boldsymbol{x}}_{\boldsymbol{p}} = \boldsymbol{A}\boldsymbol{x} + \boldsymbol{B}\boldsymbol{u} = \boldsymbol{A}\boldsymbol{x}_{\boldsymbol{p}} + \boldsymbol{B}\left(\bar{\boldsymbol{r}} - \boldsymbol{K}\boldsymbol{x}_{\boldsymbol{p}}\right) = (\boldsymbol{A} - \boldsymbol{B}\boldsymbol{K})\boldsymbol{x}_{\boldsymbol{p}} - \boldsymbol{B}\bar{\boldsymbol{r}} = (\boldsymbol{A} - \boldsymbol{B}\boldsymbol{K})\boldsymbol{x}_{\boldsymbol{p}}. \qquad (2.2.1.1)$$

Since the solution of the linear differential equation is $\boldsymbol{x}(t) = e^{(\boldsymbol{A}-\boldsymbol{B}\boldsymbol{K})(t-t_0)}\boldsymbol{x}(0)$ (with zero input) and by spectral decomposition, $e^{(\boldsymbol{A}-\boldsymbol{B}\boldsymbol{K})t} = \sum_i^n e^{\lambda_i t}\boldsymbol{r}_{\boldsymbol{i}}\,\boldsymbol{l}_i^T$ (Skogestad and Postlethwaite, 2005, pg 518) where λ_i is an eigenvalue of $(\boldsymbol{A} - \boldsymbol{B}\boldsymbol{K})$, and $\boldsymbol{r}_{\boldsymbol{i}}$ and $\boldsymbol{l}_{\boldsymbol{i}}$ are the corresponding right and left eigenvectors, the effect of a positive eigenvalue gives an unbounded exponential term in the solution. Hence the closed-loop system is stable if and only if the eigenvalues of $(\boldsymbol{A} - \boldsymbol{B}\boldsymbol{K})$ are negative. The feedback matrix $\boldsymbol{K}$ can be chosen so that the closed-loop poles lie on the left side of the complex plane. When the reference signal changes in the configuration above, it appears as a perturbation in the system, therefore large changes in the reference signal can potentially destabilize the system. In *Matlab*™, one can use the $place(\dots)$ function to generate a state-feedback gain $\boldsymbol{K}$ that positions the closed-loop poles to specified locations.

Linear Quadratic Regulator

When the controller $\boldsymbol{K}$ is chosen to minimize the objective function (or the quadratic cost function)

$$J = \int_{t=0}^{T} (\boldsymbol{x}^T \boldsymbol{Q} \boldsymbol{x} + \boldsymbol{u}^T \boldsymbol{R} \boldsymbol{u}) dt, \tag{2.2.1.2}$$

the controller is called a linear quadratic regulator (*LQR*) controller. The matrices $\boldsymbol{Q}$ (positive semi-definite) and $\boldsymbol{R}$ (positive definite) are symmetric weighting matrices chosen by the designer (Sidi, 2001, pp 327-328). Equation (2.2.1.2) suggests that the choice of the $\boldsymbol{Q}$ matrix relates to the regulation bandwidth for each state and the choice of the $\boldsymbol{R}$ matrix relates to the control effort for each actuator. LQR theory falls under the "modern" (optimal) control framework because of the time of its development and the use of optimization to determine the controller gain. A problem with this design method is that it is not quantitative in capturing plant uncertainty. The weighting matrices are usually chosen in an iterative manner to ensure specifications are met for uncertain plants. An additional difficulty with this method is that plant states are not easily obtained in practice and that leads to more complexities.

Estimating the State

In most practical systems it is infeasible to have a sensor for each state variable. Therefore the plant's state in most systems are estimated using a structure in the dashed block shown in Fig. 2.2.1.2. The structure is called a Luenberger observer or an estimator because it provides a calculated conjecture based on the inputs, outputs and the known dynamics of the plant. The matrices $\boldsymbol{A}, \boldsymbol{B}, \boldsymbol{C}$ and $\boldsymbol{D}$ are the matrices of the state and output equations for the plant. The observer gain is $\boldsymbol{L}$. The choice of $\boldsymbol{L}$ determines how fast the structure estimates the plant's state. The plant state estimate is denoted by $\hat{\boldsymbol{x}}_p$.

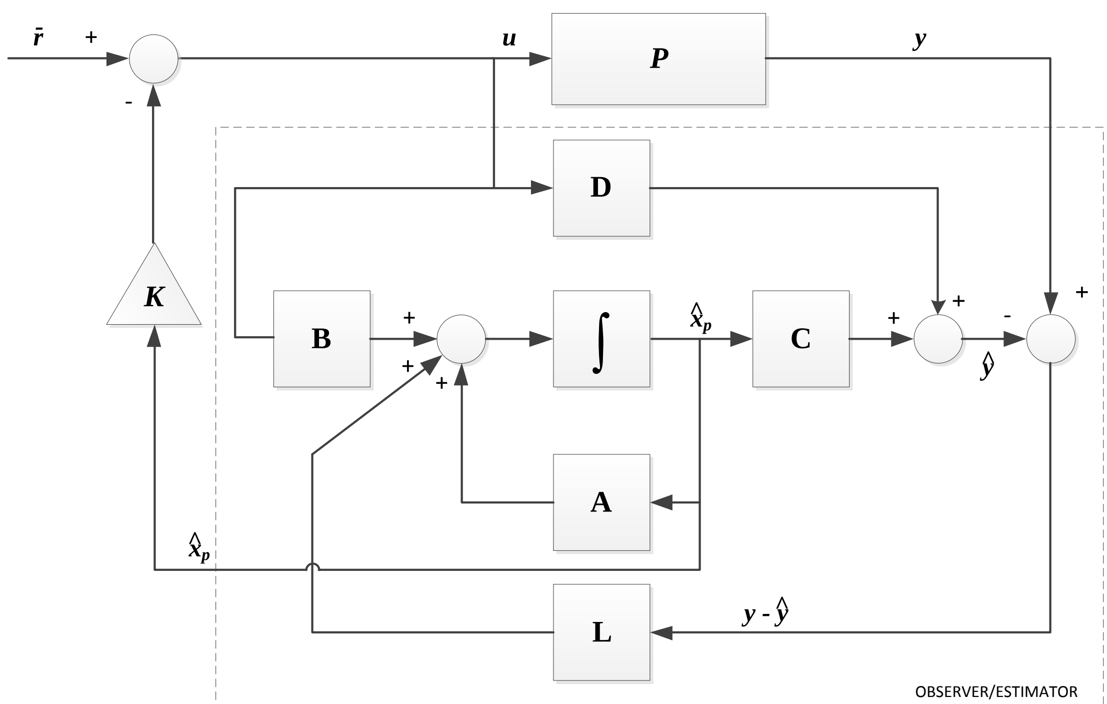

Figure 2.2.1.2 State-feedback control structure with state estimation

When the observer gain is chosen to minimize the expectation of the error between the actual state and the estimated state, the structure is a representation of a Kalman filter and the observer gain is known as the Kalman gain.

Incorporating Integral Action in State-feedback Design

To obtain good low frequency sensitivity an integrator is usually added into the control system, and if implemented with LQR is referred to as LQR with integration. The open-loop plant state-space description is augmented with the integrator to obtain the integral gain via pole placement. An artificial state $\boldsymbol{e}(t)$ is introduced, which represents the integral of the error between the reference and the output (Nagamune, 2008, slides 17-18) i.e. $\boldsymbol{e}(t) = \int_0^T [\boldsymbol{y}(\tau) - \boldsymbol{r}(\tau)]d\tau$. The state that will be augmented to the system, with the reference assumed to not deviate largely from the origin is

$$\dot{\boldsymbol{e}} = \boldsymbol{y} - \boldsymbol{r} = \boldsymbol{Cx} + \boldsymbol{Du}. \tag{2.2.1.3}$$

The result of this addition gives a control system shown in Fig. 2.2.1.3. The gain $\boldsymbol{K_i}$, in Fig. 2.2.1.3 is obtained as a result of the LQR optimization of an augmented plant including the integrators.

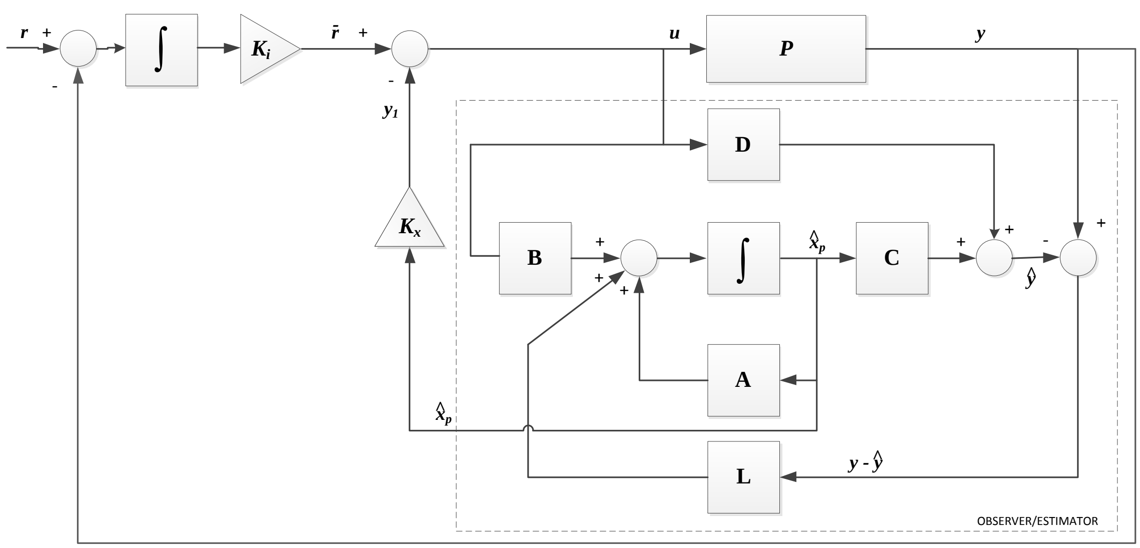

Figure 2.2.1.3 State-feedback system with integral action

Frequency Domain Perspective of State-space Design

In order to get a more compact form of the state-feedback system with an estimator and integral action, the components of Fig. 2.2.1.3 is described next using the state-space form and then converted into the classical frequency domain representation.

The plant has the following state equation and output equation

$$\dot{\boldsymbol{x}}_{\boldsymbol{p}} = \boldsymbol{A}\boldsymbol{x}_{\boldsymbol{p}} + \boldsymbol{Bu}, \tag{2.2.1.4}$$

$$\boldsymbol{y} = \boldsymbol{C}\boldsymbol{x}_{\boldsymbol{p}} + \boldsymbol{Du}. \tag{2.2.1.5}$$

The input to the plant is given by

$$\boldsymbol{u} = \bar{\boldsymbol{r}} - \boldsymbol{y_1} = \bar{\boldsymbol{r}} - \boldsymbol{K_x}\widehat{\boldsymbol{x}}_{\boldsymbol{p}}. \tag{2.2.1.6}$$

The integral operation block consisting of the integrator and the gain multiplier can be represented by the state Eq. (2.2.1.7) and output Eq. (2.2.1.8).

$$\dot{\boldsymbol{x}}_i = \mathbf{0}\boldsymbol{x}_i + \boldsymbol{I}(\boldsymbol{r} - \boldsymbol{y}), \tag{2.2.1.7}$$

$$\boldsymbol{y}_i = \bar{\boldsymbol{r}} = \boldsymbol{K}_i\boldsymbol{x}_i + \mathbf{0}(\boldsymbol{r} - \boldsymbol{y}). \tag{2.2.1.8}$$

Substituting Eq. (2.2.1.6) and subsequently Eq. (2.2.1.8) into Eq. (2.2.1.4) gives the revised plant state equation as

$$\dot{\boldsymbol{x}}_{\boldsymbol{p}} = \boldsymbol{A}\boldsymbol{x}_{\boldsymbol{p}} + \boldsymbol{B}\left(\bar{\boldsymbol{r}} - \boldsymbol{K}_x\widehat{\boldsymbol{x}}_{\boldsymbol{p}}\right) = \boldsymbol{A}\boldsymbol{x}_{\boldsymbol{p}} + \boldsymbol{B}\boldsymbol{K}_i\boldsymbol{x}_i - \boldsymbol{B}\boldsymbol{K}_x\widehat{\boldsymbol{x}}_{\boldsymbol{p}}. \tag{2.2.1.9}$$

The observer block is described by the state equation

$$\dot{\widehat{\boldsymbol{x}}}_{\boldsymbol{p}} = \boldsymbol{A}\widehat{\boldsymbol{x}}_{\boldsymbol{p}} + \boldsymbol{B}\boldsymbol{u} + \boldsymbol{L}(\boldsymbol{y} - \widehat{\boldsymbol{y}}) = \boldsymbol{A}\widehat{\boldsymbol{x}}_{\boldsymbol{p}} + \boldsymbol{B}\bar{\boldsymbol{r}} - \boldsymbol{B}\boldsymbol{K}_x\widehat{\boldsymbol{x}}_{\boldsymbol{p}} + \boldsymbol{L}\boldsymbol{y} - \boldsymbol{L}\boldsymbol{C}\widehat{\boldsymbol{x}}_{\boldsymbol{p}} - \boldsymbol{L}\boldsymbol{D}\boldsymbol{u}, \tag{2.2.1.10}$$

$$= \boldsymbol{A}\widehat{\boldsymbol{x}}_{\boldsymbol{p}} + \boldsymbol{B}\boldsymbol{K}_i\boldsymbol{x}_i - \boldsymbol{B}\boldsymbol{K}_x\widehat{\boldsymbol{x}}_{\boldsymbol{p}} + \boldsymbol{L}\boldsymbol{y} - \boldsymbol{L}\boldsymbol{C}\widehat{\boldsymbol{x}}_{\boldsymbol{p}} - \boldsymbol{L}\boldsymbol{D}\boldsymbol{K}_i\boldsymbol{x}_i + \boldsymbol{L}\boldsymbol{D}\boldsymbol{K}_x\widehat{\boldsymbol{x}}_{\boldsymbol{p}}. \tag{2.2.1.11}$$

If $\boldsymbol{y}$ is expanded in Eq. (2.2.1.11) in terms of the other states, it becomes

$$\dot{\widehat{\boldsymbol{x}}}_{\boldsymbol{p}} = \boldsymbol{L}\boldsymbol{C}\boldsymbol{x}_{\boldsymbol{p}} + (\boldsymbol{A} - \boldsymbol{B}\boldsymbol{K}_x - \boldsymbol{L}\boldsymbol{C})\widehat{\boldsymbol{x}}_{\boldsymbol{p}} + \boldsymbol{B}\boldsymbol{K}_i\boldsymbol{x}_i. \tag{2.2.1.12}$$

If $\boldsymbol{y}$ is expanded in Eq. (2.2.1.7) in terms of the other states, it becomes

$$\dot{\boldsymbol{x}}_i = \boldsymbol{r} - \left(\boldsymbol{C}\boldsymbol{x}_{\boldsymbol{p}} + \boldsymbol{D}\boldsymbol{u}\right) = \boldsymbol{r} - \boldsymbol{C}\boldsymbol{x}_{\boldsymbol{p}} - \boldsymbol{D}\boldsymbol{K}_i\boldsymbol{x}_i + \boldsymbol{D}\boldsymbol{K}_x\widehat{\boldsymbol{x}}_{\boldsymbol{p}}. \tag{2.2.1.13}$$

By augmenting Eq. (2.2.1.9), Eq. (2.2.1.12) and Eq. (2.2.1.13), the state and output equation for the complete system from reference $\boldsymbol{r}$, to output $\boldsymbol{y}$ may be written as

$$\begin{bmatrix} \dot{\boldsymbol{x}}_{\boldsymbol{p}} \\ \dot{\widehat{\boldsymbol{x}}}_{\boldsymbol{p}} \\ \dot{\boldsymbol{x}}_i \end{bmatrix} = \begin{bmatrix} \boldsymbol{A} & -\boldsymbol{B}\boldsymbol{K}_x & \boldsymbol{B}\boldsymbol{K}_i \\ \boldsymbol{L}\boldsymbol{C} & \boldsymbol{A} - \boldsymbol{B}\boldsymbol{K}_x - \boldsymbol{L}\boldsymbol{C} & \boldsymbol{B}\boldsymbol{K}_i \\ -\boldsymbol{C} & -\boldsymbol{D}\boldsymbol{K}_i & \boldsymbol{D}\boldsymbol{K}_x \end{bmatrix} \begin{bmatrix} \boldsymbol{x}_{\boldsymbol{p}} \\ \widehat{\boldsymbol{x}}_{\boldsymbol{p}} \\ \boldsymbol{x}_i \end{bmatrix} + \begin{bmatrix} \mathbf{0} \\ \mathbf{0} \\ \boldsymbol{I} \end{bmatrix} [\boldsymbol{r}], \tag{2.2.1.14}$$

$$[\boldsymbol{y}] = \begin{bmatrix} \boldsymbol{C} & -\boldsymbol{D}\boldsymbol{K}_x & \boldsymbol{D}\boldsymbol{K}_i \end{bmatrix} \begin{bmatrix} \boldsymbol{x}_{\boldsymbol{p}} \\ \widehat{\boldsymbol{x}}_{\boldsymbol{p}} \\ \boldsymbol{x}_i \end{bmatrix} + [\mathbf{0}][\boldsymbol{r}]. \tag{2.2.1.15}$$

In order to get the equation of the controller, the state-equation must be written in terms of the *input* $\boldsymbol{y}$ and $\boldsymbol{r}$, and the *output* of the controller $\boldsymbol{u}$. This obviously results in a two-degree of freedom controller.

Augmenting the states for the integrator and the observer, results in the following state equation for the controller

$$\begin{bmatrix} \dot{\widehat{\boldsymbol{x}}}_{\boldsymbol{p}} \\ \dot{\boldsymbol{x}}_i \end{bmatrix} = \begin{bmatrix} \boldsymbol{A} - \boldsymbol{B}\boldsymbol{K}_x - \boldsymbol{L}\boldsymbol{C} + \boldsymbol{L}\boldsymbol{D}\boldsymbol{K}_x & \boldsymbol{B}\boldsymbol{K}_i - \boldsymbol{L}\boldsymbol{D}\boldsymbol{K}_i \\ \mathbf{0} & \mathbf{0} \end{bmatrix} \begin{bmatrix} \widehat{\boldsymbol{x}}_{\boldsymbol{p}} \\ \boldsymbol{x}_i \end{bmatrix} + \begin{bmatrix} \boldsymbol{L} & \mathbf{0} \\ -\boldsymbol{I} & \boldsymbol{I} \end{bmatrix} \begin{bmatrix} \boldsymbol{y} \\ \boldsymbol{r} \end{bmatrix}. \tag{2.2.1.16}$$

The output of the controller is

$$[\boldsymbol{u}] = [-\boldsymbol{K}_x \quad \boldsymbol{K}_i]\begin{bmatrix}\widehat{\boldsymbol{x}}_p \\ \boldsymbol{x}_i\end{bmatrix} + [\boldsymbol{0} \quad \boldsymbol{0}]\begin{bmatrix}\boldsymbol{y} \\ \boldsymbol{r}\end{bmatrix}. \qquad (2.2.1.17)$$

The result above is two transfer function matrices, one acting as a feedback controller and the other as a pre-filter. In order to get the feedback controller, one must suppress the reference signal $\boldsymbol{r}$, and find the output due to $\boldsymbol{y}$ (application of linear superposition). Similarly, one gets the pre-filter by suppressing the output $\boldsymbol{y}$, and finding result due to $\boldsymbol{r}$. By superposition, the sum of the outputs of the pre-filter and the feedback controller must equal to the input signal to the plant $\boldsymbol{u}$.

If the plant input signal comprises of the signal from the feedback controller denoted as $\boldsymbol{u_g}$ and the signal due to the pre-filter denoted as $\boldsymbol{u_f}$, the feedback controller state and output equations are given by

$$\begin{bmatrix}\dot{\widehat{\boldsymbol{x}}}_p \\ \dot{\boldsymbol{x}}_i\end{bmatrix} = \begin{bmatrix}\boldsymbol{A}-\boldsymbol{B}\boldsymbol{K}_x-\boldsymbol{L}\boldsymbol{C}+\boldsymbol{L}\boldsymbol{D}\boldsymbol{K}_x & \boldsymbol{B}\boldsymbol{K}_i-\boldsymbol{L}\boldsymbol{D}\boldsymbol{K}_i \\ \boldsymbol{0} & \boldsymbol{0}\end{bmatrix}\begin{bmatrix}\widehat{\boldsymbol{x}}_p \\ \boldsymbol{x}_i\end{bmatrix} + \begin{bmatrix}\boldsymbol{L} \\ -\boldsymbol{I}\end{bmatrix}[\boldsymbol{y}], \qquad (2.2.1.18)$$

$$[\boldsymbol{u}_g] = [\boldsymbol{K}_x \quad \boldsymbol{K}_i]\begin{bmatrix}\widehat{\boldsymbol{x}}_p \\ \boldsymbol{x}_i\end{bmatrix} + [\boldsymbol{0}][\boldsymbol{y}]. \qquad (2.2.1.19)$$

In Eq. (2.2.1.19), the term due to the plant observer state is negated to allow for the negative feedback convention. The pre-filter state and output equations are given by

$$\begin{bmatrix}\dot{\widehat{\boldsymbol{x}}}_p \\ \dot{\boldsymbol{x}}_i\end{bmatrix} = \begin{bmatrix}\boldsymbol{A}-\boldsymbol{B}\boldsymbol{K}_x-\boldsymbol{L}\boldsymbol{C}+\boldsymbol{L}\boldsymbol{D}\boldsymbol{K}_x & \boldsymbol{B}\boldsymbol{K}_i-\boldsymbol{L}\boldsymbol{D}\boldsymbol{K}_i \\ \boldsymbol{0} & \boldsymbol{0}\end{bmatrix}\begin{bmatrix}\widehat{\boldsymbol{x}}_p \\ \boldsymbol{x}_i\end{bmatrix} + \begin{bmatrix}\boldsymbol{0} \\ \boldsymbol{I}\end{bmatrix}[\boldsymbol{r}], \qquad (2.2.1.20)$$

$$[\boldsymbol{u}_f] = [-\boldsymbol{K}_x \quad \boldsymbol{K}_i]\begin{bmatrix}\widehat{\boldsymbol{x}}_p \\ \boldsymbol{x}_i\end{bmatrix} + [\boldsymbol{0}][\boldsymbol{r}]. \qquad (2.2.1.21)$$

By using the transform, $\boldsymbol{X}(s) = \boldsymbol{C}'(s\boldsymbol{I}-\boldsymbol{A}')^{-1}\boldsymbol{B}' + \boldsymbol{D}'$, where $\boldsymbol{A}', \boldsymbol{B}', \boldsymbol{C}'$ and $\boldsymbol{D}'$ are the augmented state-space and output matrices, the frequency domain representation of the pre-filter and the controller can be obtained. The compact version of the control system in Fig. 2.2.1.3 can be seen in Fig. 2.2.1.4.

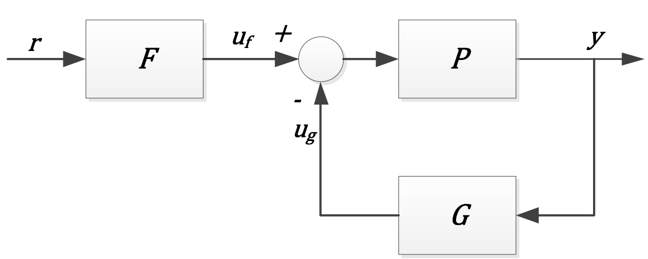

Figure 2.2.1.4 Frequency domain representation of state-feedback system with integral action

To get the $\boldsymbol{K_i}$ and the $\boldsymbol{K_x}$ LQR gains, the plant must be augmented with Eq. (2.2.1.3). The result of this operation is shown in Eq. (2.2.1.22).

$$\begin{bmatrix} \dot{\boldsymbol{x}}_p \\ \dot{\boldsymbol{e}} \end{bmatrix} = \begin{bmatrix} \boldsymbol{A} & \boldsymbol{0} \\ \boldsymbol{C} & \boldsymbol{0} \end{bmatrix} \begin{bmatrix} \boldsymbol{x}_p \\ \boldsymbol{e} \end{bmatrix} + \begin{bmatrix} \boldsymbol{B} \\ \boldsymbol{D} \end{bmatrix} \boldsymbol{u}. \tag{2.2.1.22}$$

When using *Matlab*™, the $lqr(\ldots)$ command produces a controller $\boldsymbol{K} = [\boldsymbol{K_x}\ \boldsymbol{K_i}]$. By dimensional analysis one can differentiate between the gains.

The Separation Principle

An important principle in state-feedback/observer design is the separation principle. At first it does not seem transparent how the dynamics of the observer affect the overall closed-loop system. The separation principle elucidates the matter. Figure 2.2.1.2 with a suppressed modified reference is used to explain the separation principle. Define the error between the actual state and the estimated states as

$$\boldsymbol{e_1} = \boldsymbol{x_p} - \widehat{\boldsymbol{x}}_{\boldsymbol{p}}. \tag{2.2.1.23}$$

The plant state equation in terms of the error is given by

$$\dot{\boldsymbol{x}}_{\boldsymbol{p}} = \boldsymbol{A}\boldsymbol{x_p} + \boldsymbol{B}\boldsymbol{u} = \boldsymbol{A}\boldsymbol{x_p} - \boldsymbol{B}\boldsymbol{K}\left(\boldsymbol{x_p} - \boldsymbol{e_1}\right) = (\boldsymbol{A} - \boldsymbol{B}\boldsymbol{K})\boldsymbol{x_p} + \boldsymbol{B}\boldsymbol{K}\boldsymbol{e_1}. \tag{2.2.1.24}$$

The observer state equation is

$$\dot{\widehat{\boldsymbol{x}}}_{\boldsymbol{p}} = \boldsymbol{A}\widehat{\boldsymbol{x}}_{\boldsymbol{p}} + \boldsymbol{B}\boldsymbol{u} + \boldsymbol{L}(\boldsymbol{y} - \widehat{\boldsymbol{y}}) = (\boldsymbol{A} - \boldsymbol{B}\boldsymbol{K} - \boldsymbol{L}\boldsymbol{C} + \boldsymbol{L}\boldsymbol{D}\boldsymbol{K})\widehat{\boldsymbol{x}}_{\boldsymbol{p}} + (\boldsymbol{L}\boldsymbol{C} - \boldsymbol{L}\boldsymbol{D}\boldsymbol{K})\boldsymbol{x_p}. \tag{2.2.1.25}$$

The time derivative of the error between the actual state and the estimated state is given by

$$\dot{\boldsymbol{e}}_{\boldsymbol{1}} = \boldsymbol{A}\boldsymbol{x_p} - \boldsymbol{A}\widehat{\boldsymbol{x}}_{\boldsymbol{p}} - \boldsymbol{L}(\boldsymbol{y} - \widehat{\boldsymbol{y}}) = \boldsymbol{A}\boldsymbol{x_p} - \boldsymbol{A}\widehat{\boldsymbol{x}}_{\boldsymbol{p}} - \boldsymbol{L}\left(\boldsymbol{C}\boldsymbol{x_p} - \boldsymbol{C}\widehat{\boldsymbol{x}}_{\boldsymbol{p}}\right) = (\boldsymbol{A} - \boldsymbol{L}\boldsymbol{C})\boldsymbol{e_1}. \tag{2.2.1.26}$$

Augmenting Eq. (2.2.1.25) and Eq. (2.2.1.26) gives

$$\begin{bmatrix} \dot{\boldsymbol{x}}_p \\ \dot{\boldsymbol{e}}_1 \end{bmatrix} = \begin{bmatrix} (\boldsymbol{A} - \boldsymbol{B}\boldsymbol{K}) & \boldsymbol{B}\boldsymbol{K} \\ 0 & (\boldsymbol{A} - \boldsymbol{L}\boldsymbol{C}) \end{bmatrix} \begin{bmatrix} \boldsymbol{x}_p \\ \boldsymbol{e}_1 \end{bmatrix}. \tag{2.2.1.27}$$

Since the state-transition matrix in Eq. (2.2.1.27) is upper triangular, the eigenvalues of the matrix is given by the union of the eigenvalues of the block diagonal matrices. This implies that the stability of the overall system is dependent separately on the stability of the state-feedback dynamics and the observer dynamics or in other words, the dynamics between the observer and the state-feedback are independent (Sidi, 2001, pg 356).

2.2.2. H-infinity Optimization

Work on H_∞ optimization started in the late 1970s after a paper written by Zames (1979) introduced the idea of norm minimization of the sensitivity function. This technique of controller generation used the ideas from the frequency domain arena to specify uncertainty, and used time domain ideas to solve the optimization problem. The main idea in H_∞ optimization is that the controller can be formulated in terms of a free parameter which can be varied to produce stabilizing controllers. This parameter is referred to as the Youla parameter. The generalized plant and control system block diagram in H_∞ optimization is shown in Fig. 2.2.2.1. This section is a summary of the main ideas from Maciejowski (1989) that is required to understand H-infinity optimization.

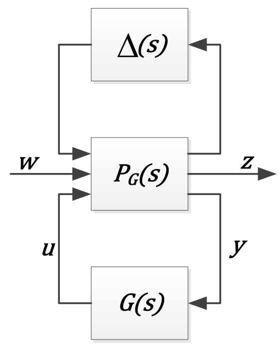

Figure 2.2.2.1 Generalized control system block for H-infinity design

In Fig. 2.2.2.1, $\boldsymbol{P_G}(s)$ represents the generalized plant which is derived from the nominal plant but may also contain weighting matrices based on the plant uncertainty; $\Delta(s)$ represents the equivalent perturbation on the system and $\boldsymbol{G}(s)$ represents the feedback controller. The signal $\boldsymbol{w}$ represents the exogenous input which usually contains the disturbance, noise and reference signals; $\boldsymbol{z}$ represents the error in the system. The aim is to minimize the infinity norm of the error due to the exogenous input. By ignoring the perturbation matrix $\Delta(s)$ and partitioning the generalized plant $\boldsymbol{P_G(s)}$ into a 2×2 system, the system error is given by

$$\boldsymbol{z} = \left[\boldsymbol{P_{G11}} + \boldsymbol{P_{G12}G}(\boldsymbol{I} - \boldsymbol{P_{G22}G})^{-1}\boldsymbol{P_{G21}}\right]\boldsymbol{w}. \qquad (2.2.2.1)$$

The aim can be restated symbolically to minimize the infinity norm of the linear fractional transform

$$\left\|\boldsymbol{P_{G11}} + \boldsymbol{P_{G12}G}(\boldsymbol{I} - \boldsymbol{P_{G22}G})^{-1}\boldsymbol{P_{G21}}\right\|_\infty = \|\boldsymbol{F_l}(\boldsymbol{P_G}, \boldsymbol{G})\|_\infty. \qquad (2.2.2.2)$$

The subscript l in Eq. (2.2.2.2) is used to denote the lower linear fractional transform of Fig. 2.2.2.1.

The H_∞ norm of a matrix transfer function $\boldsymbol{F}(s)$ is defined by $\|\boldsymbol{F}(s)\|_\infty = sup_\omega \bar{\sigma}\big(\boldsymbol{F}(j\omega)\big)$, where $\bar{\sigma}$ is the maximum singular value (Maciejowski, 1989, pg 99). By definition, the singular value decomposition (SVD) of the matrix $\boldsymbol{F}$ is given by $\boldsymbol{F} = \boldsymbol{U\Sigma V^H}$, where $\boldsymbol{U}$ and $\boldsymbol{V}$ are the output and input directions (are also unitary matrices) that produce the corresponding gains or singular values contained in $\boldsymbol{\Sigma}$ which is diagonal The superscript $\boldsymbol{H}$ denotes the Hermitian transpose. Using the above definition for SVD it can be seen that $\boldsymbol{F^H F} = \left(\boldsymbol{U\Sigma V^H}\right)^{\boldsymbol{H}}\boldsymbol{U\Sigma V^H} = \boldsymbol{V\Sigma^2 V^H}$ is an eigen decomposition of $\boldsymbol{F^H F}$, which implies that the singular values of the matrix $\boldsymbol{F}$ is given by $\sigma_i = \sqrt{\lambda_i(\boldsymbol{F^H F})}$ or $\sigma_i = \sqrt{\lambda_i(\boldsymbol{F F^H})}$ (depending on the dimensions of $\boldsymbol{F}$) (Skogestad and Postlethwaite, 2005, pg 521).

By definition (Maciejowski, 1989, pg 56) a system is internally stable if and only if, for the configuration in Fig. 2.2.2.2 (NB. Positive feedback convention), the transfer function matrix that results from the signal $[\boldsymbol{u_1}\ \boldsymbol{u_2}]^{\boldsymbol{T}}$ to $[\boldsymbol{e_1}\ \boldsymbol{e_2}]^{\boldsymbol{T}}$ is exponentially stable i.e.

$$\boldsymbol{H} = \begin{bmatrix} \boldsymbol{H_{11}} & \boldsymbol{H_{12}} \\ \boldsymbol{H_{21}} & \boldsymbol{H_{22}} \end{bmatrix} = \begin{bmatrix} (\boldsymbol{I} - \boldsymbol{GP})^{-1} & (\boldsymbol{I} - \boldsymbol{GP})^{-1}\boldsymbol{G} \\ (\boldsymbol{I} - \boldsymbol{PG})^{-1}\boldsymbol{P} & (\boldsymbol{I} - \boldsymbol{PG})^{-1} \end{bmatrix}, \tag{2.2.2.3}$$

is exponentially stable.

The H_∞ optimization problem is to find a controller that internally stabilizes the feedback system and minimizes Eq. (2.2.2.2).

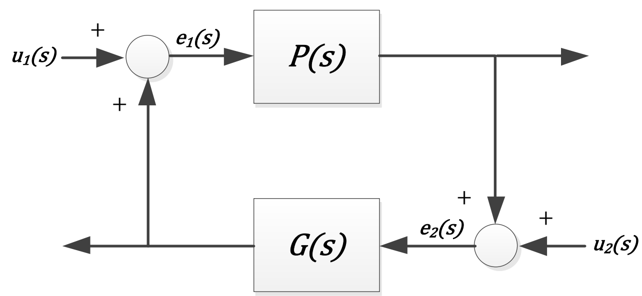

Figure 2.2.2.2 Feedback system for internal stability test

To illustrate this method, (Maciejowski, 1989, pp 267-268) uses a disturbance rejection problem to motivate why H_∞ optimization may be a feasible design tool. The sensitivity of the SISO system in Fig. 2.2.2.3 is given by, $S = (I + PG)^{-1}$. Minimizing $\|S\|_\infty$ is equivalent to pushing down on the peak of the sensitivity function (Kwakernaak, 1993, Section 2). But not only does the peak sensitivity need to be below certain limit; disturbance rejection in the low frequency region is also usually required. In order to include this requirement into the optimization problem, a weighting function is introduced so that the new aim is to minimize the weighted sensitivity $\|W_p S\|_\infty$. By choosing the inverse of the weighting function to be the ideal sensitivity requirement, achieving $\|W_p S\|_\infty \leq 1$ with the controller obtained through the optimization process will result in the specification being met. When there are multiple objectives in the control design as usually is the case, one may stack the performance objectives into the minimization. The specifications for the system may include restrictions on the complementary sensitivity and the reference to plant input response. Accordingly, the optimization will require $\left\| \begin{matrix} W_p S \\ W_t T \\ W_u GS \end{matrix} \right\|_\infty \leq 1$, where W_p, W_t and W_u are the weighting matrices; this is usually referred to as the mixed sensitivity problem.

Youla Parameterization

The Youla parameter is in general an $n \times n$ matrix from a set of stable transfer functions in the H_∞ space (Hardy space). The intention is to get the controller, in some simple relation, in terms of the plant and the Youla parameter. The key step done in Maciejowski (1989,pg 268) towards fulfilling this goal is to set the Youla parameter $Q(s)$ as in Eq. (2.2.2.4) for a feedback configuration shown in Fig. 2.2.2.3.

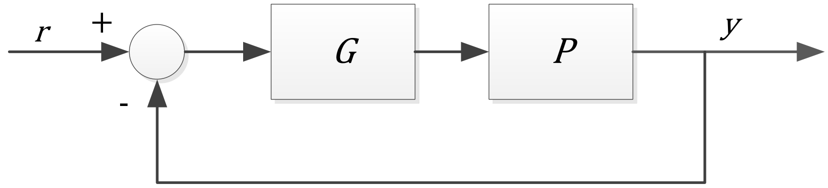

Figure 2.2.2.3 SISO feedback system used to investigate Youla parameterization

$$Q(s) = G(I + PG)^{-1} \tag{2.2.2.4}$$

Then the sensitivity is given by

$$S = I - T = I - PG(I + PG)^{-1} = I - PQ. \tag{2.2.2.5}$$

Solving Eq. (2.2.2.4) for the controller

$$Q(I + PG) = G, \tag{2.2.2.6}$$

$$G = (I - QP)^{-1}Q. \tag{2.2.2.7}$$

For both MIMO/SISO case, internal stability will be guaranteed if $\boldsymbol{Q}$ is stable since the internal stability matrix $\boldsymbol{H}$ in Eq. (2.2.2.3) can be rewritten as

$$\boldsymbol{H} = \begin{bmatrix} \boldsymbol{H}_{11} & \boldsymbol{H}_{12} \\ \boldsymbol{H}_{21} & \boldsymbol{H}_{22} \end{bmatrix} = \begin{bmatrix} \boldsymbol{I} - \boldsymbol{QP} & \boldsymbol{Q} \\ (\boldsymbol{I} - \boldsymbol{PQ})\boldsymbol{P} & \boldsymbol{I} - \boldsymbol{PQ} \end{bmatrix}. \tag{2.2.2.8}$$

The sensitivity problem can be restated in terms of the Youla parameter as

$$min\left\|W_p S\right\|_\infty = \min_{Q \in H_\infty} \left\|W_p(I - PQ)\right\|_\infty. \tag{2.2.2.9}$$

Using Matrix Fractional Representation

This section restates the theorems and definitions that appear in (Maciejowski, 1989, Section 6.42) which are relevant to simultaneous stabilization. The aim is to understand the solution of H-infinity problems so that they may be modified for new applications or can be ameliorated. The parameterization is done in terms of matrix fractional representations of the plant $\boldsymbol{P}$.

Definition: Every proper transfer function matrix can be written in the form

$$\boldsymbol{P} = \boldsymbol{N}(s)\boldsymbol{M}^{-1}(s) = \widetilde{\boldsymbol{D}}^{-1}(s)\widetilde{\boldsymbol{M}}(s), \tag{2.2.2.10}$$

where $\boldsymbol{N}, \boldsymbol{M}, \widetilde{\boldsymbol{N}}, \widetilde{\boldsymbol{M}}$ are stable transfer functions, with $\boldsymbol{N}$ and $\boldsymbol{M}$ right coprime and $\widetilde{\boldsymbol{N}}$ and $\widetilde{\boldsymbol{M}}$ left coprime.

As shown in Maciejowski (1989, Section 6.4), left coprime realization of the plant $(\boldsymbol{P}: \boldsymbol{A}, \boldsymbol{B}, \boldsymbol{C}, \boldsymbol{D})$ can be obtained by contriving a state-feedback structure with stabilizing state-feedback gain $\boldsymbol{F}$. For right coprime matrices the realization of $\boldsymbol{P}$ is

$$\boldsymbol{M}(\boldsymbol{s}) = \boldsymbol{F}(s\boldsymbol{I} - \boldsymbol{A} - \boldsymbol{BF})^{-\mathbf{1}}\boldsymbol{B} + \boldsymbol{I}, \tag{2.2.2.11}$$

$$\boldsymbol{N}(s) = (\boldsymbol{C} + \boldsymbol{DF})(s\boldsymbol{I} - \boldsymbol{A} - \boldsymbol{BF})^{-\mathbf{1}}\boldsymbol{B} + \boldsymbol{D}. \tag{2.2.2.12}$$

For left coprime matrix realization of the plant, a stable observer gain $\boldsymbol{H}$ is chosen such that the eigenvalues of $(\boldsymbol{A} + \boldsymbol{HC})$ are in the left hand plane. The realization of $\boldsymbol{P}$ is

$$\widetilde{\boldsymbol{M}}(\boldsymbol{s}) = -\left[\boldsymbol{C}(s\boldsymbol{I} - \boldsymbol{A} - \boldsymbol{HC})^{-\mathbf{1}}\boldsymbol{H} + \boldsymbol{I}\right], \tag{2.2.2.13}$$

$$\widetilde{\boldsymbol{N}}(s) = \boldsymbol{C}(s\boldsymbol{I} - \boldsymbol{A} - \boldsymbol{HC})^{-1}(\boldsymbol{B} + \boldsymbol{HD}) + \boldsymbol{D}. \tag{2.2.2.14}$$

It is also shown in Maciejowski (1989, Section 6.4.2) that if the plant $\boldsymbol{P}$ and controller $\boldsymbol{G}$ have fractional representation $\boldsymbol{P} = \boldsymbol{NM}^{-1}$ and $\boldsymbol{G} = \boldsymbol{UV}^{-1}$, the feedback loop is stable if and only if

$$\begin{bmatrix} \boldsymbol{M} & \boldsymbol{U} \\ \boldsymbol{N} & \boldsymbol{V} \end{bmatrix}^{-\mathbf{1}} \tag{2.2.2.15}$$

and

$$\begin{bmatrix} \widetilde{\boldsymbol{V}} & -\widetilde{\boldsymbol{U}} \\ -\widetilde{\boldsymbol{N}} & \widetilde{\boldsymbol{M}} \end{bmatrix}^{-\mathbf{1}} \tag{2.2.2.16}$$

are stable.

Another important theorem (Maciejowski, 1989, Theorem 6.3) in the Youla parameterization development states that the matrices $\boldsymbol{M}, \boldsymbol{N}, \boldsymbol{U}, \boldsymbol{V}, \widetilde{\boldsymbol{M}}, \widetilde{\boldsymbol{N}}, \widetilde{\boldsymbol{U}}$ and $\widetilde{\boldsymbol{V}}$ can be chosen so that

$$\begin{bmatrix} \widetilde{\boldsymbol{V}} & -\widetilde{\boldsymbol{U}} \\ -\widetilde{\boldsymbol{N}} & \widetilde{\boldsymbol{M}} \end{bmatrix} \begin{bmatrix} \boldsymbol{M} & \boldsymbol{U} \\ \boldsymbol{N} & \boldsymbol{V} \end{bmatrix} = \begin{bmatrix} \boldsymbol{I} & \mathbf{0} \\ \mathbf{0} & \boldsymbol{I} \end{bmatrix}, \tag{2.2.2.17}$$

where the controller is represented by $\boldsymbol{G} = \boldsymbol{UV}^{-\mathbf{1}} = \widetilde{\boldsymbol{V}}^{-\mathbf{1}}\widetilde{\boldsymbol{U}}$. The proof of the theorem (Maciejowski, 1989, pg 277) above shows that all stabilizing controllers have state-feedback/observer configuration.

The Bezout theorem is used to test for coprimeness. It states that $\boldsymbol{U}$ and $\boldsymbol{V}$ are coprime if and only if there exits stable matrices $\boldsymbol{X}$ and $\boldsymbol{Y}$, such that $\boldsymbol{XU} + \boldsymbol{YV} = \boldsymbol{I}$. By applying the Bezout theorem to Eq. (2.2.2.17) it can be shown that the four fractional representations (for the controller and the plant) are indeed coprime.

The last important theorem for the Youla parameterization section is that if a controller can be chosen as, $\boldsymbol{G_0} = \boldsymbol{U_0}\boldsymbol{V_0^{-1}} = \widetilde{\boldsymbol{V}}_\mathbf{0}^{-\mathbf{1}}\widetilde{\boldsymbol{U}}_\mathbf{0}$ such that Eq. (2.2.2.17) is satisfied, any $\boldsymbol{Q} \in \boldsymbol{H}_\infty$ can be chosen so that a stabilizing controller given by

$$\boldsymbol{G} = (\boldsymbol{U_0} + \boldsymbol{MQ})(\boldsymbol{V_0} + \boldsymbol{NQ})^{-1} = \left(\widetilde{\boldsymbol{V}}_\mathbf{0} + \boldsymbol{Q}\widetilde{\boldsymbol{N}}\right)^{-\mathbf{1}}\left(\widetilde{\boldsymbol{U}}_\mathbf{0} + \boldsymbol{Q}\widetilde{\boldsymbol{M}}\right), \tag{2.2.2.18}$$

$$= \boldsymbol{G_0} + \widetilde{\boldsymbol{V}}_\mathbf{0}^{-\mathbf{1}}\boldsymbol{Q}\left(\boldsymbol{I} + \boldsymbol{V_0^{-1}}\boldsymbol{NQ}\right)^{-\mathbf{1}}\boldsymbol{V_0^{-1}}, \tag{2.2.2.19}$$

exists.

By drawing a block diagram representation of Eq. (2.2.1.19) or by applying the reverse linear fractional transform in Eq. (2.2.2.2), one can split the controller into a fixed part and a varying parameter. Figure 2.2.2.1 is redrawn in Fig. 2.2.2.4 without the perturbation and the controller split into a fixed part $\boldsymbol{J}$ and the Youla parameter $\boldsymbol{Q}$. The controller is given by the linear fractional transform $\boldsymbol{G}=\boldsymbol{F_l}(\boldsymbol{J},\boldsymbol{Q})$.

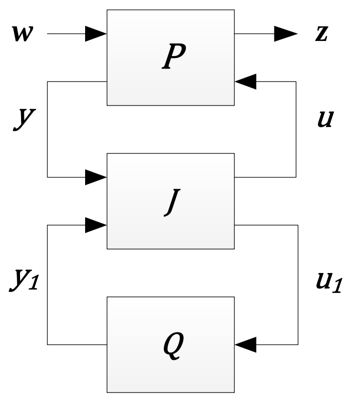

Figure 2.2.2.4 Block diagram of H-infinity system with controller $\boldsymbol{G}=\boldsymbol{F_l}(\boldsymbol{J},\boldsymbol{Q})$

It is shown in (Maciejowski, 1989, Section 6.43) that the fixed part of the controller has state-space realization given by

$$\boldsymbol{J}\!:\left(\boldsymbol{A}+\boldsymbol{BF}+\boldsymbol{HC}+\boldsymbol{HDF},[-\boldsymbol{H}\;\;\boldsymbol{B}+\boldsymbol{HD}],\begin{bmatrix}\boldsymbol{F}\\ -(\boldsymbol{C}+\boldsymbol{DF})\end{bmatrix},\begin{bmatrix}\boldsymbol{0} & \boldsymbol{I}\\ \boldsymbol{I} & -\boldsymbol{D}\end{bmatrix}\right), \qquad (2.2.2.20)$$

where the matrix elements are as defined in the section above. The state-space realization of $\boldsymbol{Q}$ can be augmented to the system to find the state-space realization of the entire controller. As stated earlier, the aim of the H_∞ optimization is to find a controller that minimizes Eq. (2.2.2.2). In order to get back in line with that idea, we need to absorb the plant dynamics into the equation that gives the exogenous input to error outputs. The absorption of the plant into the fractional transform gives Fig. 2.2.2.5 and the resulting equation for the exogenous input to error output is given by (NB. $\boldsymbol{P_{22}}=\boldsymbol{P}$)

$$\left[\boldsymbol{T_{11}}+\boldsymbol{T_{12}}\boldsymbol{Q}(\boldsymbol{I}-\boldsymbol{T_{22}}\boldsymbol{Q})^{-1}\boldsymbol{T_{21}}\right]=\boldsymbol{F_l}(\boldsymbol{T},\boldsymbol{Q}) \qquad (2.2.2.21)$$

$$=\boldsymbol{F_l}(\boldsymbol{P},\boldsymbol{K})=\boldsymbol{P_{11}}+\boldsymbol{P_{12}}\boldsymbol{G}(\boldsymbol{I}-\boldsymbol{P_{22}}\boldsymbol{G})^{-1}\boldsymbol{P_{21}}. \qquad (2.2.2.22)$$

By the substituting of Eq. (2.2.2.18) into Eq. (2.2.2.22) one obtains

$$\boldsymbol{F_l}(\boldsymbol{P},\boldsymbol{K})=\boldsymbol{P_{11}}-\boldsymbol{P_{12}}(\boldsymbol{U_0}+\boldsymbol{MQ})\widetilde{\boldsymbol{M}}\boldsymbol{P_{21}}=\boldsymbol{P_{11}}-\boldsymbol{P_{12}}\boldsymbol{U_0}\widetilde{\boldsymbol{M}}\boldsymbol{P_{21}}-\boldsymbol{P_{12}}\boldsymbol{MQ}\widetilde{\boldsymbol{M}}\boldsymbol{P_{21}}. \qquad (2.2.2.23)$$

Equation (2.2.2.21) and Eq. (2.2.2.23) are compared to obtain the following $\boldsymbol{T}$ components and their respective state-space realization

$$\boldsymbol{T_{11}}=\boldsymbol{P_{11}}-\boldsymbol{P_{12}}\boldsymbol{U_0}\widetilde{\boldsymbol{M}}\boldsymbol{P_{21}}\!:$$
$$\left(\begin{bmatrix}\boldsymbol{A}+\boldsymbol{B_2F} & -\boldsymbol{B_2F}\\ \boldsymbol{0} & \boldsymbol{A}+\boldsymbol{HC_2}\end{bmatrix},\begin{bmatrix}\boldsymbol{B}\\ \boldsymbol{B_1}+\boldsymbol{HD_{21}}\end{bmatrix},[\boldsymbol{C_1}+\boldsymbol{D_{12}F}\quad -\boldsymbol{D_{12}F}],\boldsymbol{D_{11}}\right), \qquad (2.2.2.24)$$

$$\boldsymbol{T_{12}}=-\boldsymbol{P_{12}}\boldsymbol{M}:\ (\boldsymbol{A}+\boldsymbol{B_2F},\ \boldsymbol{B_2},\ \boldsymbol{C_1}+\boldsymbol{D_{12}F},\ \boldsymbol{D_{12}}), \qquad (2.2.2.25)$$

$$\boldsymbol{T_{21}} = \widetilde{\boldsymbol{M}}\boldsymbol{P_{21}} : \ (\boldsymbol{A} + \boldsymbol{HC_2},\ \boldsymbol{B_1} + \boldsymbol{HD_{21}}, \boldsymbol{C_2}, \boldsymbol{D_{21}}), \tag{2.2.2.26}$$

$$\boldsymbol{T_{22}} = \boldsymbol{0}. \tag{2.2.2.27}$$

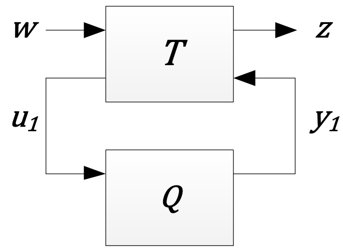

Figure 2.2.2.5 Optimization problem drawn with the plant absorbed into $\boldsymbol{T}$

The solution to the optimization problem can now be stated as to find

$$\min_{\boldsymbol{Q}\in\boldsymbol{H}_\infty} \|\boldsymbol{F_l}(\boldsymbol{P}, \boldsymbol{K})\|_\infty = \min_{\boldsymbol{Q}\in\boldsymbol{H}_\infty} \|\boldsymbol{T_{11}} + \boldsymbol{T_{12}}\boldsymbol{Q}\boldsymbol{T_{21}}\|_\infty. \tag{2.2.2.28}$$

This is equivalent to solving the Hankel approximation problem (Maciejowski, 1989, pg 293). The matrices $\boldsymbol{T_{12}}$ and $\boldsymbol{T_{21}}$ can be made all pass by appropriate choice of $\boldsymbol{F}$ and $\boldsymbol{H}$. For now we assume that they are square matrices. Eq. (2.2.2.28) becomes

$$\begin{aligned} &\min_{\boldsymbol{Q}\in\boldsymbol{H}_\infty} \|\boldsymbol{T_{11}} + \boldsymbol{T_{12}}\boldsymbol{Q}\boldsymbol{T_{21}}\|_\infty \\ &= \min_{\boldsymbol{Q}\in\boldsymbol{H}_\infty} \left\|\boldsymbol{T_{12}}\left(\boldsymbol{T_{12}^H}\boldsymbol{T_{11}}\boldsymbol{T_{21}^H} + \boldsymbol{Q}\right)\boldsymbol{T_{21}}\right\|_\infty = \min_{\boldsymbol{Q}\in\boldsymbol{H}_\infty} \left\|\boldsymbol{T_{21}}\boldsymbol{T_{11}^H}\boldsymbol{T_{12}} + \boldsymbol{Q^H}\right\|_\infty. \end{aligned} \tag{2.2.2.29}$$

(NB. In the last step that $\sigma(\boldsymbol{XAY}) = \sigma(\boldsymbol{A})$, where $\boldsymbol{X}$ and $\boldsymbol{Y}$ are all pass. Also, $\boldsymbol{A^H}$ denotes the Hermitian transpose of $\boldsymbol{A}$). The optimization problem gets reduced to trying to approximate $\boldsymbol{T_{21}}\boldsymbol{T_{11}^H}\boldsymbol{T_{12}}$ with $-\boldsymbol{Q^H}$. This is known as the 1-block problem for the un-stacked sensitivity problem. When $\boldsymbol{T_{12}}$ has more rows than columns *(thin)* and $\boldsymbol{T_{21}}$ has more columns than rows *(fat)*, the problem becomes more complicated, resulting in the 2- and 4- block problems which is the case for mixed sensitivity problems (see Maciejowski, 1989, Section 6.5.3 for result).

This section gives one method that is used to solve the H-infinity problem i.e. through model matching. The constraints on the Youla parameter is very abstract, hence it is not clear how this solution may be modified to improve the H-infinity design method. The next section contains a different approach to the solution of the H-infinity problem which at first seems as a promising avenue to investigate.

2.2.3. Simultaneous Stabilization

The motivation for simultaneous stabilization is to find a controller that stabilizes a number of discrete plant cases. Simultaneous stabilization in SISO QFT is lucidly inherent in the methodology. As pointed out by Professor Boje, the H_∞ design may be made less conservative if the problem can be broken down into a number of "smaller" (re-formulated) H_∞ problems. This idea is illustrated in this section. If the plant is uncertain and the multiplicative perturbation model is used, the uncertainty is bounded by a disk which is the source of conservatism in the design; this is shown for a SISO system in Fig. 2.2.3.1.

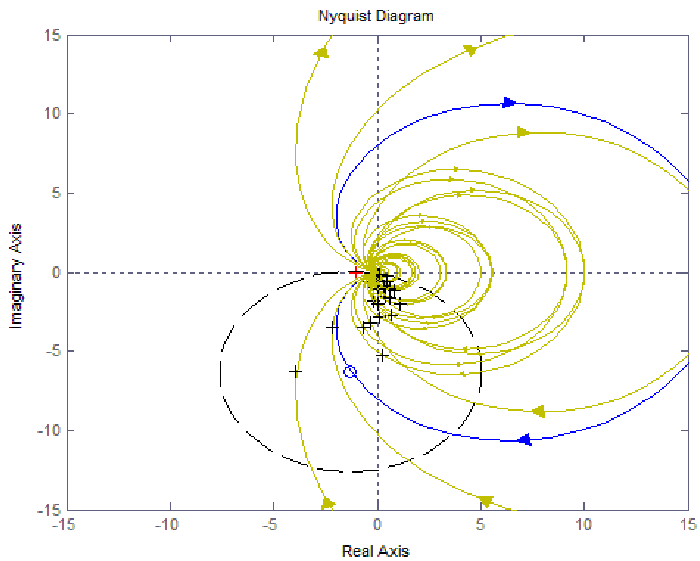

Figure 2.2.3.1 Nyquist plot of an uncertain system; nominal plant shown in blue; plant location for some $\omega = \omega_1$ shown as crosses

If the problem can be re-formulated into finding a controller that would stabilize "multiple nominal" loops with smaller uncertainty disks, the solution will be less conservative. For example, if the problem is broken down into two parts, an illustration of reducing the conservatism through simultaneous stabilization is shown in Fig. 2.2.3.2. The H_∞ optimization paradigm seems like the appropriate method to investigate this idea because of the parameterization of the stabilizing controllers. If a set of stabilizing controllers can be found for each nominal loop, the intersection of the controllers will result in a controller that stabilizes all plants with their smaller respective uncertainty disks.

A Linear Matrix Inequality (LMI) approach initially seemed liked a propitious way to solving the simultaneous stabilization H_∞ problem. A LMI has the canonical form

$$\boldsymbol{L}(\boldsymbol{x}) = \boldsymbol{L_0} + x_1\boldsymbol{L_1} + \cdots + x_N\boldsymbol{L_N} < \boldsymbol{0} \qquad (2.2.3.1)$$

where $\boldsymbol{L_0}, \dots, \boldsymbol{L_N}$ are symmetric matrices and $\boldsymbol{x} = (x_1, \dots, x_N)^{\boldsymbol{T}}$ is the vector of scalar variables to be determined. Many control problems can be manipulated into a convex optimization problem which can then be solved with LMI tools if a solution exists. There are very efficient computational solvers available for solving LMI's.

An alternative to the model matching solution to the H_∞ problem is an explicit solution in terms of the solution of two algebraic Riccati equations (ARE), this idea is expounded in (Glover and Doyle, 1988).

Due to certain limitations in this method such as the applicability to regular plants only, other techniques for solving the H_∞ problem was investigated. One of these investigations was into the LMI solution to the H_∞ problem.

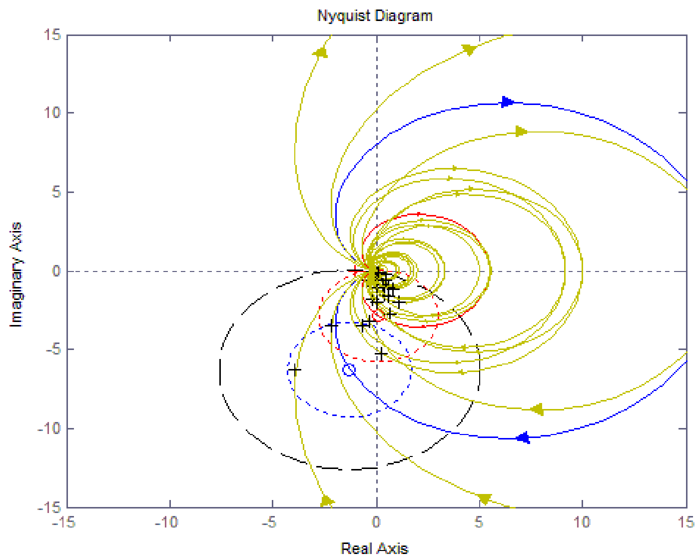

Figure 2.2.3.2 Nyquist plot of an uncertain system showing the use of two nominal loops to reduce conservatism of H-infinity design

The critical Lemma to formulating the H_∞ solution in terms of LMI's is the Bounded Real Lemma which is given below.

Given the continuous-time transfer function $\boldsymbol{T}(s) = \boldsymbol{C}(s\boldsymbol{I} - \boldsymbol{A})^{-1}\boldsymbol{B} + \boldsymbol{D}$, the following statements are equivalent (Gahinet and Apkarian, 1994):

i) $\left\|\boldsymbol{C}(s\boldsymbol{I} - \boldsymbol{A})^{-1}\boldsymbol{B} + \boldsymbol{D}\right\|_\infty < \gamma$, and $\boldsymbol{A}$ is stable;

ii) There exists a symmetric positive definite solution $\boldsymbol{X}$ to the LMI:

$$\begin{pmatrix} \boldsymbol{A}^T\boldsymbol{X} + \boldsymbol{X}\boldsymbol{A} & \boldsymbol{X}\boldsymbol{B} & \boldsymbol{C}^T \\ \boldsymbol{B}^T\boldsymbol{X} & -\gamma\boldsymbol{I} & \boldsymbol{D}^T \\ \boldsymbol{C} & \boldsymbol{D} & -\gamma\boldsymbol{I} \end{pmatrix} < 0 \tag{2.2.3.2}$$

The state-space form of the generalized plant (may include weighting matrices) in Fig. 2.2.2.1 can be written in block matrix form (excluding the perturbation matrix) as

$$\boldsymbol{P_G}: \left(\boldsymbol{A}, [\boldsymbol{B}_1, \boldsymbol{B}_2], \begin{bmatrix} \boldsymbol{C}_1 \\ \boldsymbol{C}_2 \end{bmatrix}, \begin{bmatrix} \boldsymbol{D}_{11} & \boldsymbol{D}_{12} \\ \boldsymbol{D}_{21} & \boldsymbol{D}_{22} \end{bmatrix}\right). \tag{2.2.3.3}$$

Using the Bounded Real Lemma, Gahinet and Apkarian (1994) proved that the solution to the two ARE's can be obtained by solving the following LMI

$$\begin{pmatrix} \boldsymbol{\mathcal{N}_R} & \boldsymbol{0} \\ \boldsymbol{0} & \boldsymbol{I} \end{pmatrix}^{\boldsymbol{T}} \begin{pmatrix} \boldsymbol{AR}+\boldsymbol{RA^T} & \boldsymbol{RC_1^T} & \boldsymbol{B_1} \\ \boldsymbol{C_1R} & -\gamma\boldsymbol{I} & \boldsymbol{D_{11}} \\ \boldsymbol{B_1^T} & \boldsymbol{D_{11}^T} & -\gamma\boldsymbol{I} \end{pmatrix} \begin{pmatrix} \boldsymbol{\mathcal{N}_R} & \boldsymbol{0} \\ \boldsymbol{0} & \boldsymbol{I} \end{pmatrix} < 0 \tag{2.2.3.4}$$

$$\begin{pmatrix} \boldsymbol{\mathcal{N}_S} & \boldsymbol{0} \\ \boldsymbol{0} & \boldsymbol{I} \end{pmatrix}^{\boldsymbol{T}} \begin{pmatrix} \boldsymbol{A^TS}+\boldsymbol{SA} & \boldsymbol{SB_1} & \boldsymbol{C_1^T} \\ \boldsymbol{B_1^TS} & -\gamma\boldsymbol{I} & \boldsymbol{D_{11}^T} \\ \boldsymbol{C_1} & \boldsymbol{D_{11}} & -\gamma\boldsymbol{I} \end{pmatrix} \begin{pmatrix} \boldsymbol{\mathcal{N}_S} & \boldsymbol{0} \\ \boldsymbol{0} & \boldsymbol{I} \end{pmatrix} < 0 \tag{2.2.3.5}$$

$$\begin{pmatrix} \boldsymbol{R} & \boldsymbol{I} \\ \boldsymbol{I} & \boldsymbol{S} \end{pmatrix} \geq \boldsymbol{0} \tag{2.2.3.6}$$

where $\boldsymbol{\mathcal{N}_R}$ and $\boldsymbol{\mathcal{N}_S}$ are bases for the null spaces of $\left(\boldsymbol{B_2^T}, \boldsymbol{D_{12}^T}\right)$ and $(\boldsymbol{C_2}, \boldsymbol{D_{21}})$, respectively.

Following the introductory idea of simultaneous stabilization of two plants, it may be plausible to find the two ARE's that satisfy a stacked LMI containing Eqs (2.2.3.4) - (2.2.3.6) for the two individual plants. The problem that was found through the investigation is that the final controller solution is given in terms of the two ARE's and the plant dynamics, and the question that remained was which plant or how must the plants be combined to reconstruct the controller.

2.2.4. Applying the H-infinity Design Method

The application of H_∞ optimization to control system design is less tedious than the QFT technique for multivariable systems. The reason for this is that the majority of the work in H_∞ design for real systems is to select proper weighting functions that will ensure that the specifications are met if the optimization is successful. There are commercially available algorithms that perform the optimization which relieves the designer of much work. In order to obtain a controller that meets the specifications for an uncertain plant, there needs to be a methodology behind obtaining the weighting functions. This will be shown next and is based largely on the work of (Sidi, 2002).

Choosing Complementary Sensitivity Weighting Function

An expected outcome of a control system design for an uncertain plant is for the system to be robustly stable i.e. the system must be stable (meet the robust stability specification) for all plant cases. The first step towards achieving this is to model the plant uncertainty. The first approach shown is to use the output multiplicative perturbation model as depicted in Fig. 2.2.4.1.

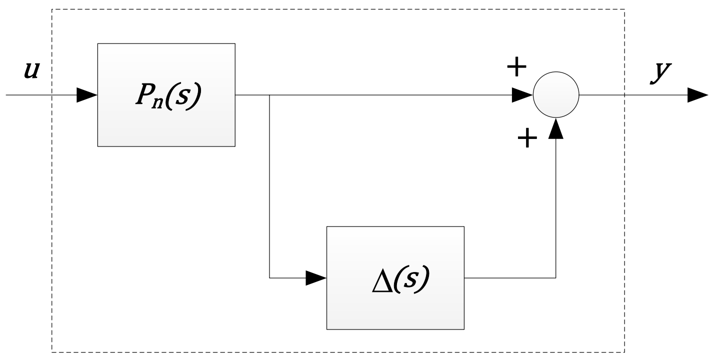

Figure 2.2.4.1 Output multiplicative modelling of plant uncertainty

The uncertain plant is given by

$$\boldsymbol{P}(s) = [\boldsymbol{I} + \Delta(s)]\boldsymbol{P}_{\boldsymbol{n}}(s), \tag{2.2.4.1}$$

with $\Delta(s) = w_0(s)\Delta_0(s)$, $\|\Delta_0(s)\|_\infty \le 1$. The function $w_0(s)$ is a scalar frequency dependent weighting function. By solving Eq. (2.2.4.1) for the weighting function, one obtains the following constraint,

$$\delta_{om}(j\omega) = \max_{\boldsymbol{P}\in\{\boldsymbol{P}\}} \bar{\sigma}\left\{[\boldsymbol{P}(j\omega) - \boldsymbol{P}_{\boldsymbol{n}}(j\omega)]\boldsymbol{P}_{\boldsymbol{n}}^{-1}(j\omega)\right\} \le |w_0(j\omega)| \tag{2.2.4.2}$$

For a SISO system, the system is stable if the maximum magnitude of the difference of the nominal loop gain and other loop gains (for the uncertain system) is less than the magnitude from the nominal loop to the -1 point for all frequencies (Kwakernaak, 1993, Section 3). This is stated as an equation below and can be derived from Fig. 2.2.4.2.

$$|L(j\omega) - L_n(j\omega)| < |-1 - L_n(j\omega)|, \qquad \forall\omega. \tag{2.2.4.3}$$

Manipulating Eq. (2.2.4.3)

$$|L(j\omega) - L_n(j\omega)| \frac{1}{|1 + L_n(j\omega)|} \times \frac{|L_n(j\omega)|}{|L_n(j\omega)|} = \frac{|L(j\omega) - L_n(j\omega)|}{|L_n(j\omega)|} |T_n(j\omega)| < 1 \quad (2.2.4.4)$$

$$\left(\frac{|P(j\omega) - P_n(j\omega)|}{|P_n(j\omega)|}\right) |T_n(j\omega)| = |W_t||T_n(j\omega)| < 1 \quad (2.2.4.5)$$

It was found (Doyle and Stein, 1981) that Eq. (2.2.4.5) also applies for multivariable systems. The term on the left hand side of Eq. (2.2.4.5) containing the plant terms is equal to the required weighting function in Eq. (2.2.4.2) for a SISO case. Since Eq. (2.2.4.5) applies for multivariable systems as well, robust stability can be guaranteed if the weighting function is chosen such that Eq. (2.2.4.2) is satisfied i.e. $\|(w_0\boldsymbol{I})\boldsymbol{T_n}\|_\infty < 1$ for multivariable systems. A common variation on this type of perturbation model is the input multiplicative perturbation model where the perturbation is reflected on the input.

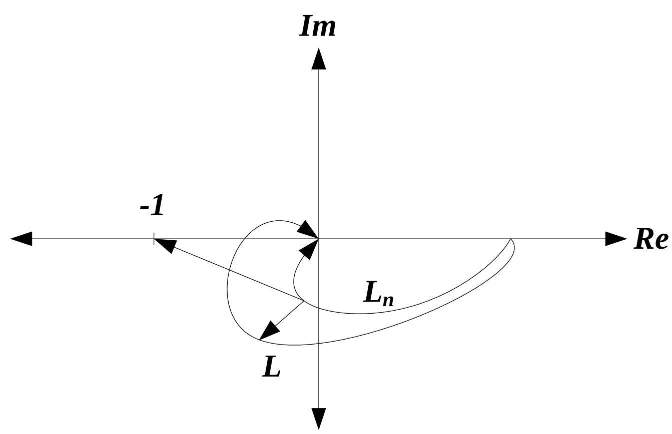

Figure 2.2.4.2 Nyquist plot of some nominal loop and a perturbed loop for a SISO system

Another perturbation model is the additive perturbation model illustrated in Fig. 2.2.4.3. The plant is given by

$$\boldsymbol{P}(s) = \boldsymbol{P_n}(s) + \Delta(s). \quad (2.2.4.6)$$

with $\bar{\sigma}\big(\Delta(j\omega)\big) < |r(\omega)| \;\; \forall\omega$.

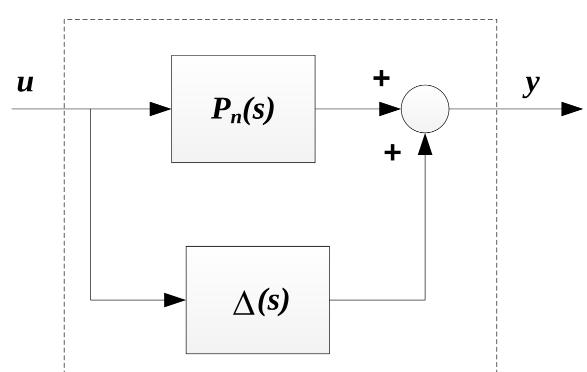

Figure 2.2.4.3 Additive perturbation model

If the plant represented by Fig. 2.2.4.3 is put into a classical positive feedback loop with controller $\boldsymbol{G}$, the resulting block diagram can be manipulated so that the perturbation is isolated in a single feedback loop. This allows for the small gain theorem to be applied. The small gain theorem states that if the norm of the elements in a feedback loop is less than unity and the elements themselves are stable, the closed loop system will be stable (Skogestad and Postlethwaite, 2005, pg 156). Performing the manipulation gives $\boldsymbol{G}(\boldsymbol{I}-\boldsymbol{PG})^{-\mathbf{1}}$ in the forward path and Δ in the feedback path. Hence the system is stable if

$$\left\|\Delta\boldsymbol{G}(\boldsymbol{I}-\boldsymbol{PG})^{-\mathbf{1}}\right\|_{\infty} < 1, \tag{2.2.4.7}$$

$$\left\|\Delta\boldsymbol{G}(\boldsymbol{I}-\boldsymbol{PG})^{-\mathbf{1}}\right\|_{\infty} = \|r^{-1}\Delta\|_{\infty}\left\|r\boldsymbol{G}(\boldsymbol{I}-\boldsymbol{PG})^{-\mathbf{1}}\right\|_{\infty} < \left\|r\boldsymbol{G}(\boldsymbol{I}-\boldsymbol{PG})^{-\mathbf{1}}\right\|_{\infty}. \tag{2.2.4.8}$$

The H_∞ problem it to $minimize$ $\|r\boldsymbol{GS}\|_\infty$, and ensure it is less than unity.

Choosing Sensitivity Weighting Function

In order for the desired disturbance rejection/tracking response to be achieved for an uncertain plant, the sensitivity needs to be designed based on the uncertainty. The sensitivity function is directly influenced by the sensitivity weighting function $\boldsymbol{W_s}$. In (Sidi, 2002), the weighting matrix is taken to be diagonal and the elements are chosen based on the definition of sensitivity

$$S_P^T = \frac{\partial T/T}{\partial P/P}. \tag{2.2.4.9}$$

For a BNIA systems the diagonal elements are chosen such that (Sidi, 2001, pg 389)

$$|1/w_{s\,ii}| \leq \frac{\Delta T_{ii}\ [dB]}{\max \Delta\, \sigma(\boldsymbol{P})\ [dB]}. \tag{2.2.4.10}$$

By using maximum change of the singular values of the plant, the uncertainty in the off-diagonal elements are also taken into account. Equation (2.2.4.10) must be calculated on a frequency basis and a curve must be fitted for the data. The weighting function $w_{s\,ii}$ must be stable and proper.

Robust performance in quantitative design is defined as the ability for the designed control system to lie within bounded specification even though the plant may be subjected to quantified perturbations. In the QFT methodology robust performance is taken care of by the use of templates. It is proven in (Sidi, 2001, pg 228) that for SISO system robust performance is achieved by ensuring

$$\max_{P\in\{P\}}[|W_P S_n| + |W_t T_n|] < 1. \tag{2.2.4.11}$$

Equation (2.2.4.11) is equivalent to the stacking the weighted sensitivity and the weighted complementary sensitivity into the $\|\cdot\|_\infty$ minimization. It is shown in (Zhou and Doyle, 1998) that this criterion can be extended for multivariable system. For multivariable systems the scalar elements of Eq. (2.2.4.11) should be replaced with the matrix equivalents and the use of maximum singular values.

Choosing Control Effort Weighting Function

The last common weighting function used in H_∞ design is for the weighting of the control effort. This matrix is usually used as a tuning matrix for the system because it can impose constraints on the actuators. The diagonal elements of the control effort weighting matrix is chosen to impose

$$\|\boldsymbol{W_u GS}\|_\infty < 1. \qquad (2.2.4.12)$$

The matrix gain $|\boldsymbol{GS}|$ describes the gain from reference/disturbance/sensor-noise to plant input. The final step in the H_∞ design procedure in (Sidi, 2002) is to design the pre-filter by using classical Bode design methods. The idea of pre-filter design in the multivariable case is the same as the SISO case i.e. shaping the closed-loop transfer function to match the reference to output desired characteristics.

2.3. An H-infinity/QFT Theory

Due to the conservativeness (through uncertainty modelling) and the lack of transparency in H-infinity design, a modification of the H-infinity design process that uses QFT may be beneficial. If a diagonal controller can be extracted from the H-infinity design, the overall design may be tuned via the diagonal controller using QFT. This will result in an H-infinity/QFT design. This design process was suggested by Professor Boje as a way to methodically reduce the conservativeness of the H-infinity controller via QFT while exploiting the controller's non-diagonal nature.

2.3.1. Methodology

Given a fully populated H-infinity controller $\boldsymbol{G}$, one can extract a diagonal matrix using the following procedure.

Define $g_{22}' = g_{22} - \frac{g_{12}g_{21}}{g_{11}}$ and multiply $\boldsymbol{G}$ from the right by a unimodular matrix to eliminate term $(1,2)$

$$\boldsymbol{GR} = \begin{bmatrix} g_{11} & g_{12} \\ g_{21} & g_{22} \end{bmatrix} \begin{bmatrix} 1 & -g_{12}/g_{11} \\ 0 & 1 \end{bmatrix} = \begin{bmatrix} g_{11} & 0 \\ g_{21} & g_{22}' \end{bmatrix}. \tag{2.3.1.1}$$

Multiply $\boldsymbol{GR}$ from the left by a unimodular matrix to eliminate term $(2,1)$

$$\boldsymbol{LGR} = \begin{bmatrix} 1 & 0 \\ -g_{21}/g_{11} & 1 \end{bmatrix} \begin{bmatrix} g_{11} & 0 \\ g_{21} & g_{22}' \end{bmatrix} = \begin{bmatrix} g_{11} & 0 \\ 0 & g_{22}' \end{bmatrix} = \boldsymbol{G_d}. \tag{2.3.1.2}$$

The H-infinity controller in terms of a diagonal controller is given by

$$\boldsymbol{G} = \boldsymbol{L^{-1}G_dR^{-1}} = \begin{bmatrix} 1 & 0 \\ g_{21}/g_{11} & 1 \end{bmatrix} \begin{bmatrix} g_{11} & 0 \\ 0 & g_{22}' \end{bmatrix} \begin{bmatrix} 1 & g_{12}/g_{11} \\ 0 & 1 \end{bmatrix}. \tag{2.3.1.3}$$

The block diagram in Fig. 2.3.1.1 is a representation of Eq. (2.3.1.3); it shows how the signal gets transferred through the split controller.

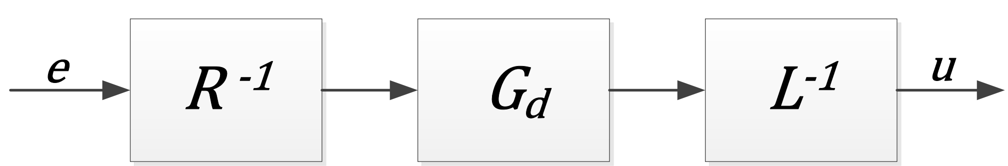

Figure 2.3.1.1 Block diagram showing signal transmission through split H-infinity controller

Reference Tracking Design

The feedback control structure is modified to resemble the classical control structure (for reference tracking) to assess how the unimodular matrices of the H-infinity controller can be mapped into the plant. The modified feedback control structure is shown in Fig. 2.3.1.2. The matrix $\boldsymbol{L}^{-1}$ does not pose a problem in the reformulation because it is simply a pre-compensator to the plant. Therefore it can be absorbed into the system as done in Section 2.1.5. As the matrix $\boldsymbol{R}^{-1}$ is situated in the usual position of the sensor (in the loop) it initially does not seem to be a problem absorbing it into the plant. But the sensor is diagonal which allows it to be absorbed into the loop without changing vector directions of the loop matrix, whereas the matrix $\boldsymbol{R}^{-1}$ is upper triangular. This does pose a problem and adds further complexities in the reformulation of the QFT design.

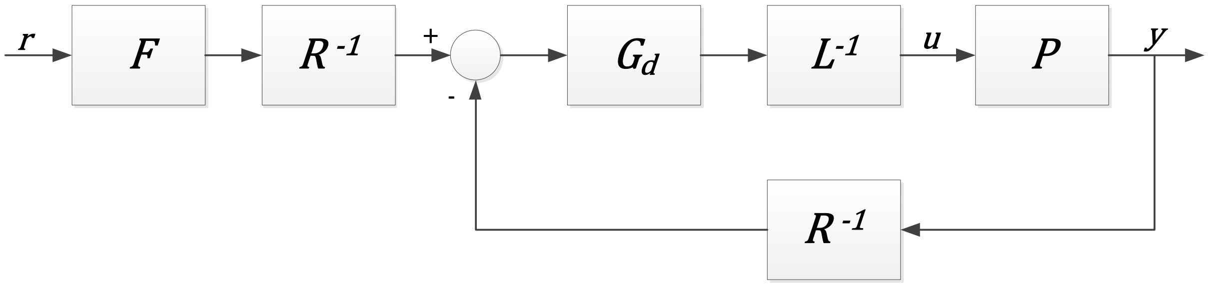

Figure 2.3.1.2 Modified feedback control structure to resemble the classical control structure

The reformulation absorbs the matrices $\boldsymbol{L}^{-1}$ and $\boldsymbol{R}^{-1}$ into the plant in the hope that it will provide some diagonalization so that QFT can be applied to achieve a less conservative controller. The reference to output tracking equation is given by

$$\boldsymbol{T} = (\boldsymbol{I} + \boldsymbol{PG})^{-1}\boldsymbol{PGF}, \tag{2.3.1.4}$$

$$\boldsymbol{T} = \left(\boldsymbol{I} + \boldsymbol{PL}^{-1}\boldsymbol{G}_d\boldsymbol{R}^{-1}\right)^{-1}\boldsymbol{PL}^{-1}\boldsymbol{G}_d\boldsymbol{R}^{-1}\boldsymbol{F}. \tag{2.3.1.5}$$

Define $\boldsymbol{R}^{-1}\boldsymbol{F} = \boldsymbol{F}_r$ and multiply both sides of Eq. (2.3.1.5) from the left by $\left(\boldsymbol{PL}^{-1}\right)^{-1}\left(\boldsymbol{I} + \boldsymbol{PL}^{-1}\boldsymbol{G}_d\boldsymbol{R}^{-1}\right)$

$$\left(\boldsymbol{LP}^{-1} + \boldsymbol{G}_d\boldsymbol{R}^{-1}\right)\boldsymbol{T} = \boldsymbol{G}_d\boldsymbol{F}_r. \tag{2.3.1.6}$$

Take out $\boldsymbol{R}^{-1}$ as a common factor from the left term of Eq. (2.3.1.6) to get

$$\left(\boldsymbol{LP}^{-1}\boldsymbol{R} + \boldsymbol{G}_d\right)\boldsymbol{R}^{-1}\boldsymbol{T} = \boldsymbol{G}_d\boldsymbol{F}_r. \tag{2.3.1.7}$$

Set $\boldsymbol{LP}^{-1}\boldsymbol{R} = \widehat{\boldsymbol{P}}'$ and perform usual QFT manipulations to Eq. (2.3.1.7) to get

$$\left(\widehat{\boldsymbol{P}}'_d + \boldsymbol{G}_d\right)\left[\boldsymbol{I} + \left(\widehat{\boldsymbol{P}}'_d + \boldsymbol{G}_d\right)^{-1}\widehat{\boldsymbol{P}}'_o\right]\boldsymbol{R}^{-1}\boldsymbol{T} = \boldsymbol{G}_d\boldsymbol{F}_r, \tag{2.3.1.8}$$

$$\boldsymbol{R}^{-1}\boldsymbol{T} = \left(\widehat{\boldsymbol{P}}'_d + \boldsymbol{G}_d\right)^{-1}\boldsymbol{G}_d\boldsymbol{F}_r - \left(\widehat{\boldsymbol{P}}'_d + \boldsymbol{G}_d\right)^{-1}\widehat{\boldsymbol{P}}'_o\boldsymbol{R}^{-1}\boldsymbol{T}. \tag{2.3.1.9}$$

Symmetry is observed between Eq. (2.3.1.9) and Eq. (2.1.3.4). The QFT philosophy can be now applied to obtain the diagonal loop gains and their respective bounds.

Rewriting Eq. (2.3.1.7) in terms of the equivalent plant inverse

$$\left(\widehat{\boldsymbol{P}}' + \boldsymbol{G}_d\right)\boldsymbol{R}^{-1}\boldsymbol{T} = \boldsymbol{G}_d\boldsymbol{R}^{-1}\boldsymbol{F}. \tag{2.3.1.10}$$

Label $\left[\widehat{\boldsymbol{P}}'\right]_{ij} = 1/q'_{ij}$ as is customary in QFT and expand Eq. (2.3.1.10) in terms of the scalar elements

$$\begin{bmatrix} \frac{1}{q'_{11}} + g_1 & \frac{1}{q'_{12}} \\ \frac{1}{q'_{21}} & \frac{1}{q'_{22}} + g_2 \end{bmatrix} \begin{bmatrix} 1 & \hat{r}_{12} \\ 0 & 1 \end{bmatrix} \boldsymbol{T} = \begin{bmatrix} g_1 & 0 \\ 0 & g_2 \end{bmatrix} \begin{bmatrix} 1 & \hat{r}_{12} \\ 0 & 1 \end{bmatrix} \begin{bmatrix} f_{11} & 0 \\ 0 & f_{22} \end{bmatrix} \tag{2.3.1.11}$$

$$\begin{bmatrix} \frac{1}{q'_{11}} + g_1 & \hat{r}_{12}\left(\frac{1}{q'_{11}} + g_1\right) + \frac{1}{q'_{12}} \\ \frac{1}{q'_{21}} & \hat{r}_{12}\frac{1}{q'_{21}} + \left(\frac{1}{q'_{22}} + g_2\right) \end{bmatrix} \boldsymbol{T} = \begin{bmatrix} g_1 & g_1\hat{r}_{12} \\ 0 & g_2 \end{bmatrix} \begin{bmatrix} f_{11} & 0 \\ 0 & f_{22} \end{bmatrix} \tag{2.3.1.12}$$

$$\begin{bmatrix} \frac{1}{q'_{11}} + g_1 & \hat{r}_{12}\left(\frac{1}{q'_{11}} + g_1\right) + \frac{1}{q'_{12}} \\ \frac{1}{q'_{21}} & \hat{r}_{12}\frac{1}{q'_{21}} + \left(\frac{1}{q'_{22}} + g_2\right) \end{bmatrix} \begin{bmatrix} t_{11} & t_{12} \\ t_{21} & t_{22} \end{bmatrix} = \begin{bmatrix} f_{11}g_1 & f_{22}g_1\hat{r}_{12} \\ 0 & f_{22}g_2 \end{bmatrix} \tag{2.3.1.13}$$

Equation (2.3.1.13) contains the row two pre-filter in the first row. This implies that row two has to be designed first and row one must be designed second. After loop two design, the controller g_2 can be incorporated into the design of row one to get exact design equations. This is done by multiplying both sides of Eq. (2.3.1.13) from the left by $\begin{bmatrix} 1 & -\frac{\hat{r}_{12}\left(\frac{1}{q'_{11}}+g_1\right)+\frac{1}{q'_{12}}}{\hat{r}_{12}\frac{1}{q'_{21}}+\left(\frac{1}{q'_{22}}+g_2\right)} \\ 0 & 1 \end{bmatrix}$. The result of this operation is

$$\begin{bmatrix} \left(\frac{1}{q'_{11}} + g_1 - \frac{\hat{r}_{12}\left(\frac{1}{q'_{11}} + g_1\right) + \frac{1}{q'_{12}}}{\hat{r}_{12}\frac{1}{q'_{21}} + \left(\frac{1}{q'_{22}} + g_2\right)}\frac{1}{q'_{21}}\right) t_{11} & \left(\frac{1}{q'_{11}} + g_1 - \frac{\hat{r}_{12}\left(\frac{1}{q'_{11}} + g_1\right) + \frac{1}{q'_{12}}}{\hat{r}_{12}\frac{1}{q'_{21}} + \left(\frac{1}{q'_{22}} + g_2\right)}\frac{1}{q'_{21}}\right) t_{12} \\ t_{11}\frac{1}{q'_{21}} + t_{21}\left[\hat{r}_{12}\frac{1}{q'_{21}} + \left(\frac{1}{q'_{22}} + g_2\right)\right] & t_{12}\frac{1}{q'_{21}} + t_{22}\left[\hat{r}_{12}\frac{1}{q'_{21}} + \left(\frac{1}{q'_{22}} + g_2\right)\right] \end{bmatrix} = \begin{bmatrix} f_{11}g_1 & f_{22}g_1\hat{r}_{12} \\ 0 & f_{22}g_2 \end{bmatrix} \tag{2.3.1.14}$$

Simplifying and rearranging the scalar terms of Eq. (2.3.1.14) result in the following design equations for row two

$$t_{21} = \frac{-t_{11}/q'_{21}}{\hat{r}_{12}\frac{1}{q'_{21}} + \left(\frac{1}{q'_{22}} + g_2\right)}, \tag{2.3.1.15}$$

$$t_{22} = \frac{f_{22}g_2 - t_{12}/q'_{21}}{\hat{r}_{12}\frac{1}{q'_{21}} + \left(\frac{1}{q'_{22}} + g_2\right)}. \tag{2.3.1.16}$$

By defining an equivalent plant according to $\frac{1}{q^*_{22}} = \hat{r}_{12}\frac{1}{q'_{21}} + \frac{1}{q'_{22}}$ and the equivalent loop gain $l^*_{22} = q^*_{22}g_2$, Eqs (2.3.1.15) - (2.3.1.16) can be simplified to

$$t_{21} = \frac{-t_{11} q_{22}^{*}/q_{21}'}{1 + l_{22}^{*}}, \tag{2.3.1.17}$$

$$t_{22} = \frac{f_{22} l_{22}^{*} - t_{12} q_{22}^{*}/q_{21}'}{1 + l_{22}^{*}}. \tag{2.3.1.18}$$

The controller g_1 is extracted from row one equations in Eq. (2.3.1.14) to yield the following design equations

$$t_{11} = \frac{f_{11} g_1}{\frac{1}{q_{11}'} - \frac{\hat{r}_{12}\frac{1}{q_{11}'} + \frac{1}{q_{12}'}}{\hat{r}_{12}\frac{1}{q_{21}'} + \left(\frac{1}{q_{22}'} + g_2\right)}\frac{1}{q_{21}'} + \left(\frac{-\hat{r}_{12}}{\hat{r}_{12}\frac{1}{q_{21}'} + \left(\frac{1}{q_{22}'} + g_2\right)}\frac{1}{q_{21}'} + 1\right) g_1} \tag{2.3.1.19}$$

$$t_{12} = \frac{f_{22} g_1 \hat{r}_{12} - f_{22} g_2 \frac{\hat{r}_{12}\left(\frac{1}{q_{11}'} + g_1\right) + \frac{1}{q_{12}'}}{\hat{r}_{12}\frac{1}{q_{21}'} + \left(\frac{1}{q_{22}'} + g_2\right)}}{\frac{1}{q_{11}'} - \frac{\hat{r}_{12}\frac{1}{q_{11}'} + \frac{1}{q_{12}'}}{\hat{r}_{12}\frac{1}{q_{21}'} + \left(\frac{1}{q_{22}'} + g_2\right)}\frac{1}{q_{21}'} + \left(\frac{-\hat{r}_{12}}{\hat{r}_{12}\frac{1}{q_{21}'} + \left(\frac{1}{q_{22}'} + g_2\right)}\frac{1}{q_{21}'} + 1\right) g_1} \tag{2.3.1.20}$$

By defining $m = \frac{1}{q_{11}'} - \frac{\hat{r}_{12}\frac{1}{q_{11}'} + \frac{1}{q_{12}'}}{\hat{r}_{12}\frac{1}{q_{21}'} + \left(\frac{1}{q_{22}'} + g_2\right)}\frac{1}{q_{21}'}$ and $n = \frac{-\hat{r}_{12}}{\hat{r}_{12}\frac{1}{q_{21}'} + \left(\frac{1}{q_{22}'} + g_2\right)}\frac{1}{q_{21}'} + 1$ then substituting these into Eqs (2.3.1.19) - (2.3.1.20) and multiplying the numerator and denominator by $1/m$ results in

$$t_{11} = \frac{f_{11}\frac{1}{m} g_1}{1 + \frac{n}{m} g_1}, \tag{2.3.1.21}$$

$$t_{12} = \frac{-f_{22}\frac{1}{m} g_2 \frac{\hat{r}_{12}\frac{1}{q_{11}'} + \frac{1}{q_{12}'}}{\hat{r}_{12}\frac{1}{q_{21}'} + \left(\frac{1}{q_{22}'} + g_2\right)} + f_{22}\left[\hat{r}_{12} - g_2 \frac{\hat{r}_{12}}{\hat{r}_{12}\frac{1}{q_{21}'} + \left(\frac{1}{q_{22}'} + g_2\right)}\right]\frac{1}{m} g_1}{1 + \frac{n}{m} g_1}. \tag{2.3.1.22}$$

The equivalent plant for row one is given by $q_{11}^{*} = \frac{n}{m}$.

Output Disturbance Rejection Design

The equation for output disturbance is given by

$$\boldsymbol{T} = (\boldsymbol{I} + \boldsymbol{P}\boldsymbol{G})^{-1}, \tag{2.3.1.23}$$

$$\boldsymbol{T} = \left(\boldsymbol{I} + \boldsymbol{P}\boldsymbol{L}^{-1}\boldsymbol{G}_{d}\boldsymbol{R}^{-1}\right)^{-1}. \tag{2.3.1.24}$$

Multiplying both sides of Eq. (2.3.1.24) from the left by $(\boldsymbol{PL}^{-1})^{-1}\left(\boldsymbol{I}+\boldsymbol{PL^{-1}G_dR^{-1}}\right)$ gives

$$\left(\boldsymbol{LP^{-1}R}+\boldsymbol{G_d}\right)\boldsymbol{R^{-1}T}=\boldsymbol{LP^{-1}}. \tag{2.3.1.25}$$

Since $\boldsymbol{LP^{-1}R}=\widehat{\boldsymbol{P}}'\rightarrow\boldsymbol{LP^{-1}}=\widehat{\boldsymbol{P}}'\boldsymbol{R^{-1}}$, Eq. (2.3.1.25) becomes

$$\left(\widehat{\boldsymbol{P}}'+\boldsymbol{G_d}\right)\boldsymbol{R^{-1}T}=\widehat{\boldsymbol{P}}'\boldsymbol{R^{-1}}. \tag{2.3.1.26}$$

Writing Eq. (2.3.1.26) in scalar form and simplifying

$$\begin{bmatrix}\dfrac{1}{q'_{11}}+g_1 & \dfrac{1}{q'_{12}}\\ \dfrac{1}{q'_{21}} & \dfrac{1}{q'_{22}}+g_2\end{bmatrix}\begin{bmatrix}1 & \hat{r}_{12}\\ 0 & 1\end{bmatrix}\boldsymbol{T}=\begin{bmatrix}\dfrac{1}{q'_{11}} & \dfrac{1}{q'_{12}}\\ \dfrac{1}{q'_{21}} & \dfrac{1}{q'_{22}}\end{bmatrix}\begin{bmatrix}1 & \hat{r}_{12}\\ 0 & 1\end{bmatrix}, \tag{2.3.1.27}$$

$$\begin{bmatrix}\dfrac{1}{q'_{11}}+g_1 & \hat{r}_{12}\left(\dfrac{1}{q'_{11}}+g_1\right)+\dfrac{1}{q'_{12}}\\ \dfrac{1}{q'_{21}} & \hat{r}_{12}\dfrac{1}{q'_{21}}+\left(\dfrac{1}{q'_{22}}+g_2\right)\end{bmatrix}\begin{bmatrix}t_{11} & t_{12}\\ t_{21} & t_{22}\end{bmatrix}=\begin{bmatrix}\dfrac{1}{q'_{11}} & \hat{r}_{12}\dfrac{1}{q'_{11}}+\dfrac{1}{q'_{12}}\\ \dfrac{1}{q'_{21}} & \hat{r}_{12}\dfrac{1}{q'_{21}}+\dfrac{1}{q'_{22}}\end{bmatrix}. \tag{2.3.1.28}$$

The final design equations for output disturbance rejection are

$$t_{11}=\frac{\dfrac{1}{q'_{11}}-t_{21}\left[\hat{r}_{12}\left(\dfrac{1}{q'_{11}}+g_1\right)+\dfrac{1}{q'_{12}}\right]}{\left(\dfrac{1}{q'_{11}}+g_1\right)}, \tag{2.3.1.29}$$

$$t_{12}=\frac{\hat{r}_{12}\dfrac{1}{q'_{11}}+\dfrac{1}{q'_{12}}-t_{22}\left[\hat{r}_{12}\left(\dfrac{1}{q'_{11}}+g_1\right)+\dfrac{1}{q'_{12}}\right]}{\left(\dfrac{1}{q'_{11}}+g_1\right)}, \tag{2.3.1.30}$$

$$t_{21}=\frac{\dfrac{1}{q'_{21}}-t_{11}\dfrac{1}{q'_{21}}}{\hat{r}_{12}\dfrac{1}{q'_{21}}+\left(\dfrac{1}{q'_{22}}+g_2\right)}, \tag{2.3.1.31}$$

$$t_{22}=\frac{\hat{r}_{12}\dfrac{1}{q'_{21}}+\dfrac{1}{q'_{22}}-t_{12}\dfrac{1}{q'_{21}}}{\hat{r}_{12}\dfrac{1}{q'_{21}}+\left(\dfrac{1}{q'_{22}}+g_2\right)}. \tag{2.3.1.32}$$

Unlike for the reference tracking problem, the output-disturbance rejection design does not have any limitation on the order of loop design.

3. Plant Model and Specifications

3.1. Plant Description

The plant is a model of a bank-to-turn (BTT) missile that was obtained from the defence company Denel Dynamics. Traditional missiles use a skid-to-turn (STT) configuration. A STT configuration minimizes the roll error of the missile and uses certain actuators (fins) as dedicated elevators and rudders. This flight configuration does not explicitly attempt to reduce the slip angle which leads to lateral strain and limitations on the possible propulsion mechanisms. A study by NASA, done in the early 1980s showed that BTT missiles in general, have lower lateral strain/forces and reduced side-slip angle (Riedel, 1980). The reduced slip angle in BTT missiles allow for ramjet engines to be used which permits for much greater range than the conventional rocket-type solid/liquid fuel propellant missiles. This has provided an impetus for the development and deployment of BTT missiles.

The most common high level guidance law implemented in missiles is the proportional navigation law. The outputs of the proportional navigational law are acceleration commands (normal and side) which are proportional to the line-of-sight rate and the closing velocity (Zarchan, 2007, pg 12). The important point to take note of in the previous statement is that there are two acceleration commands that need to be tracked. In a STT configuration, the control task does not seem too challenging because the problem is posed in a decoupled manner. In a BTT configuration, the missile is allowed to rotate and the objective is for the acceleration vector to point towards the target. A polar coordinate transformation of the normal and side acceleration vectors are performed to accommodate the new homing approach. A unit called the BTT logic in the flight control system converts the acceleration commands (in polar coordinates) to yaw and roll rate commands (Lee, Langehough and Chamberlain, 1992, pg 216). A partial functional block diagram of the control structure of a BTT missile is shown in Fig. 3.1.1.

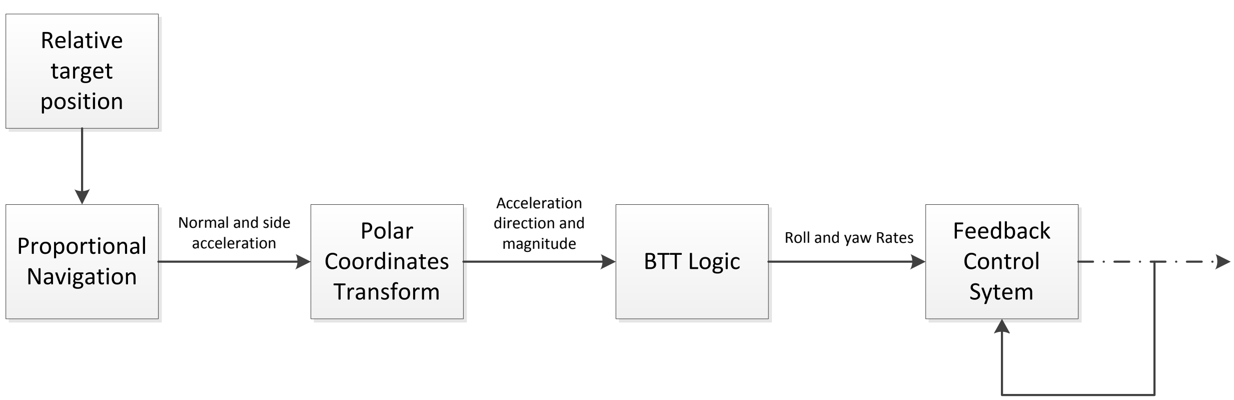

Figure 3.1.1 Partial functional block diagram of BTT control system

The plant obtained is a two-input two-output (2×2) model. The control (output) variables are the roll rate and the yaw rate of the missile which are measured in rad/s. The plant inputs are the aileron and rudder angles which are measured in rad. A block diagram of the plant showing the inputs and outputs is shown in Fig. 3.1.2. Using the output of the BTT logic as the reference commands, derived from outer loops, the design task from a feedback controller design perspective is a tracking design problem. The requirement is to find a controller that stabilizes the system for all plant cases while satisfying the bandwidth requirement for roll and yaw rate reference tracking.

Figure 3.1.2 Plant input and output variables

An illustration of the missile body frame together with the coordinate axes and angles relative to the velocity vector are shown in Fig. 3.1.3 (convention adopted from Zarchan, 2007, pg 462). The angle of attack is denoted by α, side-slip angle β, incidence angle γ and the velocity vector $\boldsymbol{v}$.

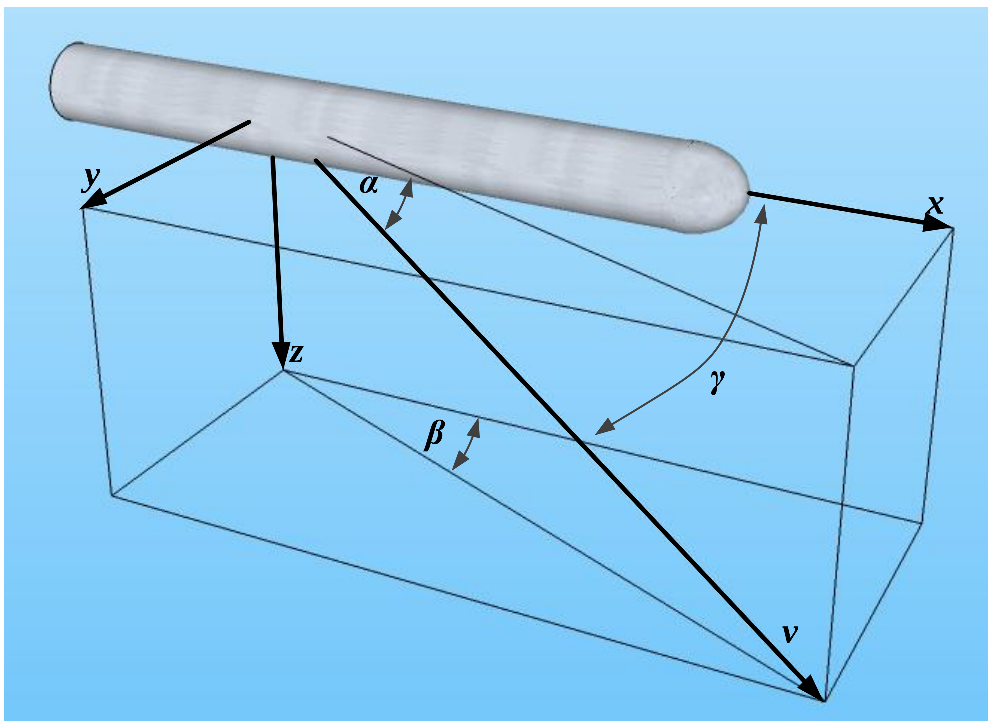

Figure 3.1.3 Missile body frame, coordinate axes and angles relative to velocity vector

The model obtained from Denel Dynamics consists of a set of six linear dynamic models (state-space form). The missile dynamics were linearized for angles of attack from $0rad$ to $1rad$ at intervals of $0.2rad$. Intuitively, the control problem gets more difficult as the angle of attack increases due to the increase in cross-coupling. From a mechanical perspective, the centre of pressure of the missile moves closer to the front of the missile as the angle of attack increases, this brings the nominal system closer to instability (Zarchan, 2007, pp 461-482). In fact, the sixth linearized plant is unstable i.e. at an angle of attack of $1rad \sim 57°$.

The plant model is third order. The state-space and output equations are used to represent the plant i.e. $\dot{\boldsymbol{x}} = \boldsymbol{A}\boldsymbol{x} + \boldsymbol{B}\boldsymbol{u}$, $\boldsymbol{y} = \boldsymbol{C}\boldsymbol{x} + \boldsymbol{D}\boldsymbol{u}$. The three states of the plant, in order are: side-slip angle, roll rate and yaw rate. The plant data for all six linearized operating points (nominal plants) are shown in Table 3.1. The data consists of the system matrix $\boldsymbol{A}$ and the control matrix $\boldsymbol{B}$.

The output matrix $\boldsymbol{C}$ and throughput matrix $\boldsymbol{D}$ for all cases are

$$C = \begin{bmatrix} 0 & 1 & 0 \\ 0 & 0 & 1 \end{bmatrix}, \; D = \begin{bmatrix} 0 & 0 \\ 0 & 0 \end{bmatrix}.$$

Based on the state declared above and the output equation, the outputs of the system are the roll and yaw rates. The output equation also implies that the system is strictly proper for all plant cases i.e. $\lim_{s\to\infty} \boldsymbol{P}(\boldsymbol{s}) = \lim_{s\to\infty} \boldsymbol{C}(\boldsymbol{sI}-\boldsymbol{A})^{-1}\boldsymbol{B} = \boldsymbol{0}$.

Table 3.1 Plant data for A and B matrices of the state-equation for each linearized point

Operating point	$\boldsymbol{A}$			$\boldsymbol{B}$	
1	-1.182	0	0.9966	-0.000378	0.8022
	-221	-5.769	-0.1728	-11290	-40.63
	-471.4	0.000261	-2.55	-0.554	-655.7
2	-1.628	-0.1763	0.9967	0.06503	0.7885
	-544.3	-5.702	0.9593	-11920	-259.9
	-612.7	-0.2034	-2.458	48.7	-604.3
3	-2.281	-0.364	0.9969	0.0686	0.6805
	2099	-5.24	3.895	-9401	-368.5
	-918.5	-0.5071	-2.278	56.67	-470.5
4	-2.951	-0.5773	0.9968	0.2626	0.5892
	9458	-4.796	5.936	-5563	1686
	-1250	-0.9272	-2.156	175.9	-414.5
5	-0.8647	-0.8391	0.9965	0.2277	0.4882
	5749	-4.001	8.193	-4682	-439.1
	341.1	-1.28	-2.042	144.1	-289
6	0.01046	-1.192	0.9958	0.2579	0.2371
	3579	-2.852	15.9	-1202	-1436
	665.8	-1.482	-2.083	107.5	-108.8

The eight independent uncertain parameters in the state-space matrices are given in Table 3.2; the element x_{ij} refers to the element that appears in the ith row and jth column of the matrix X.

Table 3.2 Plant element uncertainty

Elements	Percentage Uncertain
$a_{21}, a_{31}, b_{21}, b_{22}, b_{31}, b_{32}$	20%
a_{22}, a_{33}	50%

Due to sampling, communication and computational delays, a lumped input delay of $10ms$ was specified. For transfer function calculations, the delay was approximated using the padé approximation. NB. Modern design methods require an approximation of the transcendental function whereas QFT does not. The error between the actual phase of the delay and the phase of the approximation is shown in Fig. 3.1.4. for first, second and third order delays. The first order padé approximation of the delay is given by (Vajta, 2000)

$$e^{-sT} \approx \frac{-sT/2+1}{sT/2+1}, \tag{3.1.1}$$

and a second order padé approximation is given by

$$e^{-sT} \approx \frac{12-6(sT)+(sT)^2}{12+6(sT)+(sT)^2}. \tag{3.1.2}$$

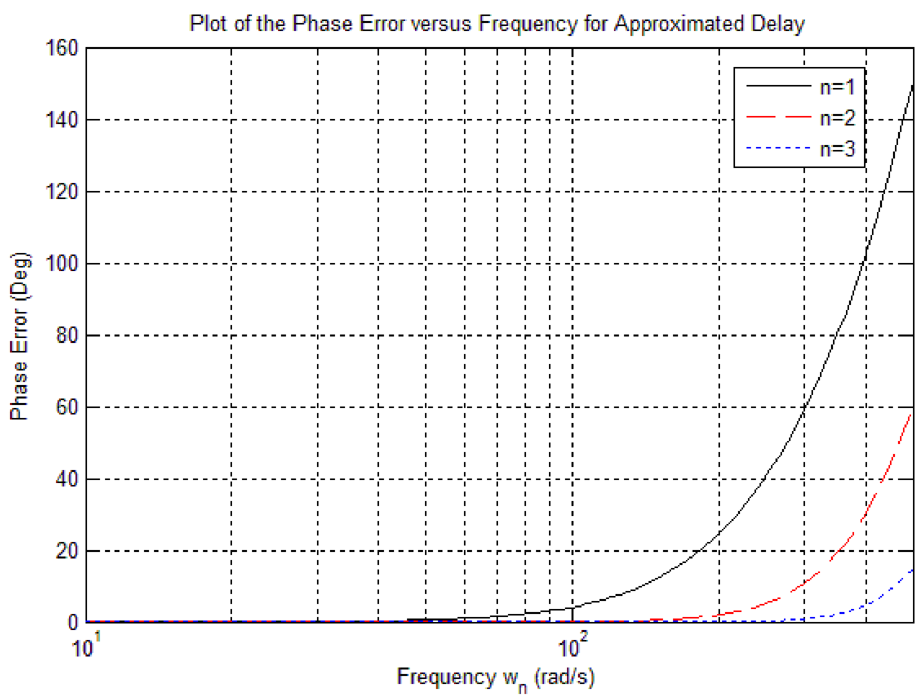

Figure 3.1.4 Phase error for different order padé approximation of delay

After the specifications are formed, the order of the padé approximation can be chosen based on the expected loop bandwidths of the system.

Although the dissertation is not aimed at nonlinear control it is important to state that the other input constraint in the system is actuator rate and amplitude saturation. This makes the designer prudent during the design process of the magnitude of controller gain and conditional stability, as not achieving the design amplification may lead to specification violation and conditional stability may make the final system unstable. The actuators have upper and lower bounds of $\pm 0.12rad$. NB. the actuator phase lag is incorporated in the plant model.

3.2. Plant Analysis

When the singular values are plotted against frequency, they are referred to as the principle gains of the system. From Section 2.2.2 it is known that SVD gives an idea of the gain in the system as the input direction changes (MIMO case). Consequently, the plot of the maximum and minimum singular values shows the limits of how the gain changes with the change in input direction. The largest ratio of the maximum singular value to the minimum singular value in a system across the frequency range is referred to as the condition number, or symbolically

$$cond(\boldsymbol{P}) = \frac{\bar{\sigma}(\boldsymbol{P})}{\underline{\sigma}(\boldsymbol{P})}. \tag{3.2.1}$$

A plot of the principal gains for each linearized point is shown in Fig. 3.2.1a. When the condition number of a plant is large, it may be difficult to control and is referred to as an ill-conditioned plant. According to (Skogestad and Postlethwaite, 2005, pg 82) having a small condition number indicates that the MIMO plant is less sensitive to uncertainty which makes the controller design less difficult but the contrary is not true in general, and large condition numbers may indicate a higher sensitivity to uncertainty.

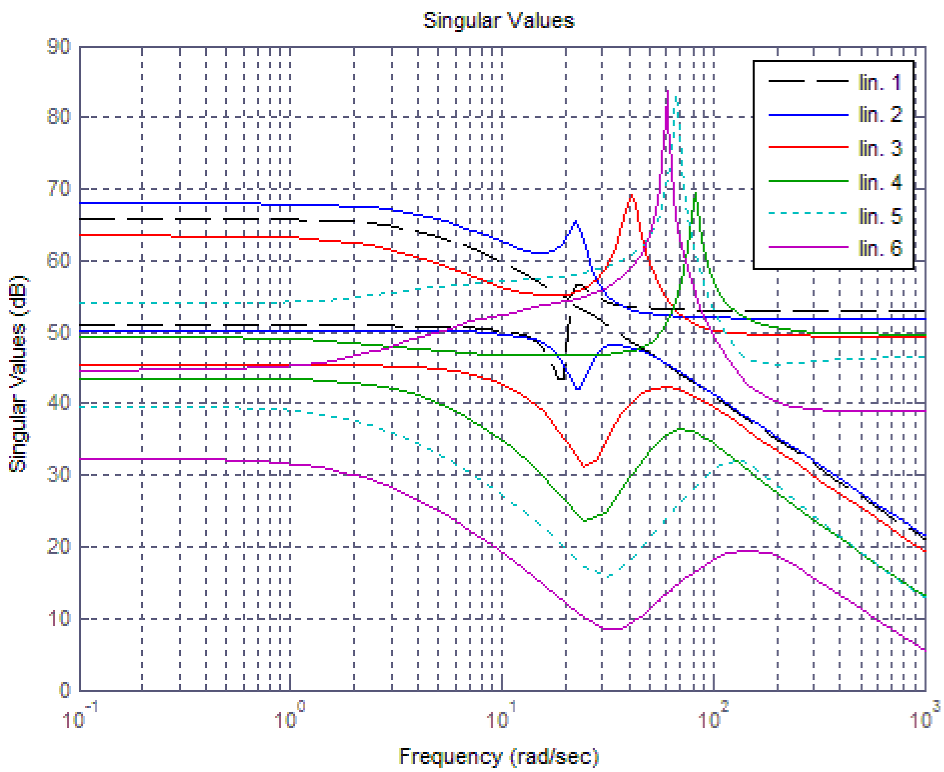

Figure 3.2.1a Singular value plot of the plant for all six nominal points

From the plot of the maximum and minimum singular values across the linearized points and frequency, it is clear to see that the condition number appears to increase as the angle of attack increases. This confirms what was initially expected, the interaction in the plant makes the control problem more difficult as the angle of attack increases. A plot of the interaction index for each linearized point is shown in Fig. 3.5b. The interaction index plot indicates that the interaction in the plant does not necessarily increase with an increase in condition number. The plot of the interaction index shows that the fourth linearized plant has the greatest amount of cross-coupling (interaction).

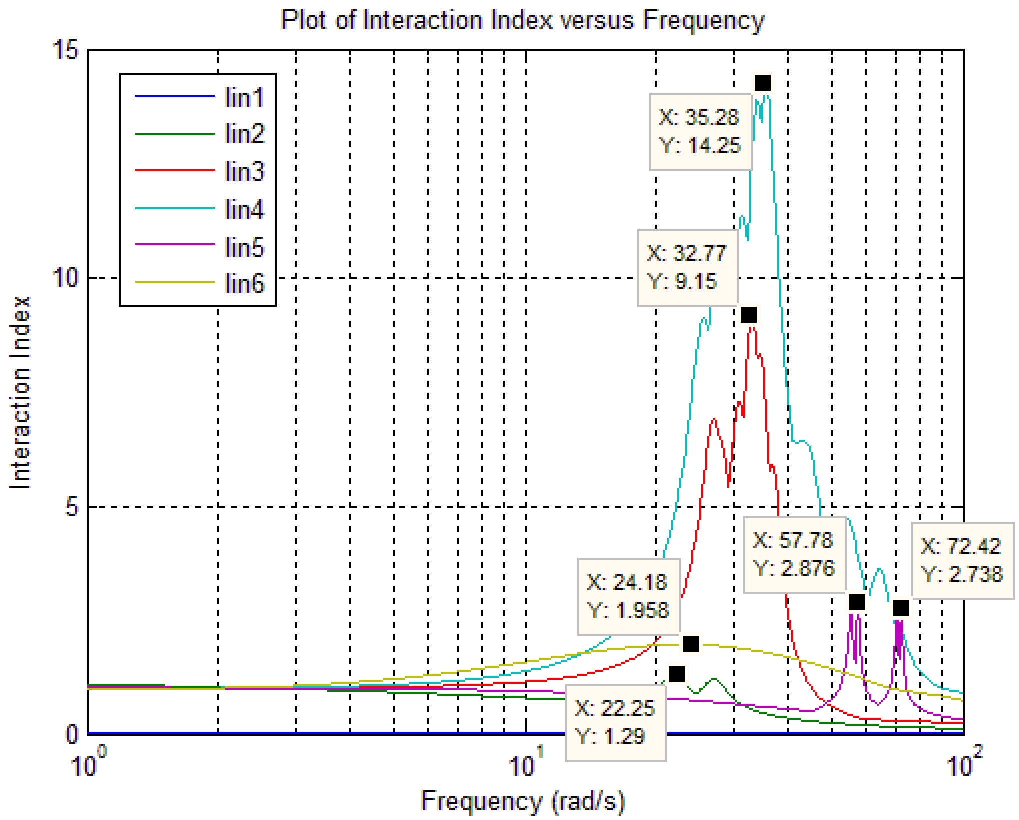

Figure 3.5b Interaction index plot of the plant for all six nominal points highlighting the peaks

3.3. System Specifications

Based on outer loop angle and acceleration demands, roll and yaw rates are derived which need to be tracked. Although bandwidth requirements for the inner loop were not stated explicitly in the specifications, informal discussions with the engineers at Denel Dynamics indicated that a bandwidth of more than $20 rad/s$ would suffice and will not restrict the outer $15 rad/s$ loop bandwidth. Therefore, the nominal tracking requirement was set as a bandwidth of $25\ rad/s$ with a $10\ rad/s$ variance to account for the uncertainty.

Using the above stated specifications as an aim, an automatic controller design method was used to get an idea of the true results one can expect (taking into account non-minimum phase lag/delays). Generation of the tracking responses were done using the LQR with integration method. The gain responsible for the bandwidth of each state's decay was tweaked until desired responses were obtained. The results of this experiment are used to refine the tracking specifications.

Specifications for linearized point 1-3

From the analysis of the plant singular values for operating points 1-3, and the knowledge of how the angle of attack affects the difficulty of the multivariable problem, it is expected that the lower angle of attack plants are the easiest from the operating points to stabilize and achieve specifications.

The $\boldsymbol{Q}$ matrix (from Section 2.2.1) that produced desirable tracking response/bandwidth for the linearized points 1-3 was $\boldsymbol{Q} = diag\{0, 25, 25, 0, 0, 16000, 16000\}$. The first three weightings are for the original plant. The other weightings were for the contrived states that were used to imbibe the delay for both input channels and add integral action for each channel (see "Frequency Domain Perspective of State-space Design" - Section 2.2.1). An observer was also included in the system to get a realistic response. The tracking magnitude response produced with the $\boldsymbol{Q}$ matrix shown above and $\boldsymbol{R} = eye(2)$ appears in Fig. 3.3.1 for 256 plants in the uncertainty set for linearized plant 1.

Using the same weighting matrices, the responses for the 2nd and 3rd operating points are shown in Figs. A1.1 - A1.2. The state-feedback and observer poles were checked to ensure the stability of the complete system [see "Separation Principle" - Section 2.2.1]. From Fig. 3.3.1 it can be seen that there is not much variation in the response of the diagonal channels with the LQR controller (plus integration). This means that the reference to output variation $max\ \Delta\left|T_{ii}^{spec}\right|$ may be relatively easy to achieve with the QFT diagonal controller. More confidence is gained by the fact that the cross-coupling is minimum in the 1st linearized plant. The iterative task of forming specifications involves assessing the magnitude of variation of $max\Delta|T_{ii}|$ and comparing it to $\Delta\left|T_{ii}^{spec}\right|$ to refine the specifications. The absolute reference-output response can be shaped in the end of the design via the pre-filter.

Knowing that the aim of $25rad/s$ with small variance is easily achievable, the specifications can be finalized. The black dashed lines in Fig. 3.3.1 show the tracking bounds that were chosen for the system. The tracking bounds are applicable for frequencies less than $60rad/s$ and sensitivity bounds will determine the closed-loop uncertainty at higher frequencies. It can be seen that the allowed variation is very large for the first linearized point but these bounds will be used for linearized points 2 and 3 as well, where it will prove challenging to achieve. Since independent control of the roll and yaw rates are required, the off-diagonal channel transmission must be minimized. So the design task is to meet the diagonal channel requirements as a first priority and minimize the off-diagonal channels magnitude response. The specifications for the off-diagonal channels shown in Fig. 3.3.1 is the worst case requirement. The step responses of the specifications are shown in Fig. 3.3.2. Specifications for the diagonal channel are

$$T_{ii}^{u}(j\omega) = \left|\frac{(j\omega/15+1)}{(j\omega/25)^2 + 2\cdot 0.6\cdot j\omega/25 + 1}\right| \qquad i = 1{,}2;\ \omega \leq 60rad/s, \tag{3.3.1}$$

$$T_{ii}^{l}(j\omega) = \left|\frac{1}{((j\omega/5\ +\ 1)\cdot(j\omega/10\ +\ 1)\cdot(j\omega/35\ +\ 1))}\right| \qquad i = 1{,}2;\ \omega \leq 60rad/s, \tag{3.3.2}$$

where the superscript l and u represent the lower and the upper bounds, respectively.

An upper magnitude limit is placed on the off-diagonal channels which is given by

$$T_{ij}(j\omega) = \left|\frac{1.3j\omega}{(j\omega/0.9+1)\cdot(j\omega/50\ +1)\cdot(j\omega/60+1)}\right| \qquad i \neq j. \qquad (3.3.3)$$

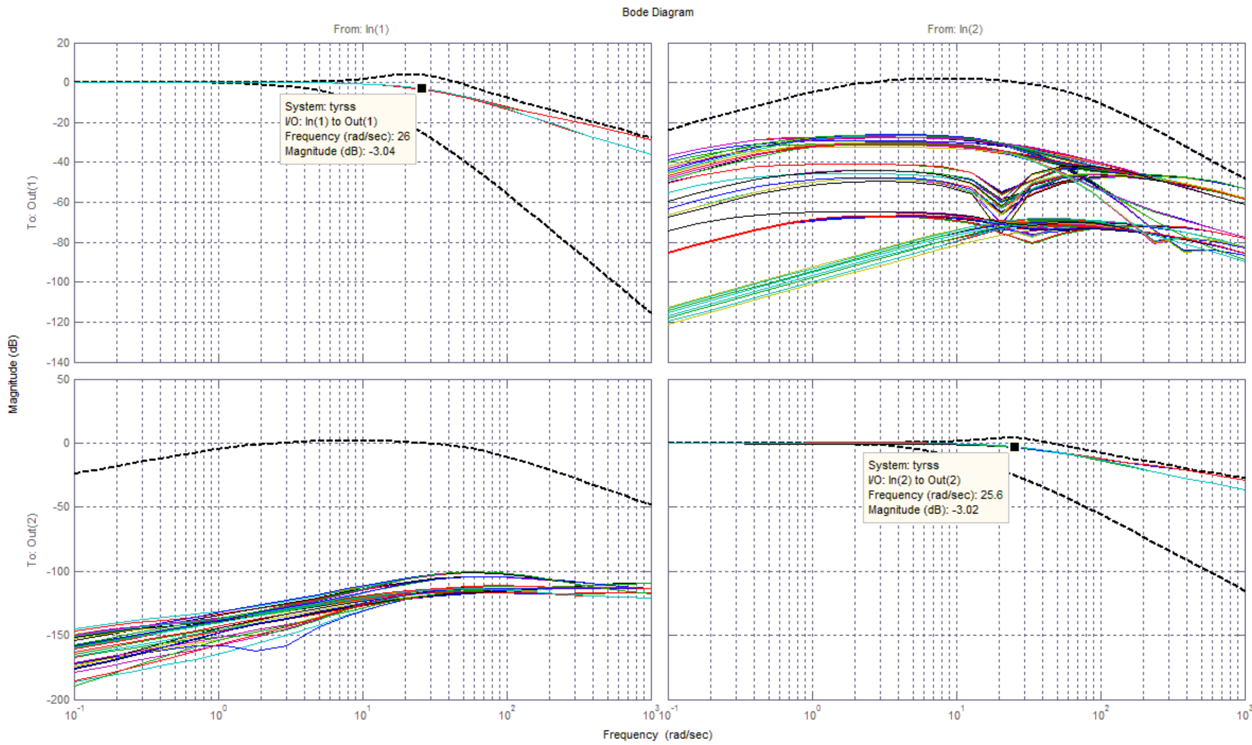

Figure 3.3.1 Reference to output magnitude plot of the automatically generated system used for refining specifications for linearized point 1

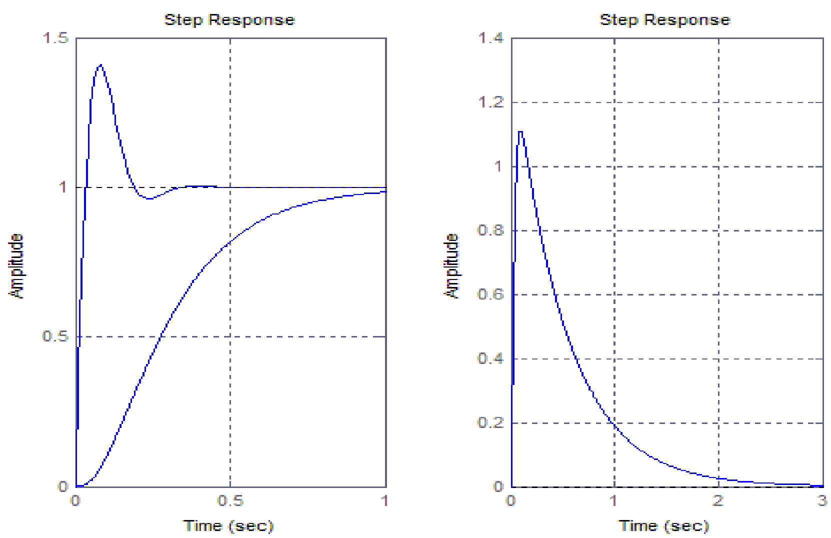

Figure 3.3.2 Step response of the system specification bounds

Specifications for linearized point 4

The same procedure done above is repeated for linearized point 4 to ensure that the obtained specifications are reasonable. The magnitude plot of the reference to output response for linearized point 4 is shown in Fig. A1.3. The complementary sensitivity variations of the diagonal channels are relatively large in comparison to the other linearized points. Specifications adjusted for this operating point are shown in Eqs. (3.3.4) - (3.3.5). The off-diagonal channels have the same specifications for all operating points.

$$T_{ii}^{u}(j\omega) = \left|\frac{(j\omega/15+1)}{(j\omega/25)^2 + 2\cdot 0.6\cdot j\omega/25+1}\right| \qquad i=1,2;\omega \le 60rad/s \tag{3.3.4}$$

$$T_{ii}^{l}(j\omega) = \left|\frac{0.99\ (j\omega/0.7\ +\ 1)}{((j\omega/0.6\ +\ 1)\cdot(j\omega/10+\ 1)\cdot(j\omega/40\ +\ 1))}\right| \qquad i=1,2;\omega \le 60rad/s \tag{3.3.5}$$

Specifications for linearized point 5

The tracking bounds for linearized point 5 are shown in Eqs. (3.3.6) - (3.3.7). Figure A1.4 shows the reference to output response of the system. It can be seen that with the refined specifications, the design is plausible. A comparison with the results of linearized point 4 indicates that linearized 5 may be easier to control than operating point 4.

$$T_{ii}^{u}(j\omega) = \left|\frac{(j\omega/20+1)}{(j\omega/25)^2 + 2\cdot 0.55\cdot j\omega/25+1}\right| \qquad i=1,2;\omega \le 60rad/s \tag{3.3.6}$$

$$T_{ii}^{l}(j\omega) = \left|\frac{0.99}{(j\omega/15\ +\ 1)^2\cdot(j\omega/35\ +\ 1)}\right| \qquad i=1,2;\omega \le 60rad/s \tag{3.3.7}$$

Specifications for linearized point 6

The final response obtained for linearized point 6 using the controller generated from the LQR design method yielded mostly unstable systems. For this reason the specifications for the 6th linearized point is to obtain maximum performance while ensuring closed-loop stability of all plants in the set.

The specifications given in this section are the first cut specifications. These tracking specification may not be achievable using QFT because of the type of design (diagonal versus optimal mixing) as well as the fact that some of the responses shown were unstable (LQR is not quantitative). From a general analysis of the reference to output response, it can be seen that the multivariable system gets more sensitive to uncertainty in the low frequency region as the angle of attack increases. This should be kept in mind during the MIMO QFT design because it may not be possible to achieve the specifications or even match the LQR *magnitude* response if a diagonal controller is used.

The control system design task is to design a feedback controller and a pre-filter to ensure closed-loop stability of the system for all plants in the uncertain set and meet the tracking requirements above.

4. Application of MIMO QFT

In this section, the multiple design methods expounded in the QFT theory section are applied to the MIMO missile plant model. First, the templates are generated for a set of pertinent frequencies and across all operating points. An analysis of these templates is done to get insight into the design problem. After template generation, the design for reference tracking specifications is done for each linearized point. The approach shown uses the algorithm in (Boje, 2004) to obtain bounds without explicitly declaring reserves for equivalent disturbance terms. The capability of non-diagonal controller design is illustrated for the 2nd linearized plant in Section 4.3. To demonstrate the use of the less conservative error-tracking specification design, a controller design using this method for the 2nd linearized point is presented in Section 4.4. Lastly, the use of the true inversion-free design equations is shown to produce less conservative bounds.

4.1. QFT Template Generation

As expressed in Section 2.1.1 ("Graphical Approach"), the uncertainty of the system is encapsulated on a frequency basis using plant templates. The intensive computational requirement was described as one of the problems in QFT design (Section 2.1.9). This section shows the method used to obtain the boundary of the templates for the missile plant.

The design frequencies should be chosen such that the resulting templates differs significantly from the other templates already plotted. This is a rule of thumb for choosing design frequencies, but in general, the more design frequencies/templates used, the more one can have confidence in specifications being met for all frequencies. The principal gain plot of the plant also indicates frequencies that may be useful for QFT design. Sufficient frequency points around resonance in the principal gains should be used for QFT design as there are quick changes (relative to frequency) in the magnitude/phase response of the plants response. The method used to generate the boundary of the templates is given by the points below.

Generation of templates:

1. Calculate the transfer functions for the equivalent plants q_{ij} in terms of the parameters that vary, for each operating point (use of *Symbolic Math Toolbox* in *Matlab*™).
2. Confirm responses as they may be numerical errors.
3. Discretize each parameter into x values ($x-1$ equal intervals). Map the edges of the multidimensional parameter box to the complex plane.
4. Discretize each parameter into y values ($y-1$ equal intervals) Find all possible combinations of mapping to the complex plane.
5. Choose z random points within the parameter multidimensional box and map them to the complex plane.

Each of steps $3-5$ should be plotted with different symbols/colours. The majority of the boundary points of the template will be a result of performing step 3. Steps 4 and 5 are performed to ensure that there are no points that result in a boundary point that is not an edge of the parameter space. For this design problem, x was chosen as 15, y was chosen as 3 and z was chosen as 10000; these parameters can be chosen based on time constraints and computational performance. It was found through practice that step 3 generally results in the majority of the points being boundary points even in special cases where there is a singularity in the plant set. The plant template of q_{11} and q_{22} for $\omega = 1rad/s$ is shown in Fig. 4.1.1 for operating point 1.

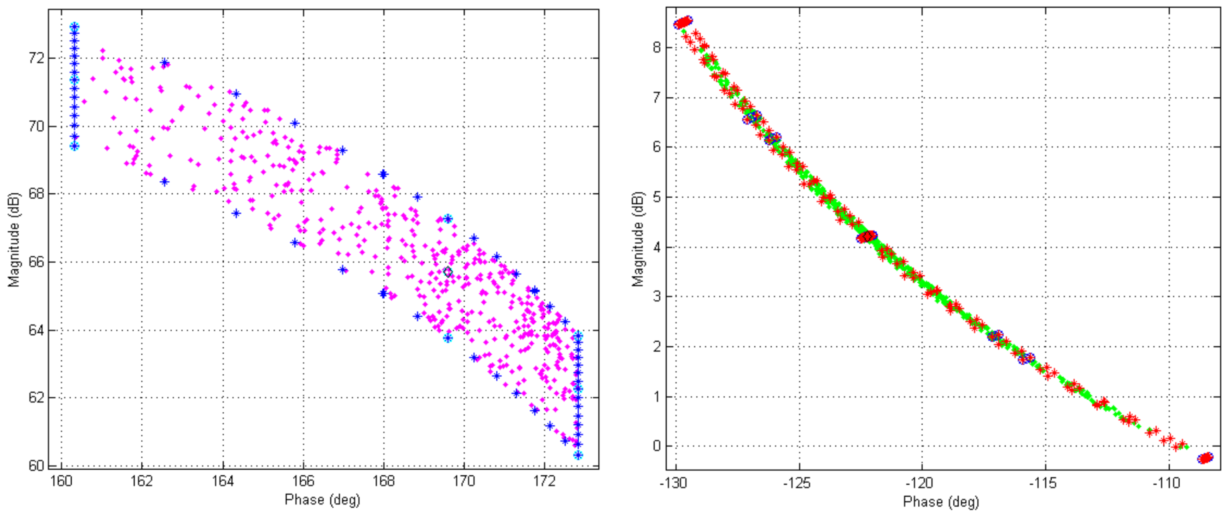

Figure 4.1.1 Templates for q_{11} (left) and q_{22} (right) for linearized point 1

The asterisks are a mapping of the edges of the parameter space. It is evident how this mapping results in the boundary of the template. The dots are plots of the mapping of random points from the parameter space to the complex plane. Also, not seen so clearly due to coinciding with the edges of the parameter space are the circles representing step 4 mapping.

This method of finding the relevant points in the parameter space is much better than just using step 4. Discretizing the parameter space into equal intervals and finding all possible mappings result in a computationally intensive task. For n parameters with m intervals, one would require $(m+1)^n$ calculations (exponential growth with number of intervals). Performing the edge mapping requires $[2^n \cdot (m+1) \cdot n]$ calculations, which grows linearly with the number of intervals. A more efficient way, is to combine steps 3 – 5 to generate the relevant points.

After the significant points of the template are generated, they are passed to an algorithm that tries to remove the interior points of the template. This algorithm simply scans from top-to-bottom and left-to-right to try to find possible boundary points. Each point is allocated into a phase interval and a magnitude interval. To determine the upper/lower boundary points, the magnitudes are assessed and the corresponding point ordered according to phase interval. To determine the left/right boundary points the phases are assessed and the corresponding point ordered according to the magnitude interval. The interval width for magnitude and phase is adjusted to get the acceptable reduction in points. The short coming of this method is that it is not automated and it cannot find the boundary of complicated templates such as circular-arc templates. Nevertheless, this method is used to reduce the number of interior points to ease the memory requirement in the subsequent step. After a reduction of interior points, the array of points is passed to a non-convex hull finding algorithm (Boje, 2000) which finds the boundary of the template. The result of each step of the above stated procedure is shown in Fig. 4.1.2 for the template of q_{11} for linearization 2 at $\omega = 1\, rad/s$. The resulting plot of the template after steps 1-5 in the procedure is given in Fig. 4.1.2a. This figure contains 35941 points. After applying the algorithm to remove some of the interior points, the resulting template looks like Fig. 4.1.2b which contains 796 points. Finally, after the non-convex hull algorithm is applied the template is given by Fig. 4.1.2c which has 205 points.

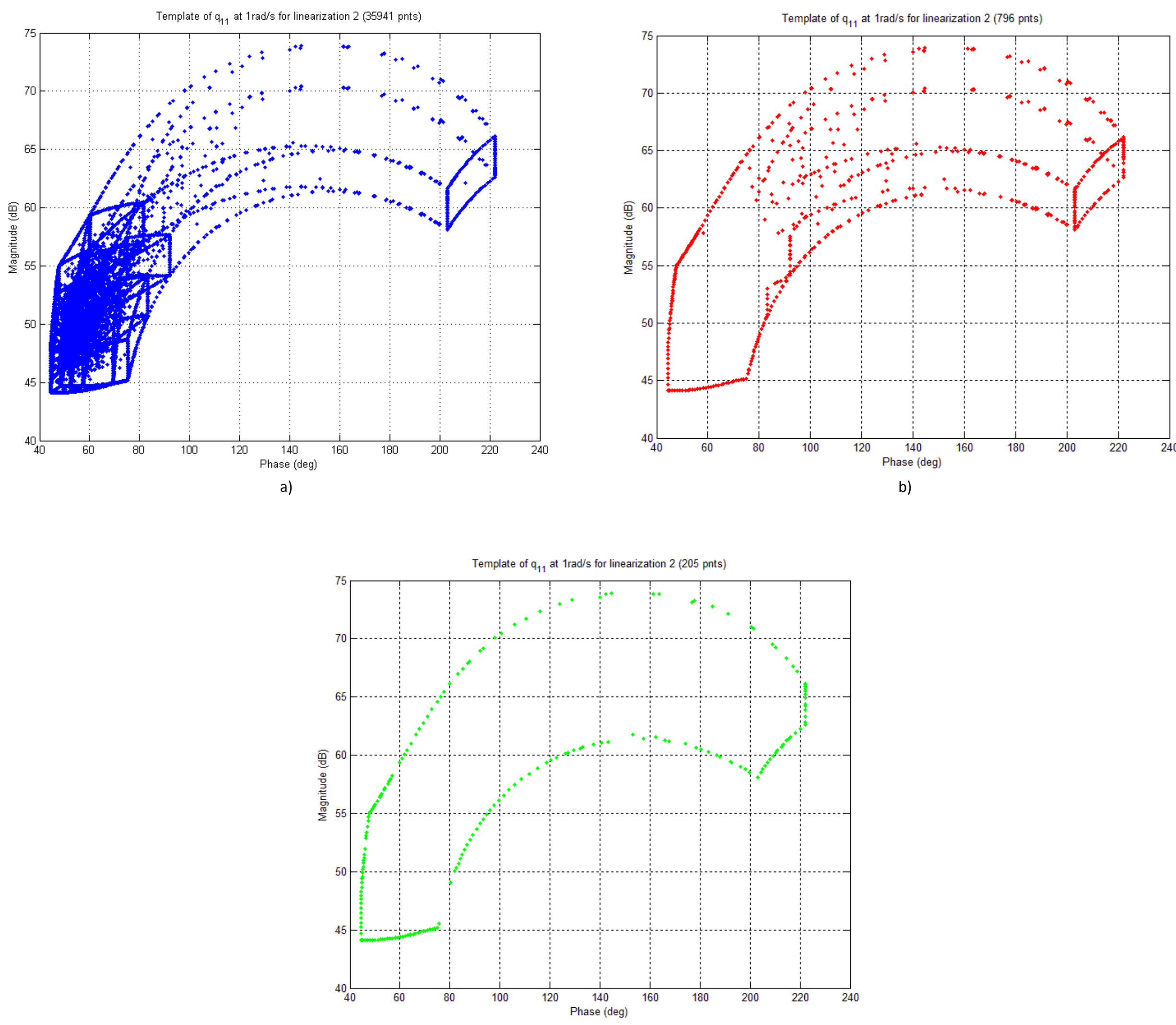

Figure 4.1.2 Template appearance after each step of reduction

The template shown in Fig. 4.1.2 is relatively wide and tall; this means there is a large uncertainty in the phase and the gain of the plant element q_{11}. But this uncertainty is not expected to pose much of an issue as the template in Fig. 4.1.2 is for a low frequency i.e. $1 rad/s$. Since the delay will produce phase lag at much higher frequency than $1 rad/s$ the large uncertainty at low frequency can be dealt with by having large loop gain. The more important frequency range that should be analysed is around the expected gain crossover frequency, as large phase and magnitude uncertainty in this region could quite easily make the system go unstable (cover the Nyquist point). Hence the next template that is analysed is at a reasonable expected gain-cross over frequency of $30rad/s$ (based on the tracking bandwidth).

The templates for plant element q_{11} and q_{22} across all linearized points for $\omega = 30\ rad/s$ are shown in Fig. A2.1 - A2.2. The template for q_{11} is approximately $200°$ wide and $60dB$ in height. From the [Inverse] Nichols chart in Fig. A2.3 (combination of conventional Nichols chart and Inverse Nichols chart – to assess both sensitivity and complementary sensitivity from open-loop gain plot), it can be observed that if a maximum sensitivity of $6dB$ is required, a $200°$ wide template will result in some loop gains having a lot of phase lead at $30\ rad/s$ (as much as $200°$ phase lead from some other plants). In order for the system to be stable a phase width of $(360° - 2 \cdot phase\_margin)$ at the gain cross-over frequency is required. But the slope of the loop gain needs to be (on average) negative in order to roll-off hence a practical constraint is a phase width of $(180° - phase\_margin)$ for frequencies near the gain cross-over frequency (Houpis, 2006, pg 231).

Figures A2.4 – A2.11 show some templates for the elements q_{11} and q_{22} across all linearized plants for frequencies $\omega = 3, 15, 60, 120$. These templates show how the uncertainty varies with frequency for the equivalent plants. The farther away templates are from each other the more difficult it is to solve the design problem with a single linear controller for all plant cases simultaneously. On the other hand, if templates are "closer" to each other or overlap each other, this indicates greater likelihood of the problem being solved with a single linear controller. From the analysis of the templates it can be seen that linearized points 1 and 2 have most of the templates overlapping or in very close proximity for various frequencies. Hence it is worthwhile investigating the use of a single linear controller for these two linearized plants. The uncertainty characteristics for linearized points 1 and 2 are the only commonalities among the set of plants. It is also clear that the uncertainty for each operating point gets smaller as the frequency increases above their respective resonance frequency.

Based on a phase margin of $30°$, the gain cross-over frequency of the system will need to be greater than $60rad/s$ if a single controller is to be designed for the set of linearized plants. This is much higher than the tracking bandwidth of the system. Preliminary experimentation attempting to stabilize higher angle of attack plants with a diagonal controller proved to be very difficult. For both of the above reasons it was decided to design a linear controller for each linearized point and schedule the controller based on the angle of attack. Such scheduling is commonly used in missile controller design. Since the angle of attack can be considered *slow varying,* the stability of the gain-scheduled system will be satisfied if the equivalent system of each linearized point is stable (Vidyasagar, 1978, pp 218-223).

4.2. Design for Reference Tracking

This section presents the diagonal controller and the pre-filter designs obtained using QFT for each linearized point. The automatic bound generation method (Section 2.1.3) is used to obtain the loop boundaries based on the specifications. This method does not require explicitly defining reserves for the cross-coupling terms and in general, is less conservative than the original MIMO QFT design methodology.

A major problem with this design method is the number of computations required to obtain the boundaries. For each ordered plant pair in the set of uncertain plants, a quartic polynomial must be solved at each design frequency and phase. If the phase range is taken to be $[0°, -360°]$ with a resolution of 5°, the loop boundary generation requires $(360/5) \cdot n^8(n^2 - 1)$ computations, where n is the number of discrete points chosen within the uncertain *parameter set*. This equates to 55296 quartic inequality solutions for 256 discrete plants. The global bound is obtained by taking the intersection of the individual solutions. It was found that at high frequency the cross-coupling and open-loop uncertainty reduces, this leads to the global solution usually producing both upper and a lower bounds at high frequency.

Application to linearized point 1

The nominal plants for all linearized points are chosen to be the plant resulting from taking the minimum value of every uncertain parameter. The equivalent nominal plants for each channel for linearized point 1 are

$$q_{11} = \frac{-13545.1363 \cdot e^{-s(10\times10^{-3})}}{(s + 8.654)}, \tag{4.2.1}$$

$$q_{22} = \frac{-786.8024 \cdot\ (s + 0.6052) \cdot e^{-s(10\times10^{-3})}}{(s^2\ +\ 5.007s\ +\ 568.3)}. \tag{4.2.2}$$

The inverse of the original plant can be written as

$$\boldsymbol{P}(s)^{-\mathbf{1}} = \frac{d(s) \cdot adj(\boldsymbol{N}(s))}{det(\boldsymbol{N}(s))}, \tag{4.2.3}$$

where $d(s)$ is the common denominator and $\boldsymbol{N}(s)$ is a numerator matrix of the original plant.

The equivalent plant elements used for the QFT design is then given by

$$q_{ij}(s) = \frac{\det(\boldsymbol{N}(s))}{d(s) \cdot adj(\boldsymbol{N}(s))_{ij}}. \tag{4.2.4}$$

By the application of Eq. (4.2.4), one can expect the occurrence of an unstable pole in $q_{ii}(s)$ if the original plant has non-minimum phase *elements*. More precisely, by calculating the adjoint of the numerator of a 2×2, which is

$$adj(\boldsymbol{N}(s)) = \begin{bmatrix} n_{22}(s) & -n_{12}(s) \\ -n_{21}(s) & n_{11}(s) \end{bmatrix}, \tag{4.2.5}$$

it can be said that one may expect an unstable pole in $q_{11}(s)$ if $n_{22}(s)$ contains a RHP zero. Similarly an unstable pole in $q_{22}(s)$ may occur if $n_{11}(s)$ contains a RHP zero.

Bounds were generated for both loops using the tracking specifications by the application of the methodology stated in Section 2.1.3. It was found that the constraints on loop gain for the second loop is relatively less severe than the first loop constraints; hence the second loop was chosen to be designed first. This is a sensible thing to do since the last loop to be designed (in this case loop one) can be solved exactly without any conservativeness.

The tracking bounds obtained for loop two together with the designed nominal loop is shown in Fig. 4.2.1.

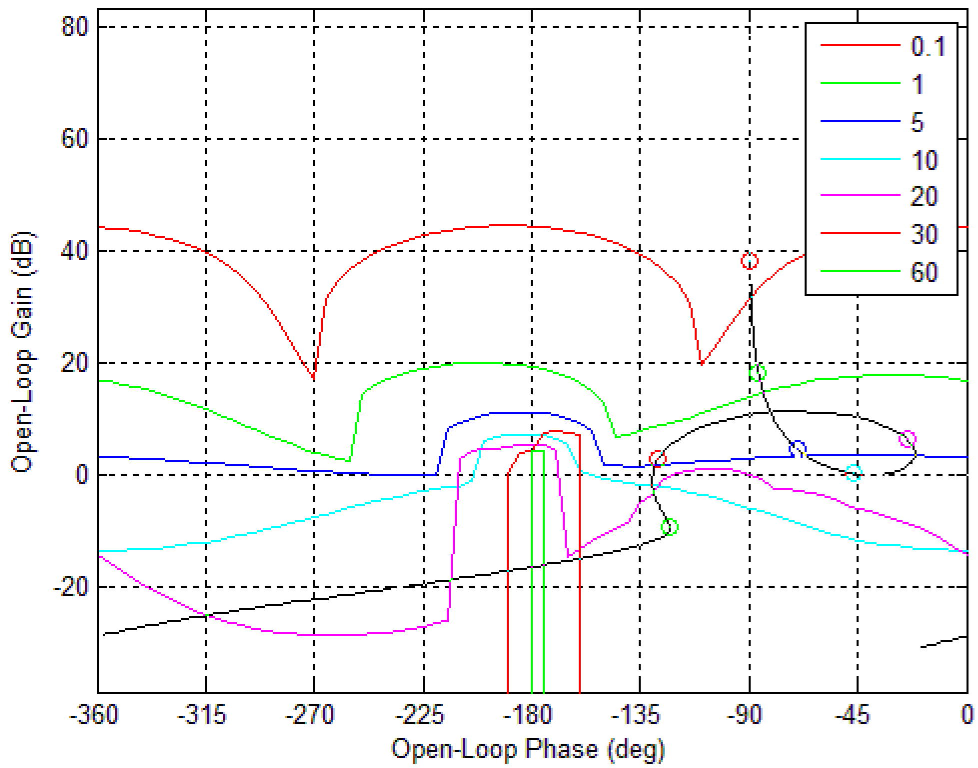

Figure 4.2.1 Nominal loop two with tracking bounds for linearized point 1

It was found that the tracking bounds were relatively easy to satisfy. Since the interaction in this plant is small compared to the higher angle of attack plants, it was desired to keep the *equivalent* second loop stable for ease of design in subsequent steps. This requirement can be satisfied if $(1 + l_2)$ has no RHP zeros. To ensure this the design constraint

$$|1 + l_2|_{dB} \geq -6dB, \tag{4.2.6}$$

is imposed. Satisfying this constraint proved more difficult than the tracking bounds. In order to satisfy the above stated constraint, the gain-cross over frequency for the equivalent second loop had to be increased from the instance which only satisfied tracking bounds. The more conservative controller also eases the pre-filter design. The bounds required to satisfy Eq. (4.2.6) are shown together with the nominal loop in Fig. 4.2.2. The robust stability bounds for frequencies $20, 22\ rad/s$ appear disjoint in Fig. 4.2.2. The reason for this is because the template for these frequencies appears as two distinct clusters. If the distance between the edges of disjoint templates at some boundary point is larger than the sensitivity bound, and at other boundary points are smaller than the sensitivity bound, the resulting robust stability bound will be disjoint. If the actual uncertain plant occupies the area between the two clusters, a solution is to use more discrete plants in the template generation. In the cases below, where disjoint boundaries where found, it was assumed that there are plant cases that lie between the two clusters hence the region between the two boundaries should be avoided. This was not required in the cases below since the reference-tracking demands resulted in loop gain (and phase) to be far from the respective robust stability boundary. The controller that meets these requirements is given by

$$g_{22} = \frac{-0.0366 \cdot (s^2 + 21.24s + 225.6) \cdot (s^2 + 61.51s + 2155)}{s \cdot (s+55)^2 \cdot (s+0.6052)}. \tag{4.2.7}$$

For an exact design of loop one, the pre-filter for channel two must be known (see Eq. (2.1.3.23)). To design f_{22} one needs to satisfy the equation (which is conservative)

$$\left| \left| \frac{l_2 f_{22}}{1+l_2} \right| - \left| \frac{q_{22}}{q_{21}} \right| A_{12} \right| \leq |t_{22}| \leq \left| \frac{l_2 f_{22}}{1+l_2} \right| + \left| \frac{q_{22}}{q_{21}} \right| A_{12} \tag{4.2.8}$$

where A_{12} is the absolute of the off-diagonal response of channel $(1, 2)$.

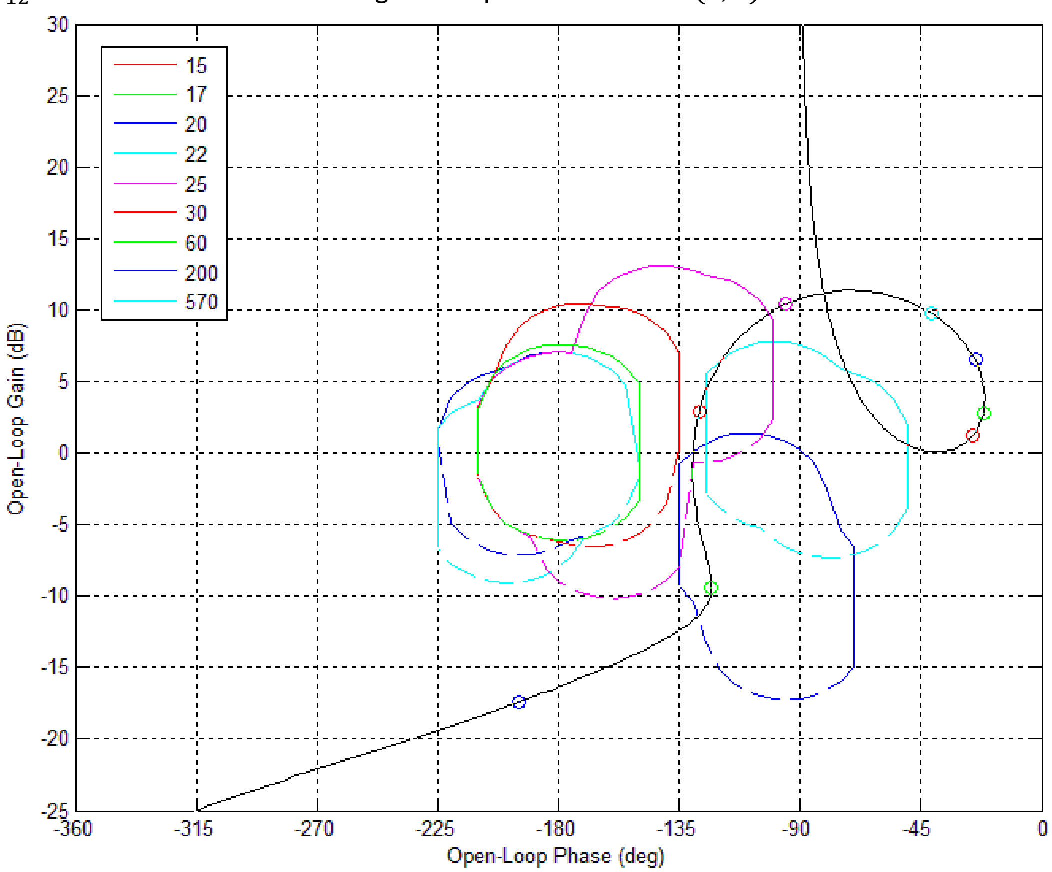

Figure 4.2.2 Nominal loop two with robust stability bounds for linearized point 1

To simplify the design, the pre-filter is chosen to be diagonal i.e. $f_{12} = f_{21} = 0$. The pre-filter element f_{22} was chosen to shape $|t_{22}|$ such that the tracking specifications are satisfied. The pre-filter that gives the response in Fig. 4.2.3 is given by

$$f_{22} = \frac{0.446 \cdot\ (s + 30)\ \cdot (s + 28.8)\ \cdot (s + 4.202)\ (s + 1)}{(s + 8) \cdot\ (s + 0.9) \cdot\ (s^2\ +\ 24s\ +\ 225)}. \tag{4.2.9}$$

The equation that may be used to check the worst case diagonal response for row two is given by

$$|t_{22}| = \left|\frac{l_2 f_{22}}{1 + l_2}\right| \pm \left|\frac{q_{22}}{q_{21}}\right| A_{12} \tag{4.2.10}$$

which is derived from Eq. (4.2.8).

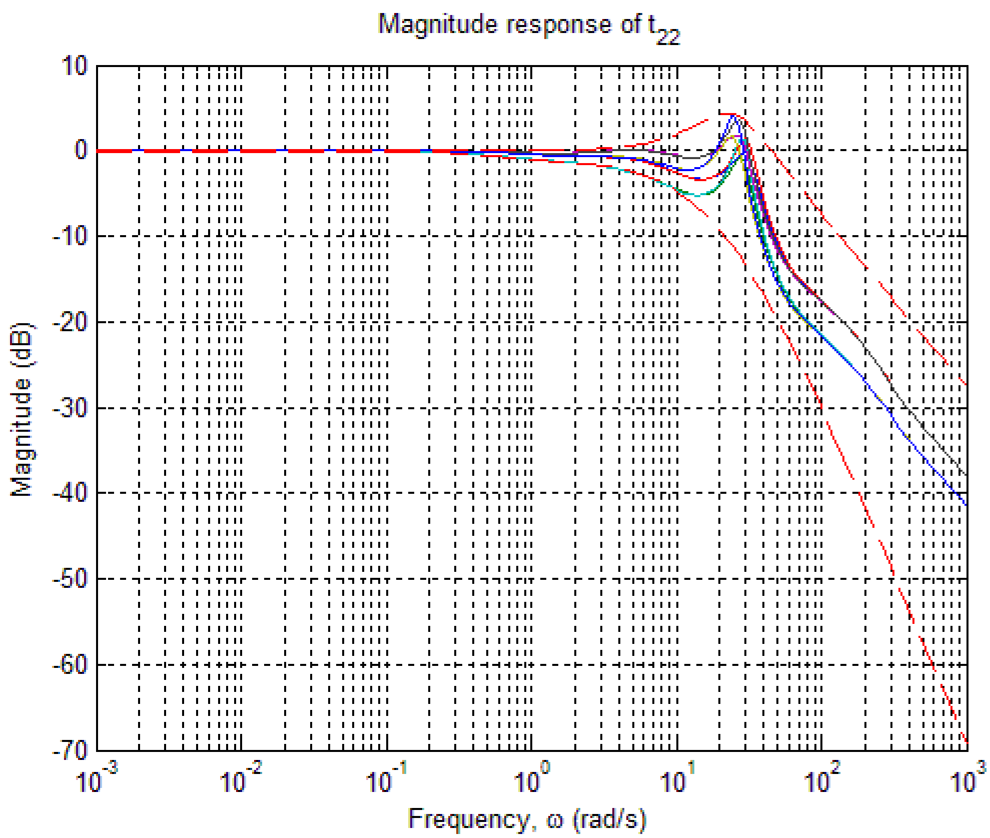

Figure 4.2.3 Magnitude response of t_{22} after row two is designed for linearized point 1

The exact design equations for loop one is given by

$$|t_{11}| \leq \left|\frac{q'_{11} g_1 f_{11}}{1 + q'_{11} g_1}\right| \leq A_{11}, \tag{4.2.11}$$

$$|t_{12}| \leq \left|-\frac{(q'_{11}/q'_{12}) g_2 f_{22}}{1 + q'_{11} g_1}\right| \leq A_{12}. \tag{4.2.12}$$

The *new equivalent* plants for loop one that incorporate loop two design are given by Eqs. (2.1.3.20) - (2.1.3.21). The loop one bounds which are obtained as a result of operations in Eqs (4.2.11) - (4.2.12) can be generated by using *genbnds(10,…)* command in the Matlab™ QFT toolbox (Borgesani, Chait and Yaniv, 1998). An alternative QFT package that one could use is the MIMO QFT CAD Package by Houpis, C. and Sating, R. (1997).

In the final loop, the robust stability constraint given by Eq. (4.2.13) is imposed to ensure that the final loop has a stability margin of $6dB$. Figure 4.2.4 shows the intersection of the tracking bounds (Eq. (4.2.11) and Eq. (4.2.12)) and the stability margin bounds for loop one as well as the nominal loop plot.

$$|1 + l_1'|_{dB} \geq -6dB \tag{4.2.13}$$

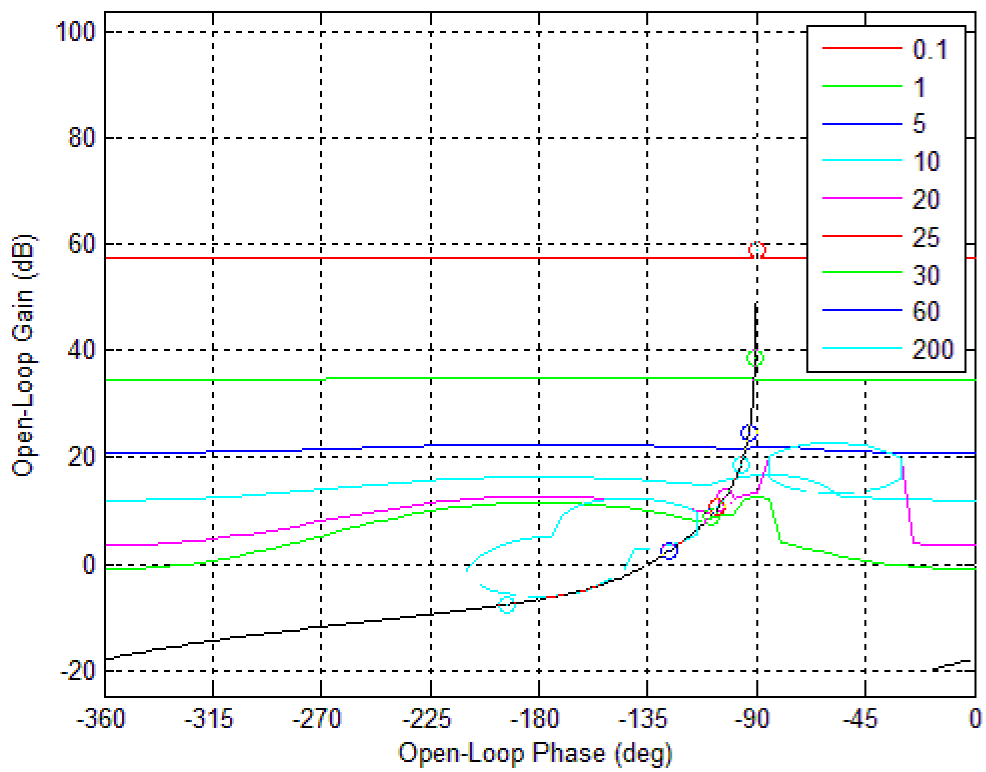

Figure 4.2.4 Nominal loop one with the intersection of tracking and robust stability bounds for linearized point 1

The controller that satisfies the global boundaries is given by

$$g_{11} = \frac{-0.0077415 \cdot (s + 8.654) \cdot (s^2 + 208.1s + 1.624 \times 10^4)}{s \cdot (s + 140.1)^2}. \tag{4.2.14}$$

To complete the design for linearized point 1 the row one pre-filter element must be design. The pre-filter that shapes the diagonal response to satisfy the reference tracking specifications for row one is

$$f_{11} = \frac{1}{(s/20 + 1)}. \tag{4.2.15}$$

The reference to output response for the closed-loop uncertain system is shown in Fig. 4.2.5. To confirm the stability of the system, a step response simulation was run and the results are shown in Fig. 4.2.6.

The magnitude and simulation results for the closed-loop system for linearized point 1 satisfy all tracking and stability specifications. The magnitude response shows that the diagonal channel for loop two dominated the loop gain requirements whereas in loop one the off-diagonal channel dominated the loop gain requirements. Figure A2.16 is a step response from the reference to the plant input. By scaling Fig. A2.16 it can be shown that the maximum reference step one can achieve without amplitude saturation in any channel is 0.1027rad/s, which is acceptable.

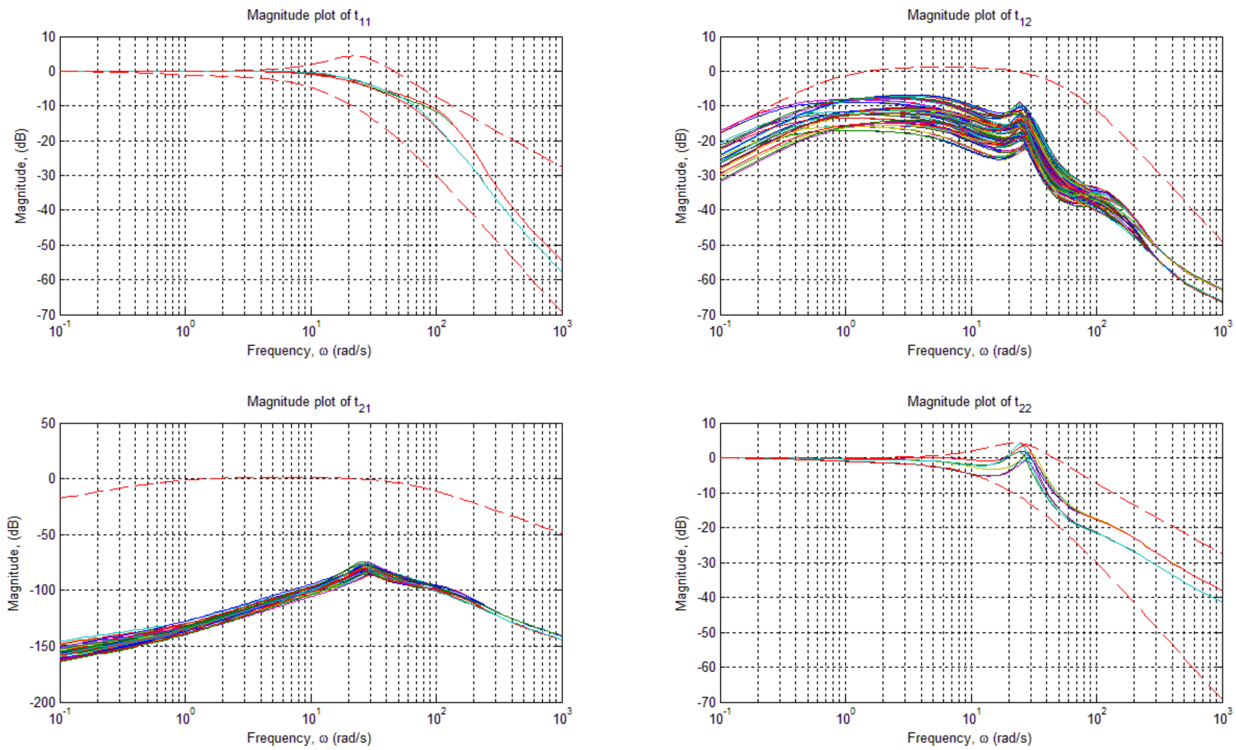

Figure 4.2.5 Magnitude plot of the closed-loop system with the specifications (red dashed) for linearized point 1

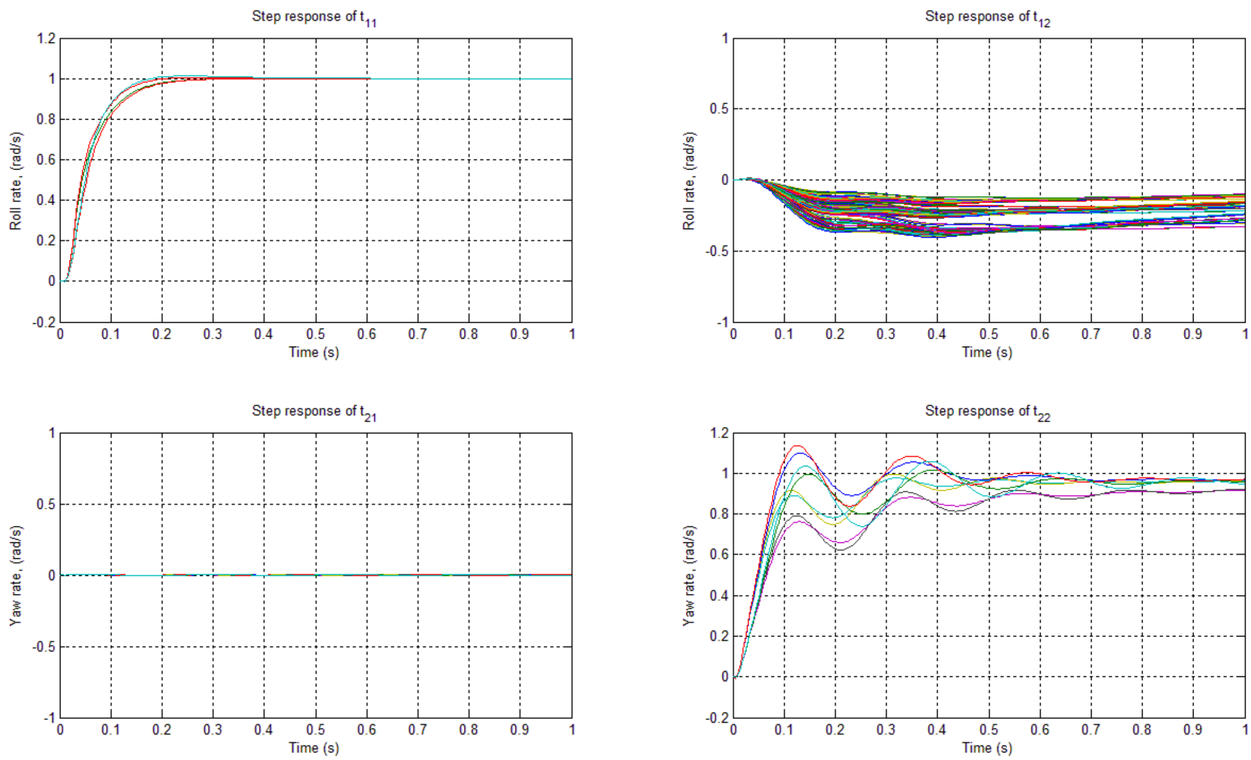

Figure 4.2.6 Step response of the closed-loop system for linearized point 1

Since the outcome of the design for linearized points 2-3 where not much different to linearized point 1, the designs for operating points 2-3 are listed in Appendix A3.

Application to Linearized Point 4

The same procedure was done for designing the controllers for the higher angle of attack plants (4-6) as was done for linearized points 1-3. In all cases, it was found that the second loop had lower loop gain demands. To illustrate this, the bounds for l_1 and l_2 are generated for linearized point 4. The bounds for each channel are shown in Fig. 4.2.7. The nominal loops are the respective nominal plants (i.e. $g_{ii} = 1$). It is clear that loop two requires a much lower gain cross-over frequency compared to loop one.

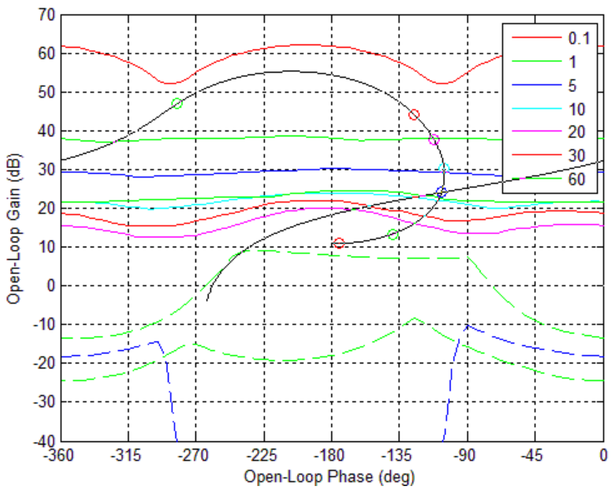

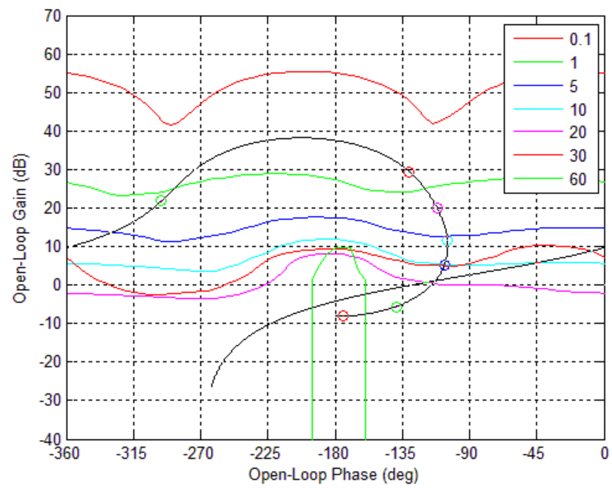

Figure 4.2.7 Tracking bounds for l_1(left) and l_2(right) with their respective nominal loops

The loop two controller that was designed for linearized point 4 satisfied all boundaries. An appropriate pre-filter design shaped the worst case reference to output response to meet design specifications as shown in Fig. 4.2.8. The controller and pre-filter that achieved row two response is given by

$$g_{22} = \frac{-482.9528\,(s+131)\,(s+28.62)\,(s+20.85)\,(s+3.798)}{s\,(s^2\;+\;3.027s\;+\;2.411)\,(s^2\;+\;1280s\;+\;6.4\times10^5)}. \tag{4.2.16}$$

$$f_{22} = \frac{24.99\,(s+10)\,(s+1.8)\,(s^2\;+\;40s\;+\;1600)}{(s+30)\,(s+18)\,(s+1.7)\,(s^2\;+\;44.8s\;+\;784)}. \tag{4.2.17}$$

After row two pre-filter design, the equivalent plants were generated to design loop one. It was found that stabilizing loop one proved to be impossible with a $6dB$ robust stability requirement, even without any tracking bounds imposed.

Figure 4.2.9 shows the loop design for linearized point 4 using the controller in Eq. (4.2.16). It can be seen that the controller was designed to be conservative with respect to the tracking bounds. This was done in an attempt to reduce the complexity of the pre-filter in the subsequent step. From the order of the pre-filter it can be seen that the over-design did not significantly ease the pre-filter design.

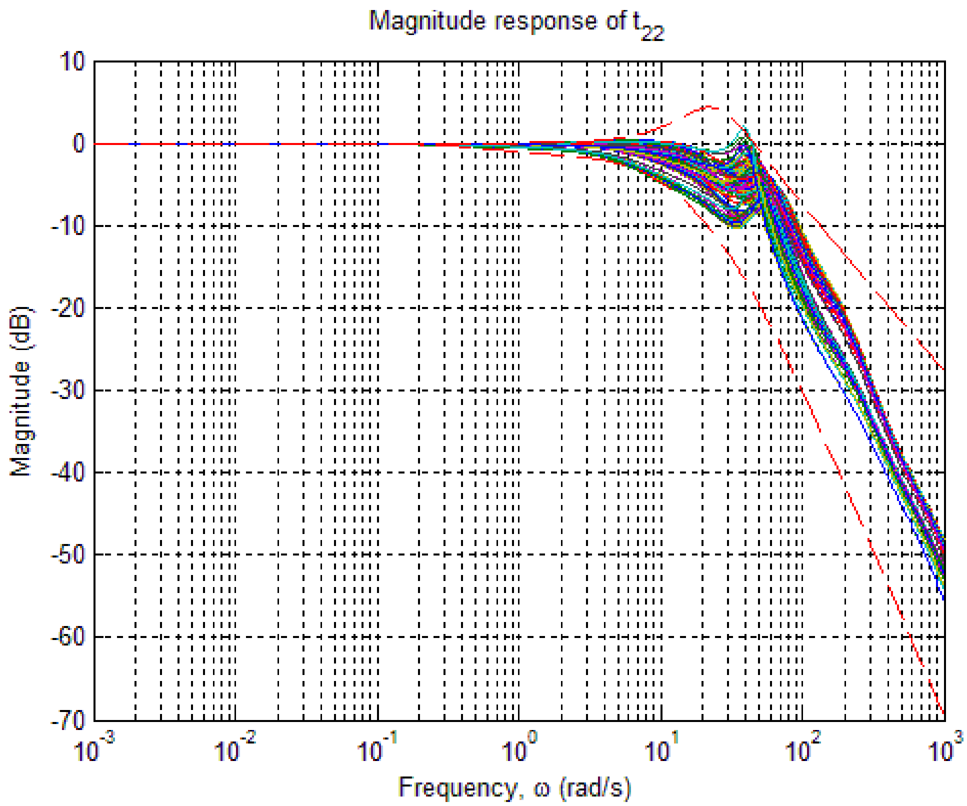

Figure 4.2.8 Magnitude response of t_{22} after row two is designed for linearized point 4

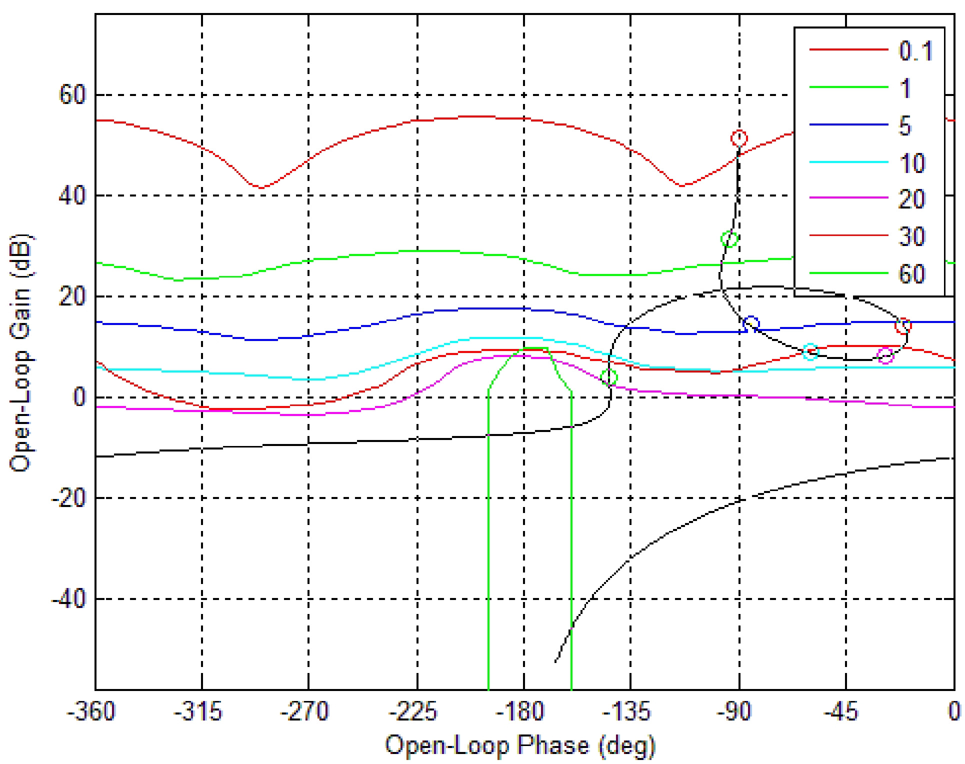

Figure 4.2.9 Nominal loop two with tracking bounds for linearized point 4

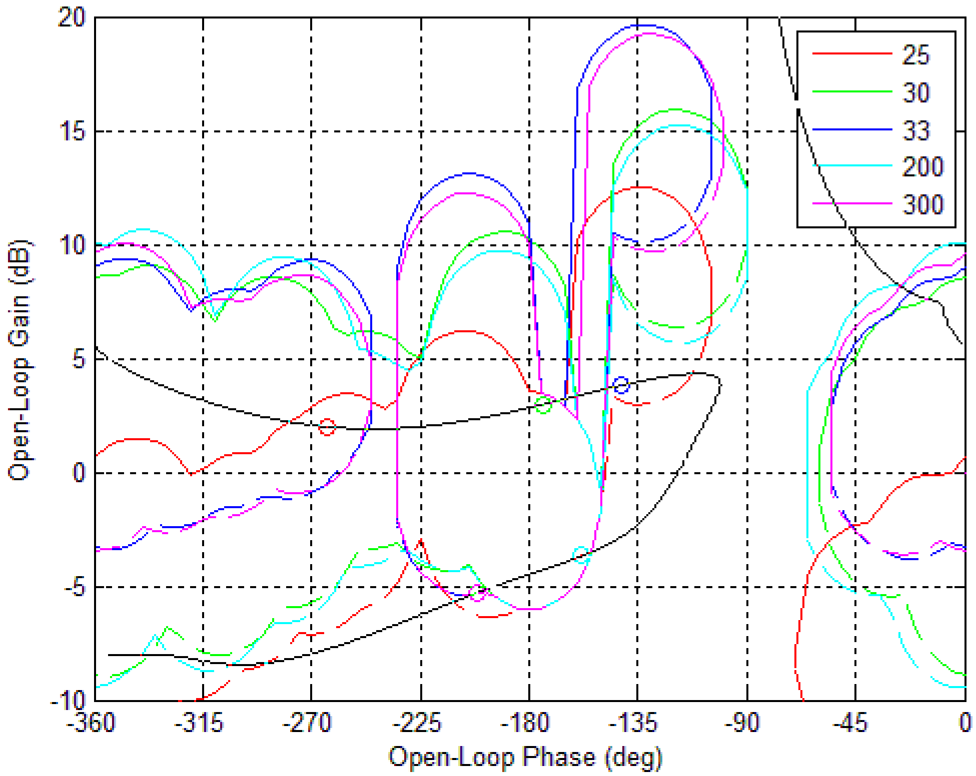

Figure 4.2.10 Nominal loop one with robust stability bounds for linearized point 4

The nominal loop for row one design is shown in Figure 4.2.10 with stability boundaries generated for a stability margin of $6dB$. The figure shows the best controller that was designed. Although the nominal plant is stable, stability of other plants cannot be guaranteed because most of the design frequency points lie in the region that violates specifications. After attempting to use a smaller stability margin it was possible to stabilize loop one, but with negligible feedback benefits. Hence a QFT solution for linearized point 4 was not found.

Application to Linearized Points 5-6

It was not possible to meet both tracking and stability specifications for the 5th and 6th linearized plants. An attempt was made to satisfy all tracking specifications for loop two of linearized point 5 while neglecting stability (i.e. loop two was allowed to be unstable). As a result of this, the equivalent loop one equations were found to contain right-hand plane zeros and poles that were very close to each other. This resulted in the last loop (nominal) being stabilized with almost no stability margin.

The last linearized point was found to be impossible to stabilize either loop with a $10dB$ stability margin due to the unstable pole and delay in the system.

The results of the attempted design for linearized points 4-6 show that simple diagonal QFT controllers are not appropriate for plants with significant cross-coupling and uncertainty. In Section 6, the theory described in Section 2.3 is applied to one of the plants that the QFT technique could not solve to show that QFT still has design benefits for more complicated plants.

4.3.Non-diagonal Controller Design

This section presents an application of the non-diagonal controller design method. The design is done for output disturbance rejection specifications and only for a single linearized point to demonstrate the concept. The pre-compensator design procedure was done for linearized points starting from six to two. From the analysis of each linearized point result, it was found that for operating points greater than 2, the combination of the uncertainty and cross-coupling makes it very difficult to get significant results. Hence the 2nd linearized point was chosen to demonstrate the quantitative decoupling theory. A design using a diagonal QFT controller is first done so that a comparison between the non-diagonal and diagonal design can be made.

Problem statement

The LTI plant is given by the 2nd linearized point with uncertainties given in Section 3.1 (Table 3.2). The task is to design a controller $\boldsymbol{G}(s)$ such that the output disturbance-to-plant output frequency (magnitude) response for the uncertain system is bounded by the specifications given below and the closed-loop system is stable for all plant cases.

$$|t_{ii}| \leq \left|\frac{j\omega/8}{(j\omega)/11.3+1}\right| = A_{ii} \quad i = 1{,}2. \tag{4.3.1}$$

$$|t_{ij}| \leq \left|\frac{j\omega/3.517}{((j\omega)/5+1)\cdot\big((j\omega)/15+1\big)}\right| = A_{ij} \quad i,j = 1{,}2. \tag{4.3.2}$$

Presentation of design using original QFT method (diagonal)

Based on observing the bounds generated for loop one and loop two, it was decided to design loop two first as it is easier to achieve the requirements. Using the original formulation (Section 2.1.2), output disturbance rejection design requires satisfying Eqs (2.1.2.16) - (2.1.2.17) for loop two. The bounds generated from the design equations and the nominal loop that satisfies those bounds are shown in Fig. 4.3.1.

Provided loop one specifications are met, the magnitude response for loop two will lie within the envelope of the uncertain system response shown in Fig. 4.3.2. The figure is obtained by plotting Eqs (4.3.3) - (4.3.4) for the uncertain plant set.

$$|t_{21}| = \left|\frac{q_{22}/q_{21}}{1+l_2}\right|(1 \pm A_{11}), \tag{4.3.3}$$

$$|t_{22}| = \left|\frac{1}{1+l_2}\right|\left(1 \pm \left|\frac{q_{22}}{q_{21}}\right| A_{12}\right). \tag{4.3.4}$$

The plot in Fig. 4.3.2 can be used to confirm that the specifications are met for design frequencies where bounds were not generated (provided loop one specifications are met). The controller that satisfies all the bounds is shown in Eq. (4.3.5).

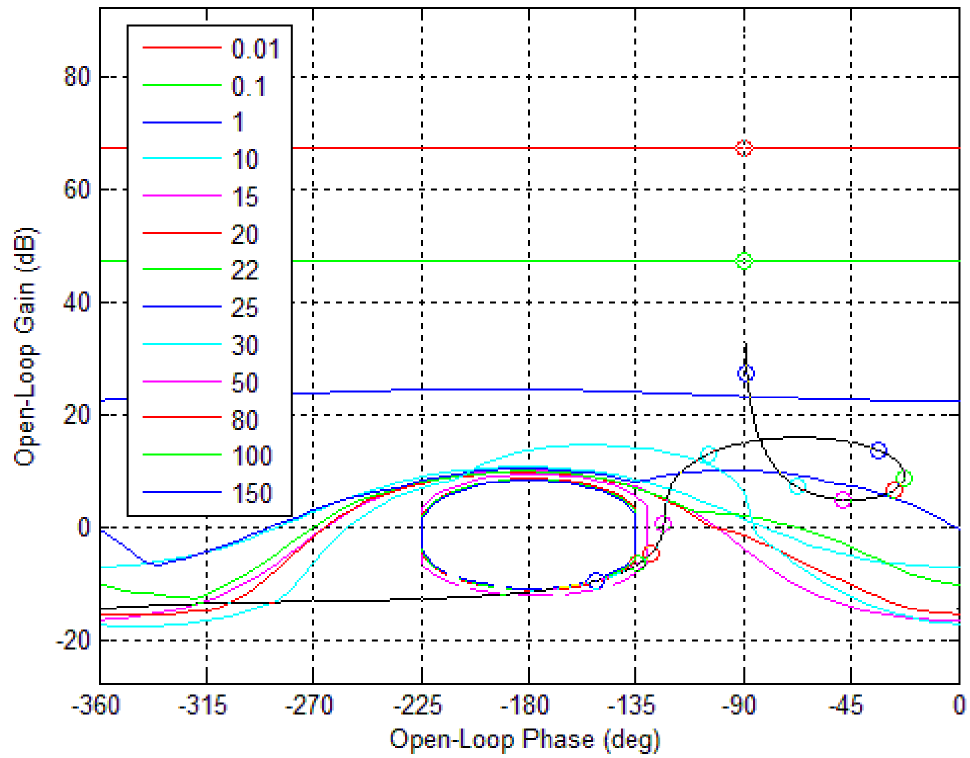

Figure 4.3.1 Nominal loop two with design bounds (disturbance rejection AND stability bounds) for linearized point 2

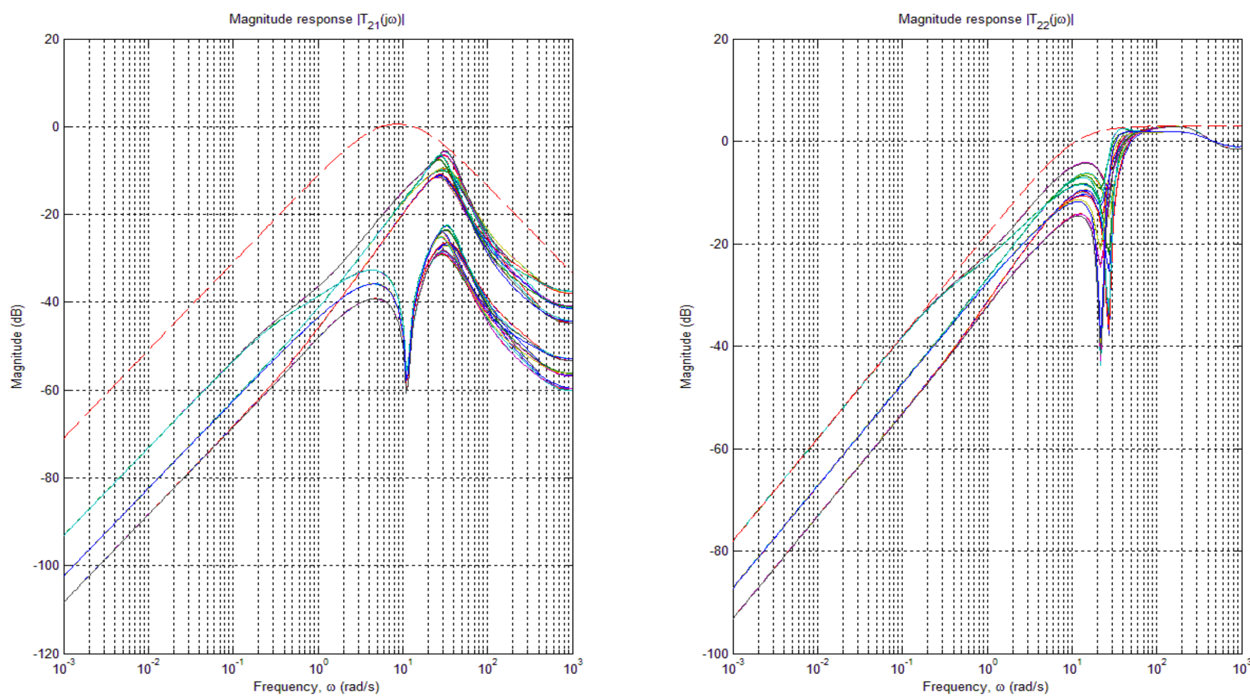

Figure 4.3.2 Magnitude response for channel T_{21} (left) and T_{22} (right) provided loop one specifications are met

$$g_{22} = \frac{-836.8\,(s + 405.1)\,(s + 251.2)\,(s^2\ +\ 18.58s\ +\ 414.2)}{s\,(s + 1300)^2\,(s + 894.9)\,(s + 0.8181)} \tag{4.3.5}$$

Since loop two has been designed, loop one can be designed without any conservativeness by solving explicitly for loop one transfer functions. By defining the equivalent plants by Eq. (4.3.6) and Eq. (4.3.7), the design equations for loop one are given by Eq. (4.3.8) and Eq. (4.3.9). These equations can be derived using a similar procedure presented in Section 2.1.3 "Design Equations for Final Loop". The nominal loop one together with the design bounds are shown in Fig. 4.3.3. As evident from the figure, the majority of the constraints cannot be achieved using this design method, hence loop one was designed with the maximum gain-cross over frequency achievable while ensuring closed-loop stability of the system.

$$q'_{11} = 1/\left(\frac{1}{q_{11}} - \frac{1}{\dfrac{1}{q_{22}} + g_2}\frac{1}{q_{12}}\frac{1}{q_{21}}\right) \tag{4.3.6}$$

$$q'_{11} = 1/\left(\frac{1}{q_{12}} - \frac{1}{\dfrac{1}{q_{22}} + g_2}\frac{1}{q_{12}}\frac{1}{q_{22}}\right) \tag{4.3.7}$$

$$|t_{11}| \le \left|\frac{1}{1 + q'_{11}g_1}\right| \tag{4.3.8}$$

$$|t_{12}| = \left|\frac{q'_{11}/q'_{12}}{1 + q'_{11}g_1}\right| \tag{4.3.9}$$

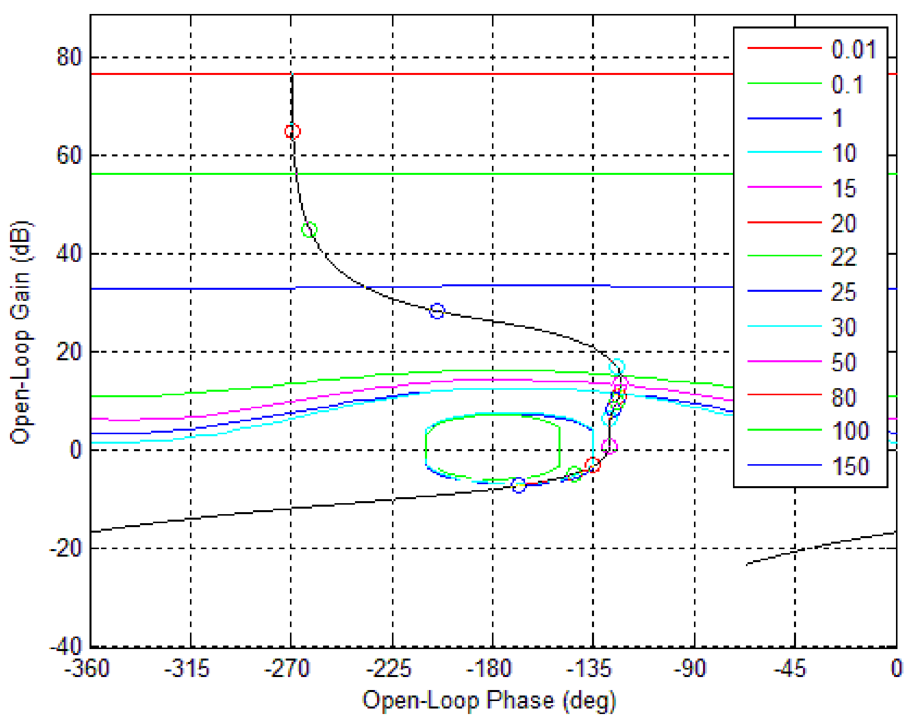

Figure 4.3.3 Nominal loop one with design bounds (disturbance rejection AND stability bounds) for linearized point 2

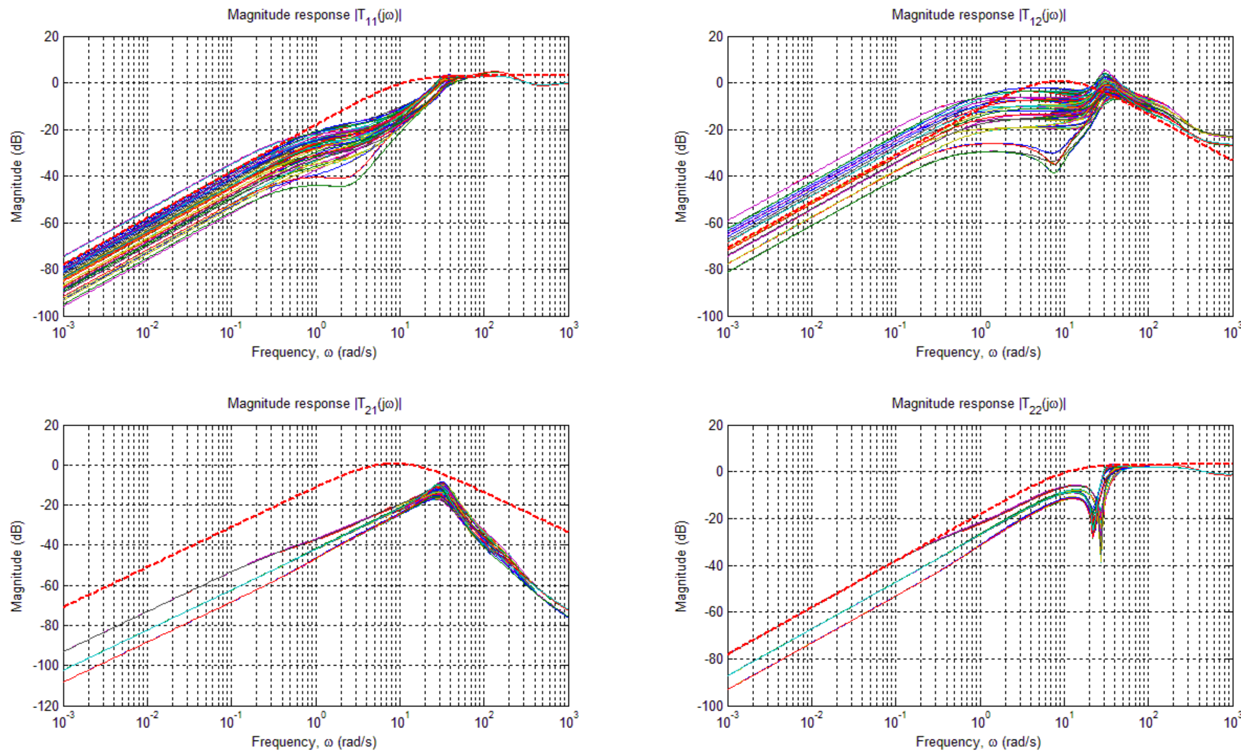

Figure 4.3.4 Magnitude plot of the closed-loop system for disturbance rejection with the specifications (red dashed)

The actual output disturbance rejection response for the final system is shown in Fig. 4.3.4 for the uncertain plant set. The first row responses clearly indicate that the specifications have not been met. This was expected since loop one design does not meet the QFT specifications. Since the first row specifications have not been met, achieving row two specifications cannot be expected (since the design equation assumes specifications are met) and the actual response for row two does not meet the specifications (cannot be seen clearly in the plot above).

In the next subsection, the non-diagonal controller will be designed and the outcome of the two design methods will be compared.

Presentation of design using Non-diagonal Controller Design

From the theory section of non-diagonal controller design (Section 2.1.5), it is known that the controller is chosen to consist of a diagonal QFT controller and unimodular matrices. To recapitulate, each unimodular matrix serves to reduce the interaction by modifying the plant in a particular row. The stability criteria (see pg 19) stated in the theory section will be used in conjunction with the non-diagonal controller design method. Therefore it is desirable to reduce the interaction index near and above the expected gain cross-over frequency to minimize the power transfer from the controller. In order to assess the interaction in the system, the open-loop interaction index given by Eq. (2.1.5.3) is plotted and shown in Fig. 4.3.5.

Figure 4.3.5 shows that there is significant interaction in the plant in the frequency range $20-30\,rad/s$. This gives an indication of the frequency range to aim to reduce interaction index when designing the pre-compensator. The interaction index is a function of the individual loop sensitivity and the equivalent plant elements from Eq. (2.1.5.2). Since the effective disturbance rejection bandwidth for this system is about $10\ rad/s$, the interaction peaks that occur between 20 and $30\ rad/s$ will require high loop gain (low sensitivity) which will in effect increase the required gain cross-over frequency of the individual loops. In the low frequency region, the low sensitivity will dominate in determining the interaction index.

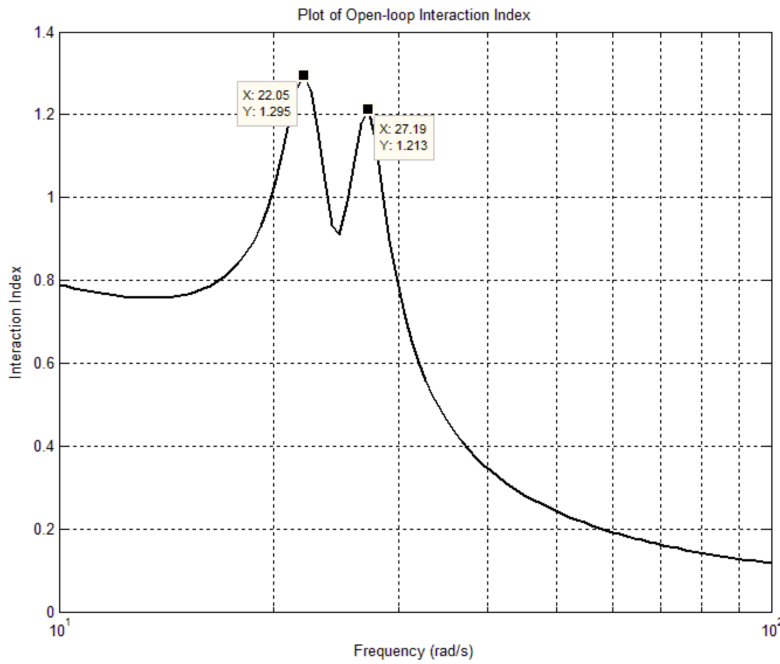

Figure 4.3.5 Open-loop interaction index

The frequencies chosen for the design of the pre-compensator are $[25, 27, 30, 40]$. The first row of the pre-compensator was designed first by choosing the element $\hat{k}_{12}$ to satisfy the bounds generated by finding the linear fractional mapping given by Eq. (2.1.5.8). The magnitude-phase plot of the designed $\hat{k}_{12}$ together with the bounds for $\alpha = [1, 0.9, 0.85]$ are shown in Fig. 4.3.6.

The pre-compensator element $\hat{k}_{12}$ that was designed is given by

$$\hat{k}_{12} = \frac{0.013521\, s^2\, (s + 109.6)\, (s + 6.973)}{(s + 22)^2\, (s^2\ +\ 7.072s\ +\ 586.6)}. \tag{4.3.10}$$

Figure 4.3.7 shows the interaction index after the row one design of the pre-compensator is incorporated into the system. The results show that the interaction index is not significantly reduced by row one design alone. A visible difference occurs about $27\ rad/s$ but the result is still above unity. Using a similar procedure $\hat{k}_{21}$ was design for row two modification which is given by

$$\hat{k}_{21} = \frac{-14426\, s^2}{(s + 225)\, (s + 12)\, (s^2\ +\ 11.76s\ +\ 138.2)}. \tag{4.3.11}$$

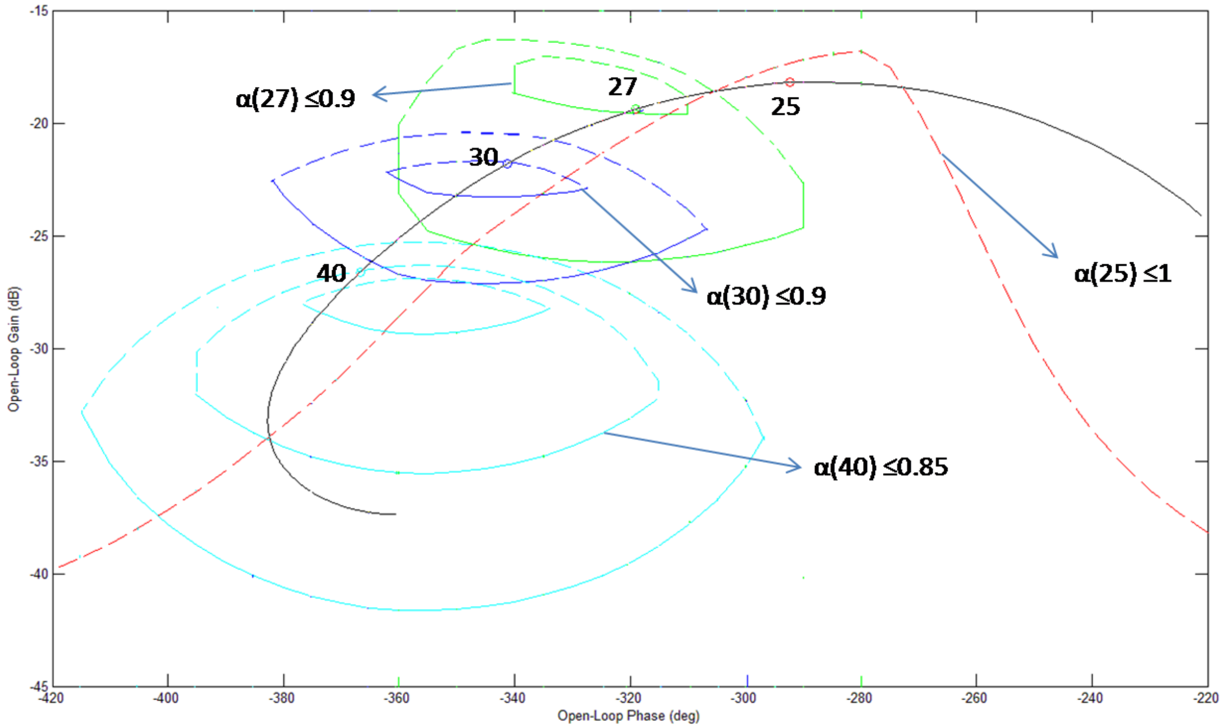

Figure 4.3.6 Design of $\hat{k}_{12}$ and the bounds that provide reduction in interaction index

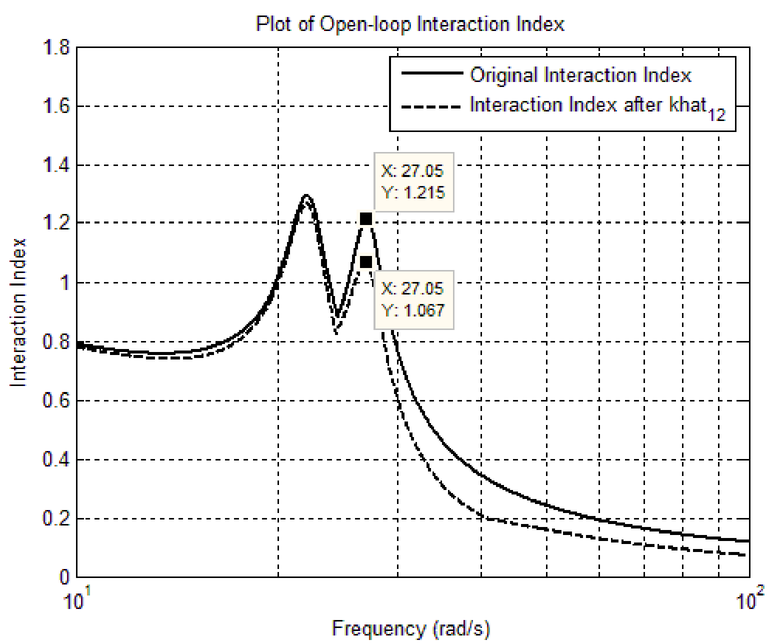

Figure 4.3.7 Interaction index of the system after row one design

The resulting improvement in the interaction index is shown in Fig. 4.3.8. The interaction index is drastically improved after the design of row two pre-compensation. From Eq. (2.1.5.5) the actual pre-compensator is given by

$$\boldsymbol{K} = \begin{bmatrix} 1 & \hat{k}_{12} \\ \hat{k}_{21} & \hat{k}_{12}\hat{k}_{21}+1 \end{bmatrix}^{-1} = \begin{bmatrix} \hat{k}_{12}\hat{k}_{21}+1 & -\hat{k}_{12} \\ -\hat{k}_{21} & 1 \end{bmatrix}. \tag{4.3.12}$$

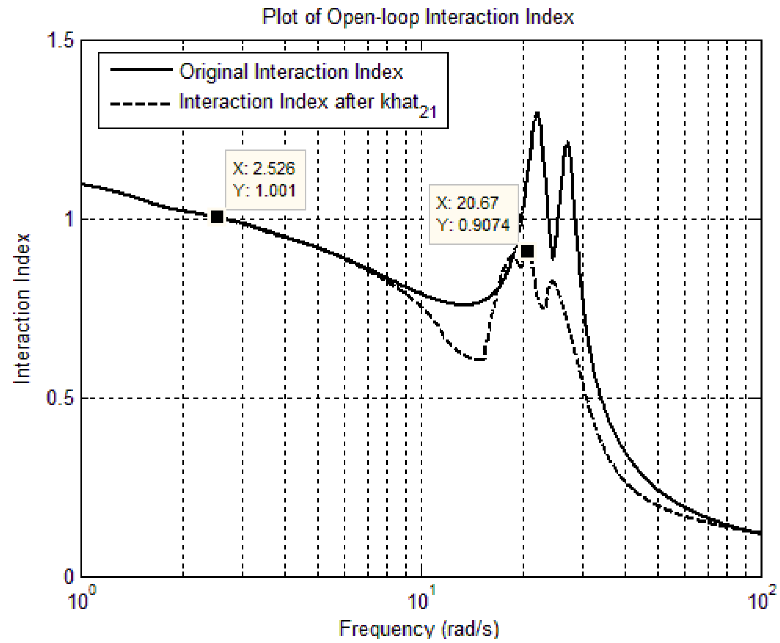

Figure 4.3.8 Interaction index after complete pre-compensator design

Now that the pre-compensator design is done, the diagonal QFT controller can be designed for the modified plant $\boldsymbol{P}' = \boldsymbol{PK}$. It will be shown how the pre-compensator reduces the conservativeness of the first loop that is designed (loop two) and how the inclusion of a pre-compensator allows the specifications to be met.

An additional constraint to the general equations used for the QFT design is given by

$$\frac{1}{1+l_i'} \leq \sqrt{\frac{q_{12}'q_{21}'}{q_{11}'q_{22}'}}. \tag{4.3.13}$$

Equation (4.3.13) can be derived from Eq. (2.1.5.2) and is used to ensure that the interaction index of the closed loop system is less than unity provided that both loops are designed to equally reduce the interaction index. Loop two was designed first and the nominal loop with the bounds are shown in Fig. 4.3.10.

The controller that meets these requirements is given by

$$g_{22} = \frac{-9.89\,(s^2 + 11.03s + 142.2)(s^2 + 6.297s + 363.1)}{s\,(s+270)\,(s+0.682)\,(s^2 + 9.861s + 97.27)}. \tag{4.3.14}$$

A magnitude plot of the controller obtained through the diagonal QFT method and the non-diagonal QFT method is shown in Fig. 4.3.9. The plot shows that the non-diagonal design has lower loop gain requirements than the original design.

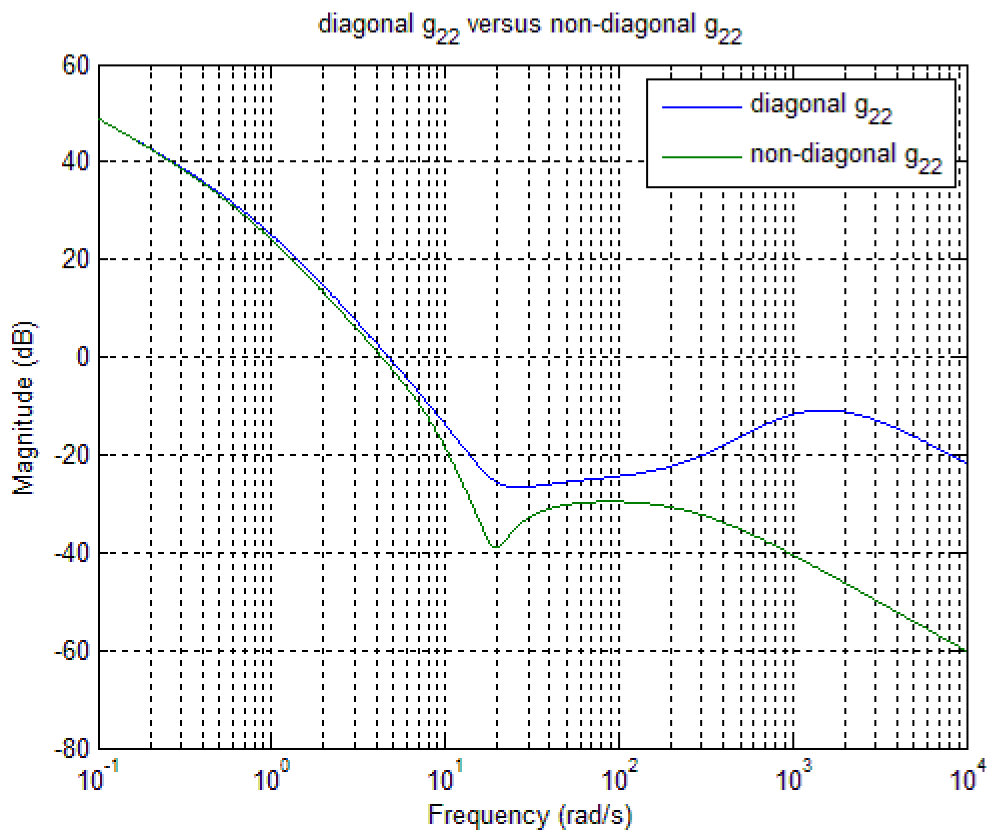

Figure 4.3.9 Magnitude plot of diagonal g_{22} and non-diagonal g_{22}

The loop one design is shown in Fig. 4.3.11 together with the nominal loop bounds. The controller that meets the disturbance rejection and stability bounds is given by

$$g_{11} = \frac{-123.3722\,(s+166.6)\,(s+24.73)\,(s+3.352)\,(s^2\ +\ 16.59s\ +\ 560)}{s\,(s+0.7384)\,(s^2\ +\ 13.25s\ +\ 702.4)(s^2\ +\ 5000s\ +\ 6.252\times 10^6)}. \tag{4.3.15}$$

Unlike the pure diagonal design case, all the constraints were met using the non-diagonal controller design method for the particular design example. The final interaction index after the non-diagonal controller is taken into account is shown in Fig. 4.3.12. Note that closed-loop stability can be inferred from the individual loop stability since the interaction index is less than unity for all frequencies. The magnitude response of the closed-loop system is shown in Fig. 4.3.13. The step response of the system confirms stability as shown in Fig. 4.3.14. From this design case study, the main advantage of the non-diagonal design method is that the specification of certain systems can be met whereas a diagonal controller may not suffice. The main disadvantage is that the overall controller structure generally gets more complicated and inevitably becomes higher order. This may lead to the loss of integrity against sensor and actuator failure in some systems. The final controller is given in symbolic form by

$$\boldsymbol{G}' = \boldsymbol{K}\cdot\boldsymbol{G} = \begin{bmatrix} \hat{k}_{12}\hat{k}_{21}+1 & -\hat{k}_{12} \\ -\hat{k}_{21} & 1 \end{bmatrix}\begin{bmatrix} g_{11} & 0 \\ 0 & g_{22} \end{bmatrix} = \begin{bmatrix} g_{11}\left(\hat{k}_{12}\hat{k}_{21}+1\right) & -g_{22}\hat{k}_{12} \\ -g_{11}\hat{k}_{21} & g_{22} \end{bmatrix} \tag{4.3.16}$$

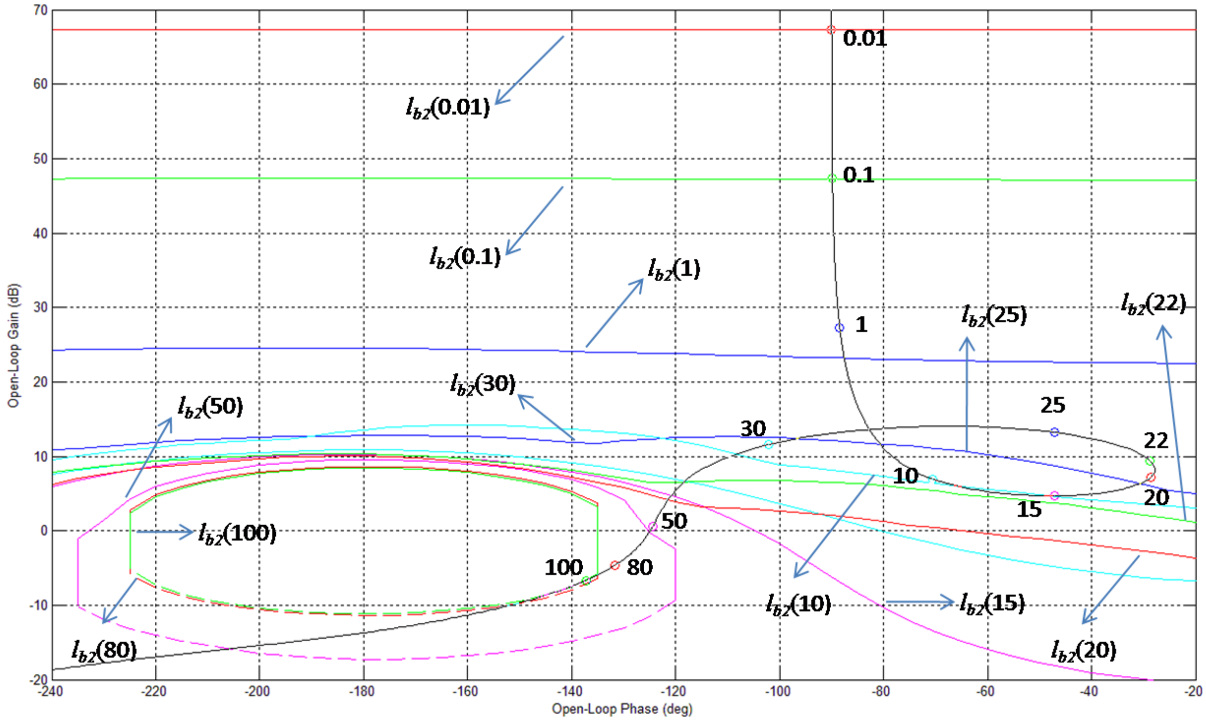

Figure 4.3.10 Nominal loop two with design bounds (disturbance rejection AND stability bounds) using the equivalent plant that incorporates the pre-compensator

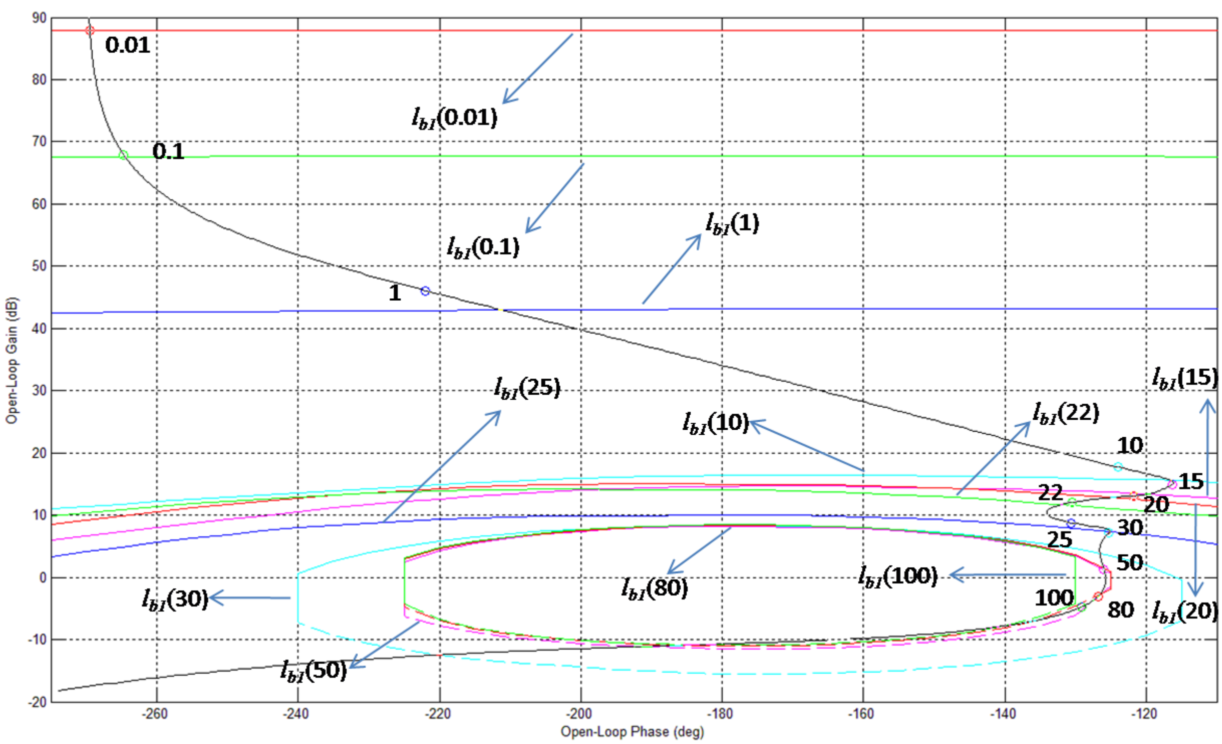

Figure 4.3.11 Nominal loop one with design bounds (disturbance rejection AND stability bounds) using the equivalent plant that incorporates the pre-compensator

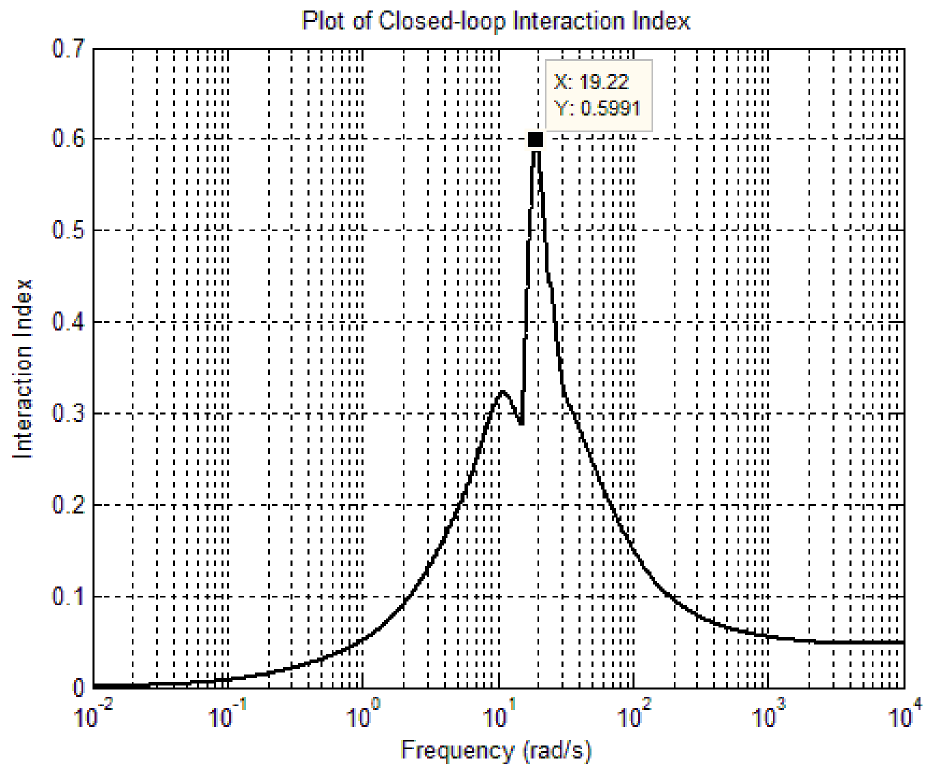

Figure 4.3.12 Closed-loop interaction index (see Eq. (2.1.5.2))

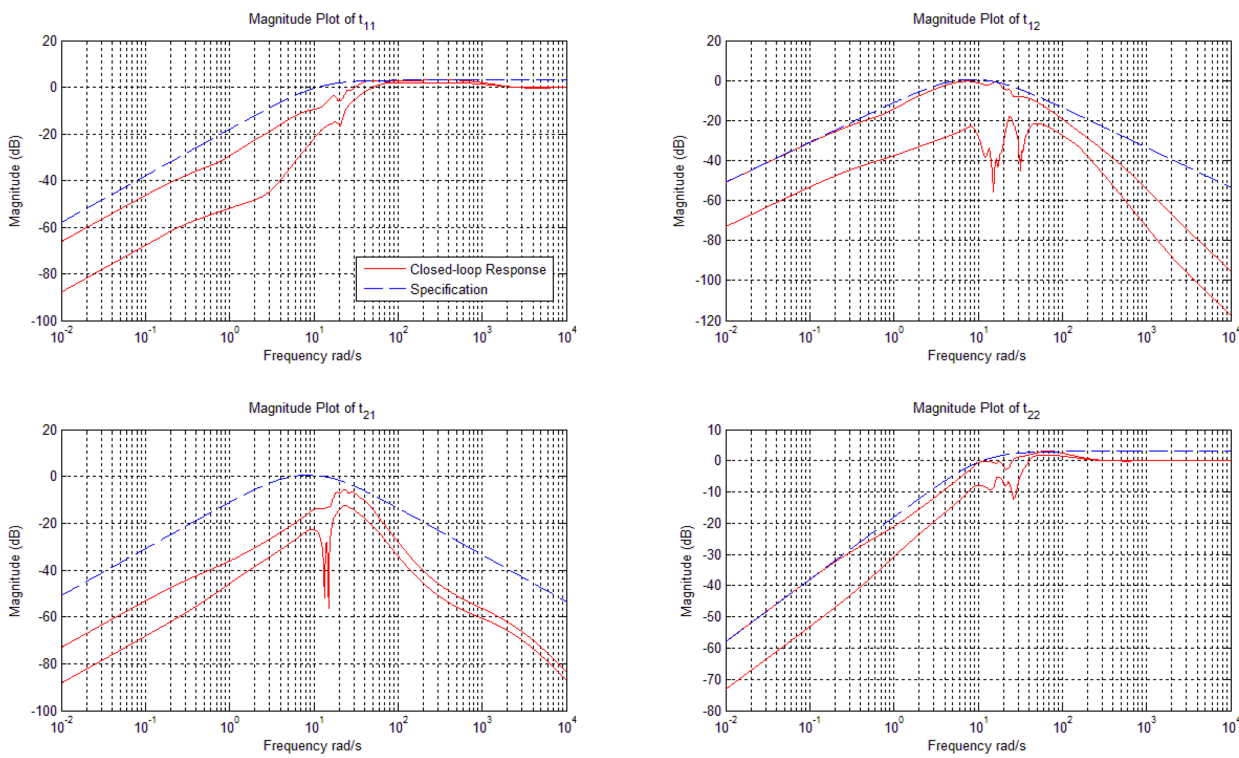

Figure 4.3.13 Magnitude plot of the closed-loop system for disturbance rejection using non-diagonal controller

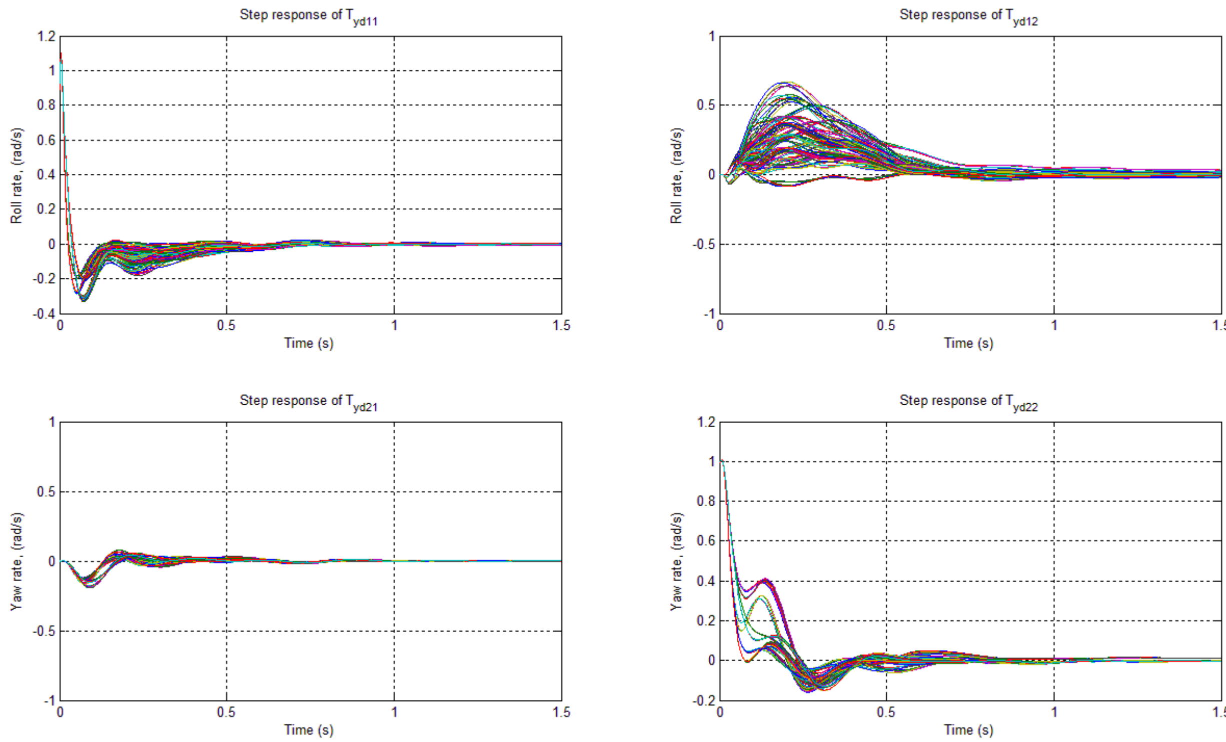

Figure 4.3.14 Step response of the closed-loop system using non-diagonal controller

4.4. Design using Error-Tracking Specifications

The specification for the error-tracking design is different from the original QFT specifications. In the original QFT design there are upper and lower bound specifications for the reference to output response. In the error-tracking design method the specifications are of disk form around some model. It was intended to generate the model transfer function from the original QFT specifications but an approximation could not be found. Therefore new specifications were generated to demonstrate the error-tracking design concept. This is done for linearized point 2 only. These specifications are comparable to the specifications used for the designs in Section 4.2. This section is an application of the theory in Section 2.1.6. The model chosen for the diagonal channel is given by

$$m_{ii}(s) = \frac{22.5108\,(s+49.49)\,(s^2 + 23.61s + 223.3)}{(s+40)\,(s+10)\,(s^2 + 30s + 625)} \cdot delay \qquad i = 1,2. \tag{4.4.1}$$

The delay is given by a second order padé approximation.

The off-diagonal channel model is given by

$$m_{ij}(s) = \frac{0.85\,s}{\left(\frac{s}{0.4}+1\right)\left(\frac{s}{60}+1\right)} \cdot delay \qquad i,j = 1,2;\ i \neq j. \tag{4.4.2}$$

The diagonal channel and off-diagonal channel specifications are shown in Fig. 4.4.1 and Fig. 4.4.2, respectively.

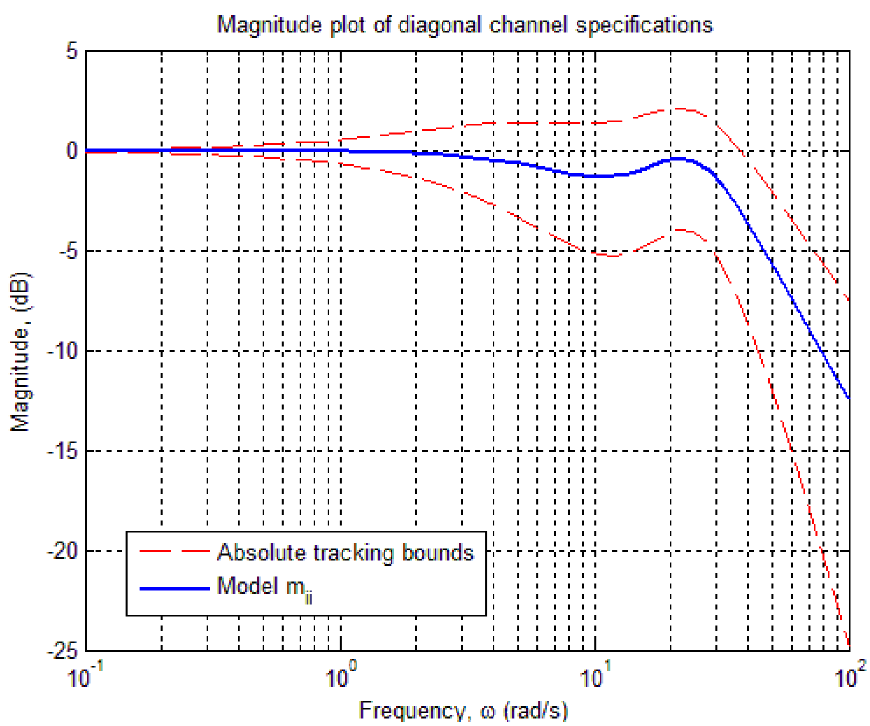

Figure 4.4.1 Diagonal channel error-tracking specifications

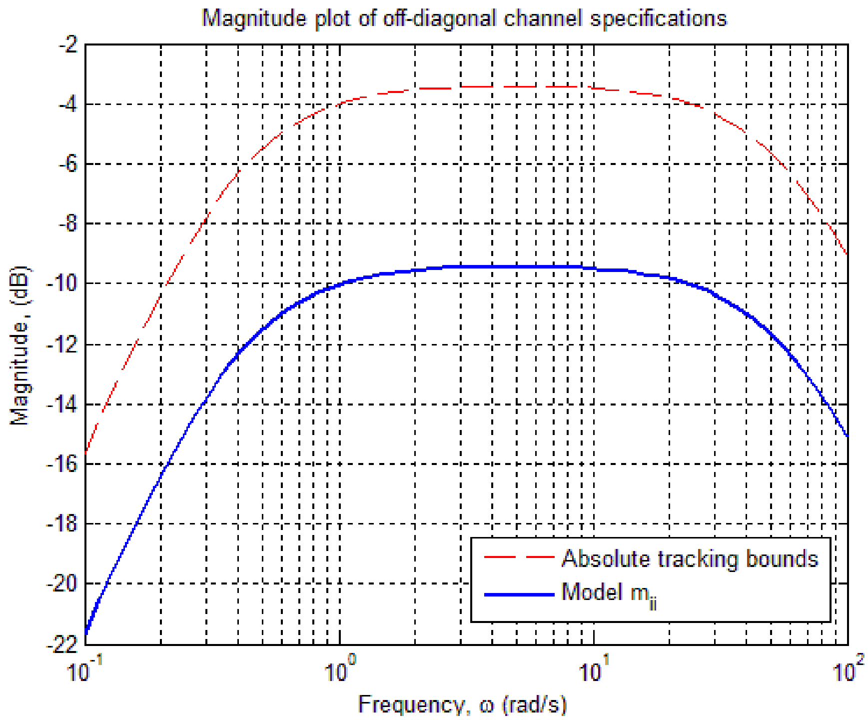

Figure 4.4.2 Off-diagonal error-tracking specifications

The error-tracking specifications were selected through an iterative procedure which involved adjusting the specifications in an attempt to approximate the original specifications. The error-tracking specifications are given by

$$a_{ii} = |e_{ii}(j\omega)| = \left|\frac{0.07\,s}{\left(\frac{s}{5}+1\right)\left(\frac{s}{60}+1\right)}\right|_{s=j\omega} \qquad i = 1,2. \tag{4.4.3}$$

$$a_{ij} = \left|e_{ij}(j\omega)\right| = 0.5 \qquad i \neq j. \tag{4.4.4}$$

Due to loop two having less severe constraints, it was designed first. The design equations that are used to obtain the tracking bounds for loop two are given by

$$e_{21} \leq \left|\frac{1}{1+l_2}\right|\left(\left|\frac{q_{22}}{q_{21}^*}\right| + \left|\frac{q_{22}}{q_{21}}\right| A_{11}\right) \leq A_{21}, \tag{4.4.5}$$

$$e_{22} \leq \left|\frac{1}{1+l_2}\right|\left(\left|\frac{q_{22}}{q_{22}^*}\right| + \left|\frac{q_{22}}{q_{21}}\right| A_{12}\right) \leq A_{22}. \tag{4.4.6}$$

The meaning of the above equations and symbols are expressed in Section 2.1.6.

The robust stability bound was chosen as $6dB$ or equivalently

$$\left|\frac{1}{1+l_2}\right| \leq 2 \quad \forall\omega. \tag{4.4.7}$$

The intersection of the error-tracking and robust stability bounds is shown in Fig. 4.4.3 together with the nominal that satisfies the bounds.

The controller that meets the bounds is given by

$$g_{22}(s) = \frac{-79409\,(s^2 + 9.329s + 135.9)}{s^2\,(s^2 + 1000s + 1 \times 10^6)}. \tag{4.4.8}$$

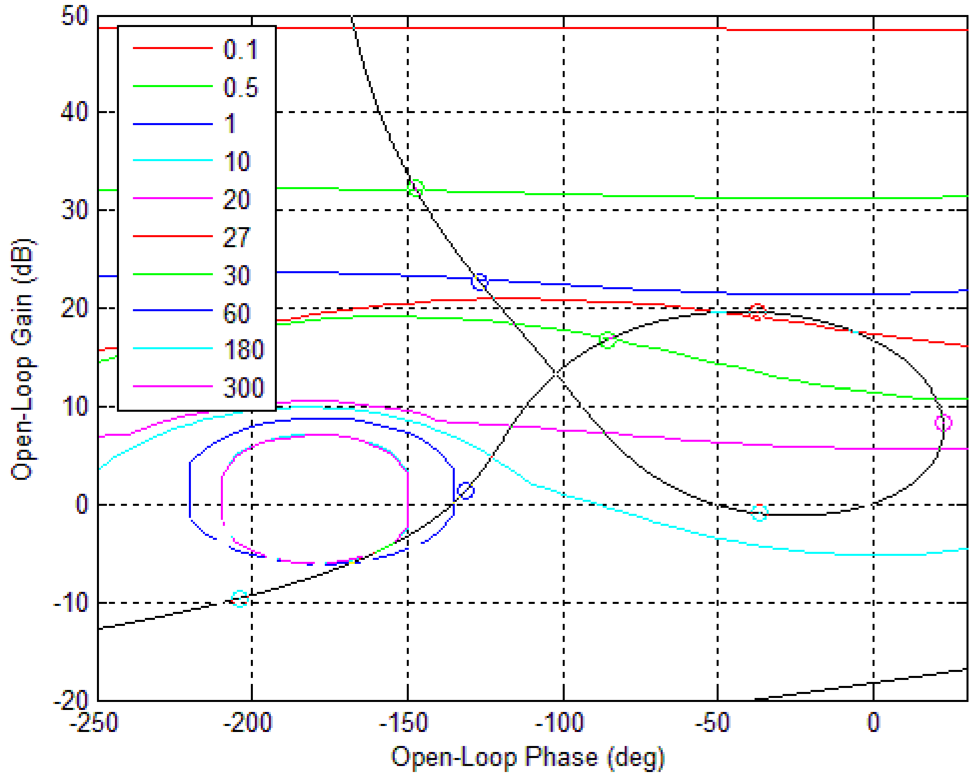

Figure 4.4.3 Nominal loop two with design bounds (error-tracking AND stability bounds)

Loop one design can be made *less conservative (not exact because pre-filter elements not known)* by the inclusion of g_{22}. The resulting loop one equations are given by

$$e_{11} \le \left| \frac{\dfrac{q'_{11}}{q^*_{11}} - \dfrac{q'_{11}q_{22}}{q_{12}q^*_{21}(1+l_2)}}{1+l'_1} \right| \le A_{11}, \tag{4.4.9}$$

$$e_{12} \le \left| \frac{\dfrac{q'_{11}}{q^*_{12}} - \dfrac{q'_{11}q_{22}}{q_{12}q^*_{22}(1+l_2)}}{1+l'_1} \right| \le A_{12}. \tag{4.4.10}$$

A robust stability bounds of $6dB$ is used. The loop one controller that meets all requirements is given by

$$g_{11}(s) = \frac{-557300\,(s+12.76)\,(s+12.04)\,(s^2 + 286.4s + 5.3 \times 10^4)}{s\,(s+1000)\,(s+452.4)\,(s+4.08)\,(s^2 + 1800s + 9 \times 10^6)}. \tag{4.4.11}$$

The bounds as a result of the intersection of the error-tracking bounds and stability bounds are shown together with the nominal loop that satisfies loop one constraints in Fig. 4.4.4. The pre-filter is obtained by the application of Eq. (2.1.6.12). The final reference to output magnitude response is shown in Fig. 4.4.5 which prove that the error-tracking specifications are met for linearized point 2. The step response in Fig. 4.4.6 confirms the closed-loop stability of the system.

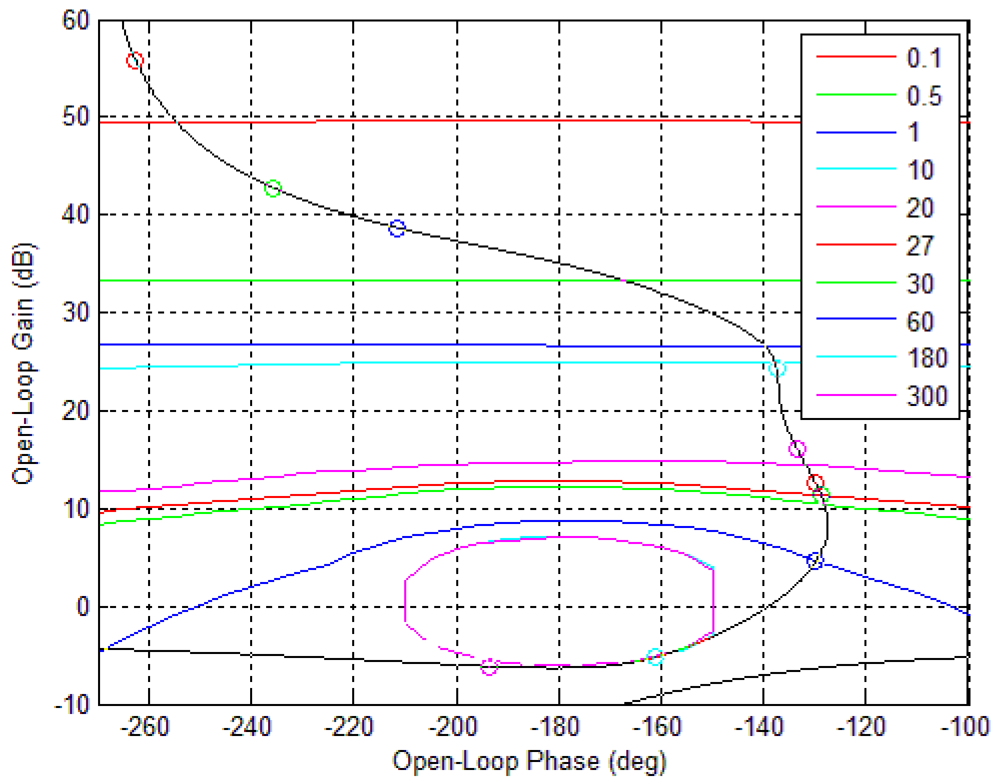

Figure 4.4.4 Nominal loop one with design bounds (error-tracking AND stability bounds)

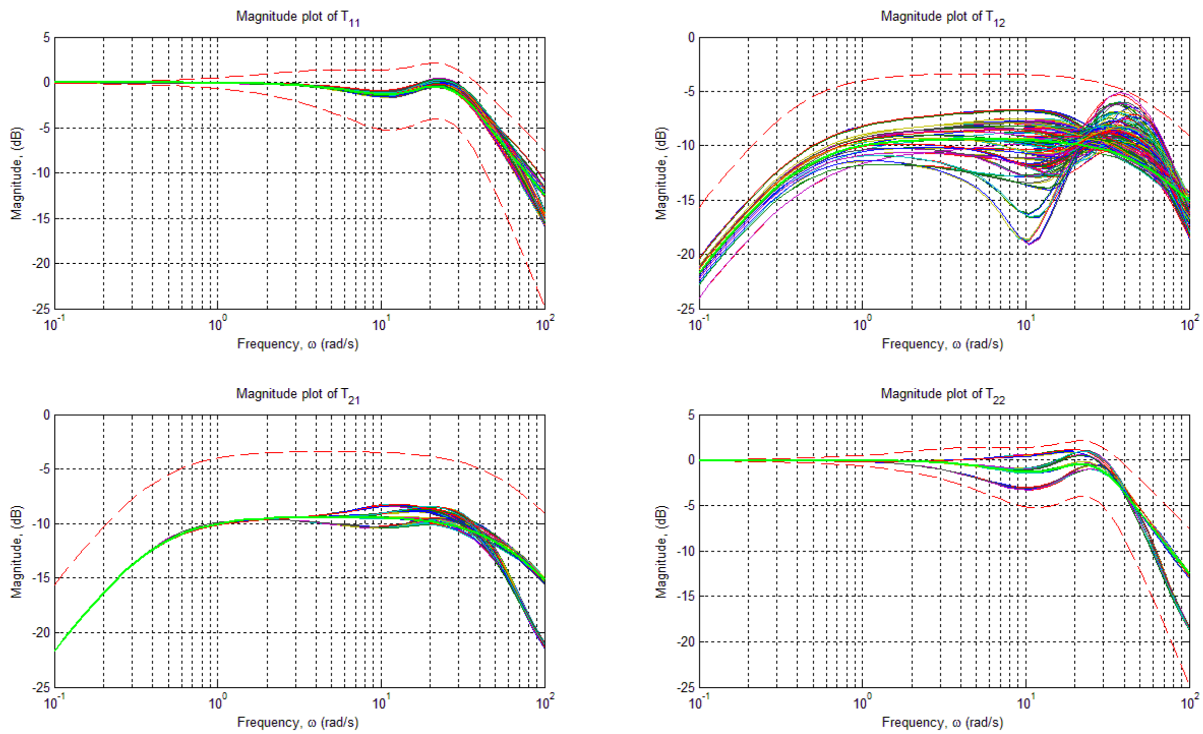

Figure 4.4.5 Reference to output magnitude response for control system designed using error-tracking specifications; the neon green line - the model; red dashed line – upper and lower bounds

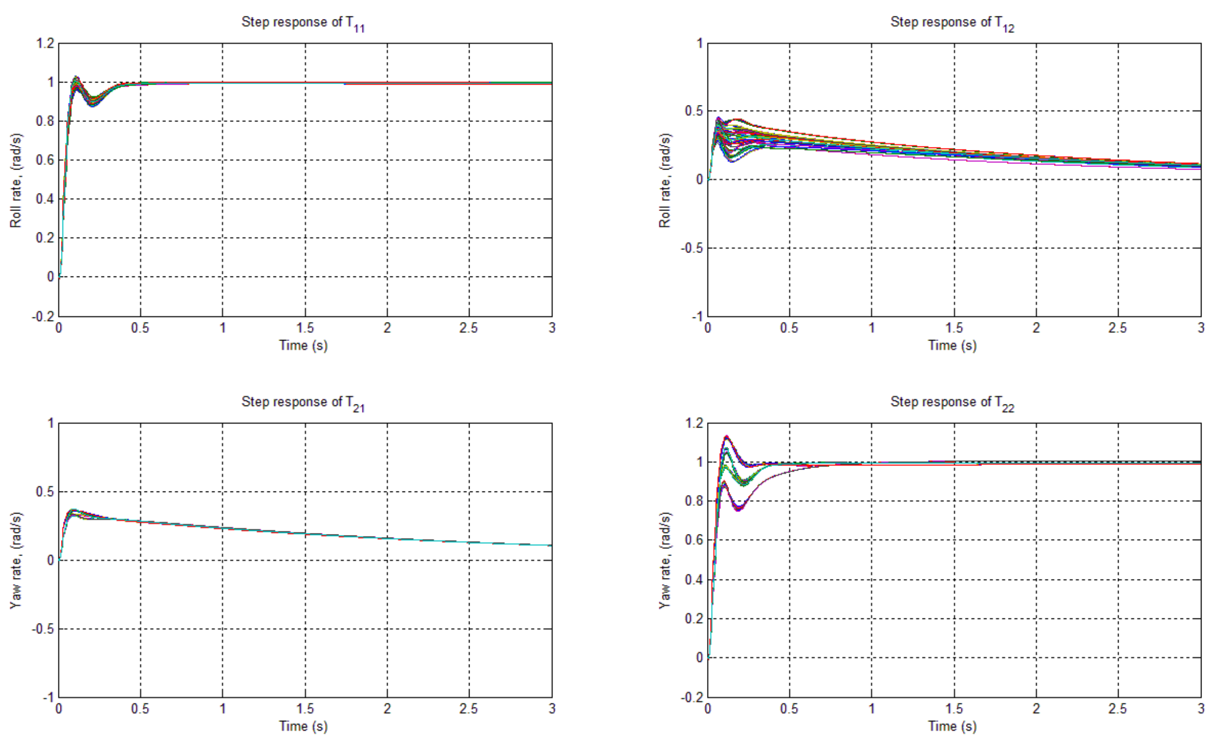

Figure 4.4.6 Step response of the control system using error-tracking design

Original QFT design for Error-Tracking Derived Specifications

For a comparison between the original QFT method for reference-tracking and error-tracking method, a traditional QFT tracking design is done for linearized point 2 using the reference-tracking specifications (upper/lower) which are derived from the error-tracking specifications. The upper reference-tracking bound is given by the magnitude of the model added to the magnitude of the error specification. Similarly, the lower reference-tracking bound is given by the model subtract the magnitude of the error specifications.

Loop two was designed first so that a meaningful comparison between the two methods can be made. Surprisingly, it was found that the original QFT tracking formulation using the algorithm (Boje, 2004) for calculating bounds were less conservative than the error-tracking bounds for loop two. This was unexpected since the error-tracking design uses phase information and was expected to yield less conservative bounds for loop two. As done in previous reference-tracking designs, the controller that satisfied the original QFT bounds was used to generate the new equivalent plant and the exact bounds for loop one. The design using the original QFT method was found to be unsuccessful at this point as loop one boundaries were not achievable due to the system delay.

Since the controller generated using the original QFT method did not prove successful, it was decided to use the controller obtained from the error-tracking design method for loop two and proceed with the usually reference-tracking design (original QFT method). Using the controller obtained from the error-tracking design method and a pre-filter that shifted the closed-loop system to meet row two demands, the worst case response shown in Fig. 4.4.7 was obtained. The pre-filter designed is given by

$$f_{22}(s) = \frac{\left(\left(\frac{s}{11}\right)^2 + 2\cdot 0.8\cdot\frac{s}{11} + 1\right)\left(\frac{s}{80}+1\right)}{\left(\left(\frac{s}{11}\right)^2 + 2\cdot 0.48\cdot\frac{s}{11} + 1\right)\left(\left(\frac{s}{35}\right)^2 + 2\cdot 0.707\cdot\frac{s}{35} + 1\right)}. \qquad (4.4.12)$$

Since this controller (obtained from the error-tracking method) was more conservative relative to the original QFT bounds, this reduced the demands in loop one design compared to the original design. But even though the constraints were eased, it was still not possible to satisfy the bounds. The loop one bounds obtained using the original QFT methodology with the error-tracking controller for loop two and pre-filter above is shown in Fig. 4.4.8. The controller that gets close to the solution is also shown in the figure and is given by

$$g_{11}(s) = \frac{-572695\,(s+12.76)(s+12.04)(s+9.687)(s^2+286.4s+5.25\times10^4)}{s\,(s+1000)(s+452.4)(s+20.44)(s+4.08)(s^2+1800s+9\times10^6)}. \qquad (4.4.13)$$

Since the application of the original QFT methodology could not generate a controller that satisfy the error-tracking derived specifications even with the use of a conservative controller it is shown here that the use of the error-tracking methodology over the original QFT methodology may have a more broad problem solving scope.

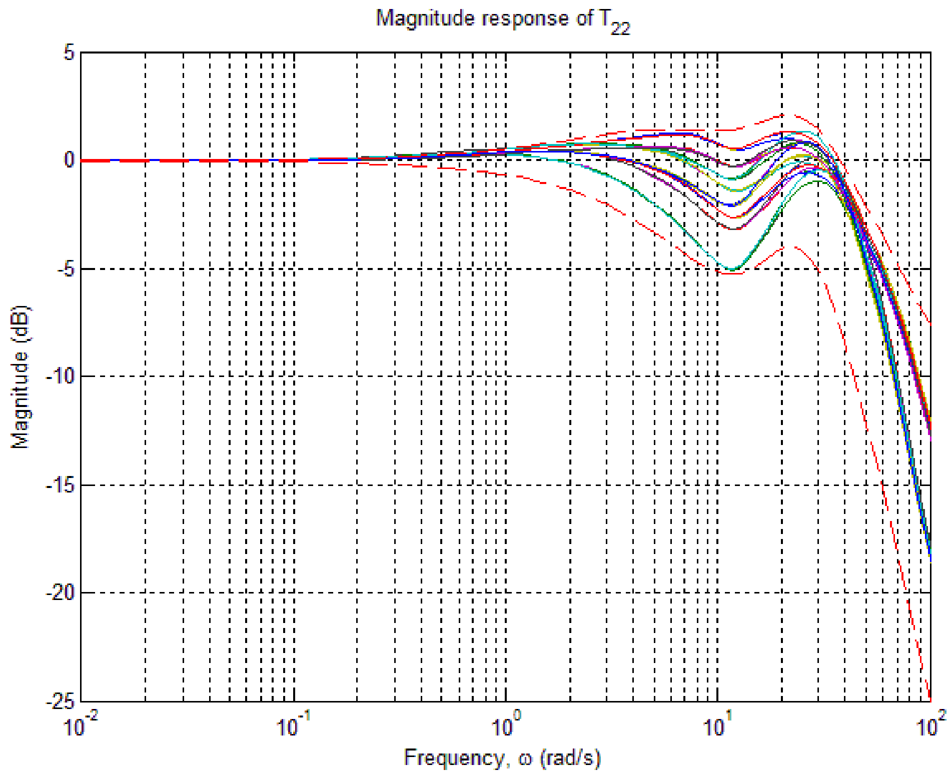

Figure 4.4.7 Worst case magnitude response of the diagonal channel for row two

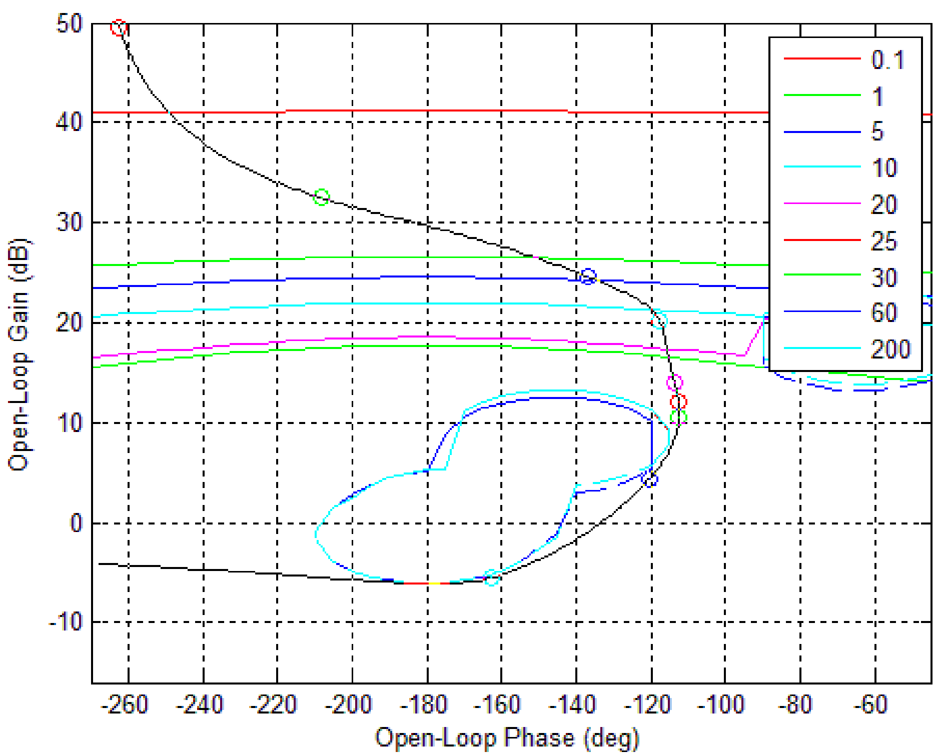

Figure 4.4.8 Nominal loop one with design bounds (reference-tracking (original QFT) AND stability bounds)

4.5. Design using True Inversion-free QFT

Less conservative bounds may be possible if a combination of the plant inversion (original formulation) method and the true inversion-free method is used (see Section 2.1.7). An example of the applications of the direct method applied solely, to the control of a CD-ROM drive can be found in (Park, Chait and Steinbuch, 1997) where Eqs (2.1.7.9) - (2.1.7.12) are applied in a different form. As stated in the theory section, the application of this inversion-free/direct method inherently results in plant inversion hence it is not a true inversion-free design. In this section, the true inversion-free method is applied as expounded in Section 2.1.7. Since both the original formulation and the true inversion-free method ensures that the closed-loop specifications are met provided all the constraints are satisfied, it implies that the union of the bounds generated using the two methods may yield less conservative bounds. A disturbance rejection design is done on linearized plant 2 to demonstrate the design concept. The same specifications are used as in the non-diagonal controller design case.

The diagonal channel boundaries for loop two for the inversion type design are shown in Fig. 4.5.1. The design equation that was used to generate the bounds in Fig. 4.5.1 is restated below.

$$\left|\frac{1}{1+l_2}\right|\left(1+\left|\frac{q_{22}}{q_{21}}\right|A_{12}\right) \leq A_{22} \tag{4.5.1}$$

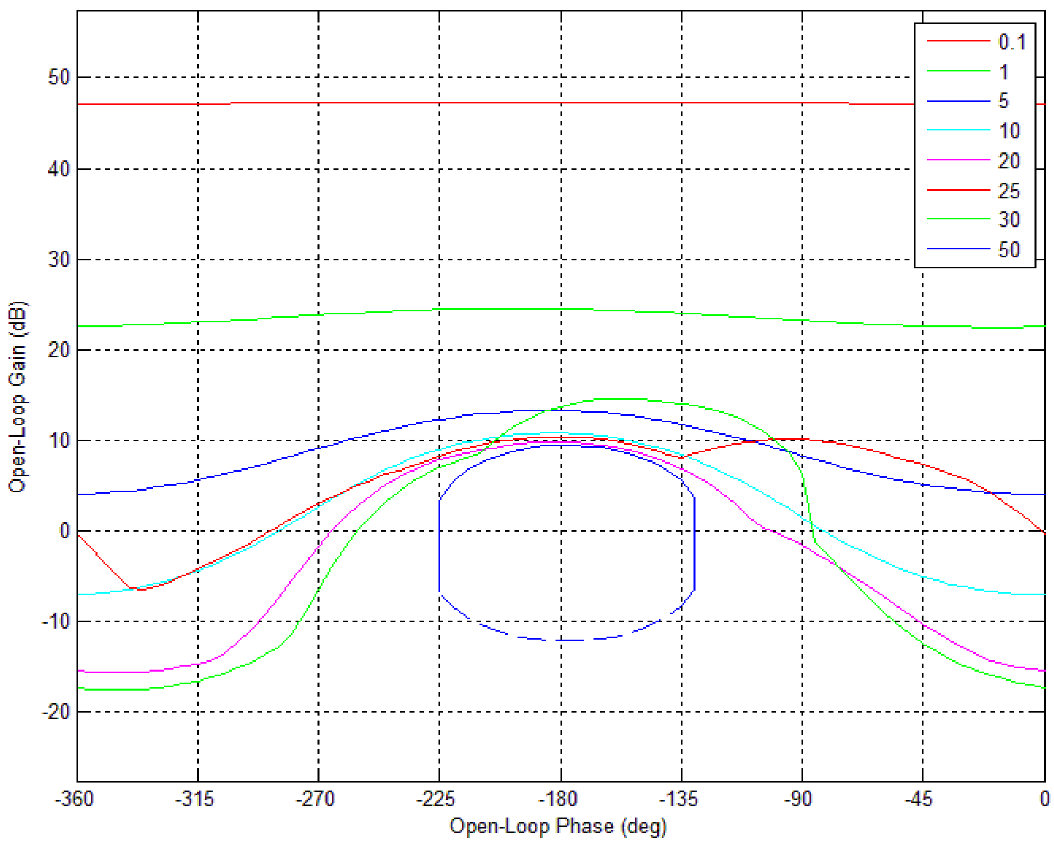

Figure 4.5.1 Loop two diagonal channel boundaries for inversion type design

The diagonal channel boundaries for loop two using the true inversion-free method can be generated by applying the Schwarz inequality twice to Eq. (2.1.7.19), which gives

$$|t_{22}| \leq \left|\frac{1 - t_{21}p_{12}g_2}{1 + p_{22}g_2}\right| \leq \left|\frac{1 + |t_{21}||p_{12}g_2|}{1 + p_{22}g_2}\right| = \left|\frac{1 + A_{21}|p_{12}g_2|}{1 + p_{22}g_2}\right| \leq A_{22}. \tag{4.5.2}$$

Manipulating Eq. (4.5.2), one gets the final constraint to be

$$\left|\frac{1/A_{21} + |p_{12}g_2|}{1 + p_{22}g_2}\right| \leq \frac{A_{22}}{A_{21}}. \tag{4.5.3}$$

The *genbnds(11,…)* command in the QFT toolbox can be used to perform the mapping in Eq. (4.5.3). The worst case closed-loop system response for channel t_{22} is given by

$$t_{22} = \left|\frac{1 \pm A_{21}|p_{12}g_2|}{1 + p_{22}g_2}\right| \tag{4.5.4}$$

The diagonal magnitude response for the controller obtained for loop two in the non-diagonal controller investigation is shown in Fig. 38.

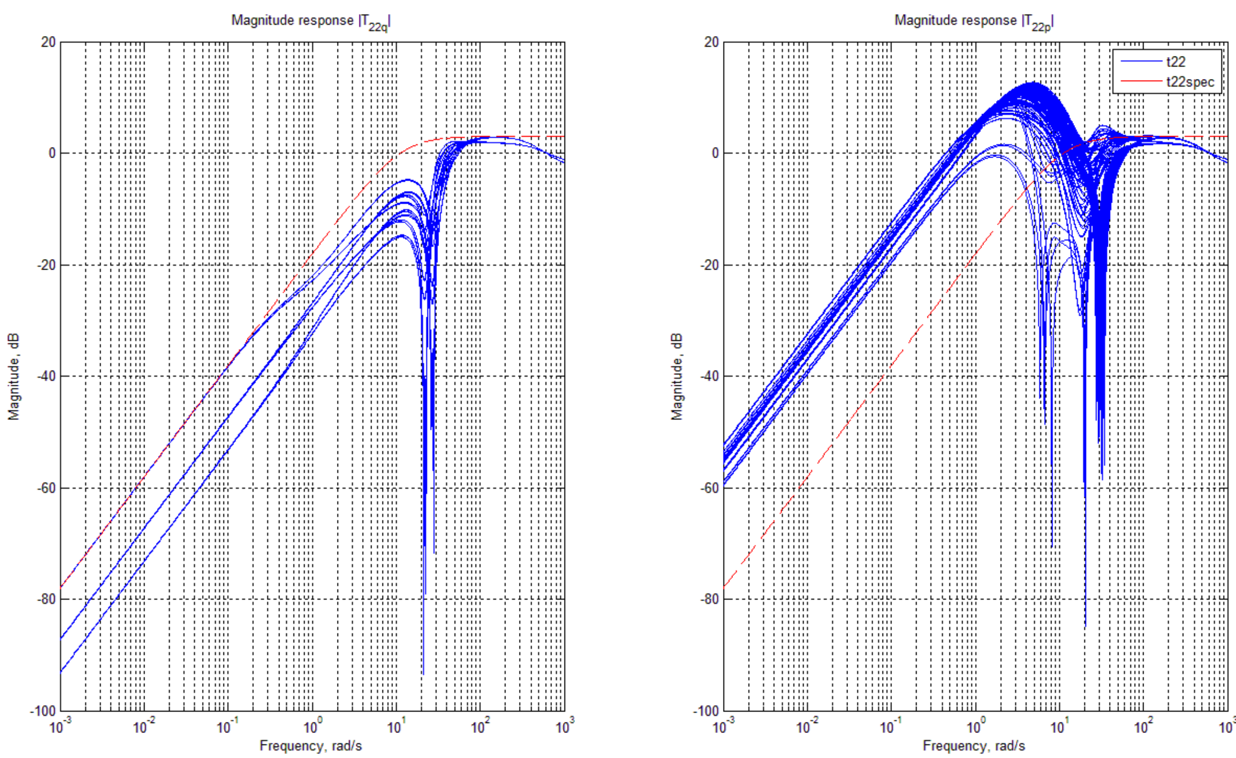

Figure 4.5.2 The worst case magnitude response; Left - original method; Right - true inversion-free method

Figure 4.5.2 show that the worst case diagonal response for the original QFT formulation does meet the specifications. This is expected since the controller used was designed using the original QFT formulation. The response on the right in Fig. 4.5.2 show that the controller gain used in the original QFT formulation is not sufficient especially at low frequencies (it is more conservative than the original QFT formulation). This indicates that the true inversion-free design method does not help much in the design at low frequencies. The true inversion-free design and the original QFT formulation design boundaries are plotted on a single figure in Fig. 4.5.3. No solution was found at low frequencies (between $0 - 10rad/s$) for the diagonal channel bounds using the true inversion-free equations (elucidated below).

The union of the diagonal bounds for the true inversion-free and original QFT formulation are shown in Fig. 4.5.4. Although the true inversion-free design bounds do not give lower loop gain requirement at important phases in this particular case, it definitely adds more possibilities for the gain. By assessing the design equations for both design methods it can be established why it makes sense to use the inversion type design equations at low frequencies and true inversion-free design equations at frequencies near and greater than the gain cross-over frequency. The diagonal output response for channel two in terms of the original QFT design is given by

$$t_{22}^{q} = \frac{1}{1+q_{22}g_2} - \frac{q_{22}/q_{21}\, t_{12}}{1+q_{22}g_2} = \frac{1}{1+q_{22}g_2} - D_{22}^{q}. \tag{4.5.5}$$

The diagonal output response for channel two in terms of the true inversion-free design is given by

$$t_{22}^{p} = \frac{1}{1+p_{22}g_2} - \frac{p_{12}g_2t_{21}}{1+p_{22}g_2} = \frac{1}{1+p_{22}g_2} - \frac{p_{12}t_{21}}{1/g_2+p_{22}} = \frac{1}{1+p_{22}g_2} - D_{22}^{p}. \tag{4.5.6}$$

It is known that the source of conservatism is the cross-coupling term (the second term) in Eqs (4.5.5) - (4.5.6). The controller gain generally starts high at low frequencies (for disturbance rejection), and decrease with an increase in frequency. Therefore it makes sense to use Eq. (4.5.5) (original QFT) for low frequency design as the cross-coupling term decreases with an increase in gain i.e. $\lim_{|g_2|\to\infty}\left|D_{22}^{q}\right| = 0$. Similarly, Eq. (4.5.6) should be used for frequencies where the gain is lower because with a decrease in controller gain the cross-coupling term in the inversion-free design equation decreases i.e. $\lim_{|g_2|\to 0}\left|D_{22}^{p}\right| = 0$.

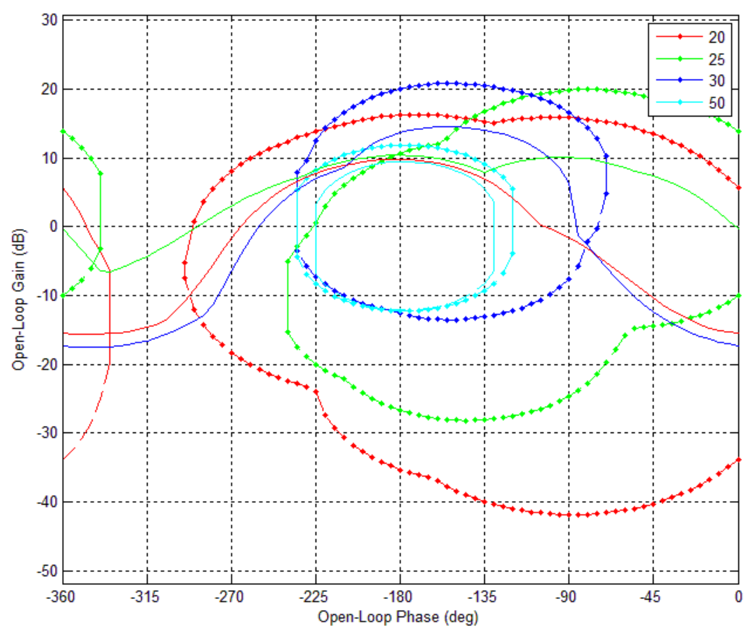

Figure 4.5.3 Composite bounds showing original QFT formulation bounds and the true inversion-free bounds (dotted lines)

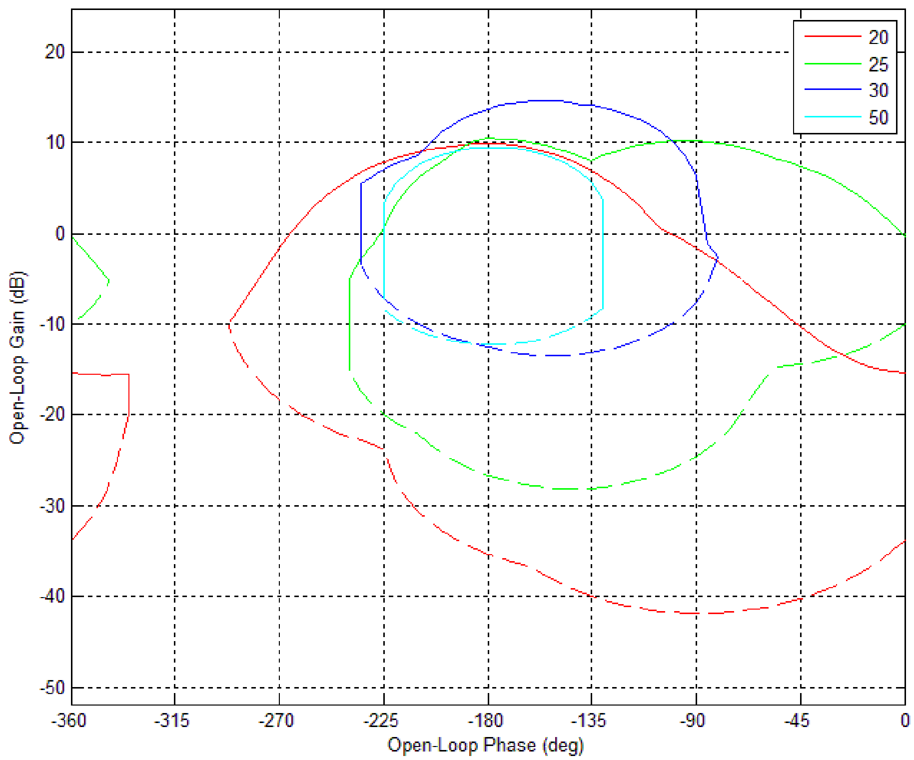

Figure 4.5.4 The union of the original QFT bounds and the true inversion-free design bounds

5. Application of H-infinity Theory

The H-infinity theory that was described in Section 2.2.4 is applied to the missile problem for each linearized point in this section. The MIMO QFT design technique is a diagonal type of control design. Therefore a QFT solution may not be possible for plants that have significant cross-coupling and uncertainty. Using the H-infinity design method, one can design a true MIMO controller (fully populated/non-diagonal) to optimally mix signals such that stability is ensured and the specifications are met. The problem with this method is that the uncertainty is captured in a manner that adds conservatism to the design and the closed-loop system is susceptible to fragility due to the high order controllers generated. Section 6 applies an H-infinity/QFT method that attempts to reduce conservatism inherent in H-infinity designs.

Application to Linearized Point 1

The first step in the H-infinity design process is to obtain the nominal plant. Unlike the QFT methodology, the conservativeness of the design is dependent on the nominal plant chosen. The nominal plant is chosen through a process of finding the required robust stability weighting function. The output multiplicative model is used to capture the uncertainty in this design. An output multiplicative model of the uncertainty results in disk shape templates. In general, different nominal plants will result in different radii templates at different frequencies. It is understood from MIMO QFT design that having a small uncertainty template at and near the gain cross-over frequency is important for obtaining less conservative designs. For this reason, the nominal is chosen that has small template radii near and above the gain cross-over frequency.

The robust stability requirements are generated for all plants using Eq. (2.2.4.2) and is shown in Fig. 5.1.

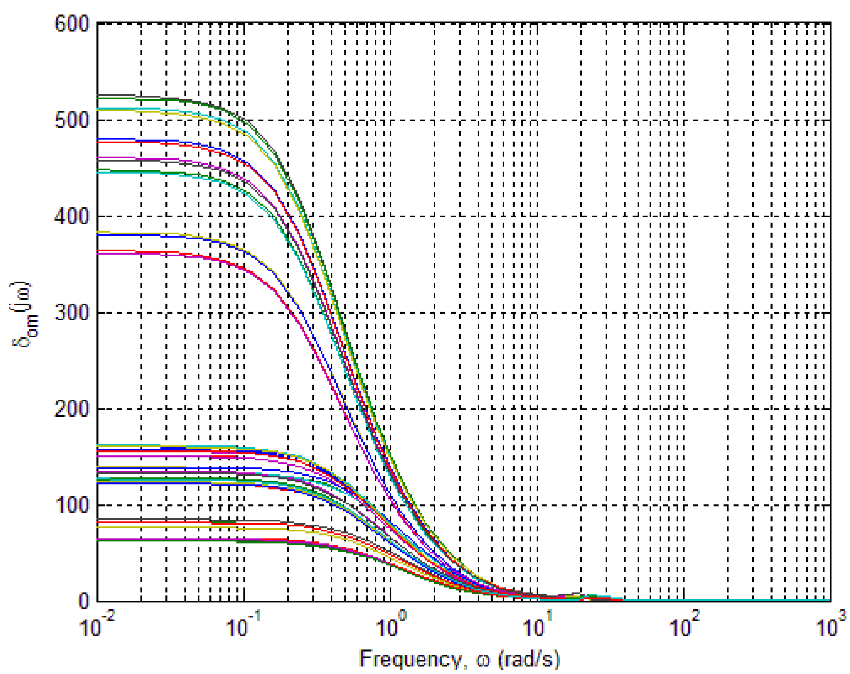

Figure 5.1 Worst case complementary sensitivity requirement for each nominal plant

The plant set for this design consists of 256 plants. It was found that plant 35 yields the smallest uncertainty radii for frequencies above $40\ rad/s$ hence it was chosen as the nominal plant. Based on the nominal chosen, the robust stability weight was chosen to satisfy Eq. (2.2.4.2). This implies that the magnitude of the weighting function must be greater than or equal to the robust stability requirement. The robust stability weighting function that satisfies Eq. (2.2.4.2) is given by Eq. (5.1), and the magnitude plot of the weighting function together with the requirement is shown in Fig. 5.2.

$$w_0(s) = 82\,\frac{s/350+1}{s/1.5+1} \tag{5.1}$$

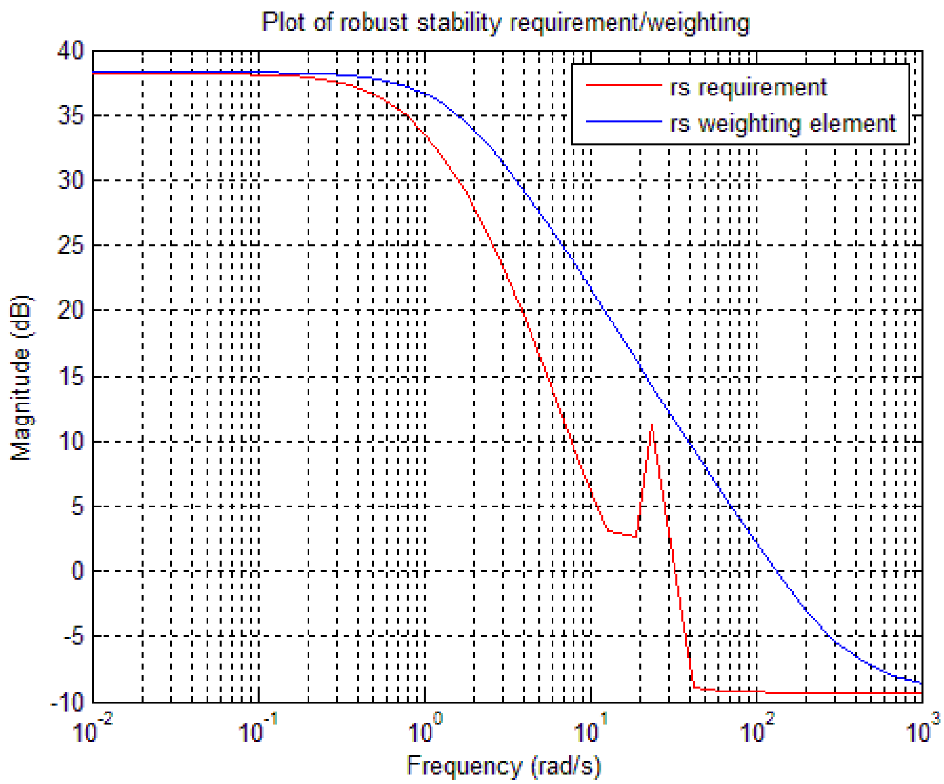

Figure 5.2 Magnitude plot showing robust stability requirement and weighting function design

The next step of the H-infinity design process is to obtain the sensitivity weighting function. This is done by choosing a weighing function that satisfies Eq. (2.2.4.10). The minimum nominal sensitivity requirement and the sensitivity weighting function are shown in Fig. 5.3. The weighting function was obtained by tuning a standard equation presented in (Skogestad and Postlethwaite, 2005, pg 64) so that its magnitude is less than the requirement at all frequencies. The sensitivity weighting function chosen is given by Eq. (5.2). Since both channels have the same specifications the weighting function for each row is the same. The design method explained in (Sidi, 2002) is used to generate the controller for the uncertain system. It is not clear to the author how the uncertainty of the system gets reflected to the nominal plant using this method, but the MIMO version of Eq. (2.2.4.11) ensures that robust performance is attained if the optimization is successful.

$$w_s(s) = \frac{s/1.2589+120}{s+120\cdot 1\times 10^{-4}} \tag{5.2}$$

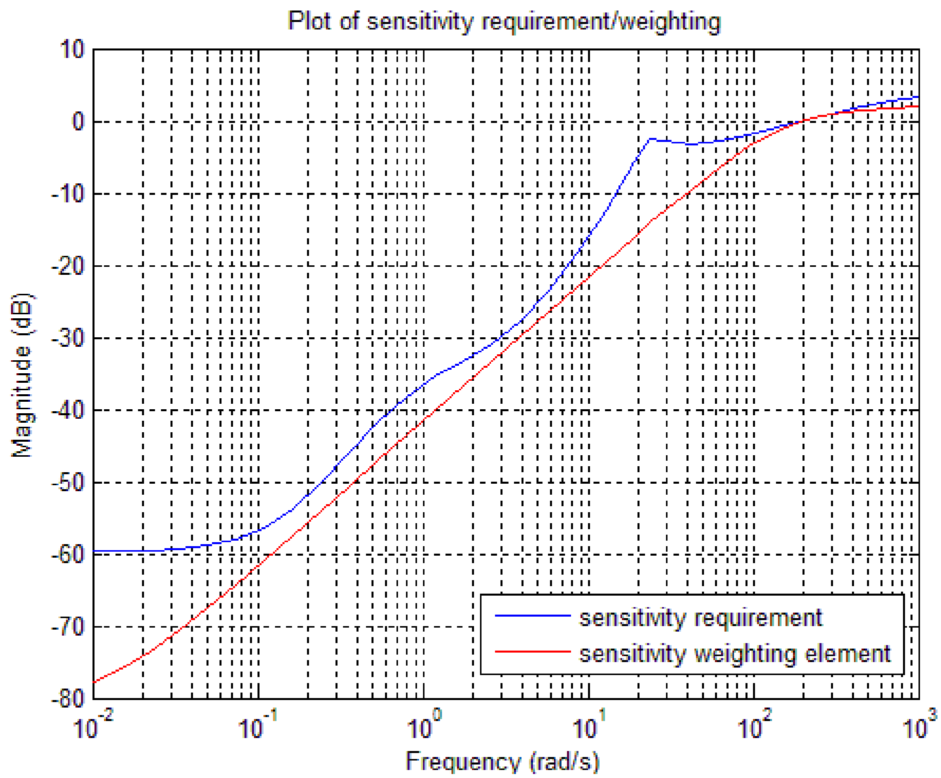

Figure 5.3 Magnitude plot of the sensitivity requirement and the weighting function

The input/tuning weighting functions were set to unity. The *Matlab*™ Robust toolbox was used to perform the H-infinity optimization. After cancelling poles and zeros that are very close to each other the final controller was obtained. The resulting elements that make up the controller are shown in Eqs (A4.1) - (A4.4). The highest order controller of the elements of the H-infinity controller is 8, which is large compared to the 4th order QFT controller. The pre-filter was made diagonal and chosen to shift the closed-loop response to be within the specifications. The equations describing the diagonal pre-filter are given by Eqs (A4.5) - (A4.6). The magnitude of the reference to output response is shown in Fig. 5.4. The step response shown in Fig. 5.5 confirms closed-loop stability.

The step response from the reference to the plant input for the H-infinity system is plotted in Fig. A2.17. In this particular case, the QFT (Fig. A2.16) and the H-infinity plant input signals were almost exact. From Fig. 5.4 one can deduce that the design is very conservative compared to the QFT design. An analysis of the controller magnitude response reveals that the H-infinity controller is much more effective in reducing the off-diagonal channel coupling via off-diagonal controller elements compared to the diagonal QFT controller.

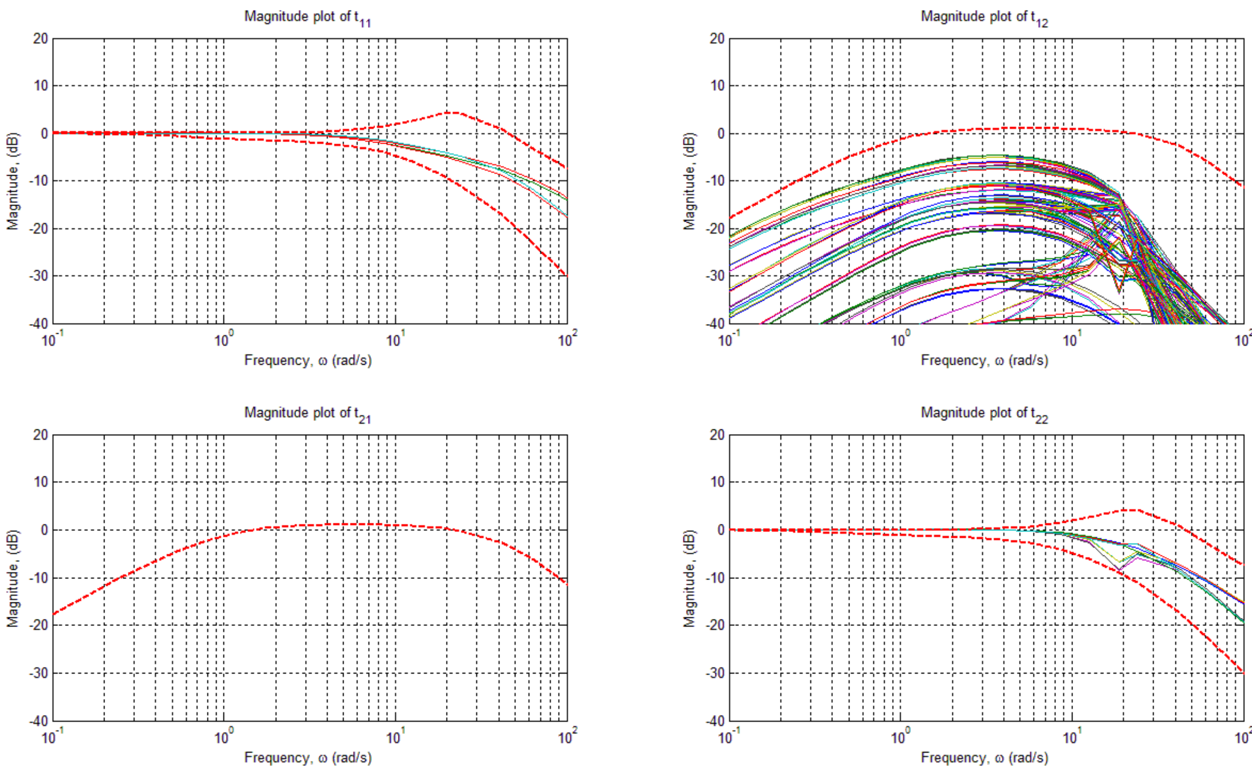

Figure 5.4 Magnitude response of the closed-loop system for linearized point 1 using H-infinity design method

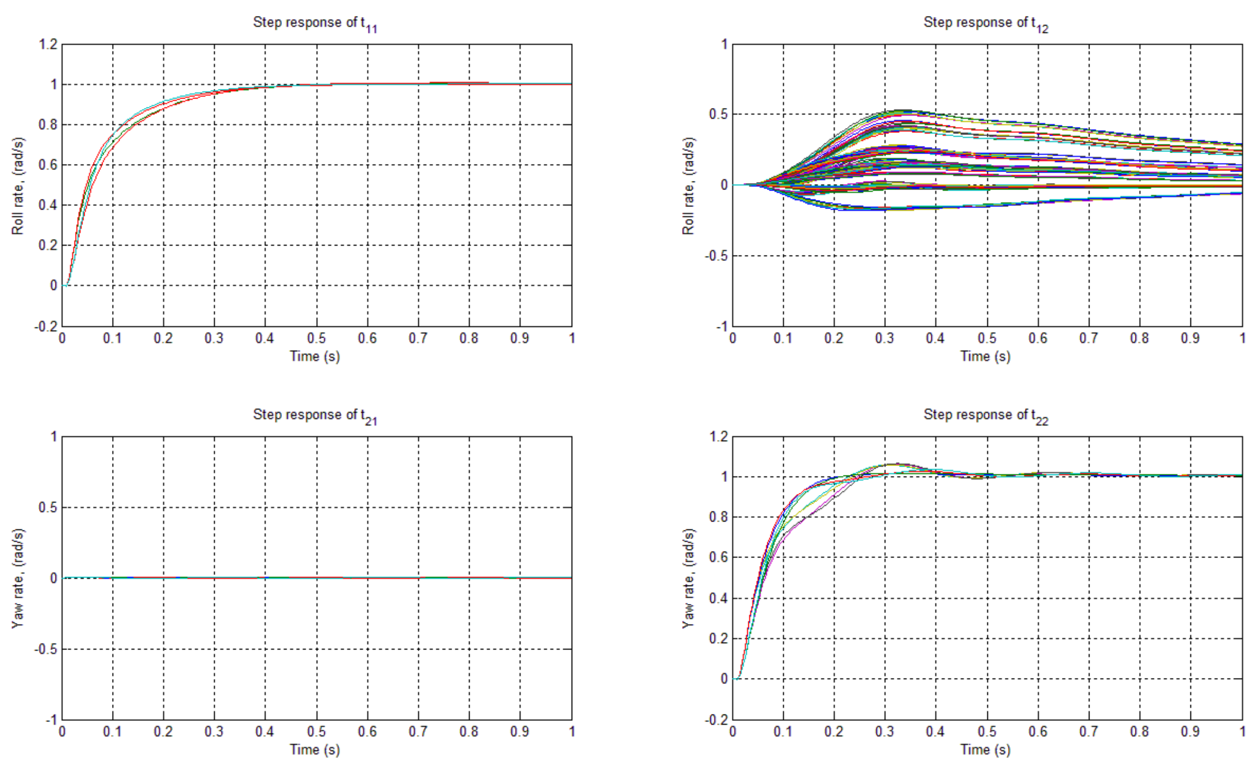

Figure 5.5 Step response of the closed-loop system for linearized point 1

Application to Linearized Point 2

Using the same procedure as above, the following results were obtained.

Table 5.1 Linearized point 2 design parameters

Nominal plant	51
Robust stability weighting function	$w_0(s) = 200\dfrac{s/700+1}{s/1.5+1}$
Sensitivity weighting function	$w_s(s) = 0.89125\dfrac{(s+233)^2}{(s+0.6957)^2}$

Figure 5.6 shows the magnitude response for the closed-loop system with a diagonal pre-filter. The step response of the system is shown in Fig 5.7. The controller and pre-filter transfer functions are given by Eqs (A4.7) - (A4.12).

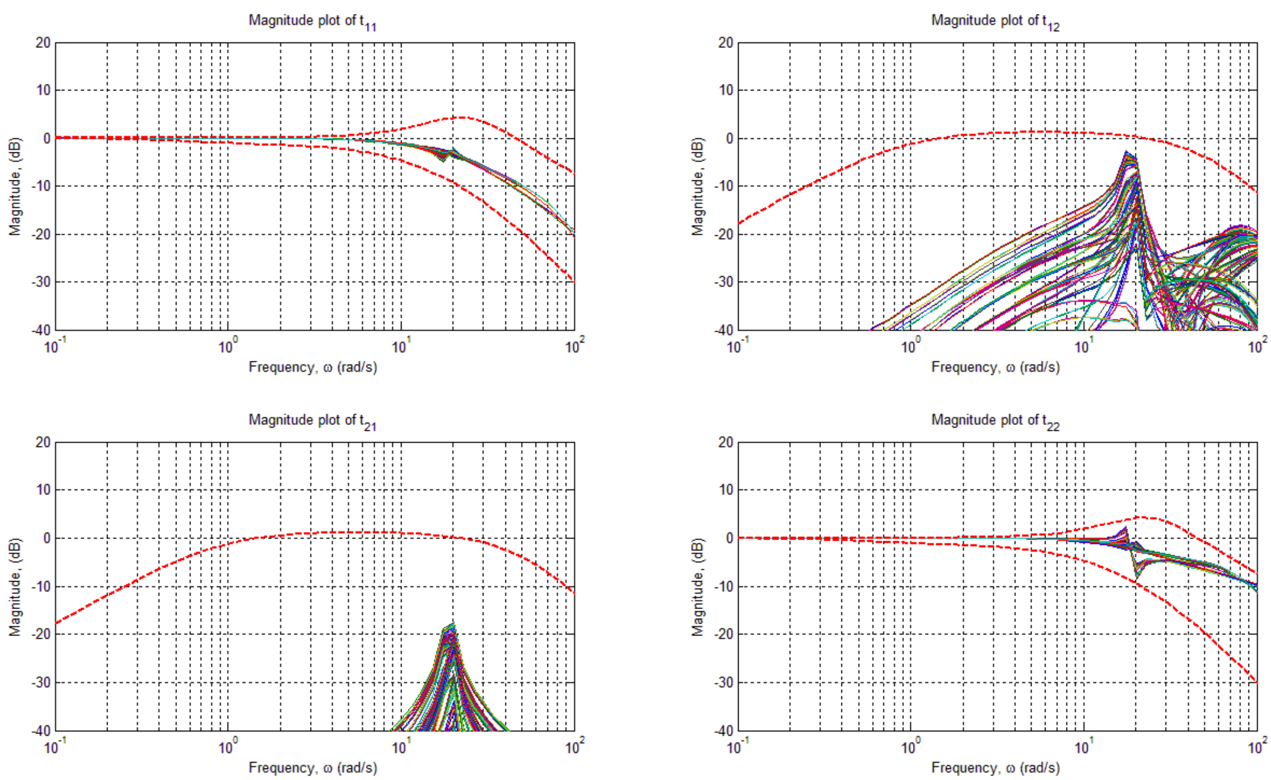

Figure 5.6 Magnitude response of the closed-loop system for linearized point 2 using H-infinity design method

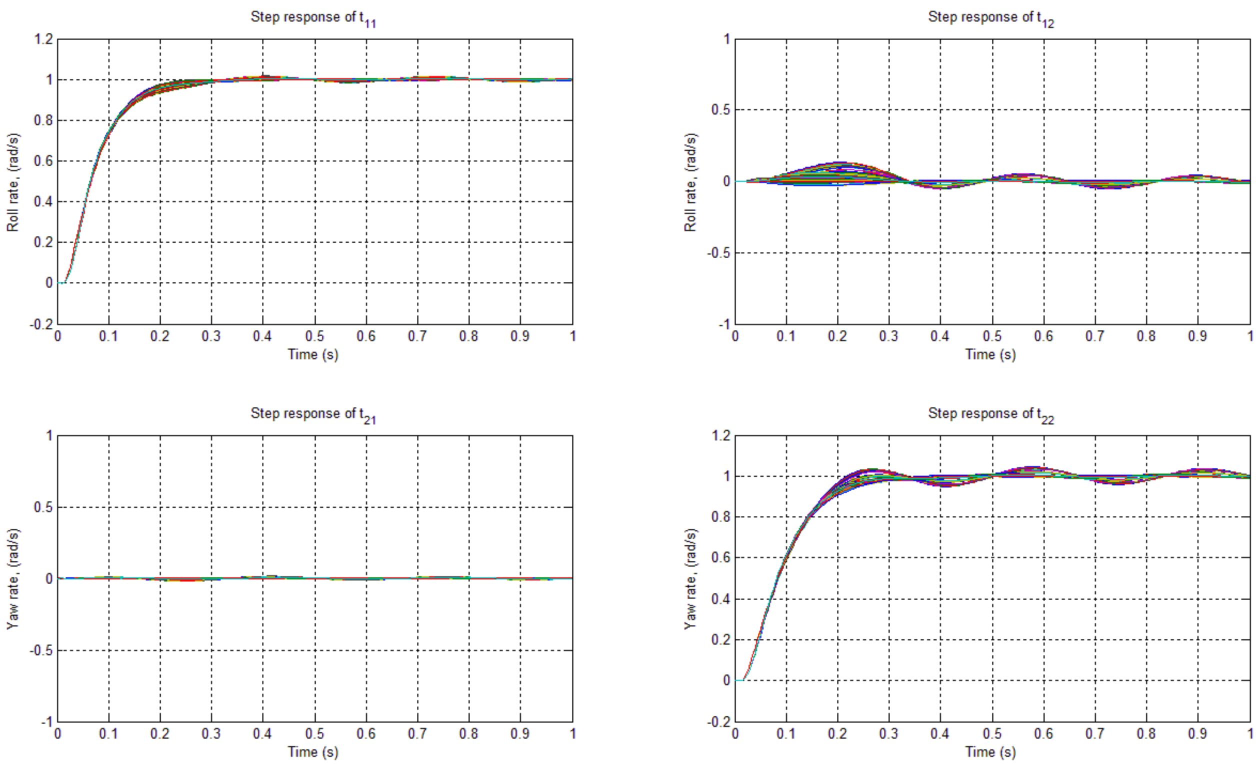

Figure 5.7 Step response of the closed-loop system for linearized point 2

Application to Linearized Point 3

Table 5.2 Linearized point 3 design parameters

Nominal plant	55
Robust stability weighting function	$w_0(s) = 300\dfrac{s/600+1}{s/1.5+1}$
Sensitivity weighting function	$w_s(s) = 0.79433\dfrac{(s+108)^3}{(s+0.04642)^3}$

Figure 5.8 shows the magnitude response for the closed-loop system with the pre-filter. The step response of the system is shown in Fig 5.9. The controller and pre-filter transfer functions are given by Eqs (A4.13) - (A4.18).

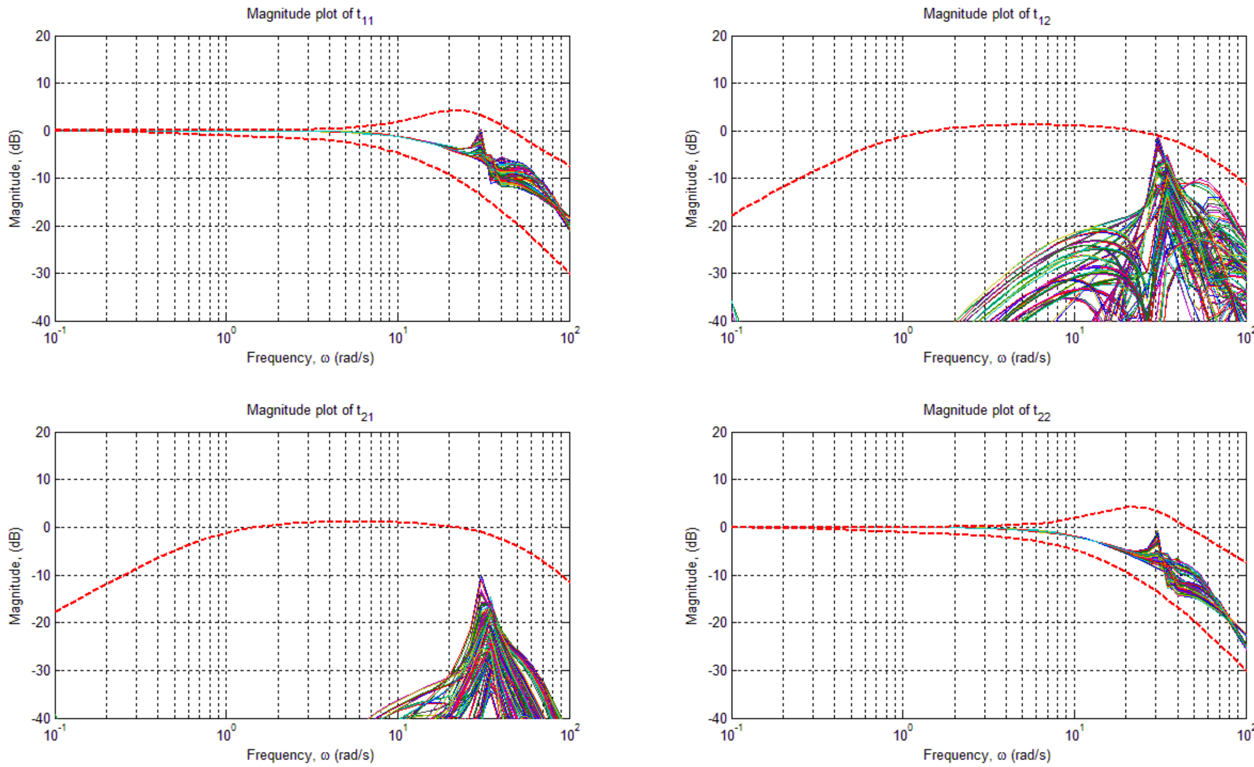

Figure 5.8 Magnitude response of the closed-loop system for linearized point 3 using H-infinity design method

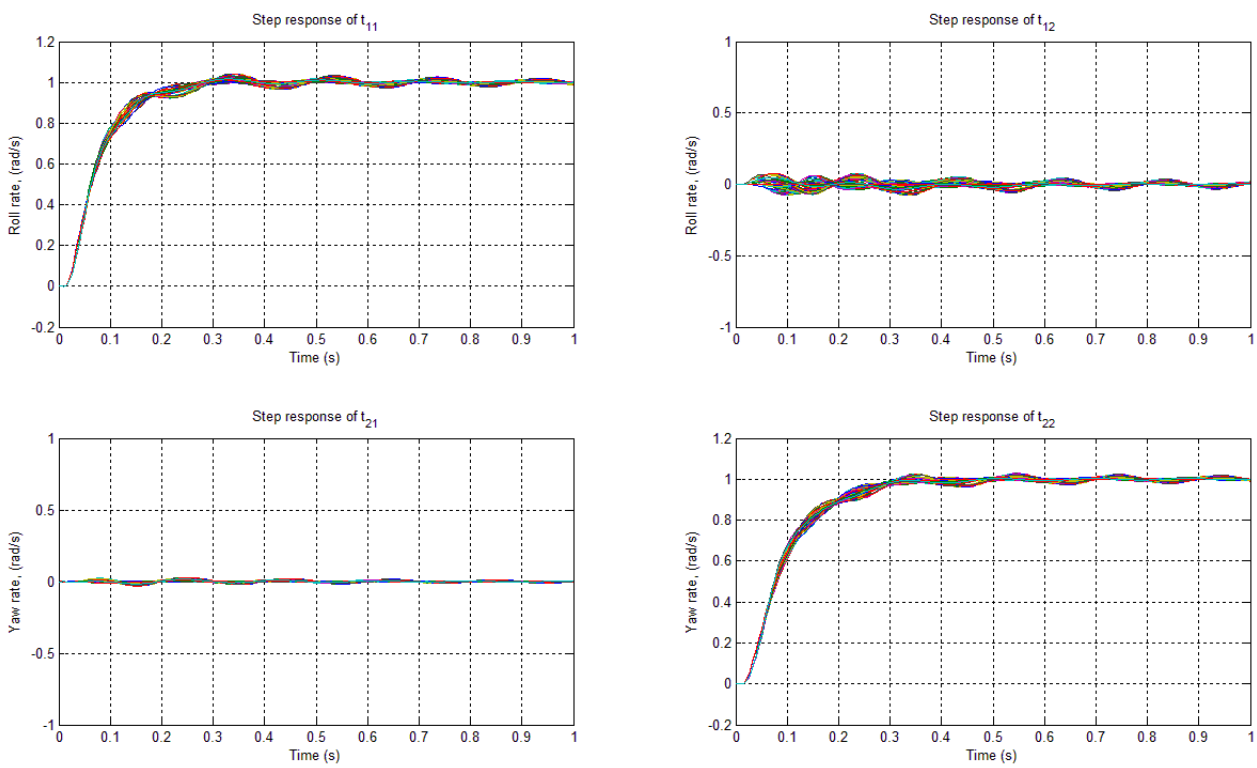

Figure 5.9 Step response of the closed-loop system for linearized point 3

Application to Linearized Point 4

In the QFT design, solutions for linearized points including and beyond 4 were not found. It is believed that this is due to the significantly larger cross-coupling in the system. It seems not "fair" to attempt a diagonal control design for such problems. But even with MIMO controllers such as the H-infinity controller, these problems are very difficult. Using the methodology in (Sidi, 2002), the generated weighting functions did not prove sufficient to meet specifications. Since the specifications could not be met, the weighting functions were adjusted so that maximum feedback benefits are attained.

Table 5.3 Linearized point 4 design parameters

Nominal plant	101
Robust stability weighting function	$w_0(s) = 470\dfrac{s/2000+1}{s/7.2+1}$
Sensitivity weighting function	$w_s(s) = 0.70795\dfrac{(s+89.76)^3}{(s+0.1724)^3}$

Figure 5.10 shows the magnitude response for the closed-loop system with the pre-filter. This clearly shows the violation of the reference tracking specifications. The step response of the system is shown in Fig 5.11. The controller and pre-filter transfer functions are given by Eqs (A4.19) - (A4.24).

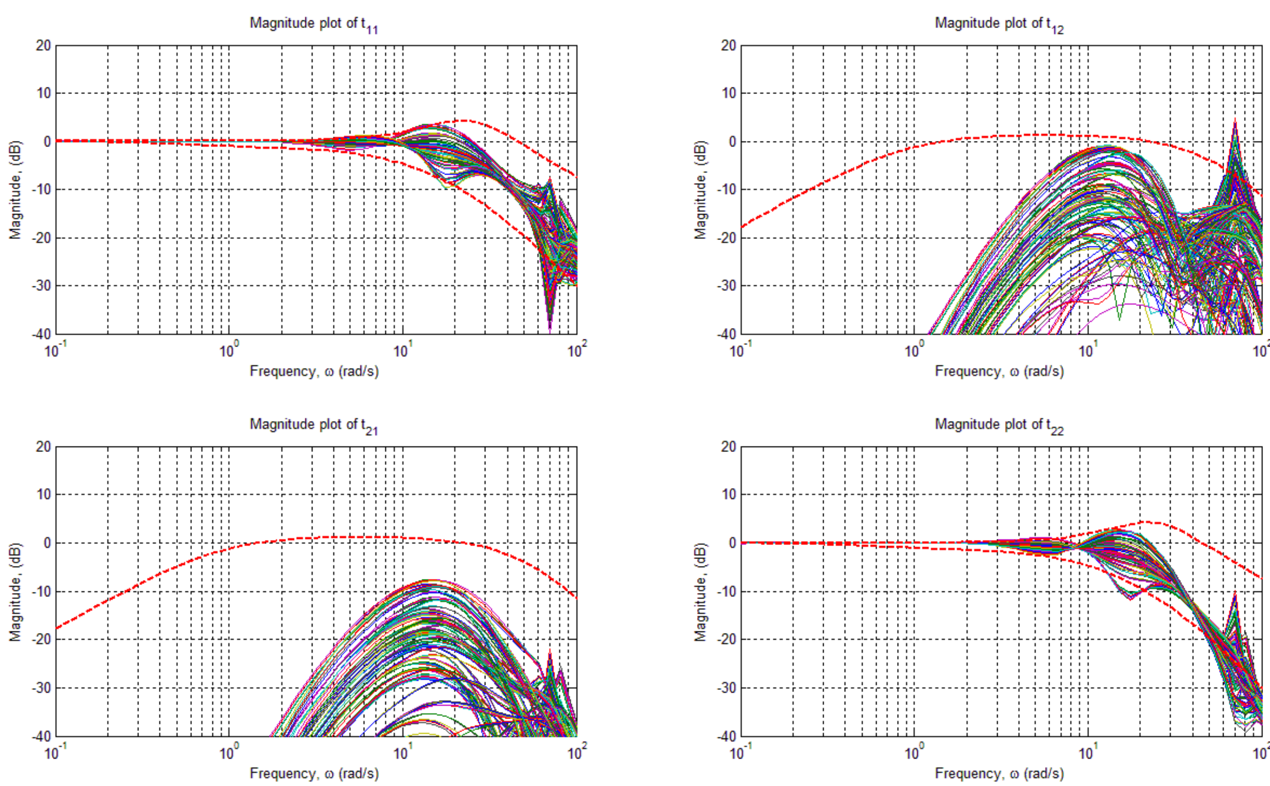

Figure 5.10 Magnitude response of the closed-loop system for linearized point 4 using H-infinity design method

The weighting requirements could not be met through the optimizations process; the gamma value obtained from the optimization was 470.

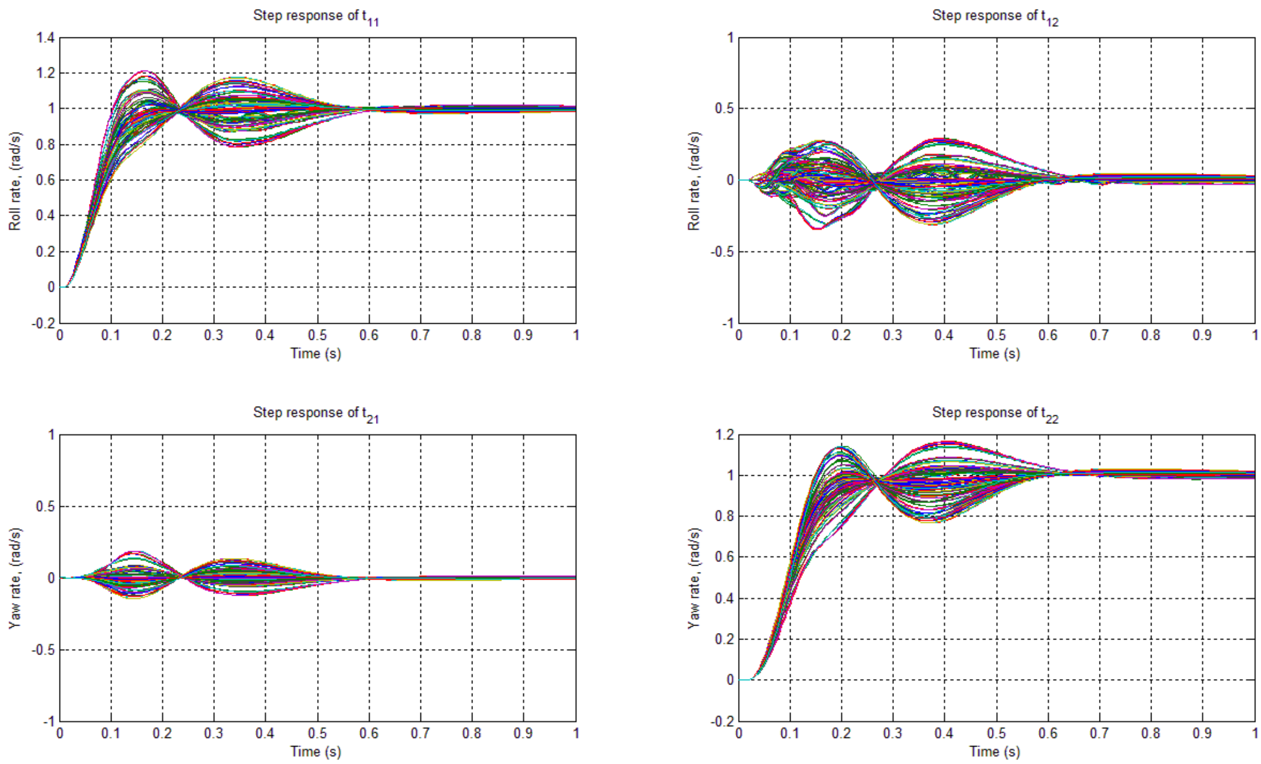

Figure 5.11 Step response of the closed-loop system for linearized point 4

Application to Linearized Point 5

Table 5.4 Linearized point 5 design parameters

Nominal plant	5
Robust stability weighting function	$w_0(s) = 160\dfrac{s/1200+1}{s/8+1}$
Sensitivity weighting function	$w_s(s) = 0.70795\dfrac{(s+178.3)^2}{(s+0.0015)^2}$

Figure 5.12 shows the magnitude response for the closed-loop system with the pre-filter. The step response of the system is shown in Fig 5.13. The controller and pre-filter transfer functions are given by Eqs (A4.25) - (A4.30).

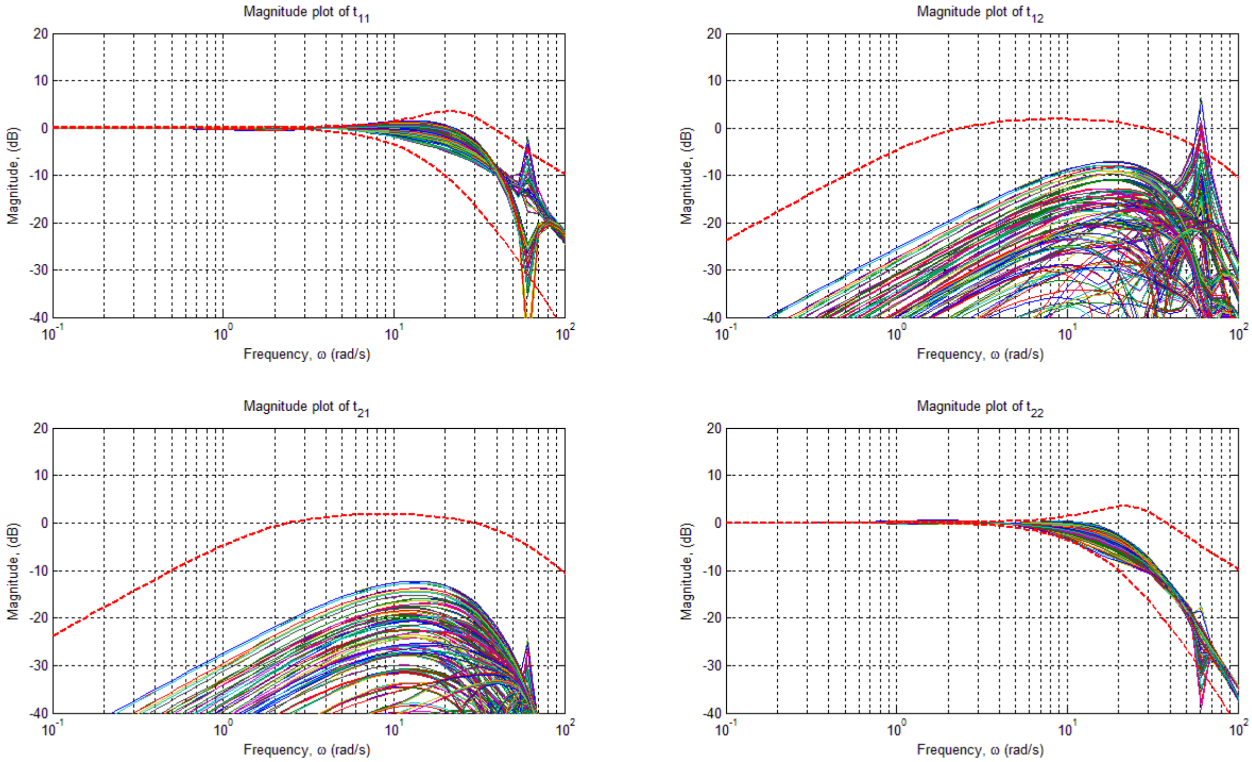

Figure 5.12 Magnitude response of the closed-loop system for linearized point 5 using H-infinity design method

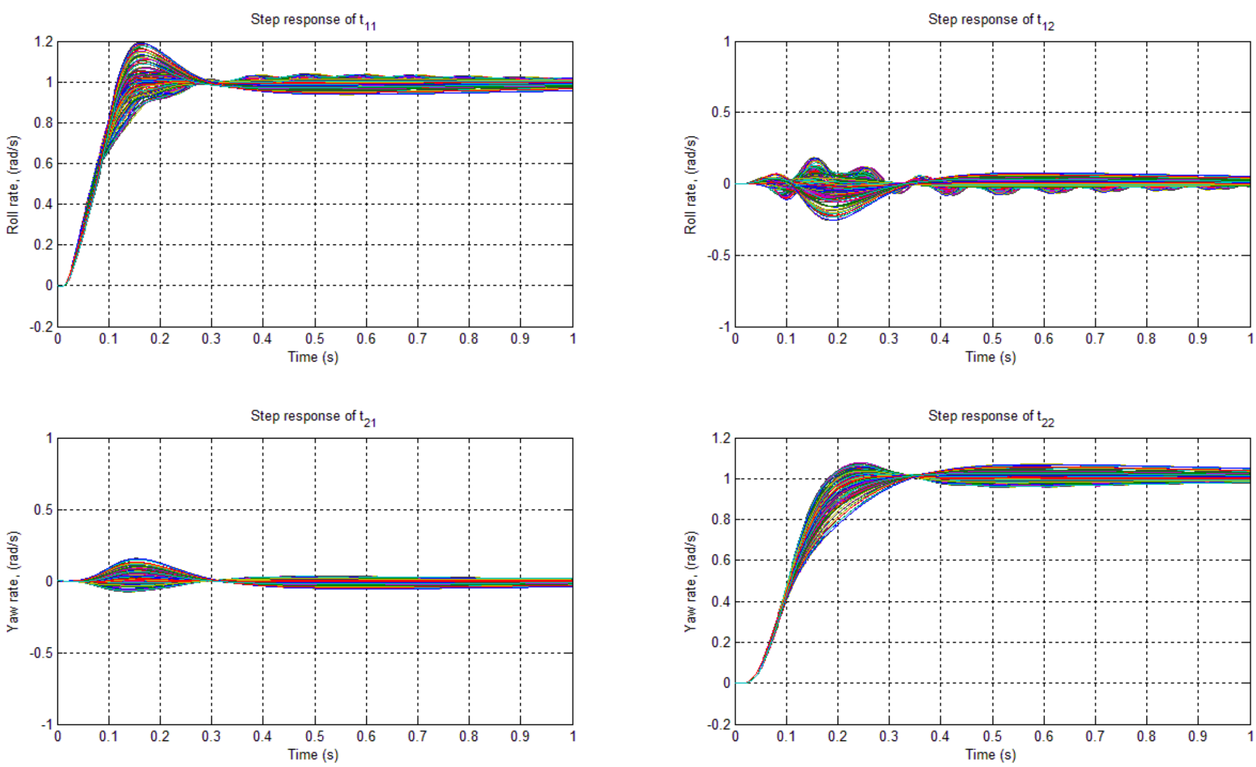

Figure 5.13 Step response of the closed-loop system for linearized point 5

Application to Linearized Point 6

After a huge effort adjusting the weighting matrices for robust stability and sensitivity, it was found that a solution for the 6^{th} linearized point could not be found using the H-infinity method either. Since H-infinity optimally mixes the signals to achieve desired closed-loop specifications it is strongly believed that there are no solutions for the 6^{th} linearized point.

6. Application of H-infinity/QFT Theory

This section demonstrates a combination of the H-infinity and QFT design methodology. The 5th linearized plant was chosen to express the design philosophy since both QFT and H-infinity design methods could not independently solve the problem. From Fig. 5.12/5.13, one can see undesired oscillations at about $60\ rad/s$, and at first it would appear unclear how to adjust the controller elements to reduce the uncertainty while ensuring robust stability. The section that documents the theory related to using H_∞/QFT combination is given in Section 2.3. The idea of using this technique is to add transparency to the H-infinity design so that tuning can be done in a quantitative manner. An H-infinity controller is first designed for the system. The optimization may generate a controller that does not result in closed-loop specifications being met. The fully-populated controller is then spilt into two unimodular matrices and a diagonal matrix as shown in Eq. (2.3.1.3). Manipulations are done in the QFT formulation of the problem to absorb the unimodular matrices into the system which allow a MIMO QFT design to be performed.

Using Eq. (2.3.1.3), the $(2,1)$ element of $\boldsymbol{L}^{-1}$ is given by Eq. (6.1), and a Bode plot of it is shown in Fig. 6.1.

$$\hat{l}_{21} = \frac{0.022293\,(s^2 + 81.72s + 2.16\times10^4)\,(s^2 + 8381s + 1.859\times10^7)}{(s^2 + 5.507s + 3583)\,(s^2 + 1284s + 1.311\times10^6)} \tag{6.1}$$

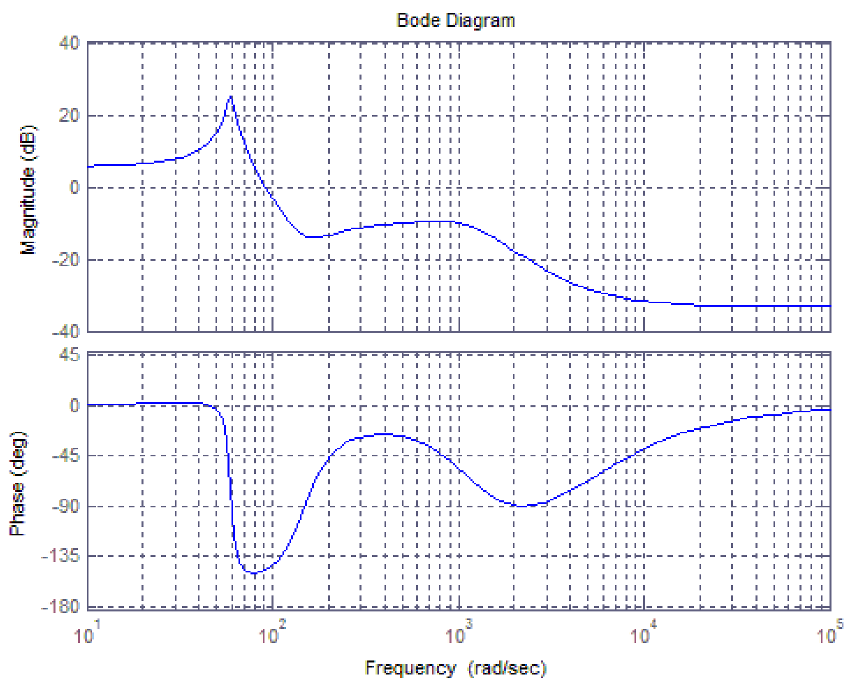

Figure 6.1 Bode plot of the dynamic element of the pre-compensator

Using Eq. (2.3.1.3), the $(1,2)$ element of $\boldsymbol{R}^{-1}$ is given by Eq. (6.2), and a Bode plot of it is shown in Fig. 6.2.

$$\hat{r}_{12} = \frac{-0.065423\,(s^2 + 18.95s + 4092)\,(s^2 + 8381s + 1.859\times10^7)}{(s^2 + 5.507s + 3583)\,(s^2 + 1284s + 1.311\times10^6)} \tag{6.2}$$

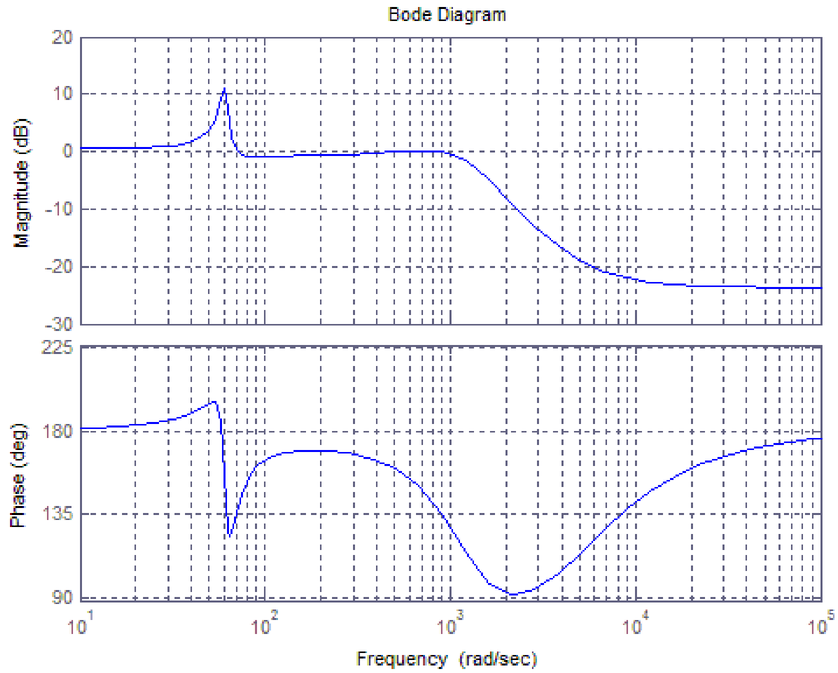

Figure 6.2 Bode plot of the dynamic part of R^{-1}

From the Bode plots above, the sharp magnitude peak at approximately $60\ rad/s$ suggests that the non-diagonal part of the H-infinity controller has some cross-feeding effect.

The equations developed in the theory section forces one to design loop two first. In order to show that incorporating the non-diagonal part of the H-infinity controller into the system may reduce the diagonal loop requirement, both the original QFT bounds and the QFT bounds after system modification with the non-diagonal part of the H-infinity controller are assessed. The original QFT bounds/system will be referred to by QFT_{orig} and the bounds/system as a result of including the non-diagonal part of the H-infinity controller will be referred to by QFT_{H_∞}. Both the bounds for QFT_{orig} and QFT_{H_∞} were generated for loop two and is shown in Fig. 6.3. The plot shows that the non-diagonal part of the H-infinity controller is effective at mid-band frequencies but not effective at lower and higher frequencies. In other words, the H-infinity modification allows for lower diagonal loop gain requirements at mid band frequencies.

The bounds are for tracking of the diagonal channel and robust stability for loop two. The intersection of these bounds together with the nominal loop is shown in Fig. 6.4. Loop two pseudo-diagonal controller is given by Eq. (6.3) (see Section 2.3.1).

$$g'_{22} = g_{22} - \frac{g_{12}g_{21}}{g_{11}} \tag{6.3}$$

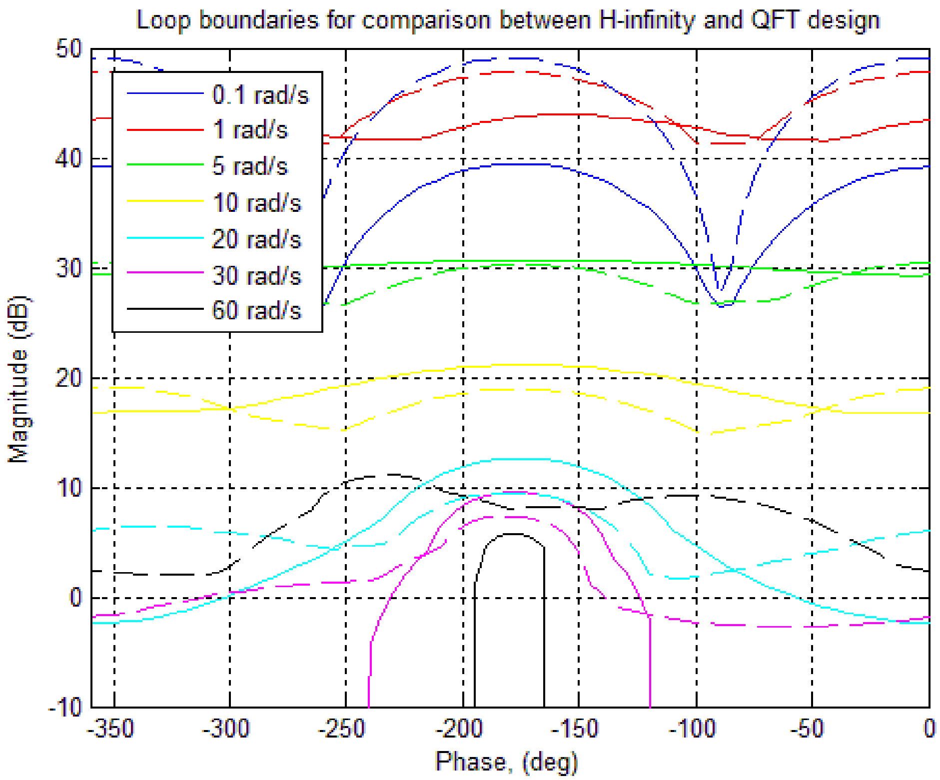

Figure 6.3 Solid lines - original QFT boundaries (QFT_{orig}); Dashed lines - new QFT boundaries with non-diagonal part of H-infinity controller absorbed into the system (QFT_{H_∞})

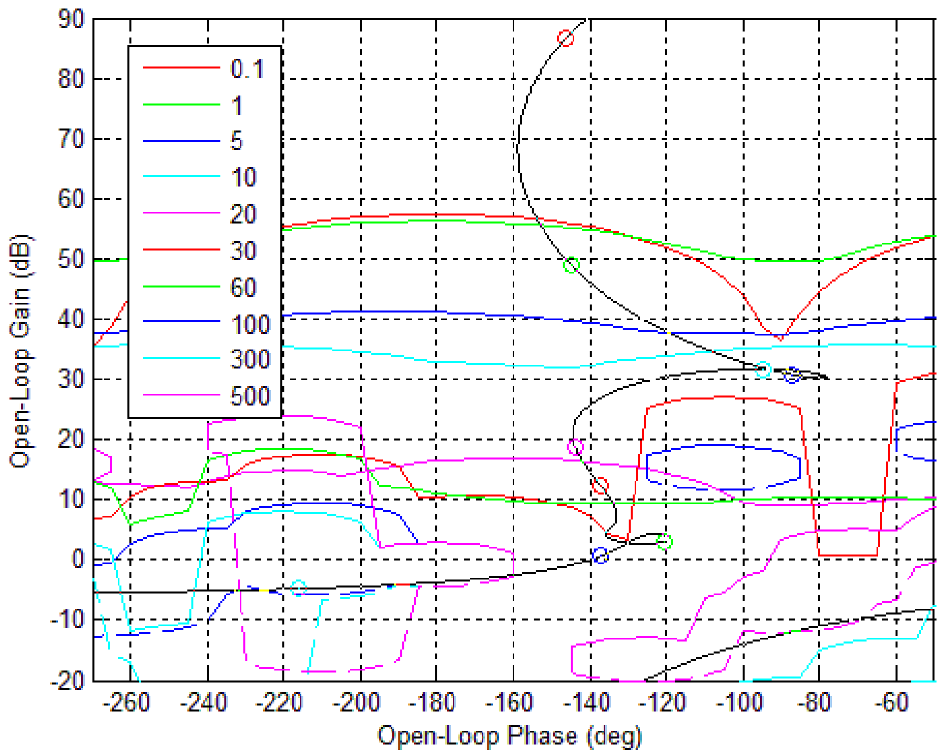

Figure 6.4 Loop two bounds and pseudo-diagonal H-infinity nominal (QFT_{H_∞})

Although conservative, the bounds in Fig. 6.4 explain why the diagonal reference to output response in loop two do not meet specifications in the frequency range $\sim 1 - 15\ rad/s$. Using this QFT/H-infinity method, the designer can tune the diagonal loops to meet the system specifications in a quantitative manner. Figure 6.5 shows the QFT_{H_∞} bounds and nominal loop for loop one. The plot shows the H-infinity design is very conservative for loop one; this completes the analysis of the pseudo-diagonal loops for the QFT_{H_∞} system.

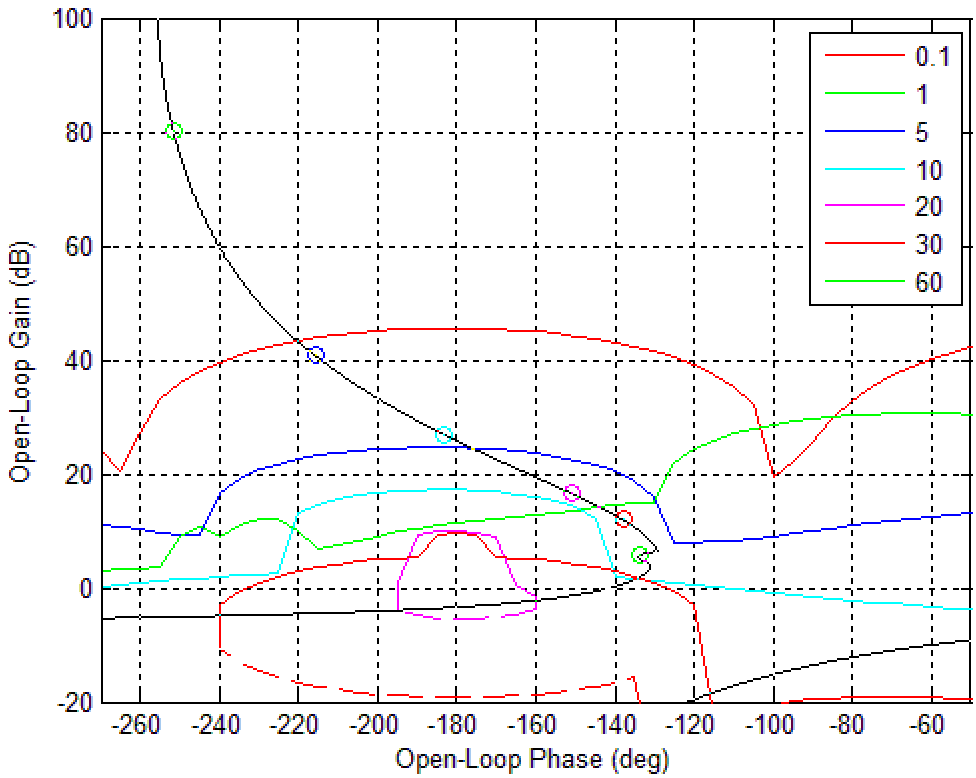

Figure 6.5 Loop one H-infinity pseudo diagonal controller

Tuning the H-infinity System using QFT

Loop two was tuned first as the design methodology requires this. The loop was modified to meet QFT_{H_∞} bounds in the frequency range $1 - 15\ rad/s$ which was not met with the original pseudo-diagonal H-infinity controller. In order to meet the bounds, the gain cross-over frequency had to be increased from $101 rad/s$ to $145 rad/s$. An $8dB$ robust stability bound was used. The tuned QFT_{H_∞} design for loop two is shown in Fig. 6.6. Both the diagonal tracking and robust stability bounds are shown so that the designer considers the trade-off during loop shaping. The tuned controller for loop two is given by

$$g_{22}^{*} = \frac{-2.8841\,(s+823.9)\,(s+201.9)\,(s+10.29)}{s^2\,(s+2.314)} \cdot \frac{(s^2 + 9.243s + 189.5)\,(s^2 + 8.946s + 707.9)}{(s^2 + 8.213s + 634)\,(s^2 + 1284s + 1.311\times 10^6)}. \tag{6.4}$$

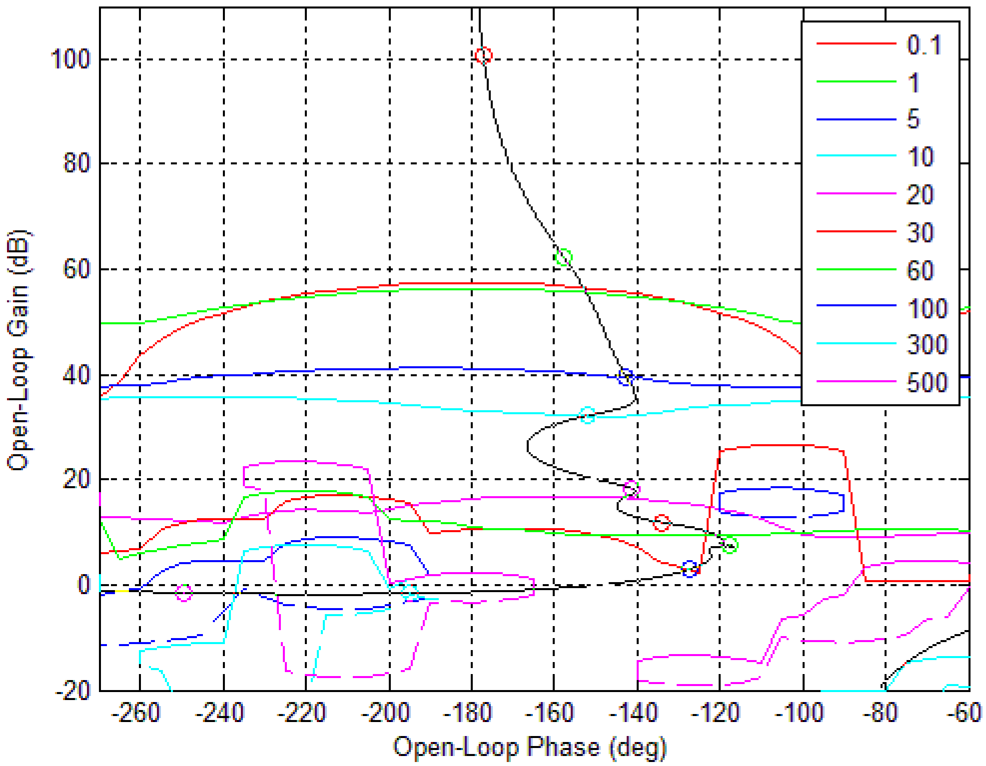

Figure 6.6 Loop two (l_2^*) design (tuned) for QFT_{H_∞}

From Fig. 6.6 it can be seen that it was not possible to meet the $60 rad/s$ tracking bound while ensuring closed-loop stability.

The original pseudo-diagonal H-infinity controller for loop one is very conservative. This allowed for the power of the QFT/H-infinity method to be shown. After tuning loop two, exact tracking bounds were calculated for loop one as described on page 56. The tuned loop together with loop boundaries for row one is shown in Fig. 6.7. Both the diagonal tracking and robust stability bounds are shown so that the designer considers the trade-off during loop shaping. The gain cross-over frequency was reduced from 96 rad/s to 14.6 rad/s while ensuring diagonal tracking and robust stability specifications are met. The tuned controller is given by

$$g_{11}^* = \frac{-168.2702\,(s+205.3)\,(s+20.86)\,(s+7.71)}{s^2\,(s+4000)^2\,(s+17.37)} \cdot \frac{(s^2\ +\ 6.36s\ +\ 10.71)\,(s^2\ +\ 5.191s\ +\ 3560)}{(s+5.075)\,(s+5.065)\,(s+1.939)}. \tag{6.5}$$

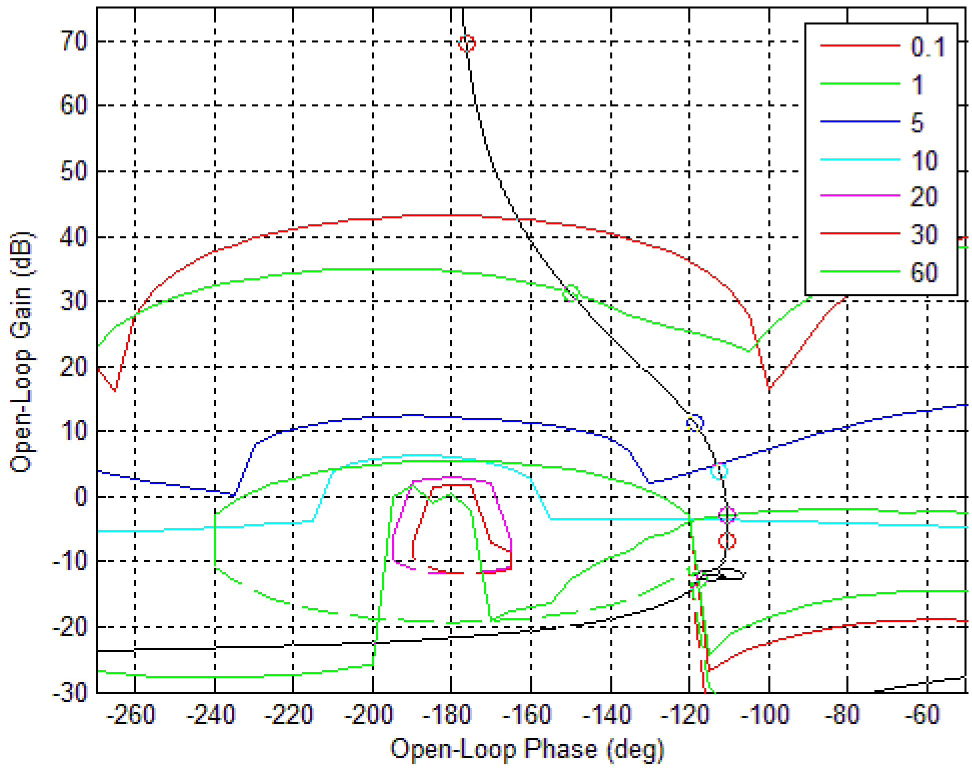

Figure 6.7 Loop one (l_1^*) design (tuned) for QFT_{H_∞}

Not only does this method allow one to obtain a less conservative diagonal controller, it also gives insight to the design. For instance, oscillations occur in the transmission response in the original H-infinity design due to the weighting requirements not being satisfied, but the QFT tuning allows one to shape the loop around more robust stability bounds which remove the sustained oscillations.

The final reference to output magnitude response is shown in Fig. 6.8 and the step response is shown in Fig. 6.9.

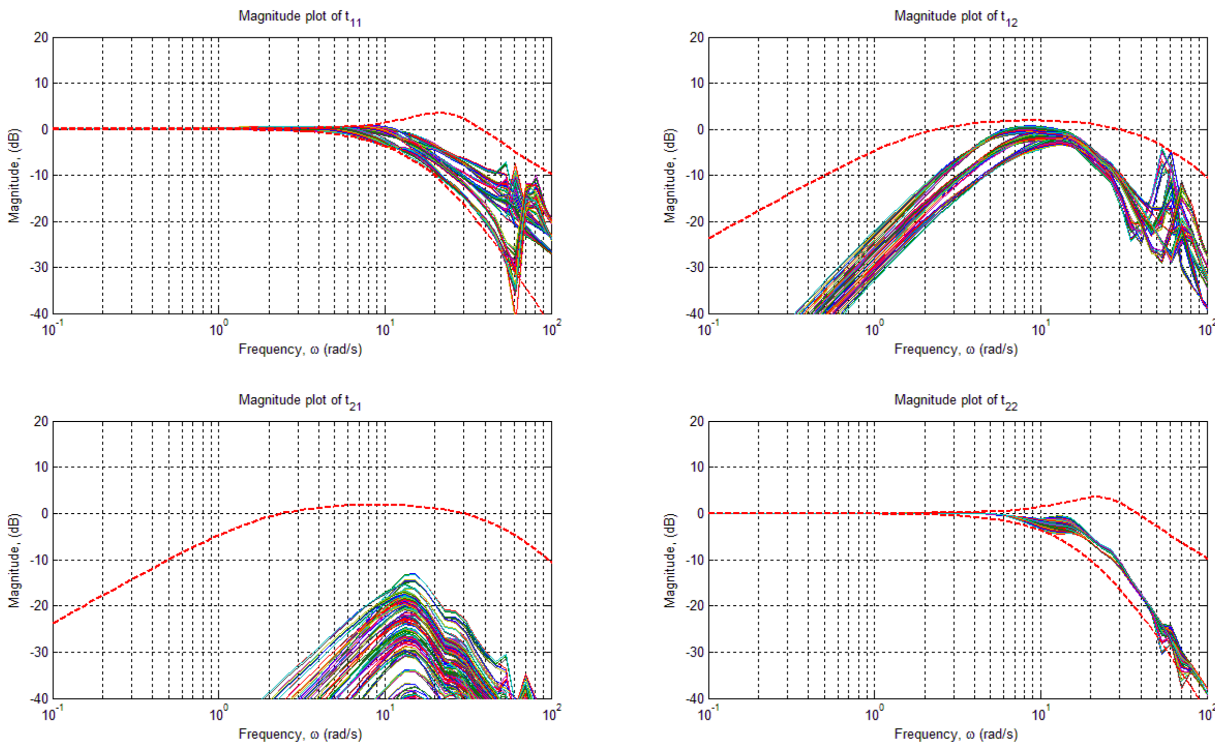

Figure 6.8 Closed-loop reference to output magnitude response for system using H_∞/QFT tuning (for linearized point 5)

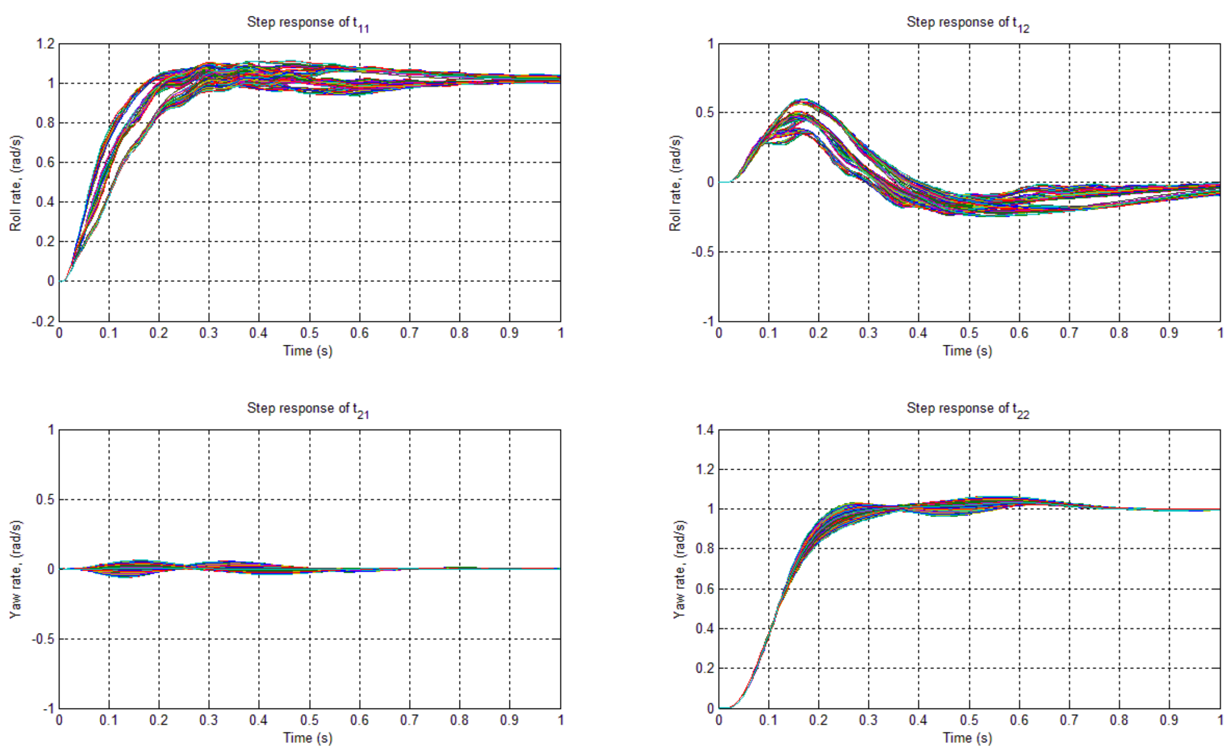

Figure 6.9 Closed-loop step response for system using H_∞/QFT tuning (for linearized point 5)

7. Discussion and Conclusions

The MIMO QFT method was found to be a very designer-intense method. The principle of transparency in SISO QFT designs was certainly carried over to the MIMO QFT extension. Although obtaining the template boundaries was a computationally intensive procedure, the insight they gave on the possible solutions and characteristics of the plant was without a doubt worthwhile. Assessing the template width at the expected gain cross-over frequency was especially useful, as it allowed the designer to determine the feasibility of using a single controller for all (or a combination) linearized points versus a gain-scheduled approach.

The first MIMO QFT technique applied was to design a diagonal controller and pre-filter for reference tracking specifications. Bounds on the cross-coupling terms were automatically generated as a result of using the algorithm in (Boje, 2004). The use of this method drastically reduced the amount of work required by the designer to obtain the loop boundaries as opposed to the alternative which demanded an iterative approach. Although this method eased the work on the designer, it shifted the effort to the computational machine. This is acceptable (in this age) with the ever increasing processing capability available. Using the method stated above, specifications were met for linearized points 1-3 with relatively low order controllers (compared to H-infinity controllers). Another benefit observed with the QFT method is that the damping factor of the controller elements could be limited (see Section 2.1.1 "Controller Preferences"). It was noticed that the design problem became more difficult as the angle of attack increased. This was expected due to the increase in cross-coupling. No QFT solution was found for linearized points 4-6. It is believed that the cross-coupling at these angles of attack were too much for the diagonal type QFT method.

The application of the non-diagonal controller design method showed significant results. Using traditional output disturbance rejection design, it was found that the specifications could not be attained. Although loop two constraints were satisfied, the exact boundaries for loop one could not be met. After pre-compensation, loop two design did not change much, but the loop boundaries in loop one were much more manageable, resulting in the closed-loop specification being met. The one problem found in this method was that the controller order is generally increased due to the multiplication between the pre-compensator and diagonal controller. This does pose a limitation to some extent, but the transparency of QFT allows trade-offs between controller order and conservativeness.

Error-tracking specifications were derived to approximate the reference tracking specifications. A traditional QFT reference tracking design and an error-tracking design was done. It was found that the reference-tracking design for loop two was less conservative than the error-tracking design for loop two. But the resulting loop one bounds could not be attained using reference tracking design. Hence the specifications could not be met with the original QFT design. The error-tracking design on the other hand, produced much lower loop one boundaries which were satisfied. This resulted in the closed-loop specifications being met using error-tracking specifications. The pre-filter order may be questionable for the error-tracking design method, but Boje (2002a) provides a method for reducing the order of the pre-filter (simplifying) by taking advantage of any over-design in the system. New specifications were created for the error-tracking design because the model $m(s)$ could not be derived from the tracking specifications. If the upper bound of the tracking specification is defined by $t_{ij}^{u}(s)$ and the lower bound defined by $t_{ij}^{l}(s)$ which correctly replicates non-minimum phase in the final system response, the model could not be obtain directly because

$$|m(s)| = \frac{\left|t_{ij}^{u}(s)\right| + \left|t_{ij}^{l}(s)\right|}{2} \geq \frac{\left|t_{ij}^{u}(s) + t_{ij}^{l}(s)\right|}{2}.$$

The application of the true inversion-free method was done for the same output disturbance rejection problem described in the non-diagonal controller design section. It was shown that the true inversion-free design equations produce less conservative bounds at frequencies near and beyond the gain cross-over frequency. Although in the case shown the results were not clear, there is indeed a theoretical advantage (shown on pg 101). From the results shown, the author believes it is justified to use the union of the original QFT bounds and the true inversion-free bounds as a common practice in QFT designs in the future.

The first distinct difference one observes between the application between QFT and H-infinity theory is the amount of work (or design time) that is required to obtain a controller that generates closed-loop responses that satisfy client specifications. Although the transparency of QFT gives insight on design problems that may not be apparent using an H-infinity approach, it is important to ask whether the design time justifies the insight. Where optimality is of interest, it is definitely justified to take a QFT approach. Both the QFT and H-infinity methods generated controllers that resulted in the closed-loop specifications for linearized point 1 being satisfied. With regards to optimality, it is important to compare the controller magnitudes for both methods used. The magnitude response of the QFT and H-infinity controllers are shown in Fig. 7.1 for linearized point 2 design. From the magnitude plot it is seen clearly (especially in output one) that the H-infinity controller uses more control effort in order to meet the specifications (more conservative). The H-infinity controller is more likely to produce nonlinear effects from saturation than the QFT controller because of the higher signal power transfer to the actuators. The work/design time required to produce a controller using QFT has drastically reduced over the years with the new computational tools available such as those used in this dissertation.

The H-infinity design methodology was successfully applied for linearized points 1-5, although specifications were not met in linearized points 4 and 5. Not meeting the tracking specifications for linearized points 4-5 using the H-infinity optimization shows the difficulty of these problems. For both linearized points 4 and 5 it was found that the specifications were violated at around $60 rad/s$. By iterative modification of the weighting functions, the specifications could have been attained but was not done so that comparisons between direct (non-iterative) designs could be made. It was found that the H-infinity controller implicitly tries to invert the plant to some extent at the resonant frequency. This resulted in controller elements with very low damping factors which are unfavourable for implementation (see 2.1.1 “Controller Preferences”). No acceptable solution was found for linearized point 6. The partial solutions that were found yielded very small stability margins (not worth stating) and no distinctive feedback benefits. The other well-known problem found with the H-infinity controller is the relatively high order (compared to QFT controller) even after controller order reduction via pole-zero cancellation. Although the H-infinity design method found solutions for the very difficult cases, the resulting controller opposes the three controller preferences stated on page 6 which makes its implementation very difficult.

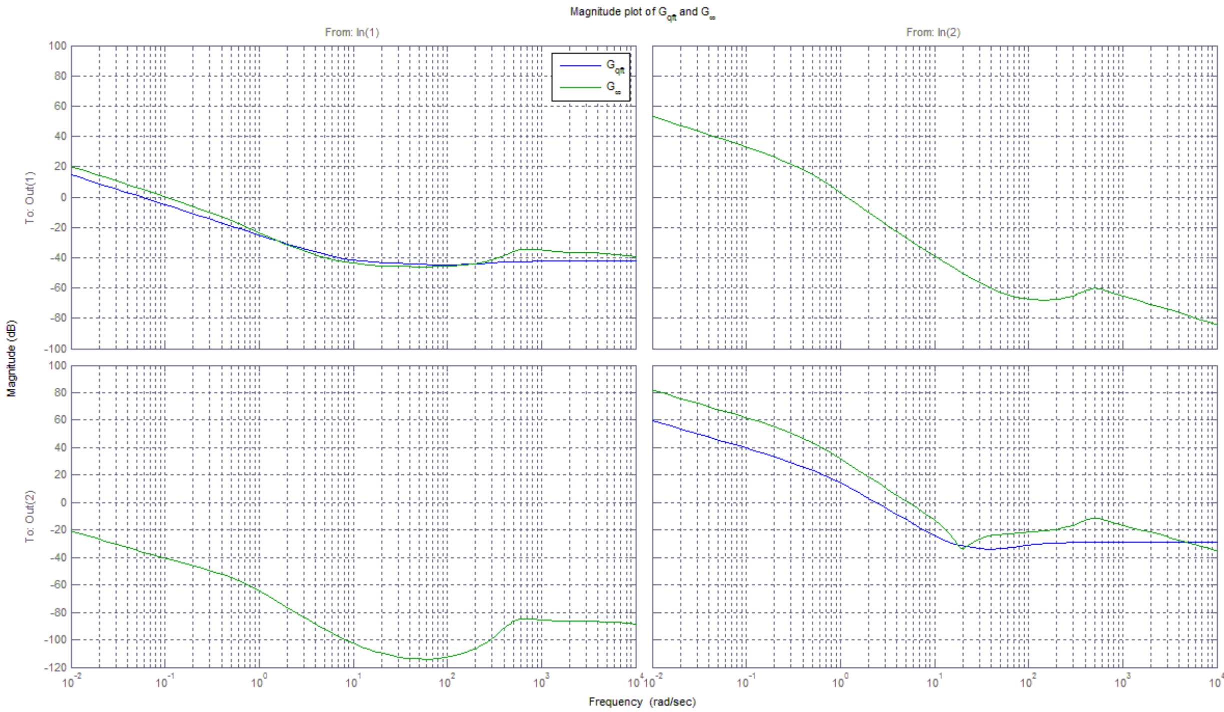

Figure 7.1 Magnitude plot of QFT and H-infinity controllers

The H-infinity/QFT combination applied in Section 6 appears to be a very promising technique that can be applied in the control industry. It combines the optimization of modern control with the transparency and insight of QFT. In the particular example demonstrated, the first design for linearized point 5 using H-infinity design yielded a controller that did not meet closed-loop specifications. Using the tuning method it was possible to "see" where loop gains were not satisfied, and tune appropriately. An impressive reduction in the final loop gain cross-over frequency from $96 rad/s$ to $14.6 rad/s$ was obtained using the QFT tuning method. Not only did the QFT tuned design produce a more optimal design, the tracking specifications were also met.

The problem of finding a QFT solution using H-infinity via simultaneous stabilization of plants promises to have significant implications for MIMO control system design. If this is possible, the MIMO problem may be solved exactly without any conservatism (using high order controller) as QFT provides for SISO system. Section 2.2.2 of this thesis investigated methods used to solve H-infinity problems so that it could be modified to solve for distinct (nominal) plants simultaneously. The one approach that appeared likely to be successful was the use of LMI's in simultaneous stabilization. Based on current LMI solutions to the H-infinity problem it was attempted to stack the LMI with additional constraints (for the other distinct plants). The obstacle that halted this approach was discovered when it was realized that the H-infinity controller was a result of the LMI's optimization AND the nominal plant. Since there are many distinct nominal plants for this method, one nominal could not be chosen. Although a solution was not found for this problem in this thesis it is worth further research as solution to this problem may be the ultimate goal of MIMO LTI control design.

References

Borgesani, C., Chait, Y., and Yaniv, O. (1998). Matlab™ quantitative feedback theory toolbox. Mathworks Inc.

Boje, E. (2000). Finding Nonconvex Hulls of QFT Templates. ASME, Journal of Dynamic Systems, Measurement and Control, 122(1), 230-232.

Boje, E., and Nwokah, O. D. I. (2001). Quantitative feedback design using forward path decoupling. ASME, Journal of Dynamic Systems, Measurement and Control, 123(1), 129-132.

Boje, E. (2002a). Multivariable quantitative feedback design for tracking error specifications. Automatica. 38(1), 131-138.

Boje, E. (2002b). Non-diagonal controllers in MIMO quantitative feedback design. International Journal of Robust and Nonlinear Control. 12(4), 303-320.

Boje, E. (2004). Algorithm for Calculating MIMO QFT Tracking Bounds. Journal of Dynamic Systems, Measurement, and Control. 126, 697.

Cohen, N. , Chait, Y., Yaniv, O. and Borghesani, C. (1992). Stability analysis using nichols charts. Proceedings of the 31st IEEE Conference on Decision and Control. 849-850.

Doyle, J. and Stein, G. (1981). Multivariable feedback design: Concepts for a classical/modern synthesis. IEEE Transactions on Automatic Control. 26(1), 4-16.

Eitelberg, E. (2000). Quantitative feedback design for tracking error tolerance. Automatica. 36(2), 319-326.

Eitelberg, E. (2006). Control Engineering. Durban: NOYB Press.

Franklin, G., Powell, J. and Emami-Naeini, A. (2006). Feedback control of dynamic systems. 5th Edition. Pearson Education.

Gahinet, P. and Apkarian, P. (1994). A linear matrix inequality approach to H∞ control. International Journal of Robust and Nonlinear Control. 4(4), 421-448

Garcia-Sanz, M. and Vital, P. (1999). Efficient computation of the frequency representation of uncertain systems. Proceedings 4th International Symposium on QFT and Robust Frequency Domain Methods. 117-126.

Garcia-Sanz, M. and Eguinoa, I. and Bennani, S. (2009). Non-diagonal MIMO QFT controller design reformulation. International Journal of Robust and Nonlinear Control. 19(9), 1036-1064.

Glover, K. and Doyle, J.C. (1988). State-space formulae for all stabilizing controllers that satisfy an H_∞ -norm bound and relations to relations to risk sensitivity. Systems and Control Letters. 11(3), 167-172.

Horowitz, I. (1979). Quantitative synthesis of uncertain multiple input-output feedback system. International Journal of Control. 30(1), 81-106.

Horowitz, I. and Loecher, C. (1981). Design of a 3 x 3 multivariable feedback system with large plant uncertainty. International Journal of Control. 33(4), 677-699.

Horowitz, I. (1982). Improved design technique for uncertain multiple-input-multiple-output feedback systems. International Journal of Control. 36(6), 977-988.

Horowitz, I. (2001). Survey of quantitative feedback theory (QFT). International Journal of Robust and Nonlinear Control. 11(10), 887-921.

Houpis, C.H. and Sating, R.R. (1997). MIMO QFT CAD Package (Ver.3) International Journal of Control. 7(6), 533-549.

Houpis, C.H. and Rasmussen, S.J. and Garcia-Sanz, M. (2006). Quantitative feedback theory: fundamentals and applications. 2nd Edition. CRC Press.

Kwakernaak, H. (1993). Robust control and H_∞ optimization--Tutorial paper. Automatica. 29(2), 255-273.

Lee, KL and Langehough, MA and Chamberlain, RA. (1992). Modern control bank-to-turn autopilot for Have Dash II missile. First IEEE Conference on Control Applications. 214-219.

Limebeer, DJN. (1982). The application of generalized diagonal dominance to linear system stability theory. International Journal of Control. 36(2), 185-212.

Maciejowski, JM. (1989). Multivariable feedback design. Addison-Wesley.

Munkres, J. (2000). Topology. 2nd Edition. Printice Hall.

Nagamune, R. (2008). Lecture slides: Continuous-time infinite horizon LQR. University of British Columbia. http://www.sites.mech.ubc.ca/~nagamune/MECH468/MECH550P_L26_CTinfiniteLQR.pdf. Last accessed: 19 May 2011.

Park, M.S. and Chait, Y. and Steinbuch, M. (1997). Inversion-free design algorithms for multivariable quantitative feedback theory: An application to robust control of a CD-ROM. Automatica. 33(5), 915-920.

Riedel, F.W. (1980). Bank-to-turn control technology survey for homing missiles. NASA Contractor Report. 3325.

Skogestad, S. and Postlethwaite, I. (2005). Multivariable feedback control analysis and design. John Wiley & Sons Ltd.

Sidi, M.J. (2001). Design of robust control systems: from classical to modern practical approaches. Krieger Pub. Co.

Sidi, M.J. (2002). A combined QFT/H∞ design technique for TDOF uncertain feedback systems. International Journal of Control. 75(7), 475-489.

Vajta, M. (2000). Some remarks on Padé-approximations. Proc. 3rd TEMPUS—INTCOM Symp. Intelligent Systems in Control and Measurement. 53-58.

Vidyasagar, M.. (1978). Nonlinear systems analysis. Printice Hall.

Vidyasagar, M. and Bertschmann, RK and Sallaberger, CS. (1988). Some simplifications of the graphical Nyquist criterion. IEEE Transactions on Automatic Control. 33(3), 301-305.

Yaniv, O. and Horowitz, I. (1986). Quantitative design method for MIMO linear feedback systems having uncertain plants. International Journal of Control. 43(2), 401-422.

Yaniv, O. (1999). Quantitative feedback design of linear and nonlinear control systems. Kluwer Academic Publishers.

Zhou, K. and Doyle, J.C. (1998). Essentials of robust control. Prentice Hall New Jersey.

Zarchan, P. (2007). Tactical and Strategic Missile Guidance. American Institute of Aeronautics and Astronautics.

Appendices

A1. LQR Responses

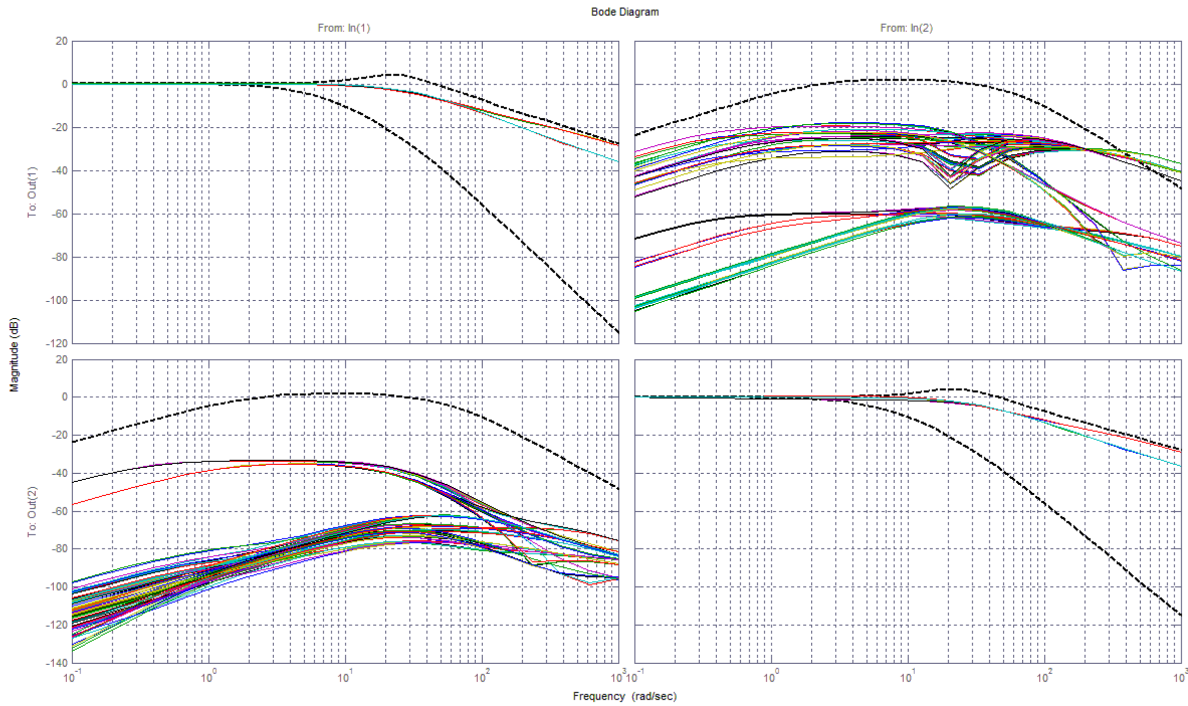

Figure A1.1 Magnitude plot of the tracking response for LQR trial for linearized point 2

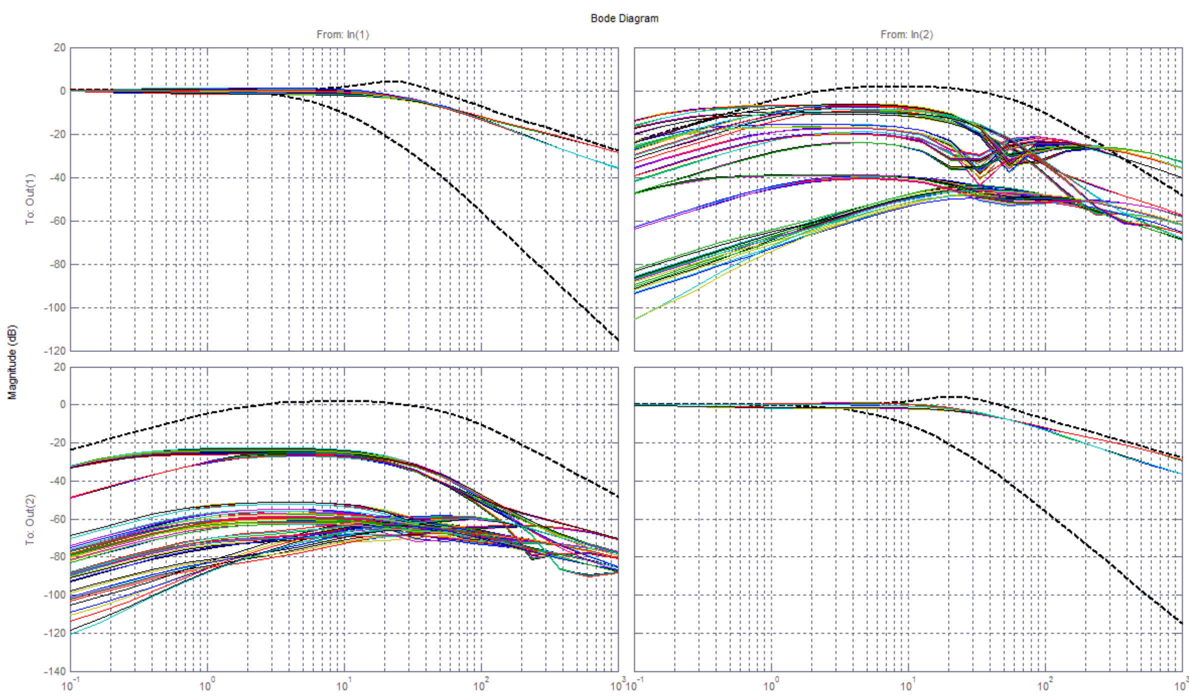

Figure A1.2 Magnitude plot of the tracking response for LQR trial for linearized point 3

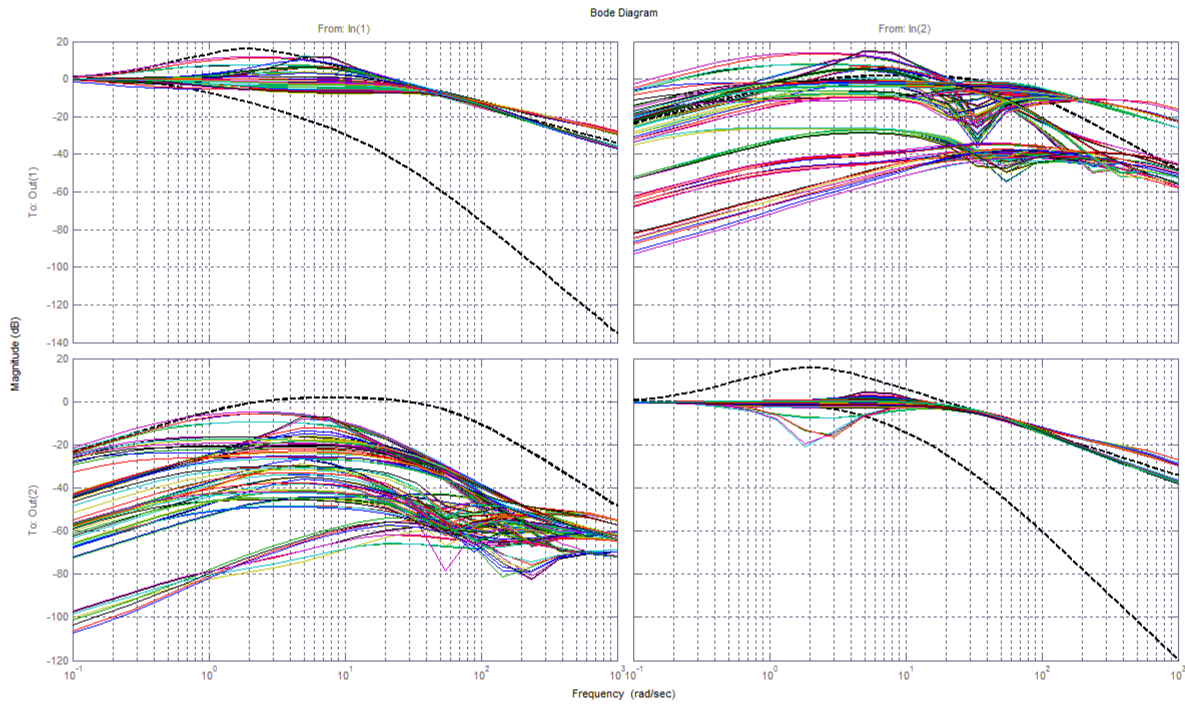

Figure A1.3 Magnitude plot of the tracking response for LQR trial for linearized point 4

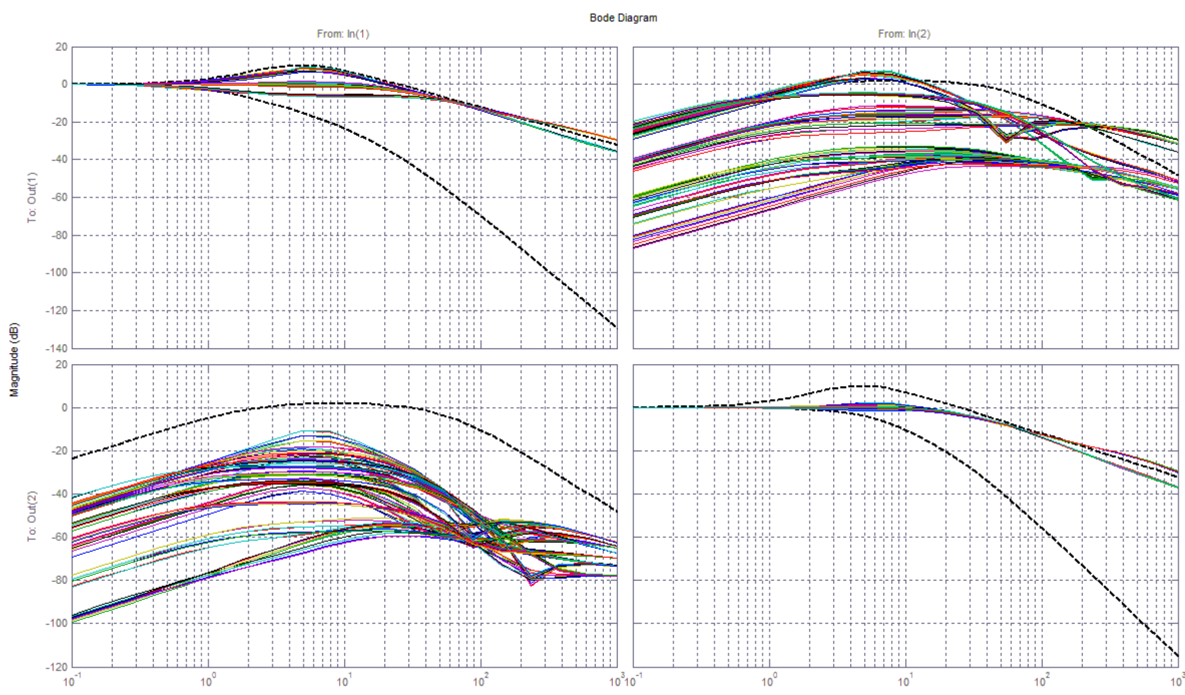

Figure A1.4 Magnitude plot of the tracking response for LQR trial for linearized point 5

A2. Plant Templates

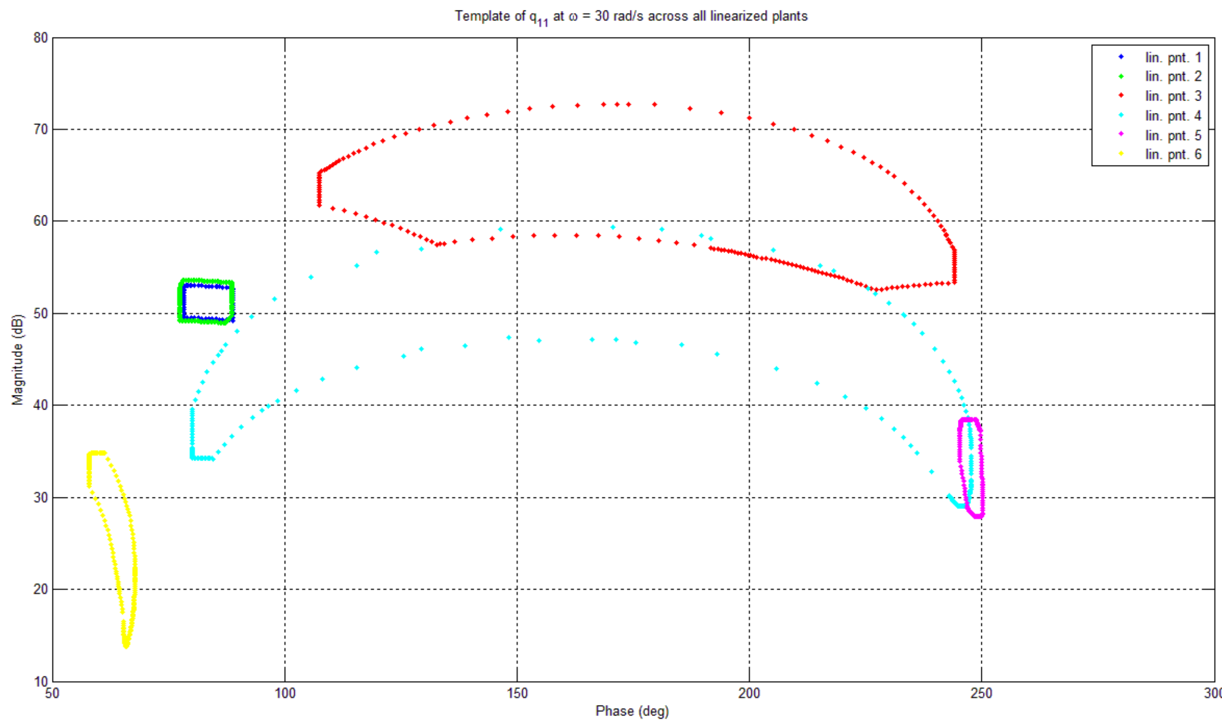

Figure A2.1 Template of q_{11} across all linearized plants for $\omega = 30\ rad/s$

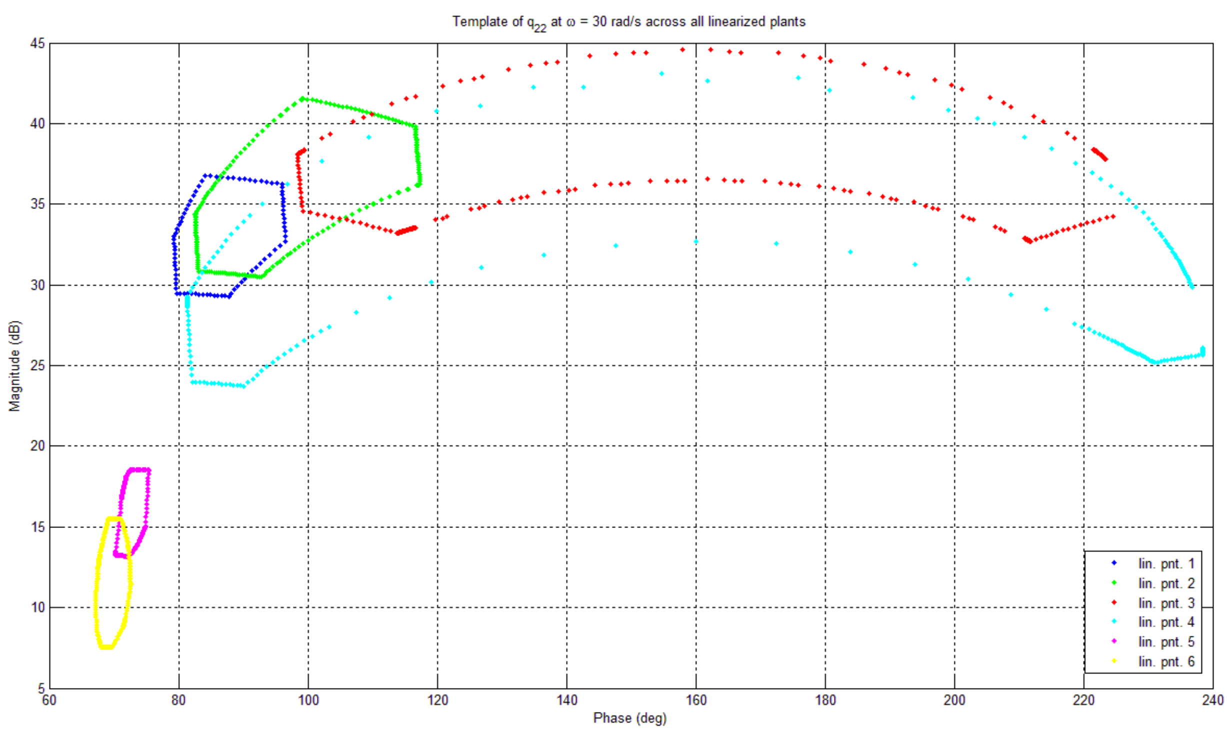

Figure A2.2 Template of q_{22} across all linearized plants for $\omega = 30\ rad/s$

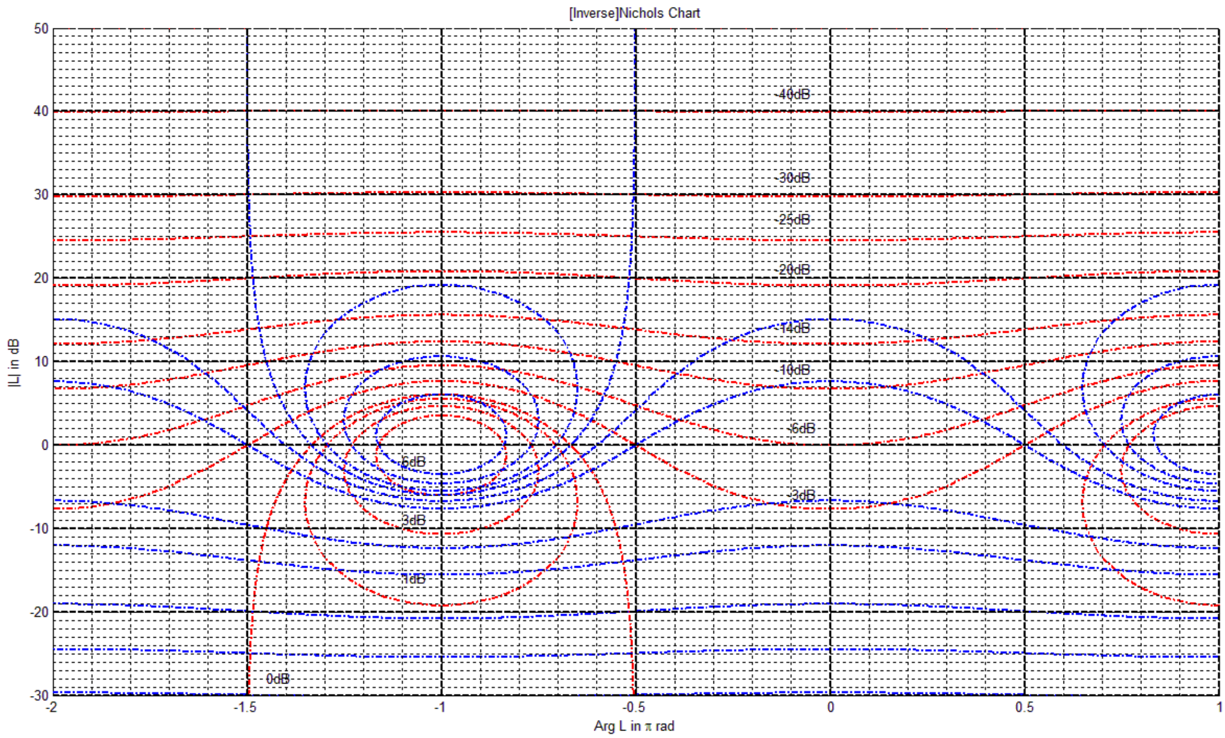

Figure A2.3 [Inverse]Nichols chart; Red '-.' – Sensitivity loci; Blue '-.' – Complementary sensitivity loci

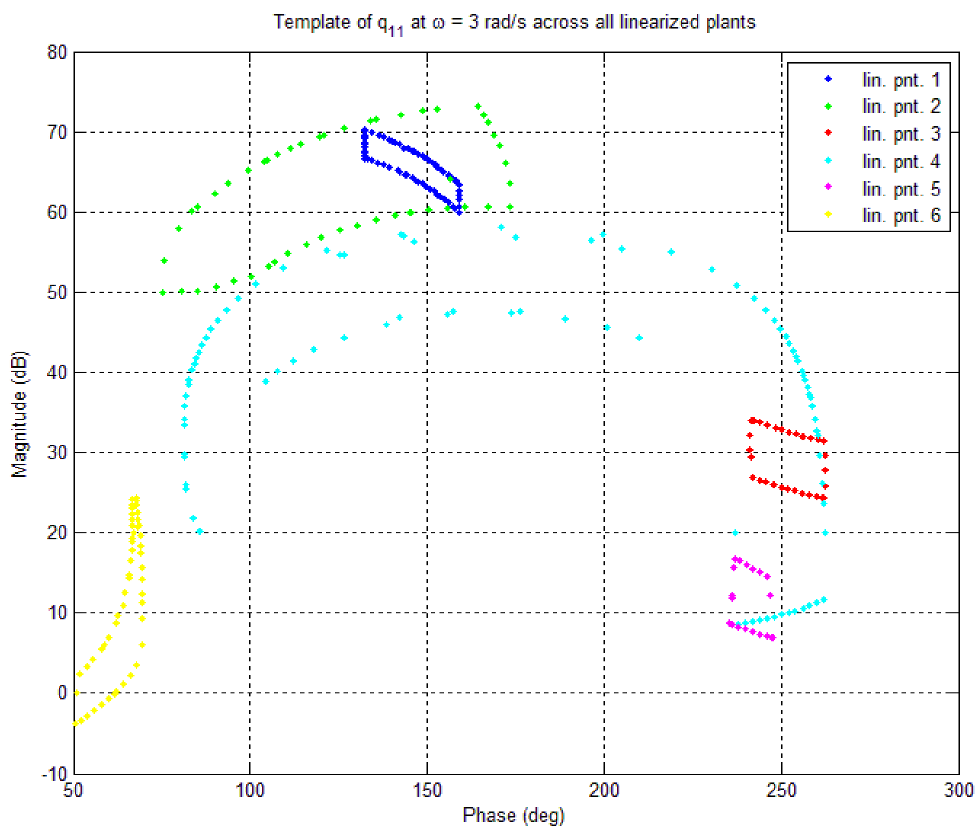

Figure A2.4 Template of q_{11} across all linearized plants for $\omega = 3\ rad/s$

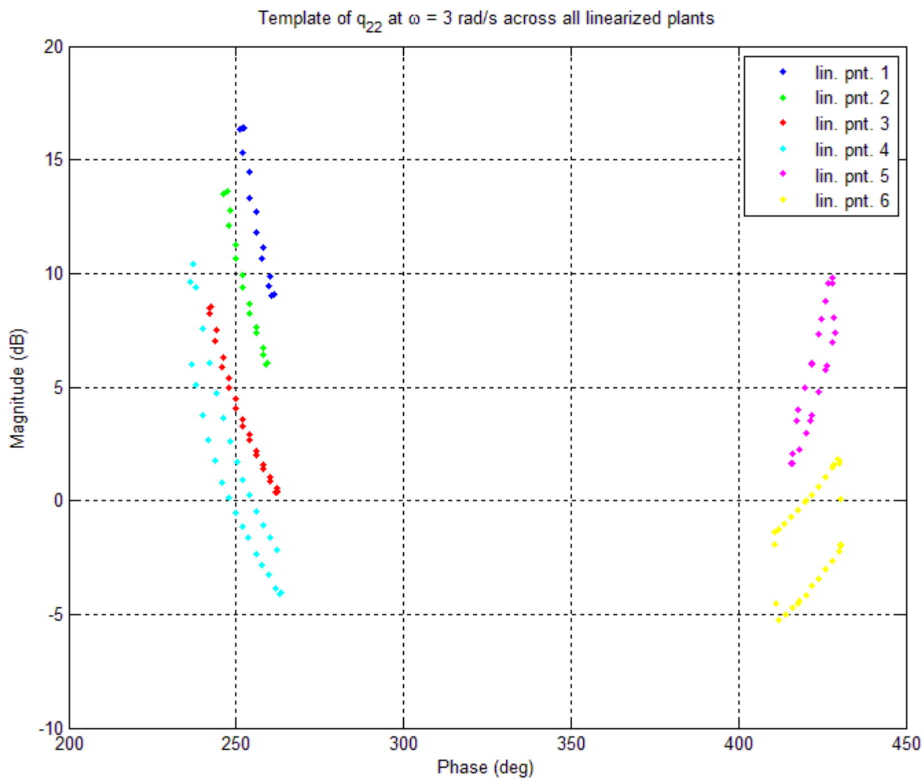

Figure A2.5 Template of q_{22} across all linearized plants for $\omega = 3\ rad/s$

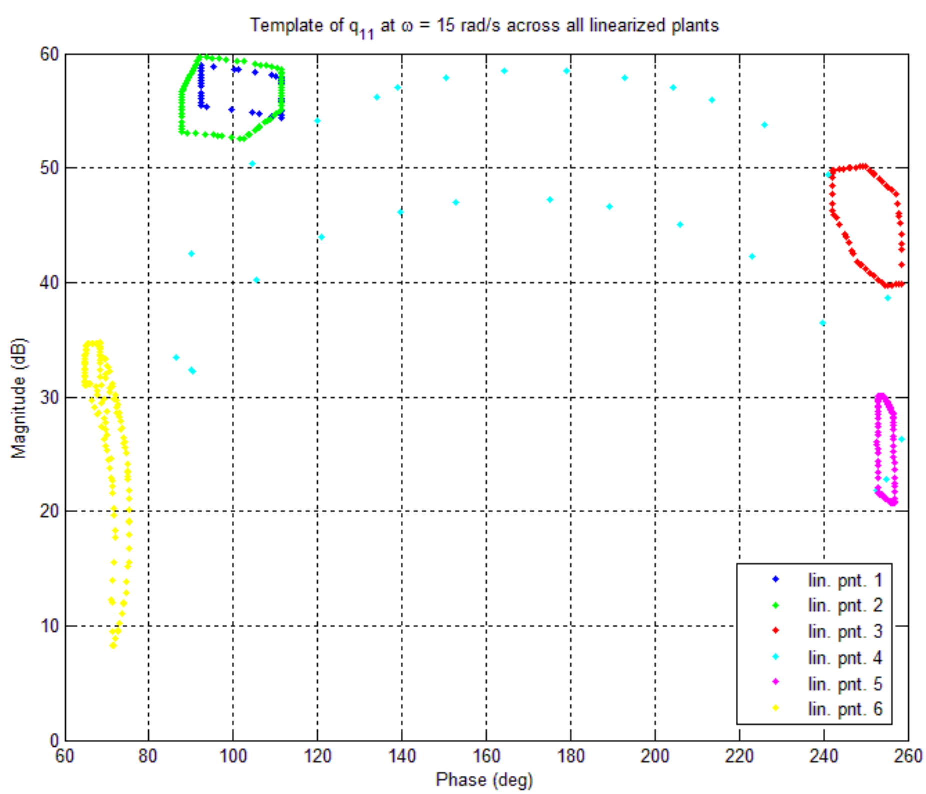

Figure A2.6 Template of q_{11} across all linearized plants for $\omega = 15\ rad/s$

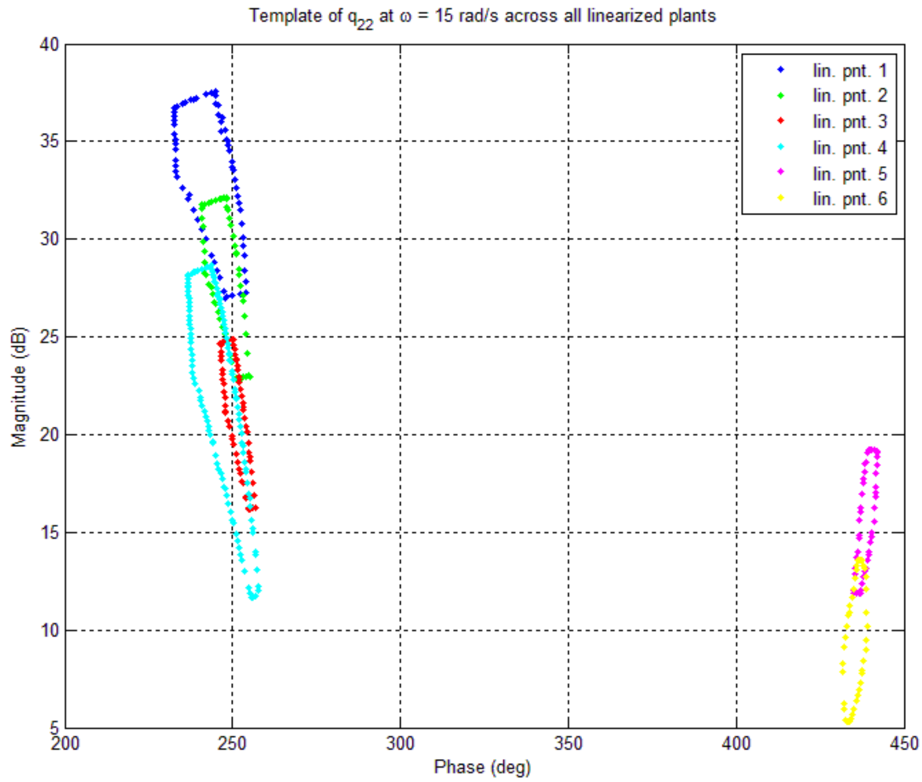

Figure A2.7 Template of q_{22} across all linearized plants for $\omega = 15\ rad/s$

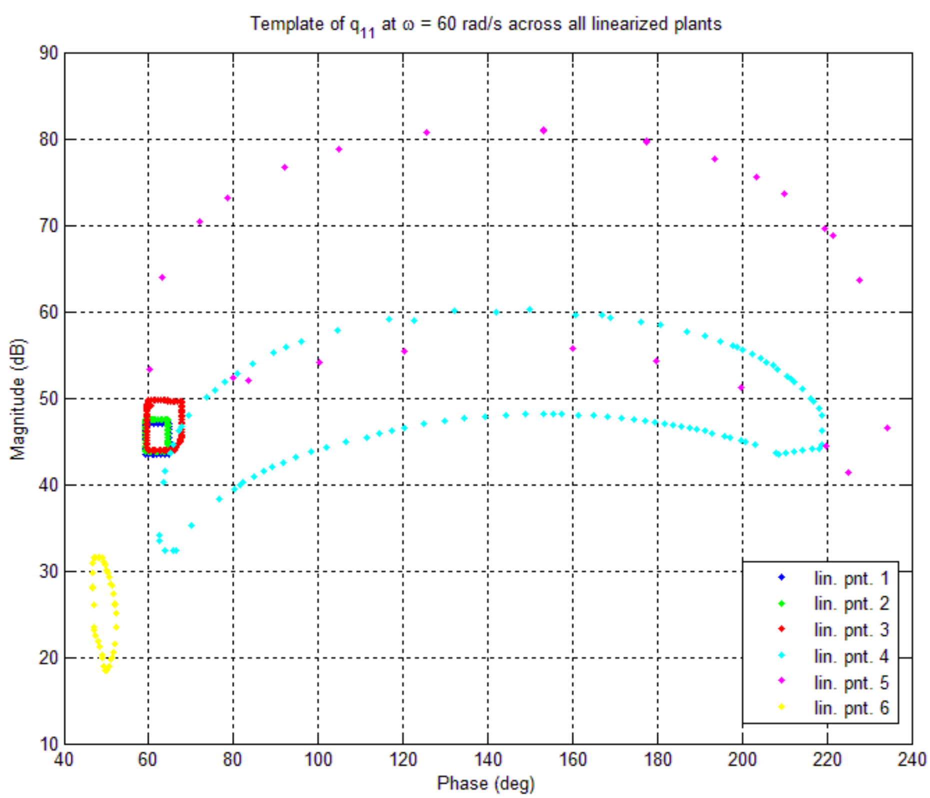

Figure A2.8 Template of q_{11} across all linearized plants for $\omega = 60\ rad/s$

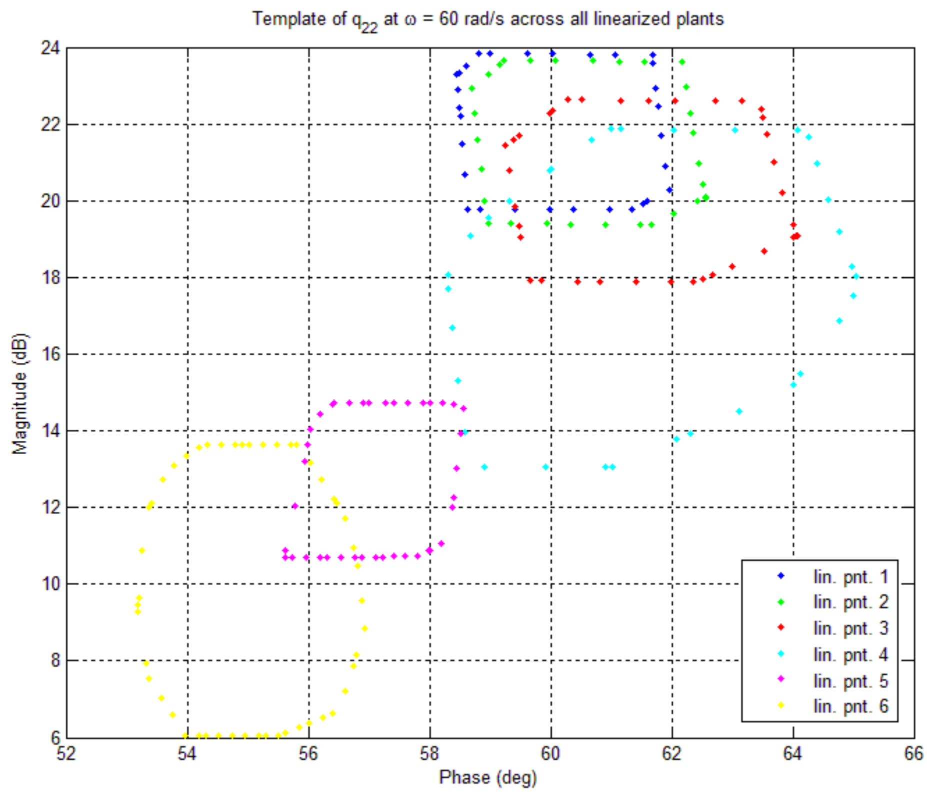

Figure A2.9 Template of q_{22} across all linearized plants for $\omega = 60\ rad/s$

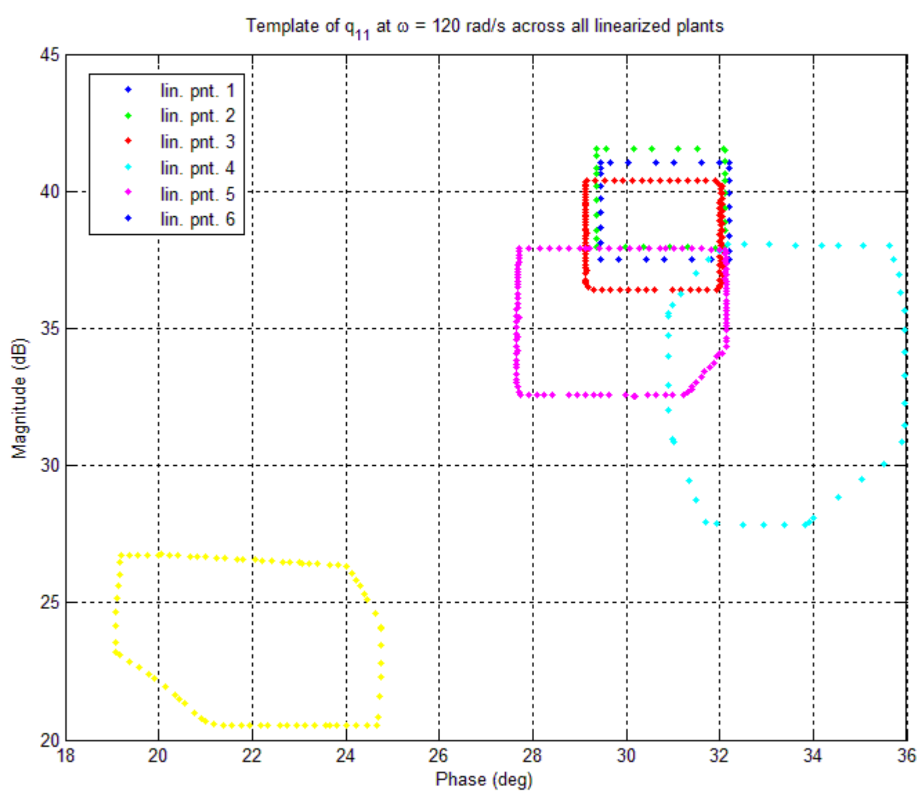

Figure A2.10 Template of q_{11} across all linearized plants for $\omega = 120\ rad/s$

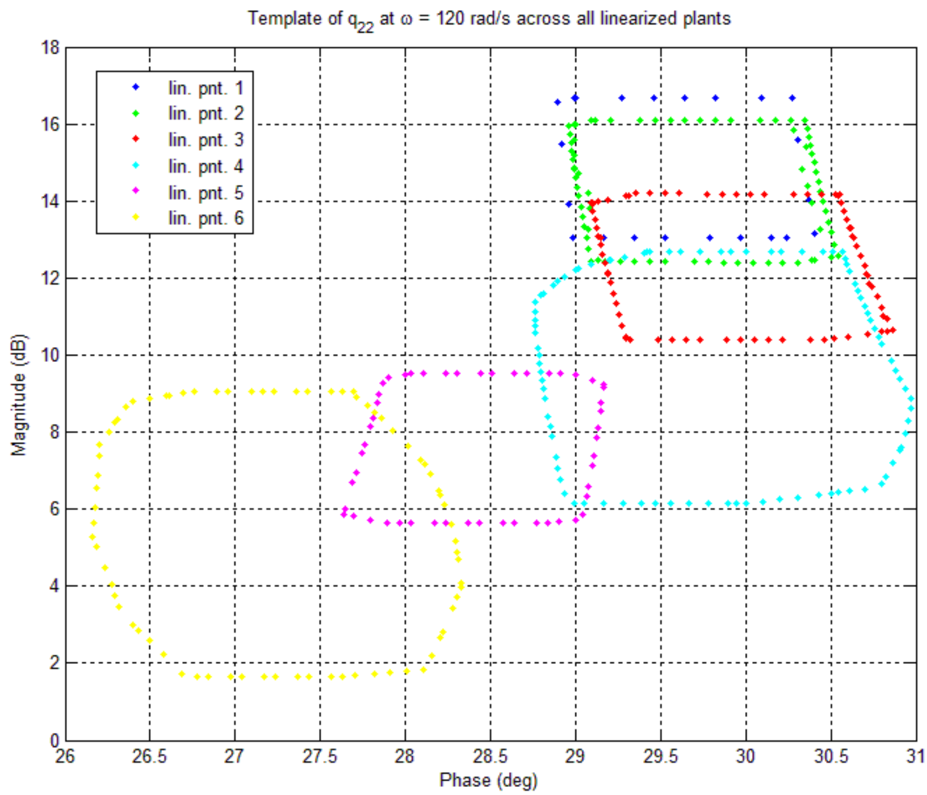

Figure A2.11 Template of q_{22} across all linearized plants for $\omega = 120\ rad/s$

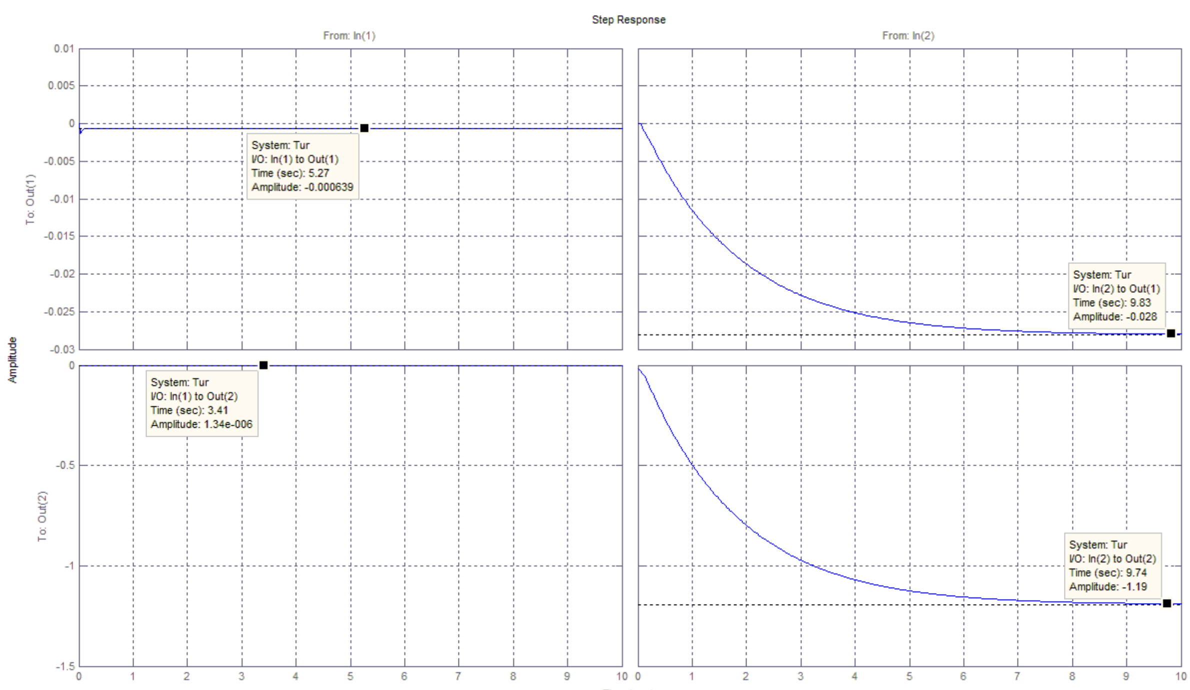

Figure A2.12 Step response from reference to plant input for linearized point 1 nominal (using QFT design)

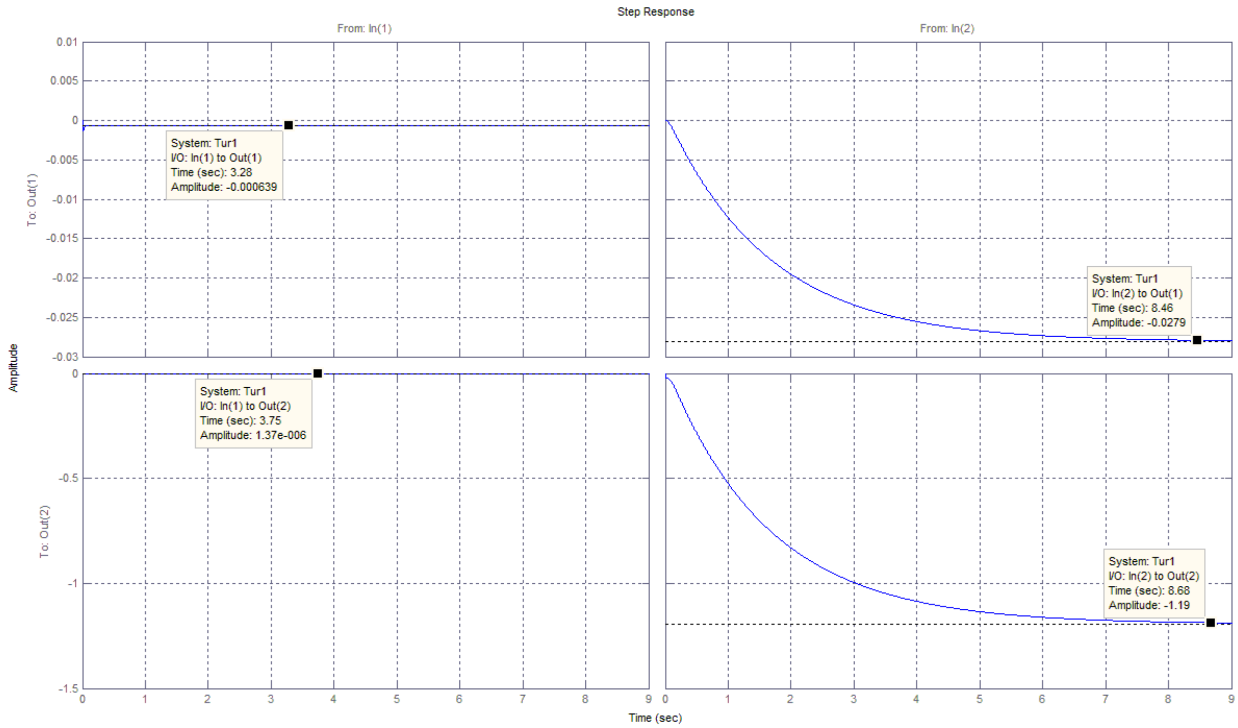

Figure A2.13 Step response from reference to plant input for linearized point 1 nominal (using H-infinity design)

A3. QFT Application to Linearized Points 2-3

Application to linearized point 2

The nominal *equivalent* plants for both channels are shown in Eqs (A3.1) - (A3.2). Note that the first equivalent plant is open-loop unstable. This certainly does not imply that the original plant element $(1, 1)$ is unstable based on Eq. (4.2.4).

$$q_{11} = \frac{-14325.046 \cdot (s + 0.8286) \cdot e^{-s(10\times10^{-3})}}{(s + 13.25) \cdot (s - 3.951)} \quad \text{(A3.1)}$$

$$q_{22} = \frac{-726.0426 \cdot (s + 0.8286)e^{-s(10\times10^{-3})}}{(s^2 + 5.316s + 740.6)} \quad \text{(A3.2)}$$

As in the linearized point 1 design, loop two was chosen to be designed first because of less severe constraints. This is expected since the plant templates for linearized points 1 and 2 have similar shapes. The idea of template shape and specifications (quantitative) determining the loop gain (bounds) is reinforced by Figure A3.1, which shows the tracking bounds and the nominal loop that appear very similar to the bounds that were obtained for linearized point 1.

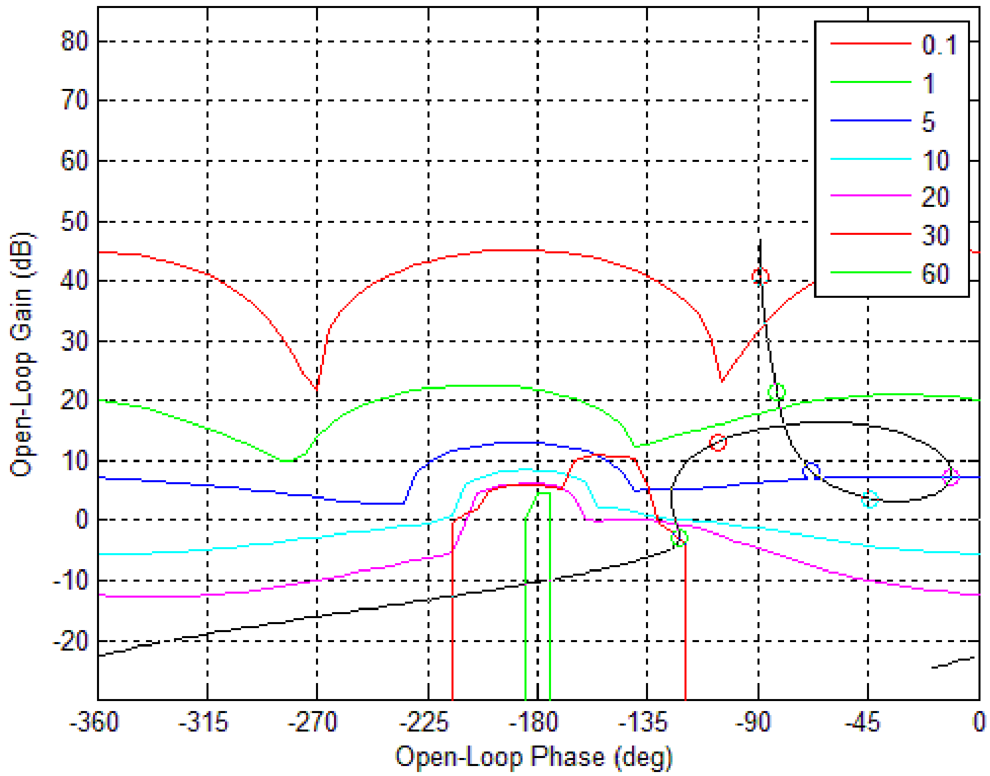

Figure A3.1 Nominal loop two with tracking bounds for linearized point 2

A robust stability margin of $6dB$ is also used for linearized point 2. The bounds required to satisfy the robust stability constraint are shown with the nominal loop in Fig. A3.2. The controller designed for loop two is a modification of the loop two controller used in linearized point 1 design. An increase in DC gain and a relocation of the first pole results in the loop two controller for linearized point 2 as

$$g_{22} = \frac{-0.08 \cdot (s^2 + 21.24s + 225.6) \cdot (s^2 + 61.51s + 2155)}{s \cdot (s+55)^2 \cdot (s+0.948)}. \tag{A3.3}$$

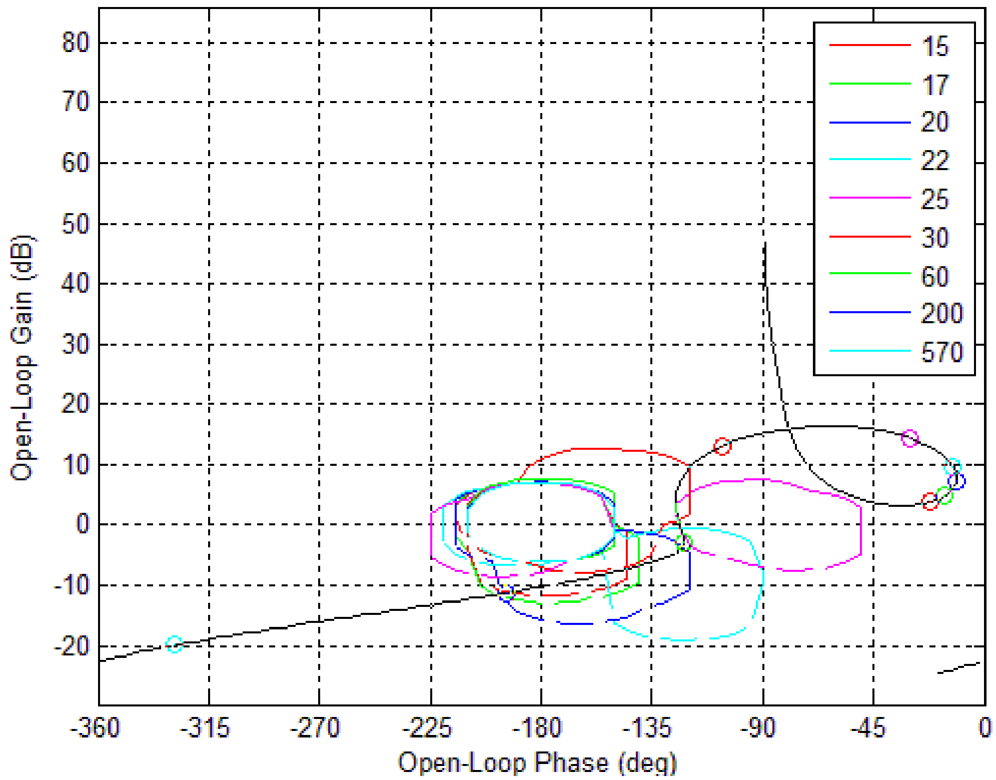

Figure A3.2 Nominal loop two with robust stability bounds for linearized point 2

Using a diagonal pre-filter, the pre-filter element for row two that shifts the worst case reference to output response to satisfy the specification is given by

$$f_{22} = \frac{13.3403 \cdot (s + 35.87) \cdot (s + 5.915) \cdot (s + 0.6386)}{(s + 17.44) \cdot (s + 0.5997) \cdot (s^2 + 20.63s + 172.8)} \tag{A3.4}$$

The worst case reference to output response with the pre-filter element above for row two is shown in Fig. A3.3.

After generating the new equivalent plants, the tracking and stability bounds ($6dB$ stability margin) for row one are found. This is shown in Fig. A3.4. The controller that satisfy all loop constraints is

$$g_{11} = \frac{-5.2 \cdot (s + 32) \cdot (s^2 + 19.7s + 124.9)}{s \cdot (s + 1085) \cdot (s + 39.16) \cdot (s + 7.882)}. \tag{A3.5}$$

The pre-filter element for row one that shifts closed-loop response to satisfy absolute specifications is

$$f_{11} = \frac{(s/1.09 + 1)}{(s/0.9 + 1) \cdot (s/25 + 1)}. \tag{A3.6}$$

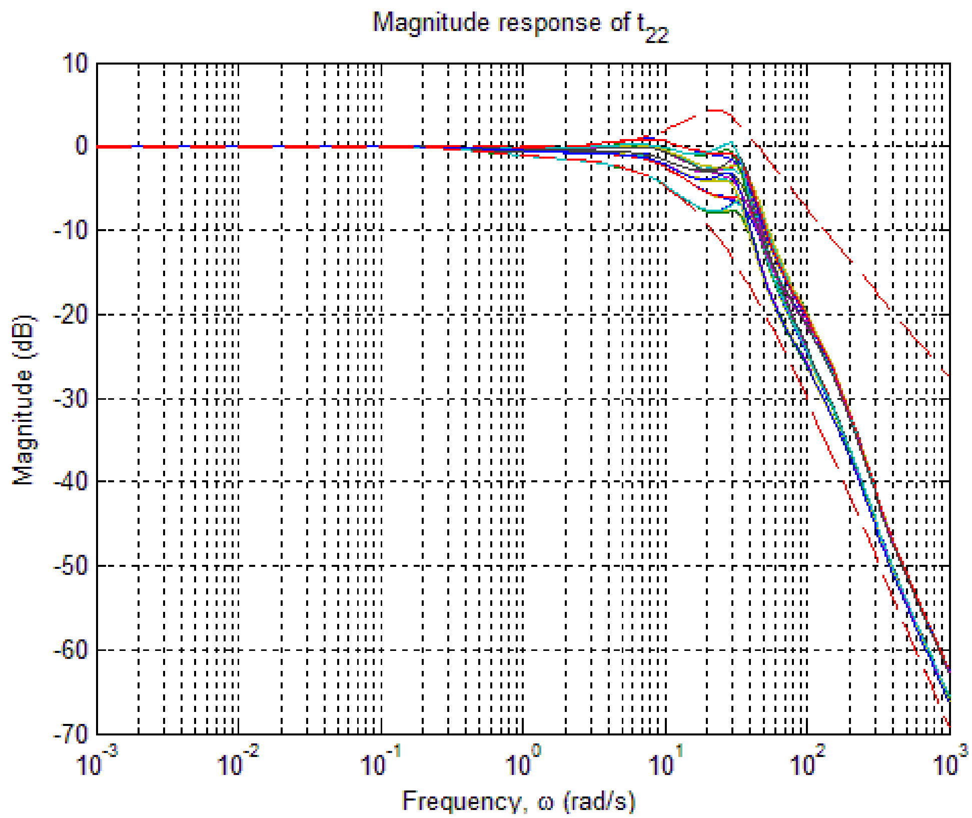

Figure A3.3 Magnitude response of t_{22} after row two is designed for linearized point 2

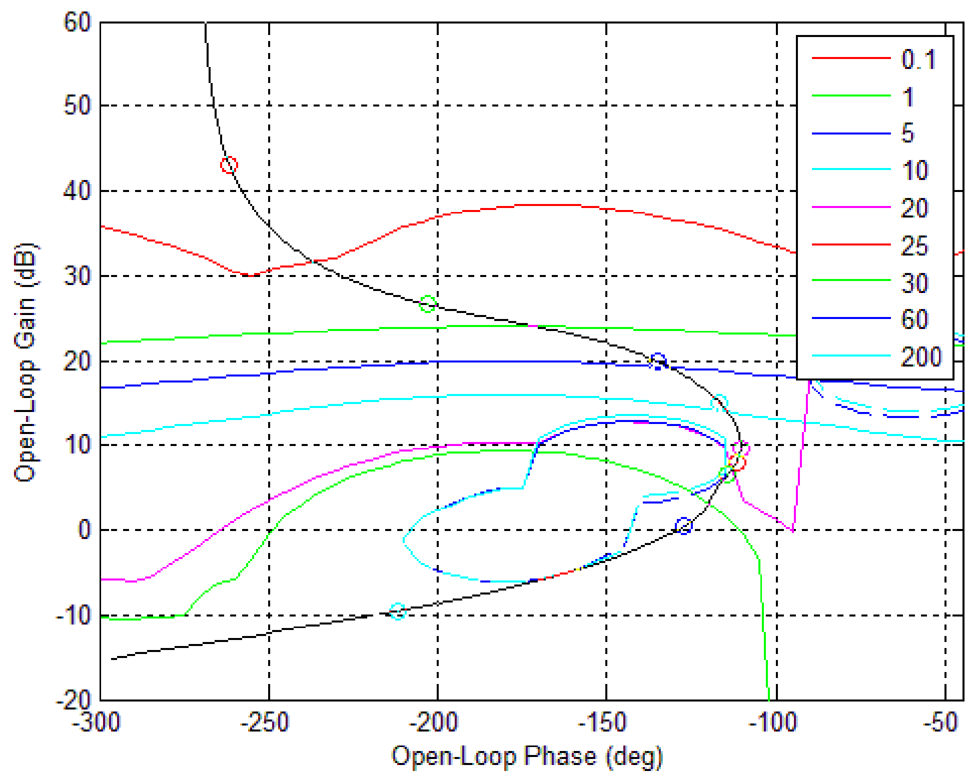

Figure A3.4 Nominal loop one with the intersection of tracking and robust stability bounds for linearized point 2

The closed-loop magnitude response and step response for linearized point 2 are shown below.

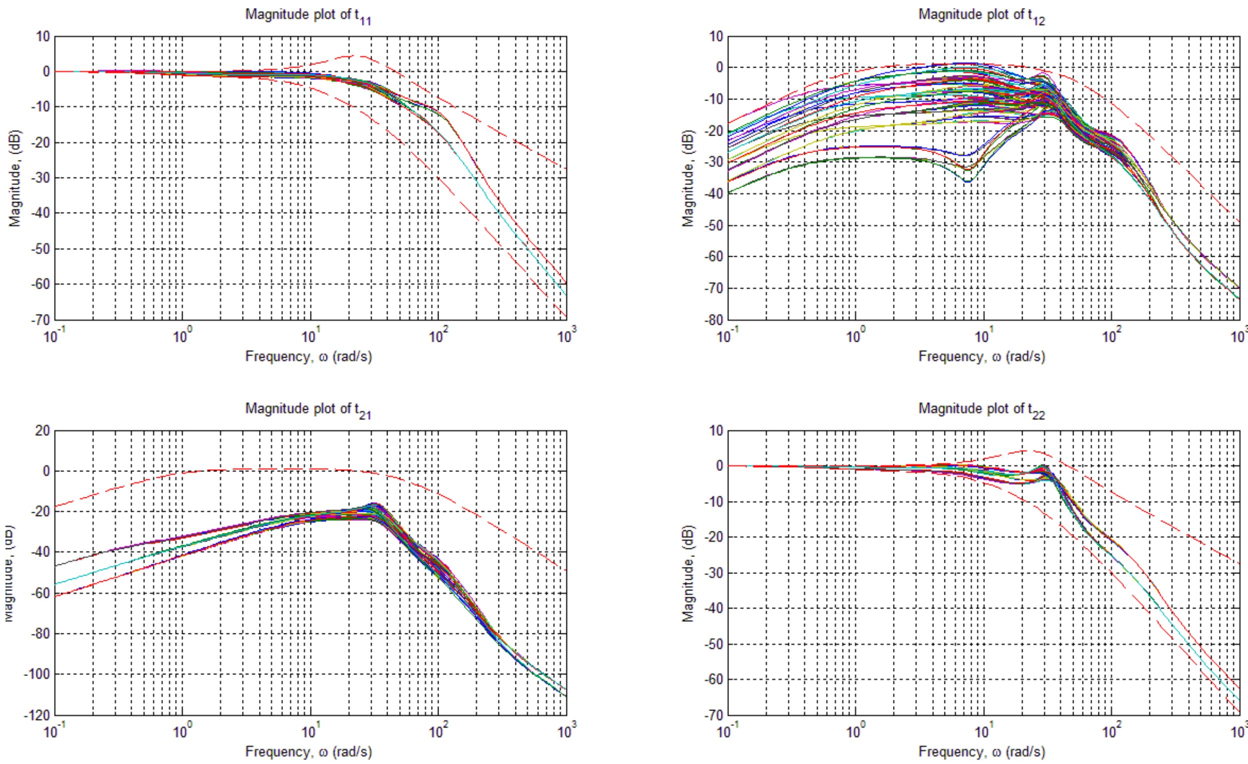

Figure A3.5 Magnitude plot of the closed-loop system with the specifications (red dashed) for linearized point 2

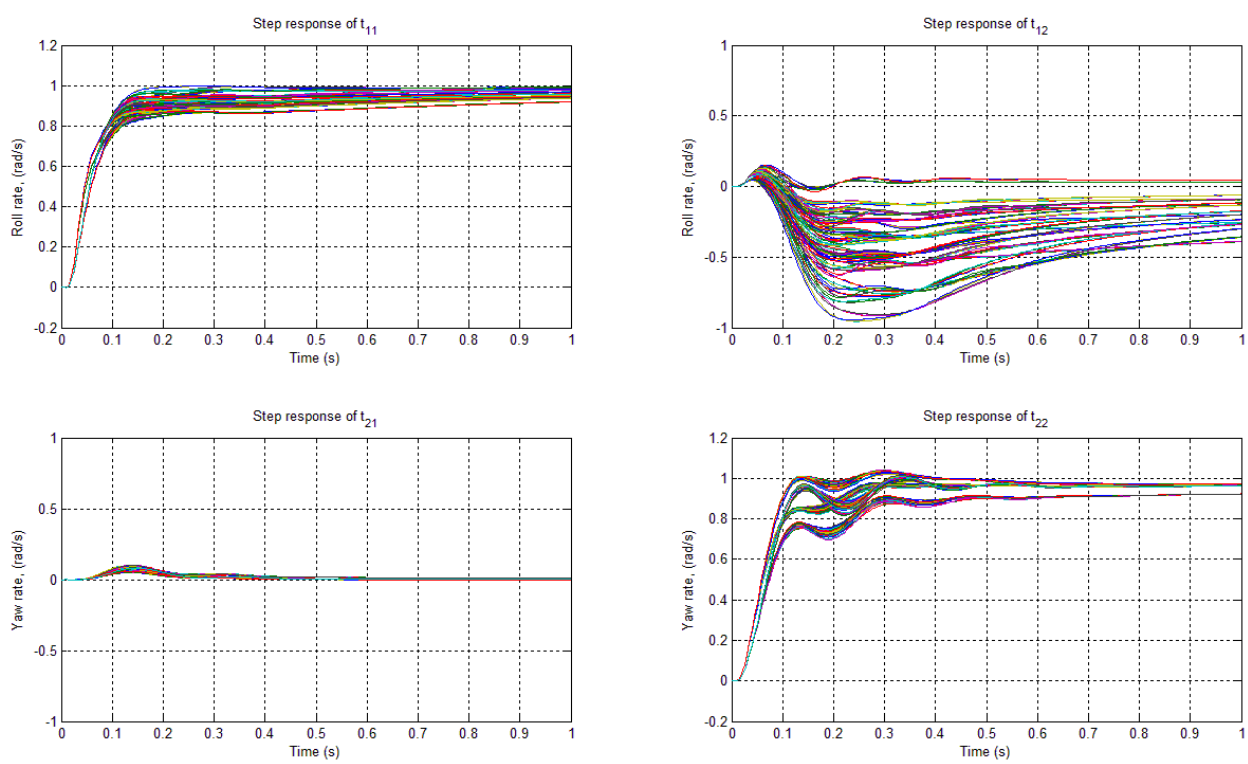

Figure A3.6 Step response of the closed-loop system for linearized point 2

Application to Linearized Point 3

The nominal *equivalent* plants for both channels are shown in Eqs (A3.7) - (A3.8).

$$q_{11} = \frac{-11316\,(s + 0.9493) \cdot\, e^{-s(10\times10^{-3})}}{(s^2\; +\; 8.415s\; + 930.8)} \tag{A3.7}$$

$$q_{22} = \frac{-566.4 \cdot\; (s + 0.9493) \cdot\, e^{-s(10\times10^{-3})}}{(s^2\; +\; 5.671s\; +\; 1100)} \tag{A3.8}$$

Once again, loop two is chosen as the first loop to design due to less stringent requirements. The loop two design is shown with the tracking bounds in Fig. A3.7. From preliminary assessment of the nominal loops, it was found that loop one boundaries were significantly more difficult to satisfy. For this reason loop two design was made more conservative than the tracking bounds required to ease loop one design.

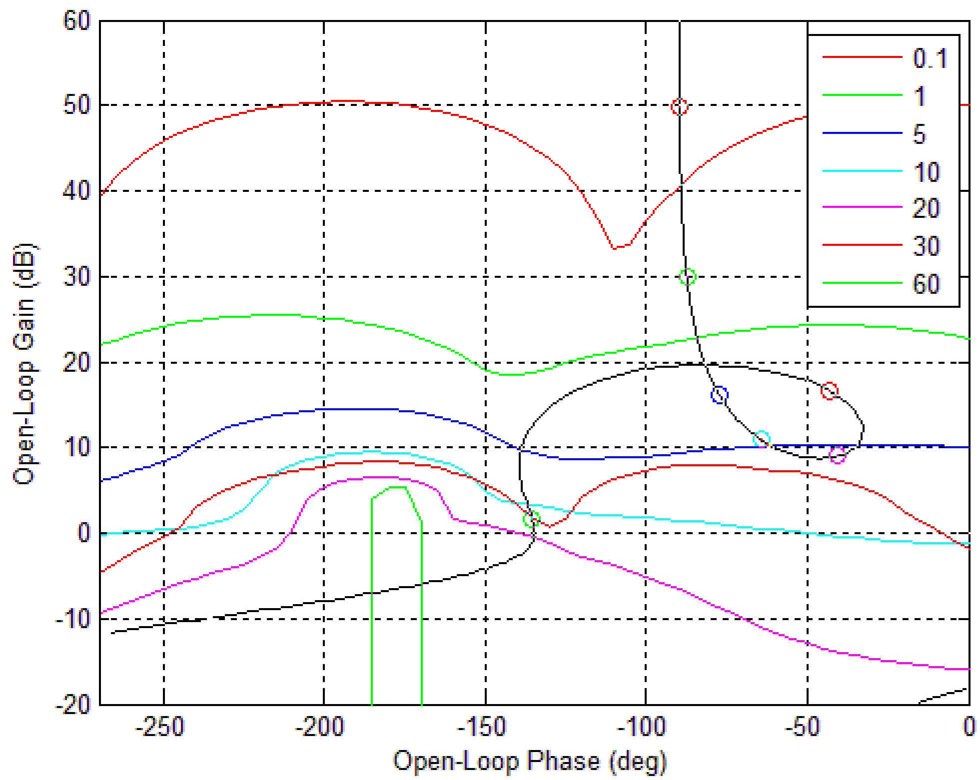

Figure A3.7 Nominal loop two with tracking bounds for linearized point 3

Using a stability margin of $6dB$, the stability boundaries with the designed nominal loop are shown in Fig. A3.8. The controller that satisfies both tracking and stability bounds is given by

$$g_{22} = \frac{-0.176 \cdot\; (s + 70.15)\;\; \cdot (s + 34.68)\;\; \cdot (s^2\; +\; 46.9s\; +\; 1100)}{s \cdot\; (s + 154) \cdot\; (s + 50.87) \cdot\; (s + 0.9493)}. \tag{A3.9}$$

The pre-filter transfer function for row two is given in Eq. (A3.10) and the worst case response for row two is shown in Fig. A3.9.

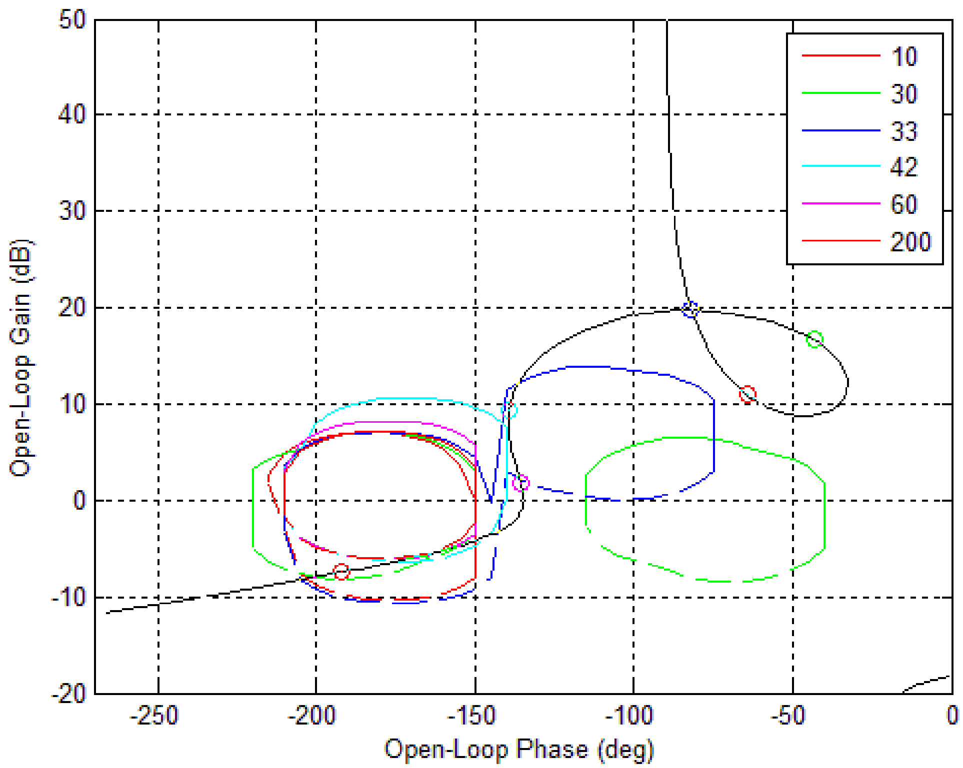

Figure A3.8 Nominal loop two with robust stability bounds for linearized point 3

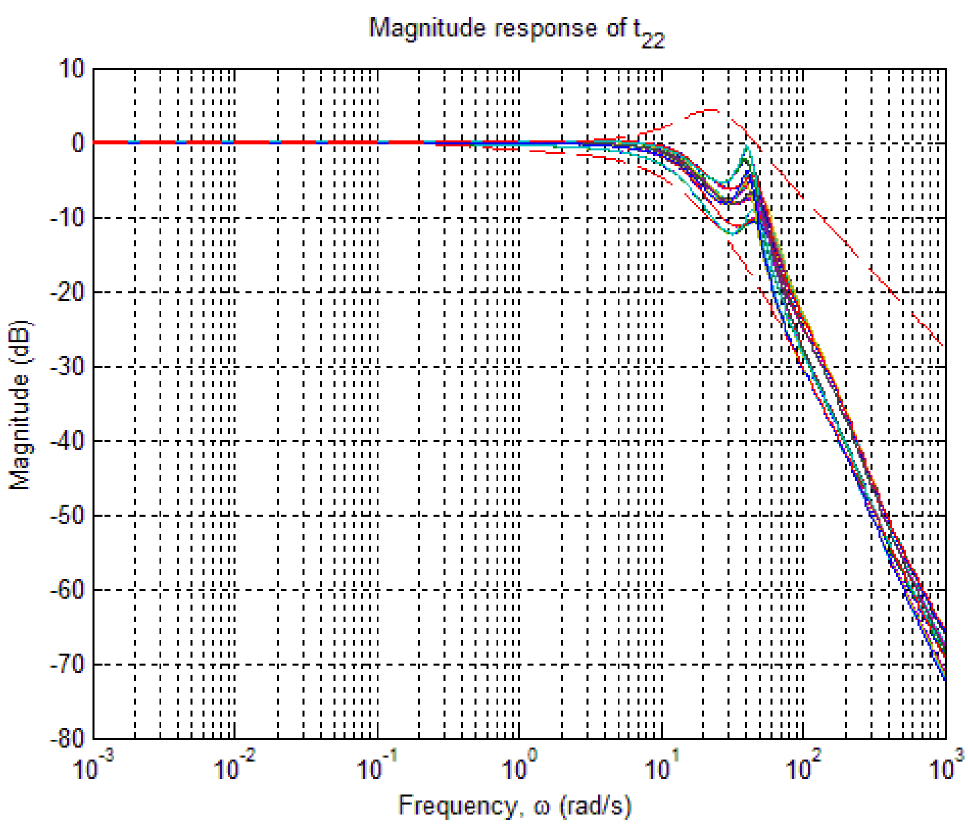

Figure A3.9 Magnitude response of t_{22} after row two is designed for linearized point 3

$$f_{22} = \frac{1}{(s/25+1)^2} \quad \text{(A3.10)}$$

The intersection of the tracking bounds and the stability bounds for loop one is shown in Fig. A3.10. The resulting controller that satisfy all constraints is

$$g_{11} = \frac{-0.00435 \cdot (s+18.7) \cdot (s^2+28.69s+411.5)}{s \cdot (s+15.42) \cdot (s+0.9493)}. \quad \text{(A3.11)}$$

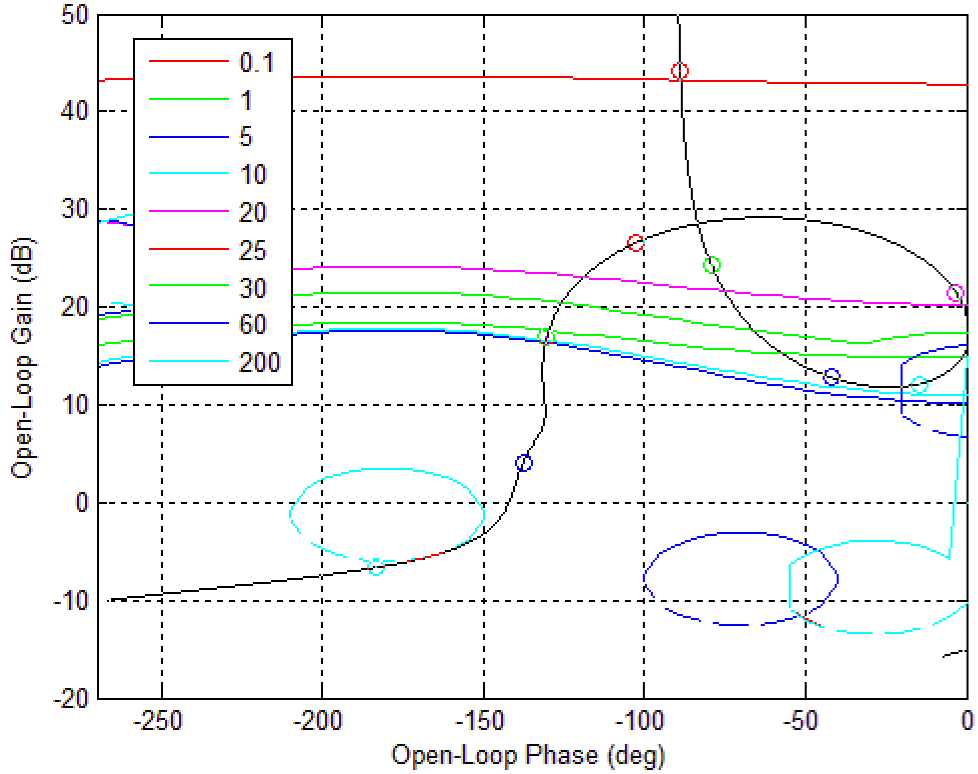

Figure A3.10 Nominal loop one with the intersection of tracking and robust stability bounds for linearized point 3

The pre-filter that shapes the uncertain set to lie within the specification bounds for row one is given by

$$f_{11} = \frac{(s/5+1)}{(s/8+1) \cdot (s/12+1)}. \quad \text{(A3.12)}$$

The reference-output response for the closed-loop uncertain system is shown in Fig. A3.11. The magnitude response shows that all specifications are satisfied. The step response of the system shown in Fig. A3.12, confirms the system stability for all plant cases.

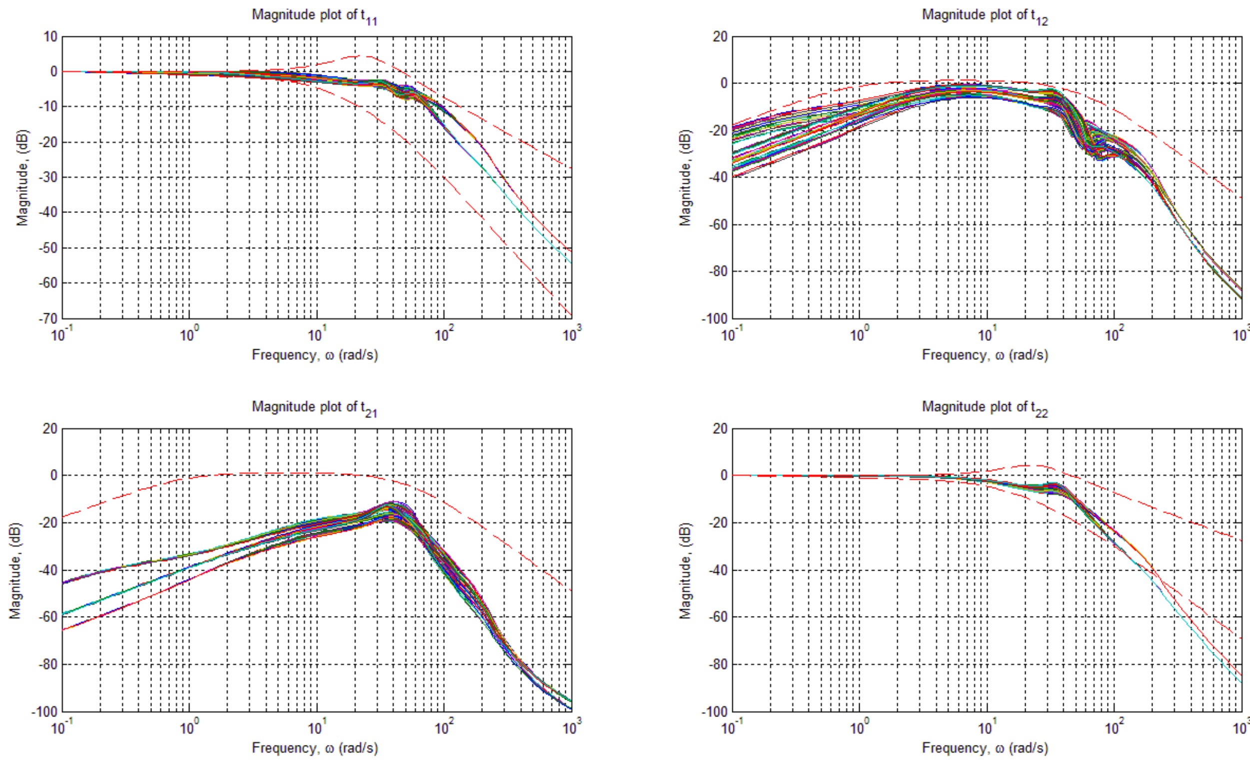

Figure A3.11 Magnitude plot of the closed-loop system with the specifications (red dashed) for linearized point 3

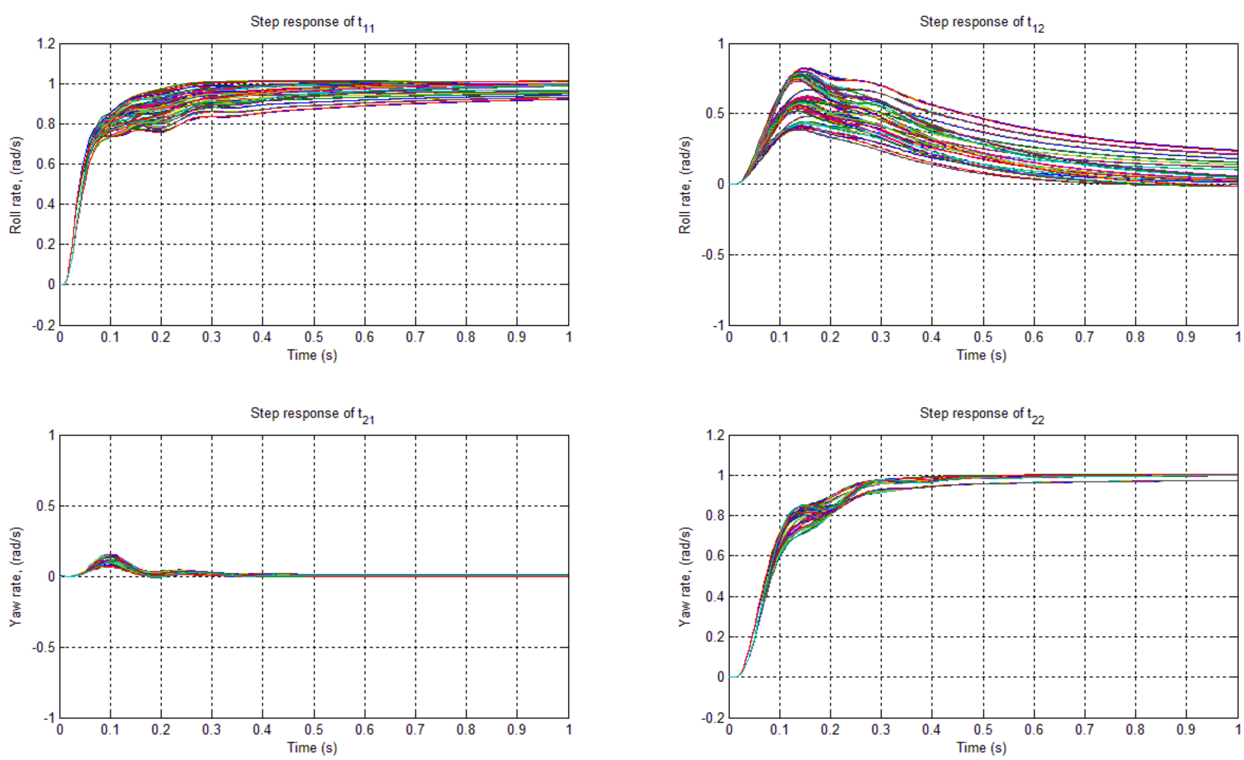

Figure A3.12 Step response of the closed-loop system for linearized point 3

A4. H-infinity Controller

The H-infinity derived controller for linearized point 1:

$$g_{11}(s) = \frac{-172.5361\,(s+8.653)\,(s+1.5)\,(s^2\ +\ 600s\ +\ 1.2\times10^5)}{(s+1.198\times10^4)\,(s+1.239)\,(s+0.012)\,(s^2\ +\ 578.9s\ +\ 3.535\times10^5)} \tag{A4.1}$$

$$g_{12}(s) = \frac{0.58314\,(s+61.43)\,(s-63.59)\,(s+1.5)\,(s^2\ +\ 600s\ +\ 1.2\times10^5)}{(s+1102)\,(s+1.057)\,(s+0.7958)\,(s+0.012)\,(s^2\ +\ 356.8s\ +\ 2.415\times10^5)} \tag{A4.2}$$

$$g_{21}(s) = \frac{-0.58103\,(s-104.2)(s+33.87)(s-10.24)(s+1.5)(s+0.1454)}{(s+1.198\times10^4)(s+1102)(s+1.239)(s+1.057)(s+0.7958)(s+0.012)} \cdot \frac{(s^2\ +\ 600s\ +\ 1.2\times10^5)(s^2\ +\ 747s\ +\ 2.218\times10^5)}{(s^2\ +\ 356.8s\ +\ 2.415\times10^5)\,(s^2\ +\ 578.9s\ +\ 3.535\times10^5)} \tag{A4.3}$$

$$g_{22}(s) = \frac{-173.1213\,(s+1.5)\,(s^2+\ 5.007s\ +\ 380.4)\,(s^2\ +\ 600s\ +\ 1.2\times10^5)}{(s+1102)\,(s+1.057)\,(s+0.7958)\,(s+0.012)\,(s^2\ +\ 356.8s\ +\ 2.415\times10^5)} \tag{A4.4}$$

The pre-filter linearized point 1:

$$f_{11}(s) = \frac{(s/15+1)}{(s/8+1)\,(s/45+1)} \tag{A4.5}$$

$$f_{22}(s) = \frac{(s/12+1)}{(s/15+1)^2} \tag{A4.6}$$

The H-infinity derived controller for linearized point 2:

$$g_{11}(s) = \frac{-1009.7567\,(s+47.98)\,(s+14.35)\,(s-4.796)}{(s+1.521\times10^4)\,(s+1.095)\,(s+0.6957)^2} \cdot \frac{(s+1.5)\,(s^2\ +\ 600s\ +\ 1.2\times10^5)}{(s+0.07448)\,(s^2\ +\ 65.85s\ +\ 9.826\times10^5)} \tag{A4.7}$$

$$g_{12}(s) = \frac{26.1724\,(s+1.355\times10^4)\,(s+45.71)\,(s+33.72)}{(s+1.521\times10^4)\,(s+1772)\,(s+1.095)\,(s+0.6957)^2} \cdot \frac{(s-30.29)\,(s+1.5)\,(s^2\ +\ 600s\ +\ 1.2\times10^5)}{(s+0.06243)\,(s^2\ -\ 9.188s\ +\ 4.814\times10^5)} \tag{A4.8}$$

$$g_{21}(s) = \frac{-25.218\,(s+3532)\,(s+178.6)\,(s-124.6)(s+48.18)\,(s+1.5)}{(s+1.521\times10^4)\,(s+1772)\,(s+1.095)\,(s+0.6957)(s+0.07448)} \cdot \frac{(s^2\ +\ 600s\ +\ 1.2\times10^5)(s^2\ -\ 10.94s\ +\ 7.392\times10^5)}{(s^2\ -\ 9.188s\ +\ 4.814\times10^5)(s^2\ +\ 65.85s\ +\ 9.826\times10^5)} \tag{A4.9}$$

$$g_{22}(s) = \frac{-1060.7414\,(s+45.68)\,(s+1.5)\,(s^2\ +\ 2.855s\ +\ 493.3)(s^2\ +\ 600s\ +\ 1.2\times10^5)}{(s+1772)\,(s+1.095)\,(s+0.6957)^2\,(s+0.06243)(s^2\ -\ 9.188s\ +\ 4.814\times10^5)} \tag{A4.10}$$

The pre-filter linearized point 2:

$$f_{11}(s) = \frac{1}{(s/25+1)^2} \tag{A4.11}$$

$$f_{22}(s) = \frac{(s/12+1)}{(s/15+1)^2} \tag{A4.12}$$

The H-infinity derived controller for linearized point 3:

$$g_{11}(s) = \frac{-1041.786\,(s^2 + 46.21s + 960.1)\,s^2 + 8.965s + 761.5)}{(s+1.387\times10^4)\,(s+0.04881)\,(s+0.004245)} \cdot \frac{(s^2 + 600s + 1.2\times10^5)}{(s^2 + 0.09045s + 0.00205)(s^2 + 164.3s + 9.09\times10^5)} \tag{A4.13}$$

$$g_{12}(s) = \frac{33.8414\,(s+1.19\times10^4)\,(s^2 + 44.84s + 910.4)}{(s+1.387\times10^4)\,(s+1631)\,(s+0.04881)(s+0.004245)} \cdot \frac{(s^2 + 14.75s + 3953)\,(s^2 + 600s + 1.2\times10^5)}{(s^2 + 0.09045s + 0.00205)(s^2 + 41.25s + 4.385\times10^5)} \tag{A4.14}$$

$$g_{21}(s) = \frac{-32.7\,(s+3670)\,(s+260.6)\,(s-178.1)(s^2 + 46.19s + 960.6)}{(s+1.387\times10^4)\,(s+1631)\,(s+0.04881)(s+0.004245)} \cdot \frac{(s^2 + 600s + 1.2\times10^5)(s^2 + 80s + 6.996\times10^5)}{(s^2 + 0.09045s + 0.00205)(s^2 + 41.25s + 4.385\times10^5)(s^2 + 164.3s + 9.09\times10^5)} \tag{A4.15}$$

$$g_{22}(s) = \frac{-1098.6542\,(s^2 + 44.84s + 910.3)}{(s+1631)\,(s+0.04881)\,(s+0.004245)} \cdot \frac{(s^2 + 3.381s + 725.4)(s^2 + 600s + 1.2\times10^5)}{(s^2 + 0.09045s + 0.00205)(s^2 + 41.25s + 4.385\times10^5)} \tag{A4.16}$$

The pre-filter linearized point 3:

$$f_{11}(s) = \frac{1}{(s/25+1)^2} \tag{A4.17}$$

$$f_{22}(s) = \frac{1}{(s/25+1)^2} \tag{A4.18}$$

The H-infinity derived controller for linearized point 4:

$$g_{11}(s) = \frac{-4194.3126\,(s+7.2)\,(s^2 + 15.13s + 118.7)}{(s+1.514\times10^4)\,(s+1.712)\,(s+0.1724)^3} \cdot \frac{(s^2 + 8.078s + 2051)\,(s^2 + 600s + 1.2\times10^5)}{(s+0.03991)\,(s^2 + 21.75s + 2.262\times10^6)} \tag{A4.19}$$

$$g_{12}(s) = \frac{-1117.6133\,(s+1.703\times10^4)\,(s+30.59)(s-28.09)\,(s+7.2)}{(s+1.514\times10^4)\,(s+2528)\,(s+1.712)\,(s+0.1724)^3} \cdot \frac{(s^2 + 14.99s + 116.9)\,(s^2 + 600s + 1.2\times10^5)}{(s+0.03991)\,(s^2 - 11.04s + 9.044\times10^5)} \tag{A4.20}$$

$$g_{21}(s) = \frac{1096.0249\ (s-1110)\ (s+180.2)\ (s-143.6)(s+7.2)\ (s^2\ +\ 15.13s\ +\ 118.7)}{(s+1.514\times 10^4)\ (s+2528)\ (s+1.712)\ (s+0.1724)\text{^}3(s+0.03991)} \cdot \frac{(s^2\ +\ 600s\ +\ 1.2\times 10^5)(s^2\ +\ 1625s\ +\ 2.343\times 10^6)}{(s^2\ -\ 11.04s\ +\ 9.044\times 10^5)(s^2\ +\ 21.75s\ +\ 2.262\times 10^6)} \tag{A4.21}$$

$$g_{22}(s) = \frac{-4256.4242\ (s+7.2)\ (s^2\ +\ 14.99s\ +\ 116.9)(s^2\ +\ 5.763s\ +\ 847.4)}{(s+2528)\ (s+1.712)\ (s+0.1724)^3\ (s+0.03991)} \cdot \frac{(s^2\ +\ 600s\ +\ 1.2e005)}{(s^2\ -\ 11.04s\ +\ 9.044\times 10^5)} \tag{A4.22}$$

The pre-filter linearized point 4:

$$f_{11}(s) = \frac{1}{(s/25+1)^2} \tag{A4.23}$$

$$f_{22}(s) = \frac{1}{(s/25+1)^2\ (s/30+1)} \tag{A4.24}$$

The H-infinity derived controller for linearized point 5:

$$g_{11}(s) = \frac{-1675.4478\ (s+200.8)\ (s+13.46)\ (s+7.835)}{(s+1.396)\ (s+0.04993)\ (s+0.001546)} \cdot \frac{(s^2\ +\ 5.543s\ +\ 3583)}{(s+0.001454)\ (s^2\ +\ 8381s\ +\ 1.859\times 10^7)} \tag{A4.25}$$

$$g_{12}(s) = \frac{137.5412\ (s+199.3)\ (s+13.13)\ (s+8.124)}{(s+1.396)\ (s+0.04993)\ (s+0.001546)(s+0.001454)} \cdot \frac{(s^2\ +\ 18.95s\ +\ 4092)\ (s^2\ +\ 6724s\ +\ 1.458\times 10^7)}{(s^2\ +\ 1284s\ +\ 1.311\times 10^6)(s^2\ +\ 8381s\ +\ 1.859\times 10^7)} \tag{A4.26}$$

$$g_{21}(s) = \frac{-134.7607\ (s+198.9)\ (s+13.46)\ (s+8.047)(s^2\ +\ 81.72s\ +\ 2.16\times 10^4)}{(s+1.396)\ (s+0.04993)\ (s+0.001546)(s+0.001454)} \cdot \frac{(s^2\ +\ 2888s\ +\ 5.114\times 10^6)}{(s^2\ +\ 1284s\ +\ 1.311\times 10^6)(s^2\ +\ 8381s\ +\ 1.859\times 10^7)} \tag{A4.27}$$

$$g_{22}(s) = \frac{-1720.7706\ (s+200)\ (s+24.3)\ (s+13.13)(s+7.965)}{(s+1.396)\ (s+0.04993)\ (s+0.001546)} \cdot \frac{(s-20.69)}{(s+0.001454)\ (s^2\ +\ 1284s\ +\ 1.311\times 10^6)} \tag{A4.28}$$

The pre-filter linearized point 5:

$$f_{11}(s) = \frac{1}{(s/25+1)^2} \tag{A4.29}$$

$$f_{22}(s) = \frac{(s/10+1)}{(s/17+1)^3\ (s/30+1)} \tag{A4.30}$$